Development and Investigation of a Rabbit Model of Tuberculosis Tissue Destruction

André Kübler

Department of Infectious Diseases and Immunity

Imperial College London

Ph.D. Thesis

Submitted July 2013

Acknowledgements

First and foremost, I would like to thank Prof. Jon Friedland, Dr. Paul Elkington and Prof. William Bishai. Without their support and inspiration, I never would have had the opportunity to pursue academic research. Prof. Friedland kindly allowed me to spend time in his laboratory as an undergraduate, where I was guided by Dr. Shivani Singh, a clinical research training fellow, who generously gave her time to teach me the fundamentals of laboratory science. Prof. Bishai took only my enthusiasm as qualification – and encouraged me to explore academic research, and the spirit of collaboration – which eventually allowed me to conduct the following studies in two laboratories of exceptional reputation, despite my relative youth and inexperience.

Dr. Elkington conceived this project, and has been a constant positive driving force, without which, a project that shared 3 principal investigators, in 3 continents, would most likely have failed.

Of those who have contributed their time and effort to the work in this project, I would like especially to thank Brian Luna, Dr. Christer Larsson and Dr. Nicole Ammerman for standing side-by-side with me, handling rabbits, discussing concepts, planning experiments and providing encouragement and support during challenges both inside and outside the lab. They have not only been co-workers, but teachers, mentors and friends. Members of both the Bishai and Friedland labs have been continuously supportive and constructively critical – with a will to push what was often a challenging project forwards.

Collaborations with Dr. Bruno Andrade and Dr. Marlene Orandle at the National Institutes of Health/National Institute of Allergy and Infectious Disease (NIH/NIAID) assisted greatly in the pathological assessment of rabbit tissue. Dr. Marc Halushka of Johns Hopkins Hospital kindly shared human histological specimens, including those stained with cathepsin K antibody (figure 77). Dr. Sanjay Jain (Johns Hopkins Center for Infection and Inflammation Imaging Research) assisted in the development of the imaging technology, and Jay Burns (Johns Hopkins Biomedical Engineering)

helped design and manufacture the equipment. Prof. David Kaczka (Harvard Medical School) and Prof. Wayne Mitzner (Johns Hopkins School of Public Health) provided useful advice in the design of the breath-hold equipment. Xylena Reed gave her time generously to proofreading early drafts of the manuscript.

I would also like to acknowledge several students; John Marshall, Donna Dang, Hui Yang, Stephanie Rincones and Michael Urbanowski who contributed to various aspects of the project, each with dedication that produced vital results.

Finally, I would like to thank those who have supported me personally at various times throughout this project. Their names are not recorded here, but their contributions, past and present, run deeper than words can possibly express. I am full of gratitude, and unworthy of such support and care.

Contents

Figure List

Abbreviations

°C	degrees centigrade
^{18}F-FDG	2-deoxyy-2-(^{18}F)fluoro-D-glucose
ASPV-IH	Inspira Advanced Safety Single Animal Pressure/Volume Controlled Ventilator
AU	arbitrary units
BCG	*bacillus Calmette-Guérin*
bp	base pairs
BSA	bovine serum albumin
BSL	bio-safety level
cAMP	cyclic adenosine monophosphate
CD	cluster of differentiation
cDNA	complementary DNA
CFP-10	culture filtrate protein 10
CFU	colony forming units
CICP	type I C-terminal collagen propeptide
cmH_2O	centimetres of water
CoMTB	conditioned media from *M. tuberculosis* infected macrophages
CPDB	Consensus Pathway Database
CT	computed tomography
ct	cycle threshold
CTSK	cathepsin K
dbcAMP	dibutyryl cyclic adenosine monophosphate
DNA	deoxyribonucleic acid
DPD	deoxypyridinoline
DTH	delayed-type hypersensitivity
ECM	extracellular matrix
ELISA	enzyme-linked immunosorbent assay
ESAT-6	early secretory antigenic target 6
FCS	foetal calf serum
FPKM	fragments per kilobases of exon per million fragments mapped
g	acceleration relative to Earth's gravitational force
gDNA	genomic DNA
GDP	gross domestic product

H+E	haematoxylin and eosin
HEPA	high efficiency particulate air
HIV	Human Immunodeficiency Virus
HP	helical peptide
HPA	Health Protection Agency
HRP	horseradish peroxidise
HU	Hounsfield units
IBMX	3-isobutyl-1-methylxanthine
IFNɣ	interferon gamma
IGRA	interferon gamma release assay
IU	international units
IV	intravenous
KEGG	Kyoto Encyclopedia of Genes and Genomes
LPS	lipopolysaccharides
M.	*Mycobacterium*
M. tb	*Mycobacterium tuberculosis*
mCi	millicuries
M-CSF	monocyte colony stimulating factor
MDR	multi-drug resistant
MMP	matrix metalloproteinase
MRM-SELDI-MSI	multiple-reaction-monitoring matrix-assisted laser desorption-ionisation mass spectrometry imaging
mRNA	messenger ribonucleic acid
NG	nasogastric
OADC	Oleic acid, albumin, dextrose, catalase
OD	optical density (at a wavelength of 600nm unless stated)
OT	old tuberculin
PBMCs	peripheral blood mononuclear cells
PBS	phosphate buffered saline
PCR	polymerase chain reaction
PET	positron emission tomography
PICC	peripherally inserted central catheter
PKA	protein kinase A
PMA	phorbol 12-myristate 13-acetate

PPD	purified protein derivative of old tuberculin
PYD	pyridinoline
qRT-PCR	quantitative real-time polymerase chain reaction
RCF	relative centrifugal force
RNA	ribnucleic acid
RNA-Seq	RNA sequencing
ROI	region of interest
RPM	revolutions per minute
rRNA	ribosomal ribonucleic acid
SARS	severe acute respiratory syndrome
SDS	sodium dodecyl sulphate
SUV	standardised uptake values
SUVmax	the SUV of the voxel with the highest emission within a region of interest
SUVmean	the mean SUV in a given region of interest
TB	tuberculosis
TB Sup	filter-sterilised supernatant of *M. tuberculosis*
TIMP	tissue inhibitor of metalloproteinase
TNFα	tumour necrosis factor alpha
TST	tuberculin skin test
UV	ultra-violet
UVTB	ultra-violet killed *M. tuberculosis*, resuspended in original supernatant
WHO	World Health Organization
wUVTB	washed ultra-violet killed *M. tuberculosis*, resuspended in fresh 7H9 media
XDR	extensively-drug resistant

Declaration of Originality

The work included in this thesis is my own, but it is not mine alone. No project containing research with rabbits could possibly be considered a truly individual pursuit. Each of the animal experiments was conducted with Nicole Ammerman, Brian Luna and Christer Larsson. Development of imaging analysis was conducted with Brian Luna. Brian also conducted the experiments on the rabbit PBMCs presented in figure 13. Michael Urbanowski and John Marshall contributed to the gene expression data, and Christer Larsson was instrumental in the RNA-Seq project. Marc Halushka and Jin Park identified samples and performed the immunohistochemistry for the human cathepsin K data, and Marlene Orandle analysed the histology presented in figures 31 and 32. Jon Friedland, William Bishai and Paul Elkington conceived and guided the project, which was funded by Imperial College London, NIH/NIAID and Howard Hughes Medical Institute (HHMI). I have endeavoured not to present any work that has been conducted by others as my own, or replicate work and claim it as my own. I have attempted to the best of my ability to reference sources of ideas and previous research.

Copyright Declaration

Abstract

Tuberculosis kills more people than any other bacterial disease. The characteristic tissue destruction that occurs during infection contributes to morbidity, mortality, and transmission. Tissue damage limits antibiotic effectiveness, and generates regions of immune privilege. Therefore, therapies that target tissue destruction may improve treatment outcomes.

Currently, modelling tissue destruction *in vivo* requires the infection of large animals for prolonged periods. These models are highly variable in outcome. This makes experimentation challenging, and limits there use in testing therapeutic strategies, which in turn limits the progression of potential therapies to clinical trials.

This thesis outlines the development of a highly consistent rabbit model of cavitary tuberculosis, in which novel therapies can be investigated, using small groups of animals. A method to assess pathology *in vivo* by breath-hold computed tomography was also developed. Matrix metalloproteinase-1 is confirmed as a potential mediator of tissue destruction, and cathepsin K is newly identified as a potential mediator of tissue destruction. These collagenases are targetable with the drugs Cipemastat and Odanacatib respectively, both of which are safe in man.

This thesis provides a novel system for trialling treatments for tuberculosis in the context of human-like, tissue-destructive pathology. This may facilitate the selection of both antibiotic and non-antibiotic treatment strategies for tuberculosis. This model will allow for a better understanding of the physical, chemical, molecular, genetic and immunological characteristics and determinants of cavitary tuberculosis.

1. Introduction

This chapter gives a brief overview of the tuberculosis (TB) epidemic, and describes why basic science is essential to TB eradication. I suggest that by defining disease by the pathology involved, we may identify specific preventative, diagnostic, and curative measures. I then describe TB pathology, focussing on the importance of tissue destruction in active disease. This forms the conceptual framework for understanding the reasons for pursuing this research. I then discuss the benefits and limitations of current animal models of TB, and how the rabbit may specifically help us to better understand tissue destruction. I summarise current evidence that suggests that matrix-degrading enzymes, especially matrix metalloproteinase-1 (MMP-1), are important in TB related tissue destruction. I explain why, in order to understand therapeutics in the context of tissue destruction, and understand the mechanisms that cause tissue destruction, we must develop a reliable model of tissue destruction, in which experiments can be carried out.

1.1. Tuberculosis; a challenging pandemic

1.1.1. Tuberculosis is a major global health concern, complicated by HIV co-infection and antibiotic resistance

TB kills more people than any other bacterial disease. The majority of its victims are immunocompetent individuals of working age, with fully-treatable pulmonary disease. In 2011, the World Health Organization (WHO) estimated that; 1.45 million people died from infection, 8.5-9.2 million new cases occurred, and 11-14 million people were living with active disease (1).

At the individual level, TB causes a debilitating disease, personal suffering and death. Within a family it often targets the bread-winners and parents of young children – in 2010, nearly 10 million children were orphaned by TB (2). In a community it evokes fear, which leads to discrimination and even persecution (3). It causes the loss of working hours in productive populations, and is a huge burden on healthcare systems in developing countries (1). TB affects global politics; it determines travel and immigration policies, foreign aid requirements and policy, not only in endemic countries, but also those seeking to interact with them. On an economic level the World Bank has estimated that TB has a total economic cost of 519 billion dollars in sub Saharan Africa alone (4). The effect of this bacterial disease is felt at every level – the 'TB problem' is both global and personal.

Mycobacterium tuberculosis (M. tb), the bacteria that causes TB, has also proven a deadly pathogen in Human Immunodeficiency Virus (HIV) infected individuals. *M. tb* infection is estimated to be responsible for 20% of HIV-related deaths, and HIV contributes to 13% of all deaths from TB (1).

Finally, as with all bacterial infections, the increasing prevalence of antibiotic resistance is concerning, especially because TB treatment options are already limited. It is estimated that 4% of new TB cases are resistant to two or more first line drugs (i.e. multi-drug resistant tuberculosis; MDR-TB) (1). Worryingly, MDR-TB appears to be epidemic in certain regions in Eastern Europe, for example, in Russia, it accounts for 20% of the 140,000 cases per annum (5). The last decade has also seen the emergence of extensively drug-resistant TB (XDR-TB), which has now been reported in

nearly every region where TB is diagnosed (1). Fatality rates of up to 97% in HIV-positive individuals with XDR-TB have been reported (6).

In 1995, the WHO declared the TB epidemic a global emergency, resulting in an increase of investment of resources for research and eradication programs. The results' of new policies and research have been modest, although, rates of disease are beginning to decline (1). There have been no specific innovations that have aided this reduction in disease. In order to further reduce the global burden of this disease, a co-ordinated effort between public-health experts, governments, industry, scientists and the public is required.

1.1.2. Is TB eradication a real possibility? A simple comparison with smallpox

Undoubtedly, the benchmark for global infectious disease eradication is smallpox. In 1967 the WHO estimates that there were 15 million people infected with the disease and that 2 million deaths resulted. Incredibly, by 1979, smallpox was eradicated (7). Why hasn't this been the case with TB?

Simply, the challenge is much more complex. The technology required to identify, eradicate and prevent smallpox was very simple and easily deployable. There was a highly effective vaccine for prevention, and a simple diagnosis achieved by merely observing an infected individuals outer appearance (8). Unfortunately with TB, there is no effective vaccine, diagnosis is challenging, transmission can occur from asymptomatic carriers, symptoms are non-specific, and disease can remain dormant for a lifetime or can reactivate unexpectedly (9, 10). This being said, TB is very rare in the developed world, and TB mortality rarer still (1). We therefore have good reason to believe that very significant reductions in TB rates are possible, if we can only understand what interventions are programmatically useful.

1.1.3. What can be learned from successes in TB eradication?

China has implemented a successful campaign against TB, with a 50% reduction in prevalence between 1990 and 2010, and an 80% reduction in mortality (1). This was likely the result of improved co-ordination of the TB surveillance program and treatment programs, following the

outbreak of severe acute respiratory syndrome (SARS) in 2003 (2). Another success story comes from Cambodia where there has been a 46% reduction in TB incidence over the past decade (1). In Cambodia, new found political stability allowed for infrastructural changes and implementation of surveillance and treatment programs, which had previously been impossible (1). In both cases, the application of current technologies has contributed to success. Similar proportional reductions in TB incidence were also seen between 1900 and 1950 in the United States of America (USA) (11). This decrease predates any specific treatment for the patient and coincides with reductions in prevalence of other infectious diseases. This indicates that socio-economic improvements can contribute significantly to reducing TB burden. The introduction of effective antibiotics did not substantially alter the rate of decline in prevalence. The USA has now seen a greater than 95% reduction in TB incidence since 1900 (11), with prevalence well below 5 per 100,000 (12). The lesson to be learned is that, in certain contexts, current technologies are effective.

In many regions of the world, especially Sub-Saharan Africa, the situation is far more worrisome. In South Africa, TB is the leading cause of death, with an incidence 200 times greater than the USA (1). This is despite the fact that South Africa has a relatively strong economy, with the gross domestic product (GDP) being at least four times that of Cambodia (13). 65% of TB cases in South Africa are HIV-positive (1).

It is clear that current strategies have not been effective enough in the settings where they are most needed. Whether this is because of high levels of HIV, modest infrastructure, political instability, economic insufficiencies, or as yet unidentified cultural or biological susceptibilities, is unclear. It must be remembered that the enormous economic burden attributed to TB, is in itself a reason for the failure to achieve the social reform required to eradicate it (14). Poverty causes TB, but TB also causes poverty.

Promoting economic development may help eradicate TB. However, strategies looking at cost-effective interventions to facilitate growth in the developing world, include the expansion of

diagnosis and treatment for TB (14). Clearly the practical solution in this situation is still beyond reach. Studying the socio-economic benefit of healthcare interventions is a complex and burgeoning science in itself. Hopefully, sustained research in this area will allow for directed efforts to solve these complex problems.

1.1.4. Summary: The eradication of TB is dependent on integration of innovative science and policy

The eradication of TB is both a social and economic necessity. It will require the simultaneous expansion of detection, and treatment, coupled with innovative solutions to prevent and cure disease. The smallpox eradication program sets a precedent for infectious disease eradication, at a relatively low cost, provided the tools required for targeted intervention are appropriate for the conditions in which they need to be deployed. Unfortunately, we lack the basic understanding of TB pathogenesis required to make targeted changes in TB endemic regions. We have not yet met the challenge of providing programmatically relevant to combat TB.

It is the duty of basic scientists to provide a knowledge base that allows TB diagnosis and treatment to be simplified. It is the duty of economists and politicians to ensure resources are correctly allocated for the application of current and future solutions. The WHO has been successful in reversing increasing rates of TB at a global level (1). However, in certain parts of the world, especially Sub-Saharan Africa, rates of TB continue to rise, even in immunocompetent individuals, despite organised programs targeting TB. It is in these regions especially, that TB is having its greatest social and economic impact, and that we are in most need of innovative solutions to simplify the prevention, identification and treatment of TB.

1.2. The tools we have and the tools we need

There are 3 clear areas where the TB epidemic requires innovative solutions:

i) Prevention: Reducing the number of new infections

ii) Diagnosis: Identifying more cases, more quickly

iii) Treatment: Shorter treatment, with less side-effects, that is easily complied with

1.2.1. Prevention of TB

1.2.1.1. Vaccination

Vaccination is the ideal manner with which to prevent infectious disease. However, the currently used vaccine, *M. bovis Bacillus Calmette-Guérin (BCG)*, has not been effective in curbing the epidemic; and multiple studies have questioned its efficacy (15-17). An immune response that protects against TB is yet to be described, despite the fact that an estimated 90% of individuals exposed to *M. tb* do not develop disease (18). Novel vaccination strategies have been shown to lead to long-lasting immune responses (19-21), but have failed to protect from disease (22). Additionally, trials are programmatically challenging, because vaccination strategies must be built in the context of BCG administration, which is effective in preventing childhood disease (23).

1.2.1.2. Non-vaccine preventative measures

The alternatives to vaccination are non-specific interventions. Economic development was discussed in section 1.1.3, and since the most cost-effective measure to achieve development is infectious disease eradication (14), the argument is circular and unhelpful. Our understanding of disease transmission is limited, and hinders development of specific prevention measures.

M. tb is transmitted by aerosol. However, we still do not have more than a preliminary understanding of the infectious dose, the mechanisms of transmission, or host susceptibility. As such, modelling transmission is extremely challenging, and identifying targets that are most likely to be effective at reducing TB burden is speculative. Very few studies have been completed in this area. Experimentally, there is a suggestion that relatively few patients transmit disease (24-26). A finding which is supported by a number of sequencing studies (27-29), although these have not been performed in endemic regions, in the context of high HIV prevalence, or with fully

validated data analysis modalities.

Lessons from combating HIV and Malaria would suggest that personal protection (condoms and mosquito nets respectively) can be effective (30, 31). Unfortunately, diseases spread by aerosol are much less susceptible to such interventions. Although some measures, such as mask-wearing, do appear to be of benefit in protecting from influenza (32-34), with TB, masks have been shown to be ineffective, even in healthcare settings (35). Architectural strategies have also been trialled (24), with interventions such as UV lighting and increased airflow showing some benefit (24, 36), but these have not dramatically changed TB prevalence. This is not to say such measures are ineffective, just that they have not been applied in a way that has significantly reduced transmission. Confined transport has been linked to increased susceptibility, suggesting that simple behaviour changes, such as opening windows, may reduce transmission, however, the overall effect of such measures is hard to ascertain (37). If we are to reduce transmission, other than by developing effective vaccines, it would appear that basic research must first identify correlates and mechanisms of transmission.

1.2.2. Diagnosis of TB

1.2.2.1. Dependence on self presentation is dangerous

Identification of TB is usually dependent on self-presentation to clinicians; which in non-medicalised cultures may be extremely late during the disease (38). Symptoms are often non-specific and usually mild during early stages of the disease, decline is insidious and pathology may be extensive (9, 10, 39). Not only does this mean that individuals often have advanced disease at presentation, but also that they may have transmitted the infection extensively (38, 40). The absence of sensitive and specific screening measures means that regional surveillance is labour-intensive and impractical in many areas. Identification of the bacteria is required for diagnosis, but is challenging.

1.2.2.2. Bacterial detection

Diagnosis is one area of TB research that has seen the translation of innovative solutions for global use (although the impact of such measures is yet to be seen). Sputum smears, chest radiography and bacterial culture have been the mainstays of diagnosis, but none are both sensitive and specific. In 2010, the WHO endorsed GeneXpert, a cartridge-based polymerase chain reaction (PCR) testing

system with the potential to diagnose TB in under 2 hours (41). Since then 1.1 million tests have been conducted (1). However, the machine is costly and dependent on electricity, therefore, its use is confined to referral centres. As such, while reducing the burden of diagnosis in some settings, this merely represents a step on the path to a point-of-care test. GeneXpert requires *M. tb* in the sputum of the patient – which may not be easily produced, or be representative of the entire lung. We still need a sensitive, rapid, point-of-care test to help identify cases. At present there is no reliable screening method for TB.

1.2.2.3. Detection of immune correlates of infection

Previous exposure to *M. tb* can be evaluated by Interferon Gamma Release Assays (IGRAs), which detect Interferon gamma (IFNɣ) release by blood in response to *M. tb* specific antigens. Because there is no way of predicting which exposed individuals will develop disease, this information is of limited use (especially in endemic regions) (42-45). Tuberculin skin tests (TSTs) use the induration resulting from cellular recruitment and inflammation that occurs during the delayed-type hypersensitivity (DTH; Type IV hypersensitivity) reaction to intradermally injected *M. tb* antigens, to assess previous exposure to *M. tb*. This test is significantly less resource intensive than IGRAs, but gives a positive result if the patient is exposed to the vaccine strain, *M. bovis BCG*. In addition to this, persons who are infected or immunosuppressed may have falsely negative tests by either measurement (46).

A highly sensitive and specific test for very early active disease and antimicrobial resistance are required. It must be point-of-care so that immediate action can be taken to treat infected individuals. A test or testing strategy for exposure in immunocompromised individuals must also be developed.

1.2.3. Treatment of TB

TB treatment consists of 6 months of antibiotics, comprised of 4 drugs (rifampicin, isoniazid, pyrazinamide and ethambutol) for 2 months followed by 2 drugs (rifampicin and isoniazid) until the end of treatment. Patient compliance during such a lengthy regimen is poor; patients often feel better after just a few weeks, and the drugs have unpleasant side-effects. In London, despite good healthcare infrastructure, the Health Protection Agency (HPA; now Public Health England) reported only 85% completion of treatment (47). This suggests that even in resource-ready settings, application of this complex regimen is problematic. Innovations are clearly needed to rapidly and simply treat TB. Novel antibiotics are helping to combat resistant disease (48-51), but extensive searches have failed to demonstrate any antibiotics likely to reduce treatment duration of susceptible disease (52). Poor antibiotic penetration into diseased tissue, and bacterial tolerance, may explain why TB treatment requires prolonged antibiotic administration (53, 54). Identification of antibiotics which overcome these problems is challenging because there are no firmly established models of the complex bacterial microenvironments found in human disease – and there is only a limited understanding of which microenvironments *M. tb* may be persisting in. It should be considered that altering these microenvironments, by targeting host mediators, may be more achievable than designing antibiotics that can function in these complex microenvironments, or against dormant bacteria.

It is also important to consider that the duration of the intervention, rather than the duration of the therapy itself, is what affects compliance. A single therapeutic event that has effects for a long duration is preferable to a shorter therapy that requires daily administration. We must aim for a single intervention strategy, which is simple, economical and safe – and we should consider all possibilities, not just novel antibiotics, to achieve this.

1.2.4. Summary: Current tools are only partially effective, innovation is required if we are to tackle TB in the developing world

TB kills more people than any other bacterial infection. Attempts to reverse the growing burden of disease have proved successful in certain socio-economic conditions, however, the tools that have helped reduce infection in these regions are not accessed in the situations where disease is most prevalent. Innovations as well as increased availability of current resources are required to relieve the burden tuberculosis in the developing world.

1.3. Defining TB: Using language to facilitate not confuse our understanding

In order to prevent, diagnose and treat TB – we must understand first what TB is. Currently, basic TB research is dependent on clinical and epidemiological definitions, which are not directly linked to the diverse underlying pathological processes. If we can better understand the phenomena that surround infection and disease in the context of the underlying pathology, we may reveal innovative strategies for combating disease.

1.3.1. Tuberculosis is the disease of humans caused by *M. tuberculosis*

TB is a broad-ranging term that describes any disease that results when *M. tb* infects a human. Historically, infection with other closely related mycobacterial species (*M. microtii, M. bovis, M. africanum, M. canettii*) have been called TB – but this adds an ambiguity in understanding the specific mechanisms of disease (that cannot be assumed to be identical for all species), and so this thesis will refer to these less common human infections as 'disease caused by *M. species*'. This is particularly true of *M. bovis*, in which human-to-human transmission is exceptionally rare (55, 56), and thus has nearly been eradicated where pasteurisation of milk products is routine (57-59). Clearly the pathogenesis of this infection is very different to *M. tb*, which is dependent on human-to-human transmission.

Since no other species is naturally infected with *M. tb*, it is an obligate human pathogen. The symptoms and disease caused by experimental *M. tb* infection in other species may resemble human disease – but is not the human disease; TB.

1.3.2. The clinical picture is related to, but not entirely dependent on, the underlying pathology

The clinical manifestations of TB are incredibly variable and dependent on numerous host and bacterial factors, as well as the anatomical location of the infection. It must be remembered that approximately 90% of individuals who are exposed to *M. tb* do not develop symptomatic illness (18). Additionally, the clinical picture does not necessarily reflect the underlying pathology; apparently healthy individuals often harbour highly destructive lesions and those with limited immunity often

have the highest bacterial burdens and the fewest symptoms (9, 10). We must remember that a clinical picture is a surrogate of these underlying processes, and although this is a vital resource to the caregiver, it is academically vague, because it does not detail the complex, varied mechanisms involved in 'active TB'. For example, destructive spinal TB and cavitary lung TB may have more in common with each other, than with granulomatous disease in a lymph node – yet most studies would group the extrapulmonary diseases together, independent of their pathology.

1.3.3. Active TB is an over-arching term defined by symptomatic disease or infectiousness

Active TB is traditionally defined by the presence of signs or symptoms of tuberculosis; cough, fever, night-sweats, weight-loss, anorexia, general malaise or a positive diagnosis (via either microscopy or culture) of *M. tb* from any site independent of symptoms (9, 10, 60). This is in contrast to latent TB, which is defined as being non-symptomatic, but having an active immune response to a subset of *M. tb* antigens. Active TB can be either pulmonary or extra-pulmonary, but all infection enters through the lungs (through inhalation) and is transmitted in exhaled aerosols (9, 10). It is also important to remember that individuals without any symptoms or signs of TB, may well be transmitting *M. tb* and so contributing to the epidemic (40). I will be defining active TB by either the ability to transmit *M. tb* to another person or symptoms and signs of tuberculosis with clinical evidence of *M. tb* infection.

With this definition, any patient who does not transmit, and does not have symptoms, does not have active TB. Maintenance of this status in all persons globally would effectively be the eradication of TB as a disease. Persons without active TB may still contain actively replicating bacilli (as evidenced by the reduced risk of active disease after prophylactic Isoniazid treatment (61)) and can be considered to have sub-clinical *M. tb* infection. If a period of active disease has been observed, asymptomatic and non-transmitting patients can be considered to be in TB remission. TB remission can result from either immune containment (spontaneous remission) alone, or in combination with antibiotic killing of bacteria (treatment induced remission). Cured TB can then be defined as

individuals in whom remission is induced to such an extent that their risk is equal, or less than, that of an individual with similar immune status, who has not previously been infected with *M. tb*.

1.3.4. Temporal definitions are inadequate: The problem with 'primary', 'secondary' and 'latent' TB

TB is often considered in a temporal framework, where 'primary' disease occurs immediately after infection (arbitrarily within 6 months of infection) and 'secondary' disease occurs after a prolonged asymptomatic period (latent disease) (62). These temporal definitions are inadequate in the context of modern disease. For example, disease resulting from immunosuppression is clinically and pathologically more similar to progressive disseminated infection; but temporal definitions would deem the former 'secondary' disease and the latter 'primary' disease. Newly acquired infection, in a previously exposed individual, may be paucibacillary, and highly destructive, but is by definition primary disease even though this same clinical picture is extremely common in older patients who most likely have reactivation of past infections. Temporal definitions are clinically useful for understanding the risk for patients exposed to *M. tb*, and estimating the time of exposure – but are academically insufficient because they are not based on biological observations. The term latency will be avoided – the definition is imprecise and unclear. Commonly, latency is defined as a period of asymptomatic infection that may become active disease. The strict clinical definition of latency is TST- or IGRA-positivity. These tests indicate that a person has immune responses to *M. tb* antigens. The assumption is that this reactivity is highly correlative with subclinical *M. tb* infection and that this subclinical infection is likely to develop to become active disease. However, since TST- or IGRA-positive individuals do not universally develop disease, even under high immunosuppression (63), it seems likely that immune responses may be maintained after exposure, without subclinical infection. This is supported by the observation that prophylactic treatment of TST-positive individuals with 9 months of Isoniazid, reduces the long-term risk of reactivation (to the levels of unexposed individuals) (61, 64, 65), but does not cause reversion of TST or IGRA responses (66-68). It follows therefore, that individuals with positive TSTs or IGRAs can only be assumed to have encountered *M. tb* (or *M. bovis* in the case of TSTs) antigens. The positive

tests therefore indicate that the individual may have subclinical infection, which in turn carries a risk of becoming active TB.

1.3.5. Resistance should be defined by the likelihood of developing active disease

Resistance to disease is the goal of any vaccination strategy. Usually this would be defined in terms of resistance to infection, but since infection with *M. tb* does not inevitably cause disease it is important to understand that resistance to disease is also a valuable, and perhaps more achievable, aim. I will define resistance as the measure of likelihood that a person will develop Active TB, (i.e. a more resistant individual is less likely to develop active TB). Crucially, this definition makes no assumption about the immune status of the patient. It is clear that immunocompromised individuals are less resistant to infection; but it must be remembered that many of the processes involved in active TB are immune-mediated – and therefore a balance of both pro- and anti-inflammatory responses must be achieved to prevent disease.

1.3.6. Summary

The language used to describe TB is unclear, and although useful for clinical studies and epidemiological data collection, the arbitrary nature of these definitions must not be broadly applied to academic thinking on the subject. By clearly defining terms as evidenced by data it is clear that:

- Cure does not require total bacterial eradication, but a return to a state where the risk of disease is equal to that of an uninfected individual.
- Latency is a clinical phenomenon, most likely explained by a variety of pathophysiological scenarios.
- 'Resistance' to disease is not necessarily dependent on resistance to *M. tb* infection alone and may be dependent on mounting the right balance between complex mediators of the immune response, rather than 'strong' or 'weak' immune responses.

TB eradication is dependent on the treatment of active disease (including asymptomatic transmission), and prevention of active disease, as distinct from eradication and prevention of *M. tb* infection. This is not to suggest that *M. tb* eradication is not a valuable therapeutic goal – but that it

may not be the only strategy.

1.4. The pathology of active TB

Active TB encompasses a spectrum of disorders resulting from the interaction between the host and bacteria as well as their individual attributes. There are 3 principal contributing factors to disease outcome (69):

i) The immune status of the infected individual

ii) The virulence, number and metabolic state of the M. tuberculosis bacilli

iii) The site of the interaction between host and bacteria

All of these variables are continually changing – in turn altering each other. As discussed in the previous section, an accurate understanding of disease processes is a prerequisite if we are to develop novel vaccines, diagnostics and treatments.

1.4.1. TB and the granuloma

There are a few principal features of tuberculosis anatomic and histologic pathology, none are unique, but in combination, they are highly indicative of TB. The most studied is the granuloma.

Granulomas are defined as '...nodular inflammatory lesions, usually small or granular, firm, persistent and containing compactly grouped modified macrophages' (70). Granulomatous responses are essential for protection against larger parasites and foreign bodies (39). Fundamentally, the response results in sequestration of the foreign body or parasite, and allows for the delivery of immune cells which can become highly activated without causing significant collateral damage to the host. Granulomas are also found in a number of conditions of unknown aetiology (39). Tuberculosis granulomas differ from granulomas found in other conditions; the main distinction is the presence of central necrosis, and the heterogeneity of the lesions. TB granulomas may be found at autopsy, in cases where there is no evidence of active TB, however, other TB pathologies are exceedingly rare in persons without active disease (69, 71).

1.4.2. Tissue destructive pathologies are the defining feature of active TB in immunocompetent hosts

The majority of TB occurs in immunocompetent adults (1); in which tissue destruction is the defining feature of active disease described by TB pathologists: Canetti, Laennac, Rich and Hunter, whose careers collectively span well over two centuries, and thousands of dissections, (69, 71-73) all describe the non-granulomatous lesion as of utmost importance in active TB. This literature is best summarised in a recent review by Hunter (73). The most up-to-date observations of human pathology describe a lipoid pneumonia which necrotises and leads to cavities in active TB. The proposed mechanism is that the lipoid pneumonia forms after proximal airway occlusion (73). Laennec describes large necrotising yellow tubercles and 'yellow infiltration' preceding caseation (72). Canetti rarely used the terms tubercle or granuloma, instead using of the non-specific term 'focus', and stating that the 'softening' of the focus is the most important event in active TB (71). Rich claimed instead that granuloma necrosis is the source of cavities (69), a hypothesis carried forwards by Lurie and Dannenberg after observing disease progression in rabbits (74, 75). The linking of granuloma formation and cavity formation has persisted, despite clear evidence that these events may occur independently (73). There has been persistent focus on the granulomatous pathology; with many high-impact reviews neglecting non-granulomatous pathology entirely (53, 76-82). The terms used in tissue destruction during TB are numerous, but whether it is called softening, cavity formation, liquefaction, this occurrence, is the most fundamental defining feature of active TB in the immunocompetent host.

1.4.3. The cavity is an environment that facilitates bacterial proliferation and immune evasion

Regions of tissue destruction represent immune failure and favour bacterial proliferation (83). Erosion of destroyed tissue leads to cavity formation, and the erosion of this tissue into airways i.e. the process of cavity formation, allows for expectoration of high numbers of bacteria, a process assumed to result in transmission (84, 85). The cavity has long been described as the most difficult lesion in TB to sterilise with antibiotics (71, 86) and extensive cavitary disease predisposes to antibiotic failure (87). It is also a key site from which drug resistant bacteria can be isolated (71). The

immune-privileged nature of this site is confirmed by the fact that even after effective antibiotic therapy, the cavity may be a site of fungal infections only otherwise seen in immunocompromised individuals (39, 60).

Understanding the process of cavity formation is fundamental to understanding what defines active disease, and also why prolonged treatment is necessary. Fundamentally, there are two key processes that occur during tissue destruction: Necrosis and extracellular matrix (ECM) degradation. In TB, matrix degradation and cavity formation is the predominant characteristic, a phenotype rarely seen in other conditions (88).

1.4.4. Tissue destruction requires ECM degradation

The lung ECM is a complex and extraordinarily resilient structure. It undergoes continuous mechanical stress during repeated expansion and contraction, whilst maintaining the delicate structure required for gaseous exchange. Although supported and maintained by the resident cells (primarily epithelial cells and fibroblasts), the lung ECM does not depend on these cells for its physical properties and can maintain its mechanical properties in the absence of cells (89, 90).

The principal mechanical components of the lung ECM are fibrillar collagens (types I and III) and elastin. The basement membrane of the alveoli is largely type IV collagen. The remaining lung matrix is composed of other collagens and glycoproteins that have some structural roles, but are also central to cell adhesion, maturation, survival and signalling (91-93). The matrix also plays a crucial role at the interface with the vascular surfaces, regulating permeability and immune cell migration (39). Given its biological importance, and the importance of its microstructure, lung ECM turnover is closely regulated. Of particular importance in the regulation of ECM are the Matrix Metalloproteinases (MMPs) and their inhibitors, tissue inhibitors of metalloproteinases (TIMPs). As their name suggests, MMPs collectively have the ability to degrade all known components of the ECM (94).

1.4.5. MMPs can collectively degrade all components of the ECM

MMPs are a family of 24 enzymes with Zn^{2+} catalytic domain. They share a conserved pro-domain and are commonly classified according to ECM substrate (collagenases, gelatinases, stromelysins *etc.*). MMPs also have many non-ECM substrates (92, 95).

MMP activity is regulated at transcriptional and translational levels, as well as by post-translational modification and finally by enzymatic activation (96). Their expression is tightly controlled, and the majority of MMPs are not expressed in healthy tissue (97). The proteolytic activity can be inhibited by TIMPs (98, 99).

Unregulated MMP expression and MMP activity have been associated with a number of disease processes (100-102), and although originally this association was linked to disease in which ECM turnover had a clearly identifiable role, such as rheumatoid arthritis, they have since been discovered in numerous inflammatory conditions, and have roles in these conditions that extend beyond ECM degradation (103).

Most importantly in terms of pulmonary ECM regulation, the MMP family includes the only enzymes known to degrade fibrillar collagen at neutral pH, the collagenases (MMPs -1, -8, -13, and -14) (104). The only other enzyme known to degrade structural collagen is cathepsin K (CTSK), a lysosomal cysteine protease with peak activity at a pH 5.0-6.0 (104).

1.4.6. MMPs and TB

It is clear that alterations in the lung ECM occur during active TB. This led to the hypothesis that MMPs may play an important role in disease. The first article in this area was published in 1996 (99), and since then, a series of studies have identified an association between MMP activity and TB (85, 105-117).

Many pulmonary cell types are found to secrete disproportionately elevated levels of MMPs, especially MMP-1, in response to TB infection (109, 110, 114, 116, 117). This explains why increased MMP-1 expression and activity is present in humans with active TB (105, 107, 109). The data strongly

indicate that MMP-1 has a central role in the cavity process in TB. Elkington *et al.* have suggested that MMP-1 expression is the most important mediator of tissue destruction, and that therapeutic targeting, with the collagenase specific inhibitor Cipemastat (which has passed phase II safety trials in man), may be beneficial to TB patients (84, 107, 109, 118). One caveat of this suggestion is the unpredictably of outcomes when inhibiting MMPs (119). MMP inhibitory therapy is fraught with complicated risks arising from disruption of proteolytic networks (120), or unexpected functions of MMPs in modulating host immune responses, either through direct function, or through modification of immune signalling, or effector molecules (119). Early MMP inhibitors also had off-target effects, which accounted for some unwanted side-effects (121-124). Interestingly, there is no identified risk associated with specifically targeting MMP-1 (119).

Currently there is only an association between collagenase activity and cavity formation, and a causative link between MMP-1 and cavity formation has not been established. Such a causative link would require trial of collagenase inhibitors in humans. Given the potential risk of such therapies, preclinical efficacy and safety trials are required. Such trials require relevant animal models of TB. However, human-like TB models, especially models of cavity formation, are challenging to use and poorly understood.

1.5. Animal models of destructive pulmonary TB

'All models are wrong, but some are useful' *G.E.P. Box* (125)

The only requirements for a model is that;

(i) The outcomes of experiments in the model can be used to accurately predict outcomes in the system they model, (ii) it can be manipulated and monitored in a manner with measureable outcomes, and (iii) it is accessible to a diverse research community.

What must be remembered in clinical medicine is that each attempt at treatment is an experiment; the variables in the biological system (i.e. the unique biology of the patient, stage of disease, the skill of the caregiver) are impossible to control. Each experiment results in either net benefit, or net harm or equivalence. If an intervention leads to reproducibly beneficial outcomes, the intervention may be broadly applicable – however, the broader the variation in subject, the less likely outcomes will correlate between patients. This concept fundamentally underpins all clinical trials.

Animal models can allow us to perform experiments which may be of unacceptable risk on an individual scale, and if interpreted correctly, with an understanding of their limitations, can allow for the first experiment on a person to be a low risk to benefit event. Animal models can also allow for investigations that are not achievable in humans, for example observations in closely matched post-mortem tissues. It must be remembered that without direct correlation to human disease, these observations are limited to being characterisations of the model, until such point as the observations are shown to relate directly to human disease.

1.5.1. Animal models of TB

Animal models of TB have a long and controversial history. Current animal models of TB show a variety of relationships to human disease, the full discussion of which is beyond the scope of this thesis. The following paragraphs focus on how well animal models of TB represent destructive TB pathology and ECM degradation.

1.5.2. Mice; bacterial growth in the absence of human-like pathology

Mice are the most commonly used animal for investigating *M. tb* infection. They are mainly used for investigating the potential efficacy of novel antibiotic regimens, as they can provide preliminary information on bioavailability, toxicity and bacterial growth (126-129), but do not show destructive pulmonary pathology. The mouse orthologs to MMP-1 (McolA and McolB) have very poor collagenolytic capacity (130). A mouse which expresses human MMP-1 in macrophages is available (131), but since *in vitro* studies suggest that fibroblasts and epithelial cells may be the most abundant source of MMP-1 (110, 117), this mouse may not fully replicate the potential role for MMP-1 in TB pathology. When infected with *M. tb*, these mice do show increased collagen destruction, but not cavity formation (109). Recently, the C3HeB/FeJ or 'Kramnik' mouse model has been used because it develops granuloma-like lesions with necrosis (127, 132-138), it is claimed that cavity formation has been observed (138), but this is exceedingly rare. Since neither human-like tissue destruction, nor MMP-1 expression, is observed mice, they are a poor candidate for investigations into the tissue destructive role of MMP-1.

1.5.3. Zebrafish; powerful tools in the absence of pulmonary tissue

The zebrafish infected with *M. marinum* has been used as a model of granuloma formation. After infection, macrophage aggregation is followed by formation of a lymphocytic cuff. Eventually caseation of the granuloma may occur (111, 139, 140). This model is particularly useful because the embryos are transparent and can be subjected to genetic knockdown (morpholinos). This means that the model can be used to simultaneously monitor bacterial infection and cellular responses at the initiation of infection, on an array of genetic backgrounds (111, 141-143). It is yet to be proven whether the dynamics of the granuloma in this model accurately replicate the events that occur in human TB. Mortality in this model is rapid (less than 100 days), and there is failure to contain infection (140, 144, 145). Extensive tissue destruction is not seen in this model (140).

1.5.4. Guinea pigs; granuloma-like lesions but high susceptibility to infection

The next most commonly used model is the guinea pig. Guinea pigs are highly susceptible to *M. tb* infection and develop progressive disease after infection with as few as 10 colony-forming units (CFU) (146). Guinea pigs develop a granulomatous response to TB that is continuously progressive and eventually forms central necrosis. Cavities and human-like tissue destruction are not observed in guinea pigs (146).

1.5.5. Non-human primates; human-like disease but in a challenging system

The cynomologous macaque model of TB is perhaps most representative of human disease. Multiple different lesion types are produced and a spectrum of outcomes, from primary progressive disease to disease resolution, are seen (147). This model is extremely useful for studying the varying outcomes of infection (148-150), but this variability makes the model challenging to use when assessing the benefits of therapeutic interventions (151). The animals are expensive to purchase and house, and difficult to handle. Rhesus macaques are more susceptible to infection and develop progressive disease after aerosol infection (152).

1.5.6. Rabbits; human-like disease in a 'small animal'

Rabbits also demonstrate a full spectrum of human-like responses to *M. tb* infection (75). Depending on the virulence and dose of the infecting organism, granulomas, necrosis and tissue destruction are observed (153-155). Commonly used out-bread New Zealand White rabbits are considered relatively resistant to active disease (75). When infected with less than 500 CFU of *M. tb H37Rv* and *CDC1551* these animals usually contain infection, and can be expected to have no countable bacteria after 3 months (155, 156).

1.5.6.1. Rabbits and cavitary pulmonary disease

The rabbit has been utilised specifically for studying cavity formation on a number of occasions. The first documented experiments took place in the 1950s, when Yamamura *et al.* described that pre-sensitisation of the rabbit by repeated subcutaneous administration of a mycobacterial extract in mineral oil and lung tissue, followed by inoculation of *M. tb* transthoracically (also in mineral oil and lung tissue) led to the reliable development of cavities (157-161). For a considerable period after

these studies, cavity formation was not specifically studied. Cavity formation was observed in a number of studies by Lurie and Dannenberg where lengthy and sustained Mycobacterial infections were achieved by inoculating either *M. tb* resistant rabbits with *M. bovis* or an inbred strain of susceptible rabbits with *M. tb* (74, 75). Subsequently, it was documented by Converse *et al.* that *M. tb H37Rv* (a virulent human isolate) infection can lead to cavity formation in resistant rabbits, but only after very high infectious doses (162). More recently, Subbian *et al.* and Via *et al.* described that high-dose aerosol delivery of *M. tb HN878*, (a virulent human isolate of the Beijing lineage), leads to progressive disease with occasional cavity development (155, 163-166). Some gene expression data from HN878 infected rabbits was published by Subbian *et al.* and suggests that TB pathogenesis in this model was associated with MMP-1 expression, but associations with cavity formation were not investigated (167).

1.5.6.2. Pre-sensitisation in rabbits, a reliable method to develop cavitary disease?

The most reproducible description of tissue destruction in TB comes from *Nedeltchev et al*. (168, 169) who modified the method of Yamamura *et al.* (157-161) to develop a reliable cavity model. Nedeltchev *et al.* performed bronchoscopic instillation of virulent *M. tb H37Rv and CDC1551 and M. bovis AF2122/97* and *ravenel* after a pre-sensitising regimen consisting of repeated injection of heat-killed *M. bovis* in incomplete Freund's adjuvant (168, 169). Unlike Yamamura, Nedeltchev did not inoculate bacteria in mineral oil and lung homogenate, and did not use transthoracic injection. Nedeltchev *et al.* observed cavity formation in all animals when sacrificed between 50 to 105 days (7 to 15 weeks) post-infection. The apparent reproducibility of cavities marked a major breakthrough in investigating this process, however, the model still resulted in diverse pathologies, and the process of cavity formation was not characterised. Because of the inconsistency in outcomes in this model, it could not readily be used for the preclinical assessment of therapeutics.

1.5.6.3. The challenge of working in rabbit models

Immunological investigations in rabbits are extremely challenging. Antibodies against even the most basic immune components are rare, and so the classic tools for the immunologist such as Flow Cytometry and ELISAs (enzyme-linked immunosorbent assays) are not readily available to rabbit researchers. Since rabbits are only distantly related to humans and mice, for which the majority of reagents are available, the level of cross-reactivity of antibodies is limited, and rarely, if ever, validated. This problem is confounded by the fact that rabbits are the primary source of commercial antibodies, which almost guarantees a lack of cross-reactivity with rabbit proteins. In addition to this, very few members of the scientific community are experienced in handling such animals and so individuals must be trained and gain experience with the animals prior to conducting, often lengthy, studies.

1.5.6.4. Rabbit models have a promising future in the '–omics era'

Despite these problems, the rabbit is an excellent TB model in a number of ways; primarily because it accurately recapitulates many human pathologies (74, 75, 155). It is clear that much could be learned from this model, and with the growing availability of antibody-free technologies for evaluating protein, lipid and carbohydrate components (in particular mass-spectrometry based platforms), and the availability of genomic databases against which RNA profiles can be matched, the paucity of immunologic reagents is becoming less of a hindrance. The development of methods for assessing tissues in these animals is essential. Since rabbits are large, comparisons can easily be made between matched tissues from the same animal. The relative ease with which biological fluids can be sampled, and high quality *in vivo* imaging can be performed, means that longitudinal assessment of disease progression can be correlated with peripheral biomarkers in individual animals (165, 170).

1.5.6.5. Summary: A reliable, well-characterised model of cavitary disease is within sight

There is no reliable, well-characterised model of pulmonary tissue destruction in response to *M. tb* infection. The Nedeltchev model is the most reliable model of tissue destruction, but correlates with

human disease have not been investigated, and the process of cavity development is poorly characterised. The aim of the work presented in this thesis was to improve both the model, and analytical methods, to a point where rabbits can be used for relevant preclinical trials of novel TB therapeutics.

1.6. Summary

TB kills more people now than at any point in history, despite the relatively wide availability of simple diagnostics and antibiotic therapy (1). We desperately need improved preventative, diagnostic and treatment measures. The uniquely destructive pathology of active TB contributes to disease progression, transmission and treatment failure (71, 84, 85, 87, 118, 171), and may therefore be therapeutically targetable. Tissue destruction is characterised by necrosis and ECM destruction. Of these two components, ECM destruction is the least well characterised and is more extensive and consistent in TB than other pulmonary diseases (88). The collagenase, MMP-1, is highly implicated in this process (99, 105, 107, 109, 110, 112-114, 116, 117). Our limited knowledge of tissue destruction is hindered by the absence of animal models of this process, although a recently developed rabbit model of cavitary disease may be useful in understanding the importance of tissue destruction in TB, as well as its molecular pathogenesis (168, 169).

This thesis describes how, using Nedeltchev's model as a basis, a novel rabbit model of tissue destruction was developed. It describes how novel technologies, especially quantification of computed tomography (CT), can be used to monitor disease in rabbits. There is an emphasis on simple and safe technologies, with translation to any facility in which animals can be bio-safety level 3 (BSL-3) contained. Finally, having generated a reliable, accessible model of human-like tissue destruction, the thesis focuses on characterising correlates to human disease, with a specific focus on molecular mechanisms of tissue destruction. The implications for these discoveries, and utility of this model, are discussed at the end of the thesis.

1.7. Hypothesis

MMP-1 has a fundamental role in TB tissue destruction.

1.8. Aims

1. Develop and characterise a rabbit model of destructive pulmonary TB. Establish protocols for investigating therapeutic regimens in this model.
2. Investigate the role of MMPs in tissue destruction in the rabbit model.
3. Investigate whether MMP-1 inhibition alters pathology in TB.

2. Materials and Methods

2.1. Materials

All reagents were purchased from Sigma-Aldrich (www.sigmaaldrich.com) unless specified. Cell culture materials were purchased from Invitrogen (www.invitrogen.com). Ro32-3555 (Cipemastat) was purchased from Tocris. Reagents were made up according to solubility information provided by manufacturers. Where possible water was used, however, DMSO was used when substances were not soluble in water.

2.2. *In vitro* experimental methods

2.2.1. Mycobacterial culture

Mycobacterium tuberculosis H37Rv and *CDC1551* (purchased from ATCC, VA, USA) was preserved as 50% glycerol frozen stocks, it was cultured for use in Middlebrook 7H9 medium (BD, Sparks, MD, USA), supplemented with 10% OADC (oleic acid, albumin, dextrose, catalase) enrichment medium, 0.5% glycerol, 0.02% Tween 80 and rotated at 200RPM (revolutions per minute) at 37°C. This was subcultured at least once with an optical density (OD) of less than 1 (measured at 600nm, by BioWave density meter, WPA, Cambridge). Midlog growth phase density cultures were used with the estimation that an OD of 1 was equivalent to $1x10^8$ CFU. CFU was measured by plating on selective 7H11 plates (BD, Sparks, MD, USA).

Mycobacterium bovis ravenel (purchased from ATCC, VA, USA) was cultured in Middlebrook 7H9 medium supplemented as above with the exception that 4.16g/l sodium pyruvate was utilised in addition to glycerol. No other strain of *M. bovis* was used.

2.2.2. TB Sup production

M. tb culture at OD 0.6 was spun down at 13000RPM for 5 minutes and the supernatant filtered through a 0.22µM Durapore (Millipore) filter. Aliquots were made and stored at -20°C.

2.2.3. UV killed *M. tuberculosis*

1ml of logarithmically growing *M. tb* was placed into a sterile 60mm petri dish, which was then sealed using parafilm. The dish is then rotated to ensure even coverage of bacteria on plate. The petri dish is then placed in a ziplock bag and irradiated for 90 minutes on a UV transilluminator (wavelength 365nm, UVP, Upland, CA, USA). This is then stored at -20°C. Effectiveness of UV killing is confirmed by culture on Middlebrook 7H11 agar supplemented with OADC enrichment medium and 0.5% glycerol. 100µl of original culture was plated as a positive control.

In figure 85, UVTB and wUVTB are used. These were made by centrifuging UV killed TB, as described above, and removing the supernatant. The cells were then washed 3x in PBS prior to resuspension in either the original supernatant (UVTB) or in the Middlebrook 7H9 (wUVTB).

2.2.4. Macrophage culture

Monocytes were isolated from donor leukocyte cones (National Blood Transfusion Service). The entire content of the leukocyte cone was mixed 50:50 with HBSS. 35mls of this mixture was then pipetted into a 50ml conical falcon tube containing 15mls Ficoll Paque (Amersham Biosciences, UK). Centrifugation at 480 RCF (relative centrifugal force) for 30 minutes followed. The serum was discarded and the monocyte layer removed into a new falcons. The cells were then washed 5 times by resuspension in 50mls HBSS then centrifugation for 5 minutes at 308 RCF. This technique yields monocyte purity over 95%, with less than 5% cells CD3 positive (our group, unpublished observations). Total monocyte concentration was calculated by incubation for 5 minutes at 37°C on a haemocytometer, then visual counting of adherent cells. Monocytes were plated at $2.5x10^5$ cells per cm^2 in 24 well plates. Adherence took place during a 1 hour incubation in supplement free RPMI. Non-adherent cells were removed after this time by washing with HBSS. Monocytes were matured into macrophages over 4 days in RPMI containing 20ng/ml macrophage colony stimulating factor (M-CSF, R&D, Abbingdon, UK) and 10% FCS (foetal calf serum). Cells were then rested for 24 hours in RPMI + 10% FCS, without M-CSF prior to starting experiments.

2.2.5. *In vitro* macrophage experimental protocol

After maturation, macrophages were either stimulated with TB Sup, UVTB, or wUVTB. They were then left for 72 hours prior to harvesting of supernatants, which were stored at -20°C.

When live infection took place, *M. tb H37Rv* OD was utilised to assess CFU/ml and ensure that a multiplicity of infection (MOI) of 1 was achieved. After 2 hours, the cell culture supernatant was changed to remove non-infecting bacteria. Supernatants were harvested at 72hours and filter sterilised through Durapore 0.22µm spin filters (EMD Millipore Corporation, MA, USA) prior to evaluation of MMP secretion.

Cells were observed by light microscopy during and at the close of each experiment to assess viability. Experiments were not analysed if alterations in cell viability were observed.

2.2.6. Sandwich ELISAs

All ELISAs were completed according to manufactures protocols: MMP-1, MMP-3 and tumour necrosis factor alpha (TNFα) levels in the cell culture supernatants were analysed by ELISA (R&D Systems Duoset ELISA) according to the manufacturer's instructions. All breakdown product assays (CICP; type I C-terminal collagen propeptide, HP; Helical Peptide, PYD; pyridinoline, DPD; deoxypyridinoline) were purchased from Quidel Corp (San Diego, CA, USA). Rabbit MMP-1 ELISA was purchased from USCN (Wuhan, China). Prior to analysis all samples were spun for 5 minutes at >10000 RCF, prior to filtration through 0.22µM Durapore spin filters (EMD Millipore Corporation, MA, USA). 96 well plates were coated with 100µl of 0.8µg/ml capture antibody and left over night. 3 washes, using 300µl of 0.05% tween in PBS (phosphate buffered saline) took place between additions of a new reagent. The plate was then blocked for 1 hour with 1% bovine serum albumin (BSA). 100µl per well of sample and standards were then added, followed by addition of 100µl per well of biotinylated detection antibody. Streptavidin horseradish peroxidise (HRP) was then added prior to the final wash. 100µl of substrate solution was then added and the plate monitored for colour change over a period of 5-30minutes. 50µl per well of 2M H_2SO_4 was added prior to analysis in a 450nm microplate reader.

2.2.7. Luminex (multiplex immunoassay)

MMP-1, -3 and -7 were analysed utilising multiplex immunoassay according to the manufacturer's instructions (R&D systems). Cell culture supernatants were diluted 1:5 prior to incubation on a pre-moistened, 96-well filter plate. The samples were incubated in a 1:1 ratio with primary antibody coated microparticles, then incubated for 2 hours, whilst shaking at 500rpm. The microparticles are then washed by repeated vacuum driven removal of fluid and addition of wash buffer. Secondary biotinylated antibody is added, and the plate is incubated for a further 1 hour with shaking. Incubation for 30 minutes with streptavidin phycoerythrin then took place, then washing and resuspension in wash buffer. Analysis was performed on the Luminex platform (BioPlex 200, BioRad).

2.2.8. Primer design for quantitative real time polymerase chain reaction (qRT-PCR) analysis

Primers were designed using Vector NTI (Life Technologies, Carlsbad, CA, USA). Primers were required to be 18 and 25 bases long, with a melting temperature between 55 and 65°C, GC content from 40-60% and a product length from 80-200bp (base pairs) long.

2.2.9. qRT-PCR analysis of rabbit lung tissue

Rabbit lung samples were cut into 0.3mm (maximum) cubes and placed into RNAlater (Qiagen) using a no touch, RNAse free technique. This was stored at 4°C for up to 1-2 days to allow for penetration, prior to removal and storage at -80°C. RNA (ribonucleic acids) were extracted under BSL-3 conditions using the following method. The RNeasy Fibrous Tissue Mini Kit (Qiagen) was utilised, although the protocol required adaptation in order to produce DNA (deoxyribonucleic acid) free RNA. Less than 30mg of tissue was homogenised in Buffer RLT and 1% β-mercaptoethanol, by 3 cycles of the following: bead-beating with 2mm beads at 250rpm followed by 30 seconds centrifugation at 13000*g*. This is followed 1:59 proteinase K:water treatment at 55°C for 10 minutes. The samples were then subjected to centrifugation at 10000*g* for 3 minutes. The supernatant is removed and added to equal volumes of 100% ethanol. The samples were then passed through an RNEasy mini spin column and cleaned with wash buffer prior to on column DNAse treatment. After 30minutes exposure to DNAse a 2x ethanol wash is performed prior to elution from the column with water. The

sample is then resuspended on a new column and retreated with DNAse, and eluted in water a second time. This re-treatment process successfully yields DNA free RNA of high quality as tested by analysis of the 28s:18s ratio on the Agilent BioAnalyser (Agilent, CA).

RNA concentration in the eluted sample is measured by Nanodrop Spectrophotometry (Nanodrop 2000C ThermoScientific, DE, USA), and the concentration adjusted to 0.5µg/µl. The RNA is then subjected to cDNA conversion utilising the Agilent Superscript cDNA synthesis kit (Agilent, CA) according to the manufacturer's instructions. 10:3:1:6 Superscript II Mastermix: Random Primers: Reverse Transcriptase: 0.5µg/µl RNA mixture were subjected to 25°C for 5 minutes, then 42°C for 15 minutes, and finally 95°C for 5 minutes prior to storage at -20°C. (-80°C if prolonged storage is to follow). A no reverse transcriptase control is also synthesised and subjected to qRT-PCR analysis with primers capable of amplifying genomic DNA sequences, to ensure the absence of genomic DNA from reaction mixtures.

qRT-PCR was carried out using SYBR II (BioRad, CA) and the iQ5 platform according to the manufacturer's instructions. 40 cycles were performed and the raw data exported to excel. This data was then analysed using LinReg software (172) to calculate efficiency, and ct (cycle threshold) values. Excel was utilised to calculate ΔΔct and fold changes.

2.2.10. Gelatin zymography

Rabbit lung samples in PBS were homogenised by bead-beating in a sealed 2ml O-ring tube, with 15 2mm glass beads. Samples were then spun at 10000*g* for 30 seconds, and then re-suspended. Bead beating was repeated until a clump-free homogenate was produced (approximately 5-10x). Samples were then filtered through Durapore spin filters (Millipore, MA). Samples were then mixed with 5x loading buffer (0.25M Tris pH 6.8, 50% glycerol, 5% sodium dodecyl sulphate - SDS, bromophenol blue) and run on an 11% acrylamide gel impregnated with 0.1% gelatin at 180V for approximately 3 ½ hours (buffer 25mM Tris, 190mM glycine, 0.1% SDS). A standard of 2ng recombinant MMP-9 (Oncogene, Nottingham, UK) were loaded on each gel. Once the marker had reached the end of the

gel, the gel was washed in 2.5% Triton-X for 1 hour, then rinsed twice in low salt collagenase buffer (55mM Tris base, 200mM sodium chloride, 5mM calcium chloride, 0.02% Brij, pH 7.6) prior to incubation at 37^{o} for 16 hours in collagenase buffer. Areas of gelatinolytic activity were revealed by a single step stain-destain method using 0.02% Coomassie Blue (Pharmacia, Sweden) in 1:3:6 acetic acid : methanol : water.

2.2.11. Casein Zymography

The samples were processed as above. The same running and loading buffer are used. The gel utilised is the commercially available 12% casein gel (Invitrogen). Samples were run at 180V for approximately 90 minutes (or until the marker reached the end of the gel), in the Invitrogen XCell SureLock MiniCell. All samples were run alongside a recombinant human 10ng MMP-1 standard (CalBiochem #444208).

2.2.12. Whole trancriptome sequencing of rabbit pulmonary tissue

Tissue was dissected under gross observation from cavity wall, contralateral upper lobe of infected lung, and uninfected lungs and stored in RNAlater (Ambion) at 4°C for 24 hours prior to transfer to -80°C. Tissue fragments <30mg were homogenized by bead beating in TRIzol, RNA extraction was achieved by the addition of chloroform, centrifugation and then isolation in ethanol. The ethanol/chloroform mix was then bound to a column (Qiagen) for cleanup. Washing preceded on-column DNAse treatment (Ambion) at 37°C for 15minutes. This was followed by further washing and elution in RNAse free water. 200-500ng of samples were then submitted to the Johns Hopkins Core sequencing facility. The sequencing facility completed the following steps; RNA integrity was tested using the Agilent 2100 Bioanalyzer (Agilent Technologies, Santa Clara, CA), mRNA (messenger RNA) was enriched using the RIBOminus kit according to the manufacturer's instructions (Life technologies, Grand Island, NY). Successful removal of rRNA (ribosomal ribonucleic acid) was verified by another Bioanalyzer assay. Fragmentation of the RNA was performed by chemically as described in Applied Biosystems SOLiD™ Total RNA-Seq Kit protocol (Applied Biosystems, Carlsbad, CA). Fragmented RNA was purified using the Invitrogen RiboMinus Concentration Module (Life

technologies, Grand Island, NY) and the size distribution and yield were assessed by Bioanalyzer using the RNA 6000 pico Chip Kit (Agilent technologies, Santa Clara, CA) and Qubit Fluorometer (Life technologies, Grand Island, NY). Once the concentration was confirmed, construction of the amplified whole transcriptome library was performed as specified in the Applied Biosystems SOLiD™ Total RNA-Seq Kit protocol, which is intrinsically strand-specific. After reverse transcription was complete, each sample was barcoded with a unique 3' primer during the library amplification step. Libraries were run on DNA1000 chip using the Agilent Bioanalyzer to assess size distribution and quality of the amplified library. Quantification of each library was performed by qPCR and equimolar concentrations of each library were pooled together prior to completion of emulsion PCR and sequencing on the AB 5500xl SOLiD sequencer (Applied Biosystems, Carlsbad, CA). Reads were aligned to OryCun 2.0 (http://www.ncbi.nlm.nih.gov/genome/316?project_id=42933) using the Bioscope 1.3 Whole Transcriptome Analysis Pipeline using default settings (Applied Biosystems, Carlsbad, CA). The number of reads mapped to each transcript was calculated using HTSeq-count v0.5.3. The overlap resolution mode was set to "intersection-nonempty" and feature type was set to "exon". (http://www.huber.embl.de/users/anders/HTSeq/doc/install.html#download)

Differential expression between the sample groups was determined using DESeq v1.4.1 (http://genomebiology.com/2010/11/10/R106), using a test based on the negative binomial distribution, modeling both biological and technical variation. *p*-values are adjusted for multiple comparisons using the Benjamini - Hochberg method. Transcripts with adjusted *p*-values less than 0.05 were considered significant.

2.2.13. Histology

Tissues were fixed by immersion in 10% neutral buffered formalin. Processing was completed by Histoserv or the Comparative Pathology Core at Johns Hopkins University. For the final rabbit study analysis was performed by Marlene Orandle at the NIH/NIAID comparative pathology laboratory (figures 31 and 32). Briefly, tissue was embedded in paraffin, sectioned at 4µm and stained with hematoxylin and eosin (H&E) for routine histopathology or with an acid fast stain for bacteria.

Sections were examined by light microscopy using an Olympus BX51 microscope and photomicrographs were taken using an Olympus DP70 camera.

2.2.14. Immunohistochemistry

This was performed by Jin Park and Marc Halushka and images of stained slides were taken to identify specific pathologies (173). Formalin-fixed and paraffin-embedded tissues were de-paraffinized with xylenes and rehydrated. Antigen retrieval was performed at 95°C in citrate buffer (DAKO, Carpinteria, CA) and endogenous peroxidase was blocked with hydrogen peroxide (DAKO) for 10 min. After blocking, tissues were incubated with mouse monoclonal antibodies directed at human cathepsin K (clone 3F9; Abcam, Cambridge, MA, USA) overnight at 4°C. After washing in PBS, HRP-conjugated secondary antibodies were applied for 1 hour at 37°C and the staining was visualized with 3,3-diaminobenzidine (DAKO) for 2 min. Nuclei were counterstained with Mayer's haematoxylin.

2.2.15. PBMC stimulation and TNFα analysis

PBMCs were collected as described below and cells were counted by Countess Automated Cell Counter (Invitrogen). Live/dead cells were stained using 0.4% trypan blue (Invitrogen T10282). PBMC stimulation was carried out in 96-well flat bottom plates (BD). 10^5 live cells were added to each well. Cells were stimulated with PMA (30 ng/mL) (Sigma P8139), PPD (5 TU) (Tubersol NDC 49281-752-22, Lot C3949AA), ESAT-6 /CFP-10 (30 µg/mL) (BEI resources, NR-14868, NR-14869), and a media only control group was also included. Cells were incubated with antigen for 24 hours and then supernatant was collected and filtered with a 0.22µm filter. Single cytokine ELISA were done according to manufacturer protocol (USCN Life Science Inc. E90133Rb for TNFα).

2.3. Animal procedures:

2.3.1. Animals

Female New Zealand white rabbits were used for all animal experiments. Animals were maintained in BSL-3 conditions in accordance with the protocols approved by the Institutional Animal Care and Use Committee (IACUC) at Johns Hopkins University, USA.

2.3.2. Sensitisation

3-3.5kg rabbits (Covance research products/Myrtles rabbitry/Robinsons) were sensitised with 5x0.2ml subcutaneous injections containing varying amounts (as dictated by experiment) of *M. bovis ravenel* at mid-log growth, that had been heat-killed (3 hours at 72°C), and mixed 50:50 with incomplete Freund's adjuvant, to form a water in oil emulsion. 18-25 days after the final injection, skin test reactivity was determined by injection of 0.1ml of old tuberculin (OT) (Synbiotics Corporation, Exdale, CA, USA) or 5IU (international units) purified protein derivative (PPD)(Tubersol) (Sanofi-Aventis, Bridgewater, NJ, USA) and read 48 hours later to assess reactivity. Measurement was performed using callipers to measure two perpendicular dimensions of the raised area in the plane of the skin and a thickness measurement by subtracting skin fold thickness in a matched untreated area of skin to the region the TST. Halving these diameters give the radii *a*, *b* and *c* respectively. Skin test volume was calculated using the volume of an ellipsoid (174):

$$\frac{4}{3}\pi abc$$

2.3.3. Rabbit infection

Rabbits were anaesthetised with intramuscular ketamine (5-10mg/kg) and xylazine (15-25mg/kg), prior to placement of a 4.5mm diameter endotracheal tube. A 3.0mm flexible Pentax FB-8V paediatric bronchoscope (Pentax Medical Company, Montvale, NJ, USA) was guided into the right lower lobe of the lung and a catheter inserted through the instrument port. The inoculums was administered through a catheter composed of a 1ml luer-lock syringe, a 22 gauge luer stub, and 90cm of TE-50 tubing (which allows the catheter tip to be visualised at the end of the bronchoscope's instrument port). Inoculum delivery was directly visualised through the bronchoscope to confirm correct placement.

2.3.4. In vivo sampling

2.3.4.1. Blood collection

Blood was collected from the middle ear artery, when animals were anaesthetised for other studies. Acepromazine (0.2mg) was utilised to cause vasodilatation. A 22 gauge canula (Smiths Medical) was

placed into the artery, and blood collected into 10ml syringes (BD, Sparks, MD, USA). Using a blunt 18G filling needle (BD, Sparks, MD, USA) blood was transferred either to tubes containing no additive (for serum), or lithium heparin (for plasma), (BD, Sparks, MD, USA), or Ficoll/Citrate for the collection of peripheral blood mononuclear cells (PBMCs). Tubes were centrifuged at 1600*g* for 15 minutes (a delay of 2 hours precedes this step if serum is being collected), prior to collection of supernatant. The brake is in the on position except for the processing of PBMCs, which was performed according to the manufacturer's instructions.

2.3.4.2. Urine collection

Urine was collected from the bladders of anaesthetised rabbits by placing firm pressure from the apex of the bladder in the direction of the sacrum. The bladder apex was palpated approximately 10cm above the pubic symphysis. Urine was collected in a receptacle (figure 38).

Lung samples were obtained at necropsy via rapid dissection. This took place after anaesthesia as above by IV (intravenous) administration of an overdose with Euthasol (Virbac Corporation, Fort Worth, TX). Samples of tissue were dissected by macroscopic appearance. Tissue for protein analysis was immediately snap-frozen in liquid nitrogen, RNA later (Ambion) was used for RNA analysis within 15minutes of overdose. Subsequently tissues were taken for histological analysis by fixation in 10% formalin, and placed in PBS for CFU enumeration. The weight of each sample was caculated by addition pre and post weighing sample collection vials.

2.3.5. Rabbit Imaging

Imaging took place under gas anaesthesia. Anaesthesia was induced using ketamine and xylazine as above, prior to transfer onto 1% isofluorane in $3lmin^{-1}$ oxygen delivered to a sealed chamber in which the anaesthetised animal was contained. IV injection of 0.2mCi of ^{18}F-FDG (2-deoxyy-2-(^{18}F)fluoro-D-glucose) via the marginal ear vein preceded transfer to the chamber if positron emission tomography (PET) imaging was utilised. The input and output of the chamber are HEPA (high-efficiency particulate air) filtered in order to contain BSL-3 conditions within the chamber. The chamber is then transferred to BSL-2 conditions where a clinical 8 slice scanner (Neruologica CereTom) is used to generate CT image data. PET scanning is performed using the Philips Mosaic HP

Small Animal PET Imager.

CT and PET scans were manually co registered using AMIRA (Visualization Sciences Group, Burlington, MA, USA). Specific regions of interest (ROIs) where used were selected using a 3 dimensional selection tool of equal size. Whole lung segmentation was completed using AMIRA as described in figure 47. Briefly a contiguous selection of region in density -1024 to -200 HU was isolated using space filling tool originating in the lung field. This was enlarged 3 pixels in all planes. Holes within the segmented region were filled. Next, regions which link non-lung regions to the lung were manually removed – and then a space-filling tool was used to remove the contiguous non-lung regions. Next, a smoothing algorithm was applied to the entire shape. If dilated, the oesophagus was removed with a space-filling tool in the range of -1024 to -800 HU. Finally, the segmented region was eroded by 3 pixels in all directions.

Breath hold scanning is described fully in the text (figure 42). Scanning required the use of a custom-built BSL-3 chamber (figure 41). Briefly, rabbits were intubated and connected via a T-tube to a HEPA filtered circuit through which $3lmin^{-1}$ of oxygen containing 1% isoflurane was delivered. Lung inflation was initiated by closing a valve in the expiratory limb. Pressure was set by immersing a division of the inspiratory limb to the required depth in a column of water. When the predetermined pressure was reached, a valve distal to the pressure trap was closed. The CT scan was acquired at this point. After acquisition both valves were opened to allow normal breathing in the rabbit.

2.3.6. Immunosuppression with dexamethasone

Immunosuppression was performed by giving a subcutaneous 10mg/kg loading-dose of dexamethasone followed by daily maintenance doses of 0.1mg/kg subcutaneously for 28 days (154, 175).

2.3.7. Culture of bacteria from rabbit tissue

Two methods were used to assess bacterial burden in tissue; biopsy sampling and whole lobe homogenisation. When lung was sampled a small piece of representative tissue was placed into a

pre-weighed o-ring tube containing approximately 2mm of glass beads and 800µl of PBS. This was stored for 24 hours at 4°C prior to homogenisation using a bead beater at 250RPM for 30 seconds, then centrifugation for 30 seconds at 13000*g*. This was repeated 3 times. 500µl of homogenised sample was plated on selective 7H11 (BD, Sparks, MD, USA). 1 to 10 serial dilutions were also plated up to 1:100 000 dilutions. CFU were enumerated 28 days after plating. The range of accurate detection was considered to be a CFU from 10 to 300. Where 2 dilutions fell into this range the count in the range from 10 to 100 was utilised for calculating CFU.

To calculate entire lobe CFUs each lobe was first weighed, then, the of specimens for histological and molecular analysis were removed and the remaining lung weighed and placed into a 50ml conical falcon tube containing 20ml of PBS. This was left for 24 hours at 4°C prior to homogenisation using a Polytron homogeniser (Kinematica, Luzern, Switzerland), in a sealed glovebox. The homogenate was then diluted to 40ml and plating proceeded as described above, except dilutions included 1:1 000 000 dilutions for highly affected lobes.

2.4. Statistical Analysis:

All statistical analysis, with the exception of that specifically listed as being performed by the sequencing facility (section 2.2.12.), was conducted using GraphPad Prism 5. Specific tests are including within the figure legends.

3. Investigating Factors That Contribute to Cavity Formation in the Rabbit Model of Tuberculosis

Cavity formation is a distinguishing feature of active TB (9, 10, 39, 60, 69, 71). It is associated with morbidity (176-179), mortality (180-183), transmission (184, 185) and treatment failure (71, 86, 87, 186). It is the site where the highest numbers of bacteria are found in post-mortem specimens (71). Targeting the processes involved in cavity formation may be beneficial in preventing morbidity, death and transmission (84, 85, 118, 171). Further examination of this process and the environment it generates may also allow us to improve the effectiveness of antibiotics, resulting in shorter regimens and preventing the emergence of resistance.

Currently the processes involved in cavity formation are poorly understood, partly because it is challenging to study experimentally. The overall aim of the following studies was to better understand pre-sensitised rabbit models and develop a model suitable for trialing novel therapeutics in the context of cavitary disease. The requirements of the model were:

i) That it recapitulates human cavity formation

ii) It is consistent in phenotype

iii) It can be easily and accurately monitored, and hence be economically viable for use in preclinical trials

The following chapter describes investigations of cavity development, using the Nedeltchev model (168, 169) as a starting point*.

**Readers may wish to read chapter 4 (in particular section 4.7), prior to reading this chapter, especially if they wish to understand, in detail, how the quantitative imaging analysis was performed. The relevant sections of chapter 4 are referenced in the text of this chapter, and could be reviewed, if necessary at the relevant points in this chapter.*

3.1. *M. tuberculosis CDC1551* infection in the pre-sensitised rabbit

Nedeltchev *et al.* noted that infection of pre-sensitised with *M. tb CDC1551, H37Rv* or *M. bovis ravenel* or *AF2122/97* resulted in cavities 7 to 15 weeks later (168). In an attempt to reproduce Nedeltchev's findings, rabbits were sensitised with 5 injections of 10^7 heat-killed *M. bovis ravenel* over 14 days. After 23 days, animals were subjected to tuberculin skin testing (TST), with 0.1ml of old tuberculin (OT). The test was read 48 hours later. After this, the rabbits were transferred to BSL-3 conditions where they were infected with 10^3 CFUs of *M. tb CDC1551* via a catheter passed through the instrument port of a bronchoscope. This strain was used because a transposon mutant library is available on this background (187), and it was hypothesised that this could be used to identify virulence factors required prior to and after cavity formation (188). The bronchoscope was wedged into a third generation airway, and the catheter tip visually introduced into a distal airway. This technique allows for direct visualisation of the delivered inoculum into a fourth generation airway. Animals were sacrificed at 6 and 10 weeks post infection, and gross pathology observations made.

Very few animals formed cavities, and often there was a complete absence of any observable gross pathology (table 1). Any pathology (lesion) was documented. When present, these lesions were small, firm nodules. These findings did not fit with the observations of Nedeltchev *et al.* (168, 169) and suggested that OT-TST positivity does not universally predispose to cavity formation as Nedeltchev described.

Study	Duration of Infection	Rabbit	OT-TST Diameter*	OT-TST Description	Gross Pathology of Lungs at Necropsy
1	6 Weeks	A	9.6	Hard	No lesions
		B	12.0	Hard	Small lesion, right lower lobe
		C	6.9	Soft	No lesions
		D	6.9	Soft	No lesions
		E	5.7	Soft	No lesions
		F	6.5	Soft	No lesions
		G	7.4	Soft	Multiple lesions in right lung, lesions in left lower lobe
		H	6.6	Soft	No lesions
2	6 Weeks	I	n.m.	Hard, large	Small lesions in right and left lower lobes
		J	*n.m.*	*Hard, large*	*Cavity in left lung, small lesions in right lung*
		K	n.m.	Hard, large	Small scattered lesions in left lung
		L	n.m.	Small	Multiple lesions in lower right lung
		M	n.m.	Small	Small lesions throughout lungs
		N	*n.m.*	*Red, Not Raised*	*Large cavity in right lung, small lesions throughout left lung*

Table 1. *M. tuberculosis CDC 1551* infection did not lead to cavity formation within 6 weeks in the majority of rabbits. OT-TST reaction did not predict cavity formation: 14 rabbits were infected with *M. tuberculosis CDC1551*. $10^{2.5}$ CFU were used in study 1, and $10^{3.5}$ CFU were used in study 2. Only 2 rabbits developed cavities and many animals showed no signs of growth pathology at necropsy. *(*Different investigators performed measurements in each experiment and so results are not comparable between studies. n.m.; not measured)*.

Study	Duration of Infection	Rabbit	OT-TST Diameter*	OT-TST Description	Gross Pathology of Lungs at Necropsy
3	10 Weeks	O	22.0	red, hard, thick	Small lesions in right lower lobe
		P	17.9	red, hard	Lesion in right lower lobe
		Q	21.3	red, hard, thick	No lesions
		R	-	no reaction	-
		S	-	no reaction	-
		T	11.8	red, not thick	No lesions
		U	17.9	red, hard, thick	Large lesion in right lower lobe
		V	-	no reaction	-
		W	15.8	red, not thick	Small lesions in both lungs
		X	-	no reaction	-

Table 2. *M. tuberculosis CDC 1551* infection did not lead to cavity formation at 10 weeks in OT-TST positive animals: 4/10 rabbits did not develop OT-TST positivity, these animals were not infected. The 6 OT-TST positive rabbits were infected with $10^{3.5}$ CFU of *M. tuberculosis CDC1551*. No rabbits developed cavities and 2/6 animals showed no signs of gross pathology at necropsy. *(*Different investigators performed measurements in each experiment and so results are not comparable between studies. n.m.; not measured)*.

It was reasoned that the period of infection may have been too brief and so a 10-week experiment was conducted, and only OT-TST positive animals were infected (table 2).

These studies demonstrated that even strongly positive OT-TST reactions did not reliably predispose to cavities at 6 or 10 weeks (table 1 and 2). As a result of these studies it was concluded that sensitisation with five injections $1x10^7$ heat-killed bacilli in incomplete Freund's adjuvant does not universally lead to OT-TST reactivity and that *M. tb CDC1551* does not reliably establish infection in pre-sensitised rabbits. Not all OT-TST positive animals developed observable cavities. It is possible that cavitary disease had occurred and that gross pathological observation was not sufficient to detect it. To address this concern *in vivo* computed tomography (CT) imaging was employed in subsequent experiments.

3.2. Investigating *M. bovis* ravenel infection in OT-TST positive and negative animals

To further investigate the relationship between OT-TST sensitivity and cavity development, three OT-TST positive and three OT-TST negative animals were infected with *M. bovis ravenel* (all animals received sensitisation as in 3.1.), which is known to have high virulence in rabbits (162, 168, 169, 174, 189). It was expected that this higher virulence would correlate with cavity development. Lung disease in the animals was assessed using CT/^{18}F-FDG PET scanning and gross pathology. All animals failed to develop cavities at 7 weeks. Surprisingly, all animals showed disease resolution by *in vivo* imaging (figure 1) and negligible pathology at necropsy (figure 2).

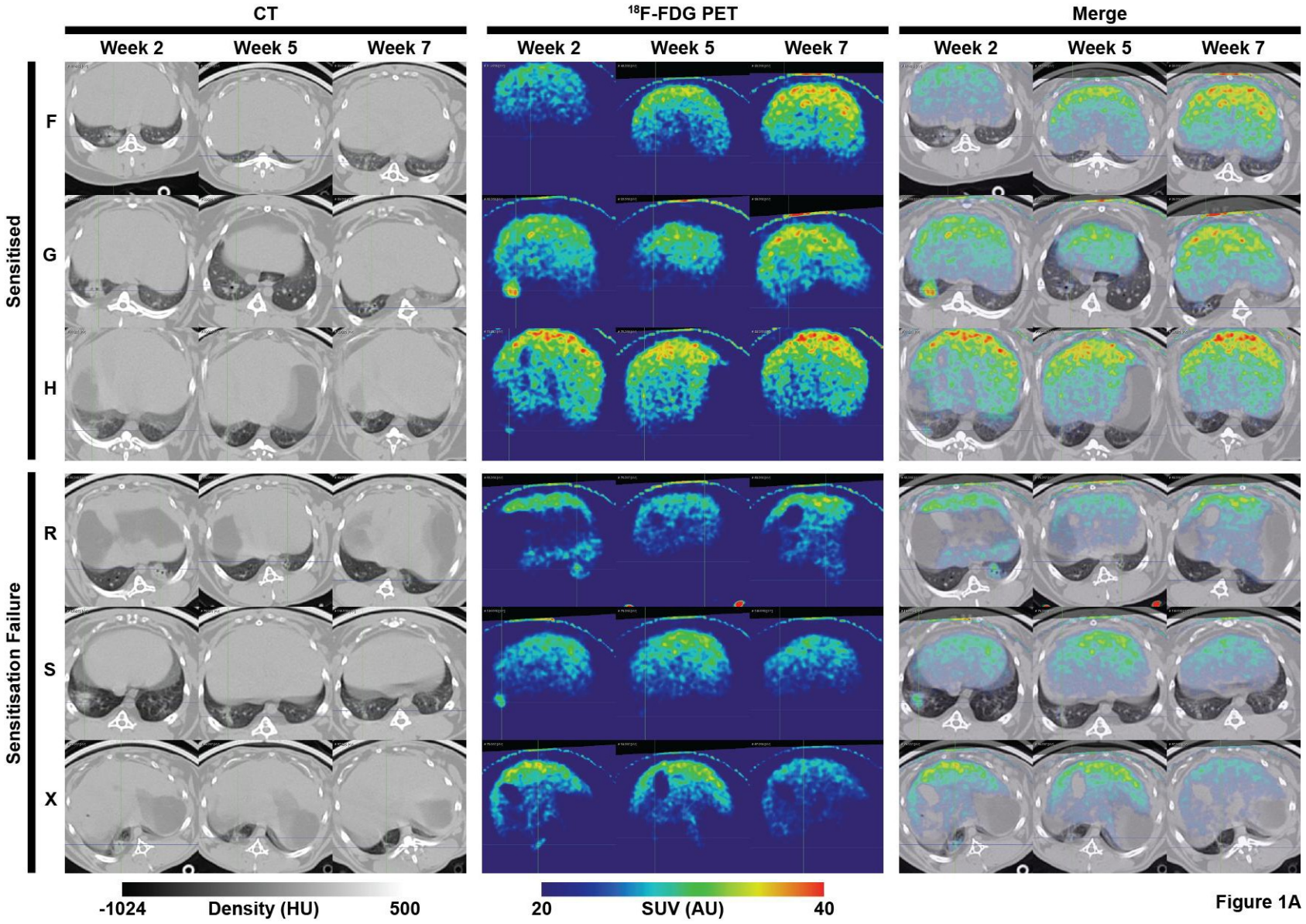
CT
18F-FDG PET
Merge
Week 2
Week 5
Week 7
Sensitised
F
G
H
Sensitisation Failure
R
S
X
-1024
Density (HU)
500
20
SUV (AU)
40

Figure 1A

Figure 1A. Subjective observations from *M. bovis* infected animals with positive and negative OT-TSTs: Qualitatively there appeared to be improvement in CT/^{18}F-FDG PET observations. Opacity and size of CT lesions diminished. ^{18}F-FDG PET uptake also appeared to decrease throughout infection.

Figure 1B. Objective observations from *M. bovis* infected animals with positive and negative OT-TSTs: To quantify the observed imaging changes a matched volume was selected from each scan co-registered CT/^{18}F-FDG PET scan. SUV max and mean decreased significantly with time *(p<0.01)* and CT density changed in similar but more significant manner *(p<0.001). (HU = Hounsfield Units; AU = arbitrary units; SUV = standardised uptake value, ROI = region of interest). Time was the only significantly contributor to variation in each graph in 'B' (p<0.01); there were no other significant contributors to variation and no significant differences between groups (Two-way ANOVA with Bonferroni multiple comparison post test). Linear trend statistics describe how significantly non-zero the change in y-values are over time.*

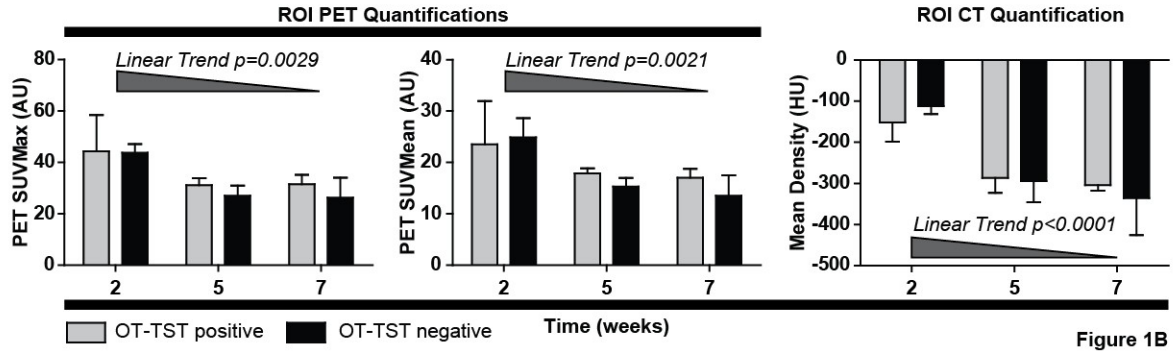

Figure 1B

The failure to develop progressive disease and extensive lesions was unexpected, and could be explained by three hypotheses: (i) The strain being utilised was exhibiting reduced virulence in the model, (ii) the sensitisation process was protecting against disease development or (iii) the experimental infection technique was not reproducible.

To address the third hypothesis, a short study investigating both the strain and method of infection was performed (figure 34). This demonstrated that the infection method was reproducible. To investigate the first hypothesis, an experiment to see whether the sensitising strain was protective against a different laboratory isolate of *M. bovis ravenel* was conducted.

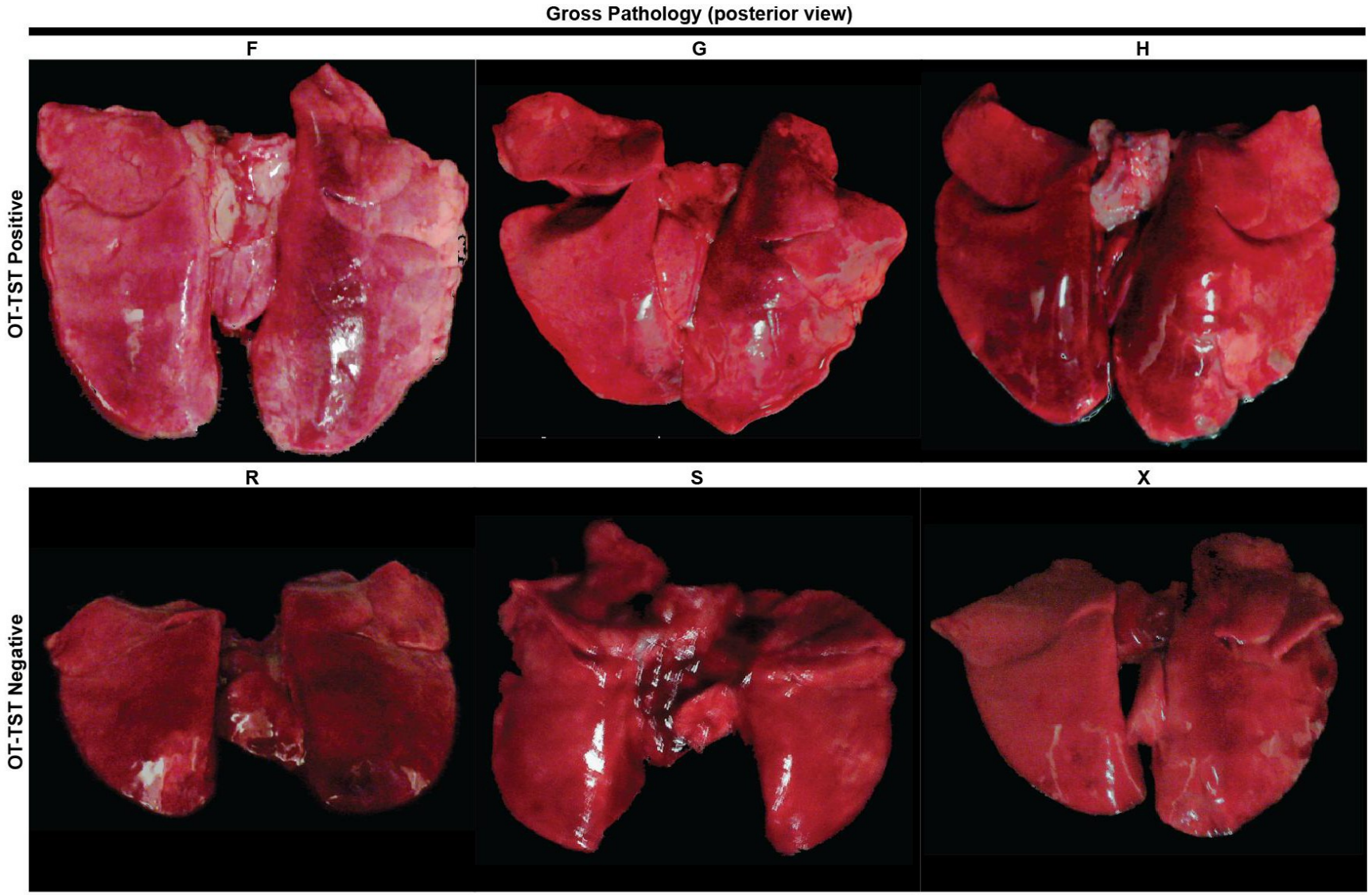

Figure 2. Gross pathology from *M. bovis* infected animals with positive and negative OT-TSTs: No significant pathology was observed 6 weeks after infection. In rabbits H and X, small lesions were observed in the lower right lobes.

3.3. Investigating the strain-specific effect on protection from extensive *M. bovis* disease

A different laboratory *M. bovis ravenel* isolate was cultured from a rabbit with extensive pathology. It was used to infect 6 rabbits sensitised with the *M. bovis ravenel* strain that had failed to show virulence in the previous experiment (section 3.2). If the strain used for sensitisation was protective from disease, containment and resolution of infection would be expected. 6 weeks after infection gross pathology (figures 3 and 4) and bacterial burden (figure 5) were analysed.

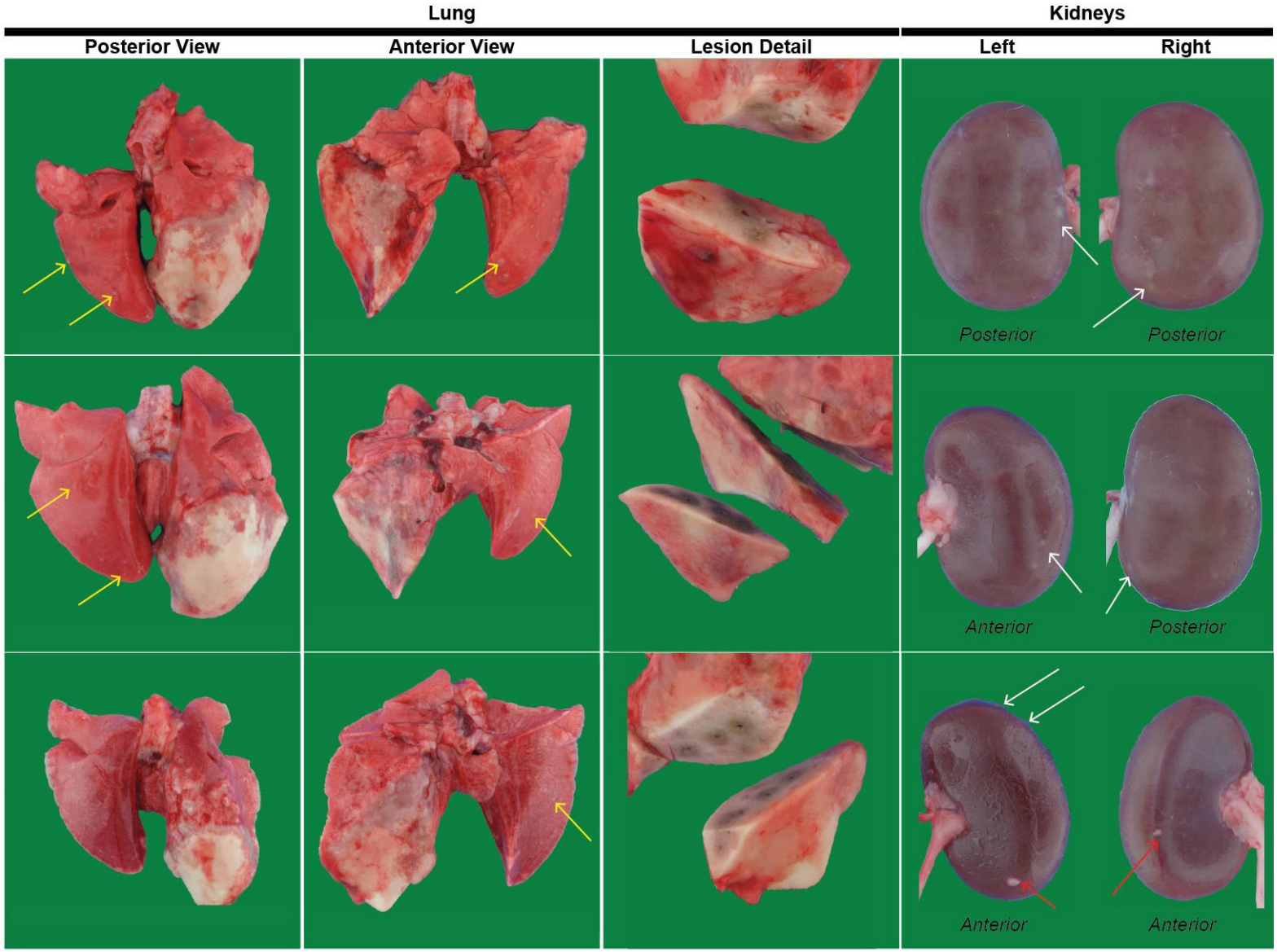
Lung
Kidneys
Posterior View
Anterior View
Lesion Detail
Left
Right
J
K
Q
Posterior
Posterior
Anterior
Posterior
Anterior
Anterior

Figure 3

Figure 3. Gross Pathology of *M. bovis ravenel* infected animals showing relatively contained pulmonary disease: Animals J, K and Q showed localised pathology. Dense infiltrates were observed at the site of infection (lesion detail), the lesions were firm. Very small pearlescent lesions were observed in the contralateral lobes (yellow arrows). Subcapsular renal lesions were observed in all animals (white arrows). *Red arrows indicate residual pericapsular fat, not lesions.*

Figure 4. Gross Pathology of animals infected with *M. bovis ravenel* showing extensive pulmonary disease: Animals N, R and L showed extensive disease throughout both lungs. Dense infiltrative lesions are seen at the site of infection, whereas punctate localised lesions, consistent with granuloma formation and haematogenous spread are seen in adjacent tissue. The lower portion of the left lobe of rabbit N appeared largely normal. In all animals the pathology at the site of infection consisted of multiple small lesions (lesion detail). In rabbit R a miliary pattern of disease was observed in the left lung; with several hundred small lesions located sub-pleurally. In rabbit L extensive infiltrates were seen in both lungs, with only a small portion of the superior lobes appearing to contain grossly normal tissue. No lesions were observed in the kidneys of rabbit L despite the extensive lung pathology, however, the digital file was corrupted and the image lost. Rabbit R had multiple large subcapsular lesions, whereas rabbit N had only a few relatively large subcapsular lesions.

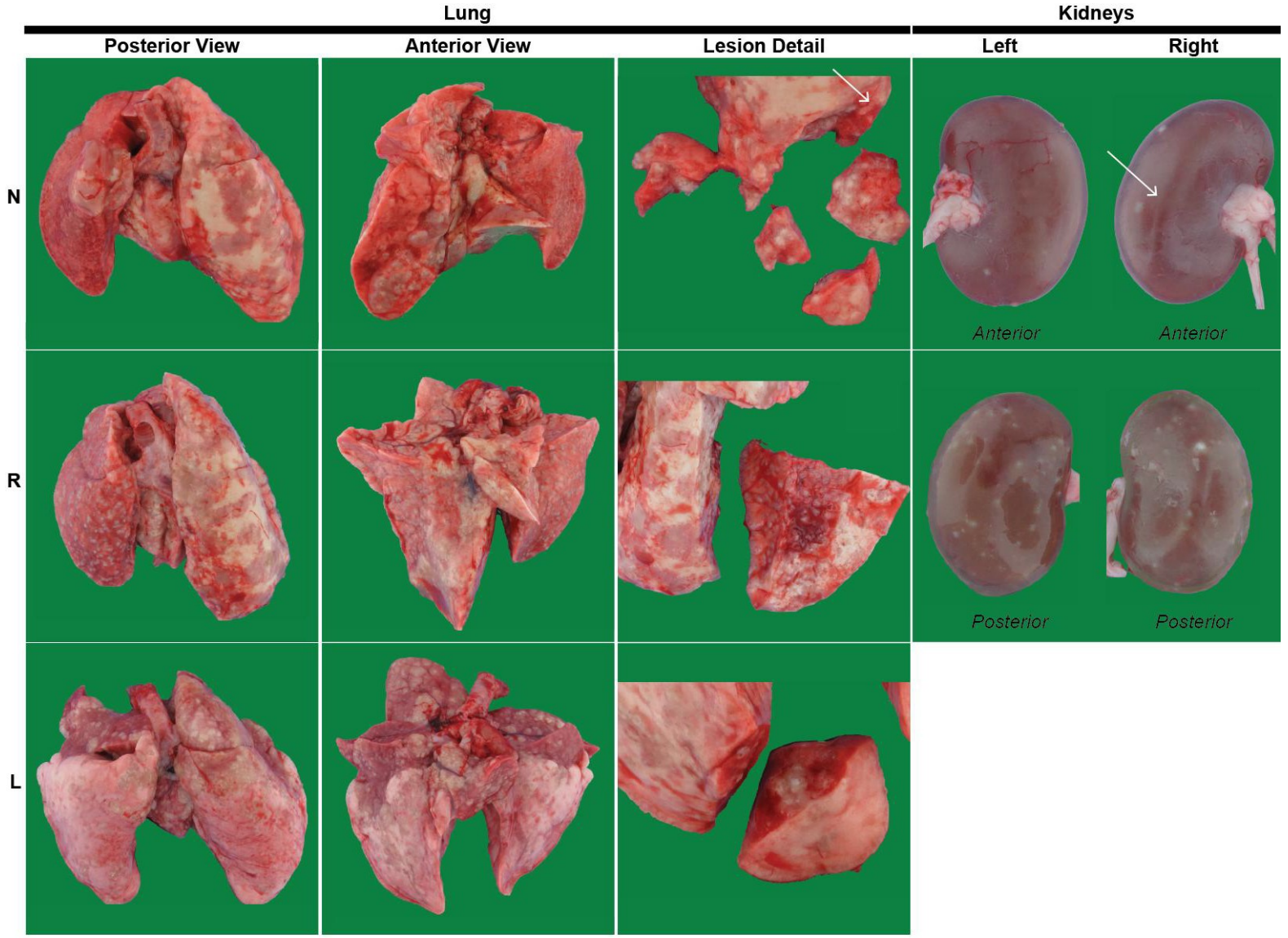
Lung
Kidneys
Posterior View
Anterior View
Lesion Detail
Left
Right
N
R
L
Anterior
Anterior
Posterior
Posterior

Figure 4

All 6 infected animals developed extensive pulmonary disease, far beyond that seen in the previous experiment, despite similar infectious doses (figure 3 and 4). This was in-keeping with the observations that *M. bovis* is highly virulent in rabbits (74, 75, 168, 169, 189). Bacteria were found in all regions of the lung sampled, with a strong concordance between regions of grossly observable pathology and bacterial burden (figure 5D). Interestingly, animal-to-animal bacterial burdens varied significantly, as did the distribution of the bacterial burden within each rabbit (figure 5E).

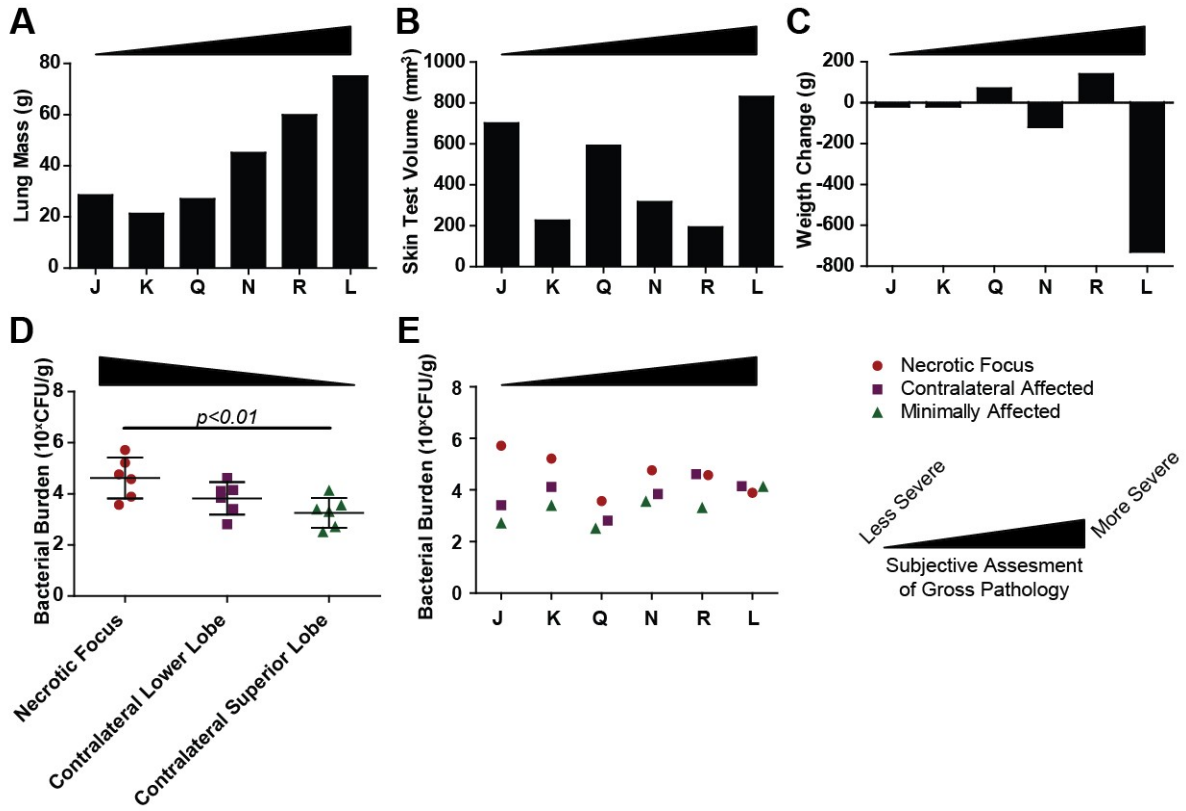

Figure 5. Outcomes in *M. bovis* infected animals were highly variable even after an infection period of only 6 weeks: (A) Lung masses of animals appeared to correlate with subjective assessment of disease pathology *(R square=0.8520, p=0.008, Pearson Correlation)*. **(B)** Degree of OT-TST positivity did not correlate with any observed gross pathological phenotype. **(C)** Excessive weight loss was noted in rabbit L, but the other animals did not have substantial changes in weight from infection. **(D)** Bacterial burden is on average greater in the necrotic region of the lung than in distant tissue *(one-way ANOVA with Tukey post-test)*. **(E)** Samples were taken from the necrotic focus (i.e. where infection took place), and two sites in the contralateral lobe; one without observable pathology (minimally affected) and one with pathology (contralateral affected). The variation in distribution of bacterial was greater in animals that had less extensive gross pathology. Bacteria were cultured in all regions of lung tested.

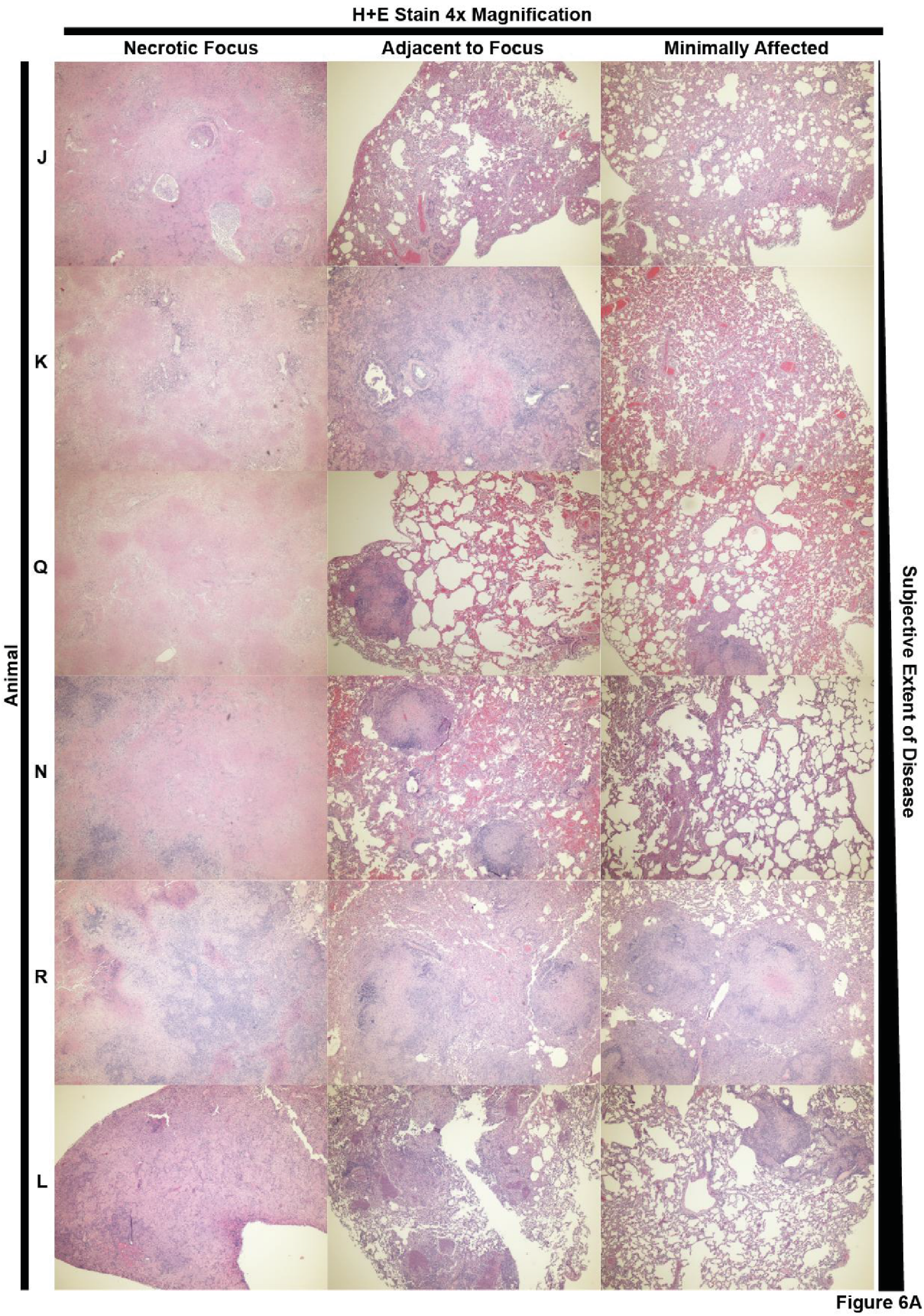
H+E Stain 4x Magnification
Necrotic Focus
Adjacent to Focus
Minimally Affected
Animal
J
K
Q
N
R
L
Subjective Extent of Disease

Figure 6A

Figure 6A. Histopathology of sensitised, *M. bovis* infected rabbits, demonstrating a range of responses to infection: Extensive necrosis is observed at the site of infection in all animals (necrotic focus). This is characterised by total destruction of the tissue architecture with infiltration of mononuclear cells accompanied by varying degrees of lymphocytic infiltration. Adjacent to this, varying degrees of necrosis with occasional granuloma forma- tion (Q,N,R and L) are observed. In minimally affected areas, granulomas are still observed in animals with more extensive gross pathology (R,L).

Figure 6B. Uninfected lung tissue from the right lower lobe showing normal lung architecture: (4x magnification, H+E stain).

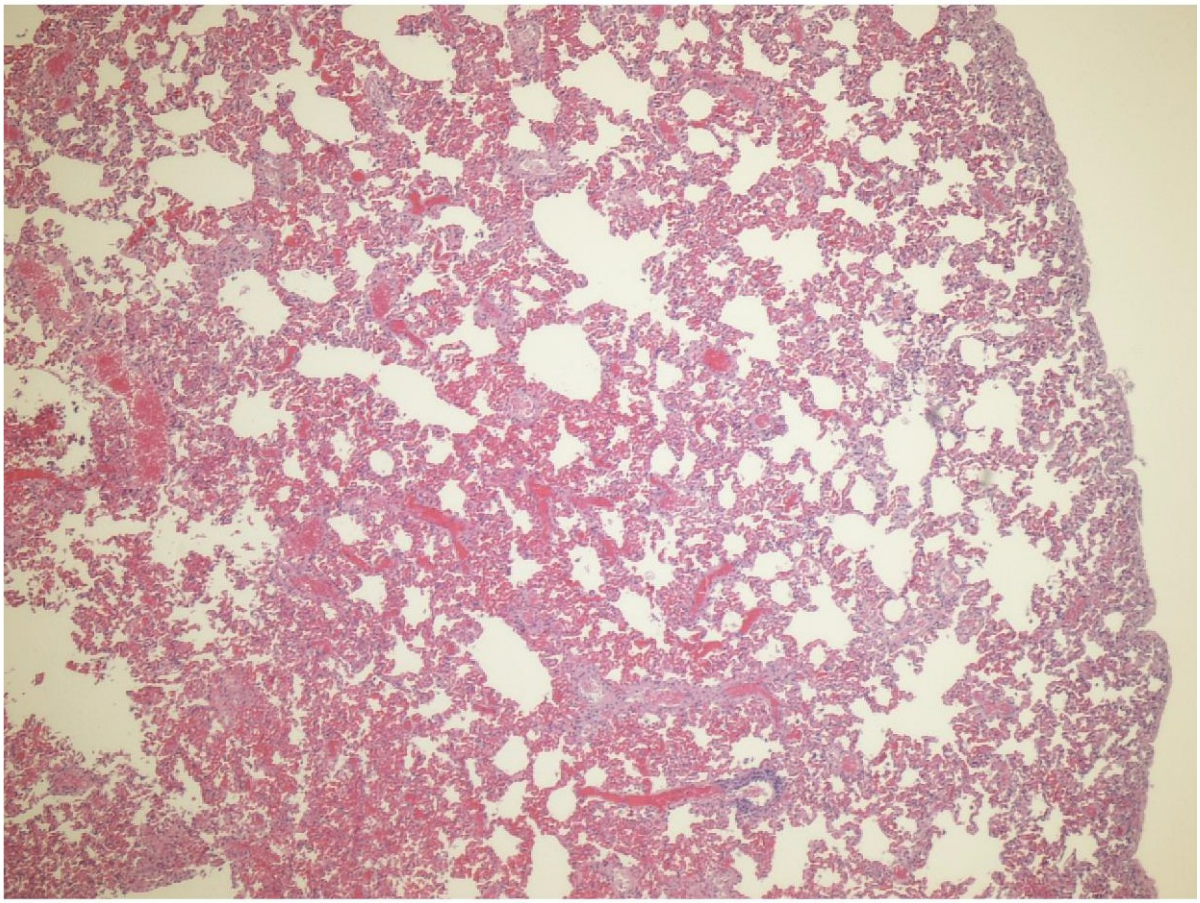

Figure 6B

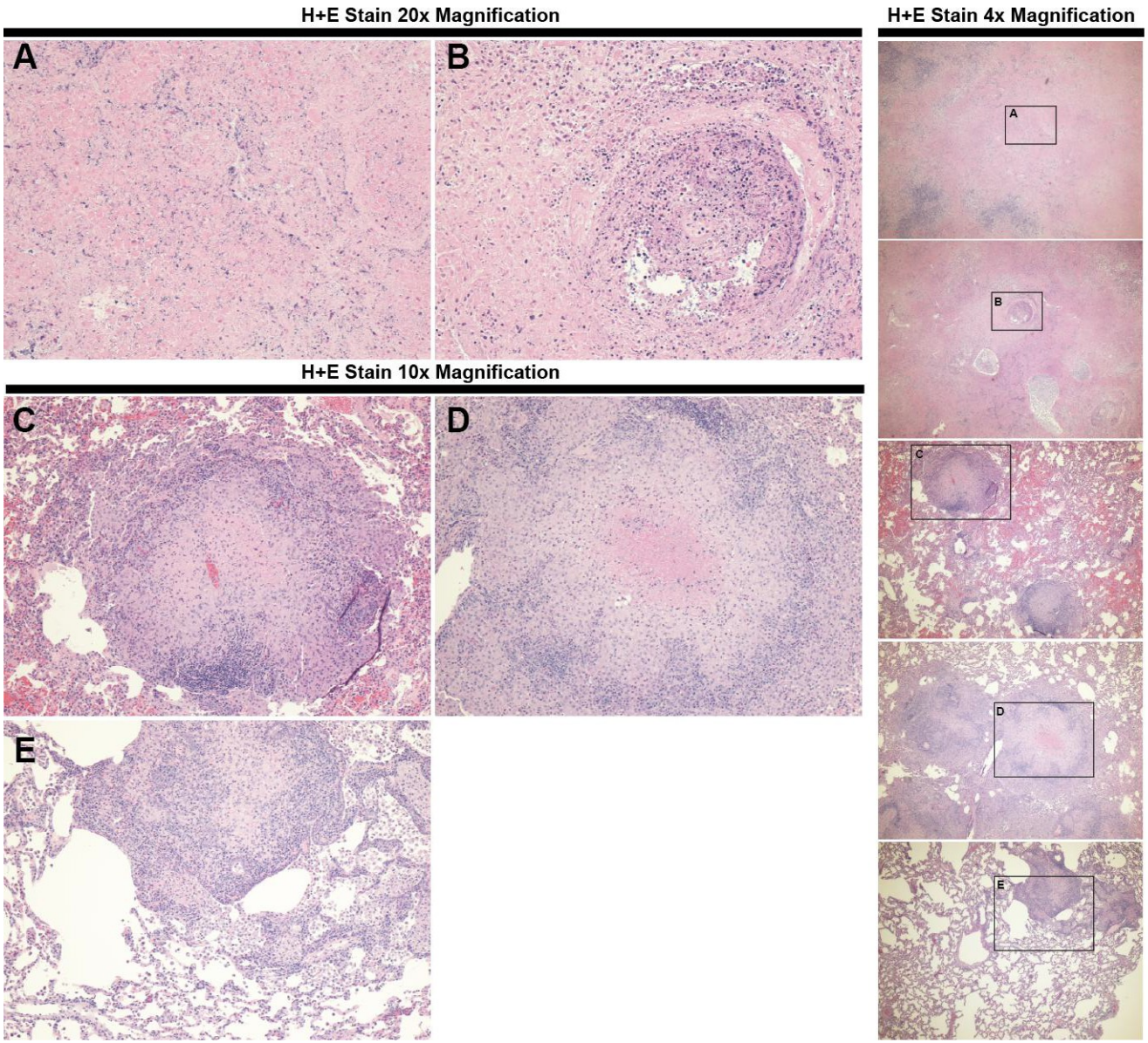

Figure 7. Detailed histopathology of sensitised *M. bovis* infected animals demonstrating a range of responses to infection: (A) The composition of the necrotic region included numerous macrophages, with occasional and varying degrees of lymphocytic infiltration. Normal alveolar structure is obliterated. **(B)** Only animal J exhibited organised lesions within this necrosis. The lesion is granuloma-like in appearance, exhibiting minimal central necrosis, and a fibrous cuff. **(C)** In animals N,R and Q organised lesions were present in the tissue adjacent to necrotic focus; these lesions had a degree of central necrosis as well as a surrounding ring of lymphocytes. Epithelioid macrophages towards the centre. No foam cells were noted and there does not appear to be a fibrotic cuff. **(D,E)** Even in tissue distant from the site of infection organised lesions could be seen. Although normal tissue was more extensive in these regions, lesions were identified in all animals except J.

The presence of extensive pathology and high bacterial burden indicated that the sensitising strain was not protective against infection, and it was concluded that the original isolate used in section 3.2 was avirulent in rabbits.

Interestingly, the *M. bovis ravenel* isolate from infected rabbits, did not cause cavities to from (as identifiable at necropsy). This was despite OT-TST positivity, extensive local necrosis and apparent tissue destruction. This added to the already substantial evidence that OT-TST positivity alone was not sufficient to cause cavitary disease.

3.4. *M. tuberculosis* infection leads to cavity formation more rapidly than *M. bovis* infection

Having established that OT-TST positivity was not sufficient to develop rapid cavities, we proceeded to investigate if the virulent *M. bovis* isolate, when utilised for sensitisation, predisposed rabbits to cavity formation. In addition to this, infection with *M. bovis ravenel* was compared to infection with *M. tb H37Rv*. Skin tests were not conducted, as OT had been removed from the market. All 10 rabbits received 5 injections of $1x10^7$ of heat-killed *M. bovis ravenel*, in incomplete Freund's adjuvant. After 25 days, 5 rabbits were infected with *M. bovis* and 4 with *M. tuberculosis* (1 animal due to be infected with *M. tuberculosis* died during anaesthesia prior to infection). The animals were monitored by CT/^{18}F-FDG PET imaging.

Cavities formed in 75% of animals infected with *M. tb* within 5 weeks (figure 8A). No cavities were observed in any animals infected with *M. bovis* during this time period; cavities were seen in 2 of these 5 animals by 10 weeks. Each group was infected with equal bacterial numbers ($10^{3.95}$ *M. tb H37Rv* and $10^{3.96}$ *M. bovis ravenel* CFU). The time to cavity formation in the *M. tb* infected animals was significantly faster than in *M. bovis* infected rabbits (p=0.025 log-rank Mantel-Cox test). Interestingly, intrapulmonary spread of *M. bovis* led to equal distribution of bacteria throughout the lung by 10 weeks, even though cavities did not form (figure 8B).

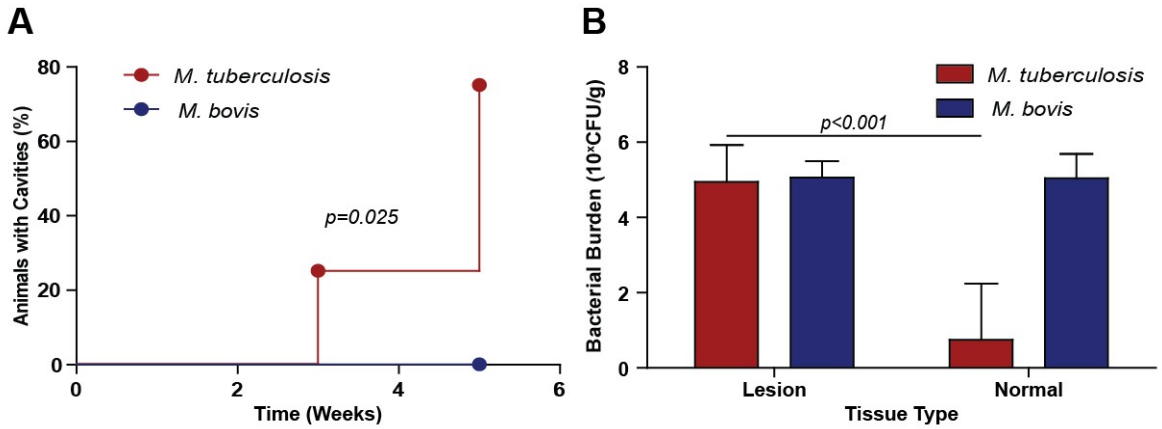

Figure 8. Cavitation occurred more readily in sensitised *M. tuberculosis* infected animals than *M. bovis* infected animals: (A) Time to cavitation curve showing increased rate of cavity formation in *M. tuberculosis* infected rabbits (*p=0.025 Log-Rank, Mantel-Cox Test*). 3/4 *M. tuberculosis* infected rabbits and 0/5 *M. bovis* infected animals developed cavities in the observed 5 week period. **(B)** Bacterial burdens were the same at the site of infection. *M. bovis* was found at equivalent levels in the contralateral lung. *M. tuberculosis* however, was found at significantly lower levels in non-lesion sites. (*one-way ANOVA, Tukey post comparison test*).

Rudimentary quantification of CT changes in matched regions of interest (ROIs) demonstrated that in *M. tb* infected animals the consolidated regions (-50 to +50 Hounsfield units; HU) did not change significantly during infection with *M. tb* (figure 9A and C). This suggested that there was relative containment of disease in the primary region of infection. This was associated with limited dissemination of bacteria to the contralateral lower lobe (figure 8B). In contrast, *M. bovis* infection resulted in continued growth of CT observable regions of consolidation. This increase resulted in significantly greater involvement of the lung by week 5 (figure 9C). The degree of ^{18}F-FDG PET uptake increased dramatically in *M. bovis* infected animals, suggesting a continued, and substantial, inflammatory response, whereas no increase was seen in the *M. tb* infected animals.

Together, these observations suggest that the degree of inflammation and pulmonary infiltrate does not correlate with cavity formation. They also indicate that *M. tb H37Rv* does not drive as extensive an inflammatory response to *M. bovis ravenel*, even thought the response to *M. tb* infection results in cavity formation. Interestingly, the bacillary burden at the site of the infection was very similar between species, suggesting that the local number of bacteria does not dictate the degree of inflammation (as measured by ^{18}F-FDG PET) or cavity formation. Two plausible explanations are: (i)

There is either a dampening of responses to *M. tb* through immune evasion or suppression or (ii) overall, but not local, bacterial burden contribute to local ^{18}F-FDG uptake. Importantly, this study demonstrated that cavity formation in this pre-sensitised model is not simply the result of an overwhelming inflammatory reaction, but a Mycobacterial species-specific process.

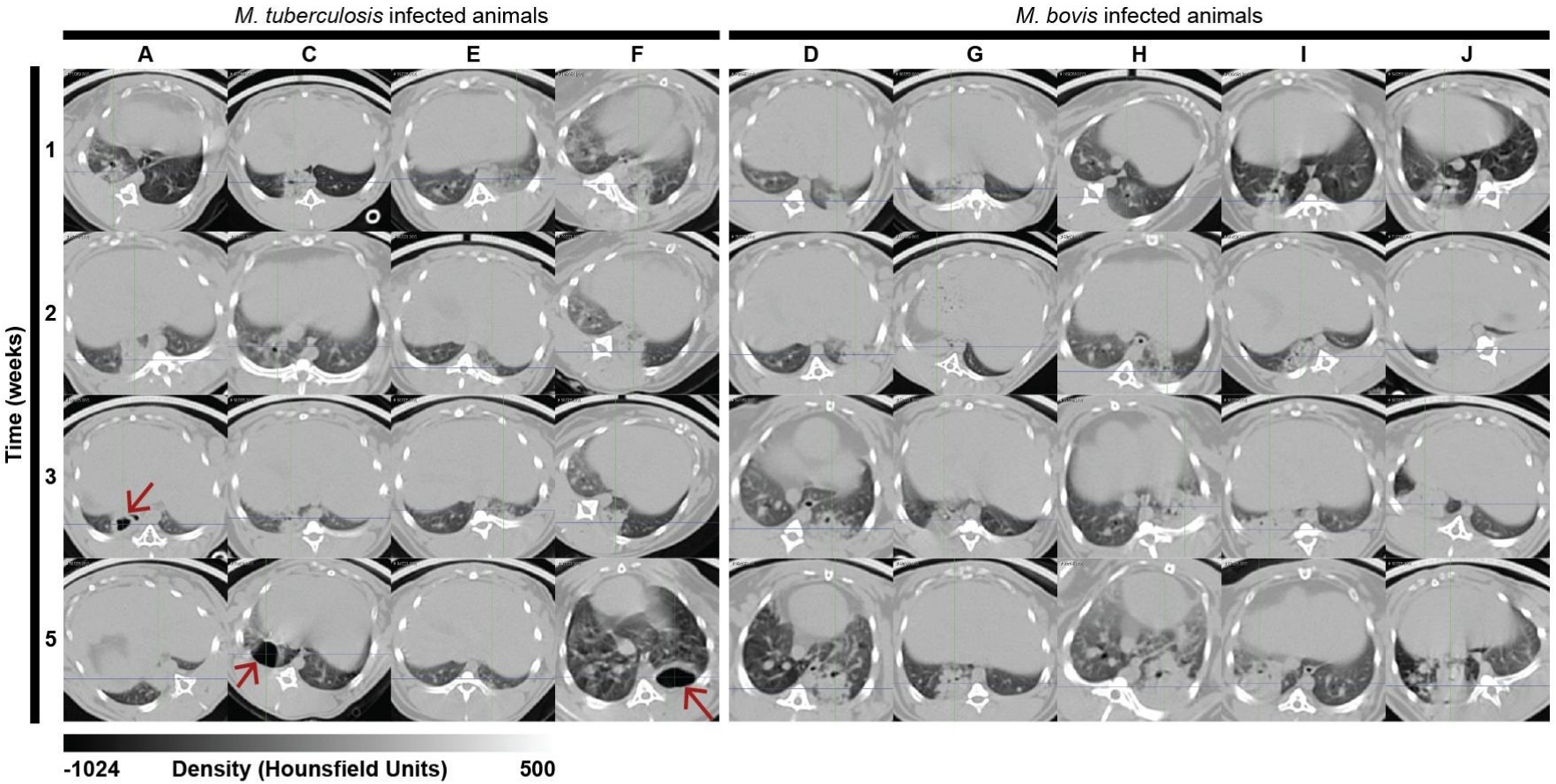

Figure 9A. ***In vivo*** **imaging showed that** ***M. tuberculosis*** **infection resulted in more rapid cavity formation than** ***M. bovis*** **infection, despite lower amounts of inflammatory change:** Transverse CT sections that demonstrating lesion progression in both infections. Cavitation events are marked by red arrows. Progressive extensive consolidation follows infection with *M. bovis* but not with *M. tuberculosis*.

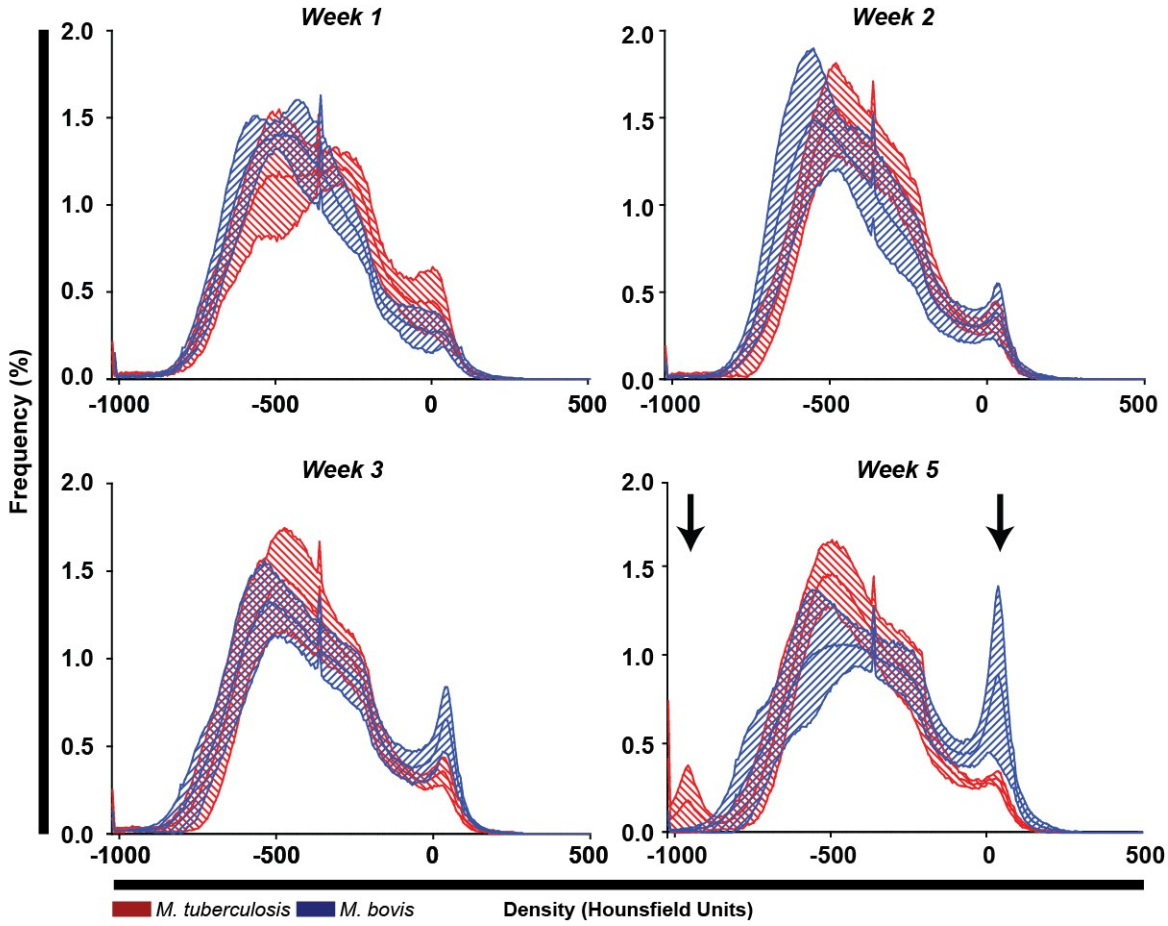

Figure 9B. *In vivo* imaging showed that *M. tuberculosis* infection resulted in more rapid cavity formation than *M. bovis* infection, despite lower amounts of inflammatory change: Histograms representing lung density. The x-axis represents hounsfield units. The y-axis shows the frequency at which this density is observed as a portion of the entire lung volume. Arrows represent regions where divergence occurs between *M. bovis* and *M. tuberculosis* animals. These regions correlate with cavity formation (-1000 to -900 HU) and consolidation (-50 to 50) (black arrows). Area represents standard deviation from the mean for all animals at each timepoint. *(HU; hounsfield units)*.

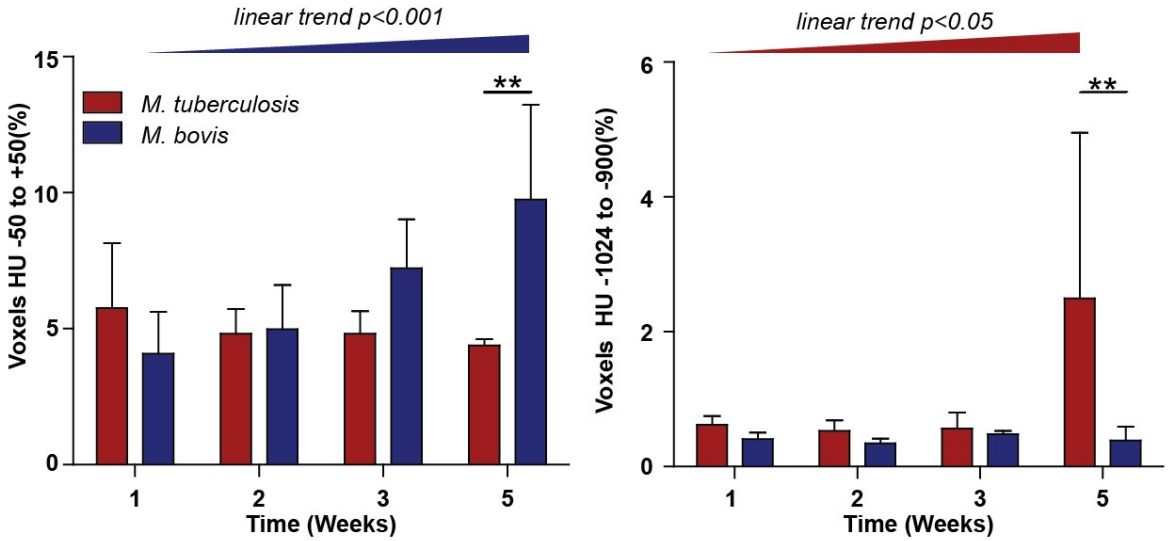

Figure 9C. Quantitative CT analysis reveals greater increases in high density tissue in *M. bovis* infected animals when compared to *M. tuberculosis* infected animals: In animals with *M. bovis* infection, densities that correlates with consolidation in the lung are significantly increased, whereas in *M. tuberculosis* infected animals, densities that correlate with air (i.e. cavities) are increased. *(*p<0.05, **p<0.01, ***p<0.001, ****p<0.0001 by two-way ANOVA with Bonferroni multiple comparisons post-test, linear trend statistics describe how signficantly non-zero the change in y is over time).*

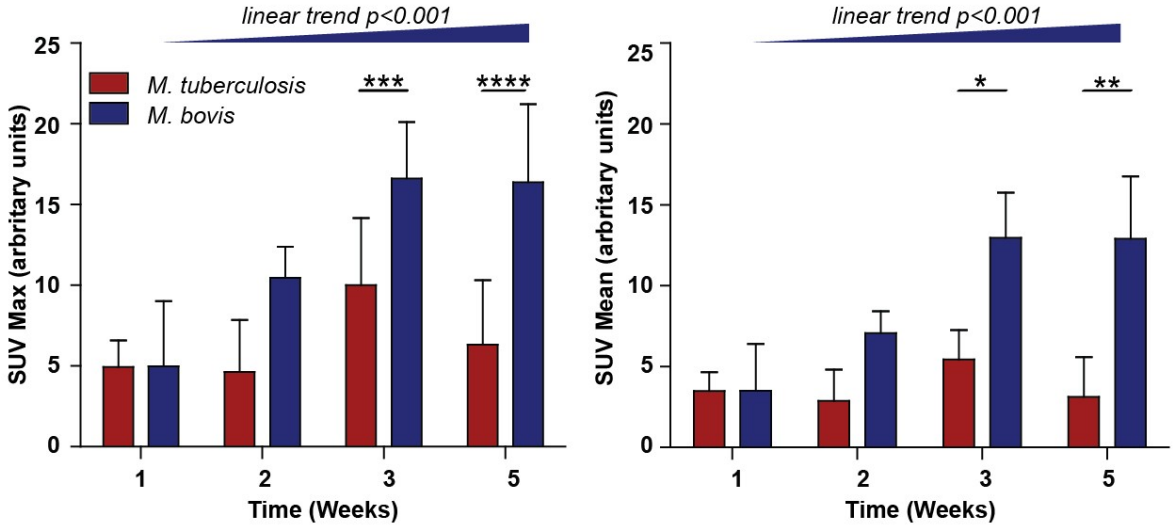

Figure 9D. Quantitative PET analysis demonstrates that inflammation is greater in *M. bovis* infected animals than in *M. tuberculosis* infected animals: ^{18}F-FDG PET uptake is vastly increased as measured by SUVmean and SUV max in *M. bovis* infected animals as compared to *M. tuberculosis* infected animals at week 3 and 5. ^{18}F-FDG uptake continues to increase throughout infection in *M. bovis* infected but not *M. tuberculosis* infected animals. *(*p<0.05, **p<0.01, ***p<0.001, ****p<0.0001 by two-way ANOVA with Bonferroni multiple comparisons post-test, linear trend statistics describe how signficantly non-zero the change in y is over time).*

To further understand the cavity formation and identify potential predictors of cavity formation; a long-term experiment using peripheral biomarkers, TST responses and *in vivo* imaging was conducted. As OT was no longer commercially available we utilised tuberculin purified protein derivative (PPD), which is precipitate of OT (190).

3.5. PPD-TST positivity is the best predictor, if not a requirement, for cavity development in the rabbit model

This study was designed to utilise the variable outcomes experienced in this model to better understand cavity formation with a view to maximising reproducibility in future experiments. The primary aim of this study was to identify peripheral markers of disease progression by intensively monitoring the early stage of infection (figure 70, section 5.6). A secondary aim was to determine the long term outcome of disease in context of immune responsiveness to the mycobacterial antigens in PPD.

10 animals were sensitised utilising the same regimen described previously (5 equally spaced injections of 10^7 heat-killed CFU of *M. bovis ravenel*), and were tested 18 days later using the PPD-TST (figure 10). 5 out of the remaining 9 animals developed positive PPD-TSTs (figure 13A). This suggested that there is either an inherent variability in response to sensitising regimens or in responsiveness to PPD antigens. Animals were infected via bronchoscope with 10^3 CFU of *M. tb H37Rv* (figure 10). The infection procedure failed in one animal – and it was subsequently excluded from the study (the skin test of this animal had been negative).

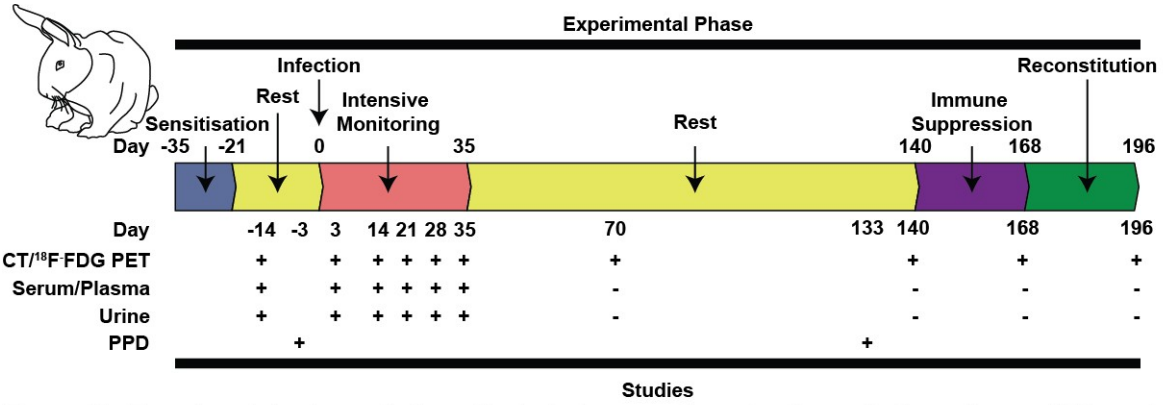

Figure 10. Experimental schema to investigate factors predisposing to cavity formation and biomarkers of cavitation: Sensitisation was achieved by delivering 10^7 heat-killed CFU in 0.2ml of a 1:1 mix of PBS and incomplete Freund's adjuvant. Animals were allowed 21 days for immune responses to develop, after which reactivity was assessed by measuring responses to 0.1ml PPD (5 tuberculin units). During this period preinfection CT/^{18}F-FDG PET scans were completed. Animals were infected with 10^3 CFU of *M. tuberculosis H37Rv*. Blood and urine samples were taken and CT/^{18}F-FDG PET scanning performed on days 3, 14, 21, 28 and 35 post-infection. Animals with extensive cavities were sacrificed and the remaining animals were followed for a further 105 days. At Day 140, the remaining animals were subjected to immune suppression using a loading dose of dexamethasone (10mg/kg) was followed by maintenance doses for 28 days (0.1mg/kg). CT/^{18}F-FDG PET scanning was completed at the initiation of treatment, at the end of treatment and 28 days after treatment was completed. The animals were sacrificed at day 196 and bacterial burdens assessed.

CT/^{18}F-FDG PET scanning demonstrated that all animals had more extensive disease at day 14 than at day 3 (figure 11), suggesting active disease progression. The primary outcomes at day 35 were divided into two types based on imaging findings; cavity forming (5 animals) and non-cavity forming (4 animals). Two cavity subtypes were defined, terminal cavities and non-terminal cavities (figure 11). A terminal cavity was characterised by being large enough that it posed an immediate threat to the well-being of the rabbit, in this case euthanasia was performed (3 animals) so that tissue samples could be collected for further analysis (figure 12). If cavities were small, and deemed not immediately life-threatening (2 animals), animal health was monitored closely, and animals were not euthanised (non-terminal cavities). There was no significant difference in the degree of ^{18}F-FDG uptake between terminal and non-terminal cavities, or between cavity and non-cavity animals prior to cavity formation (figure 13B).

Figure 11A

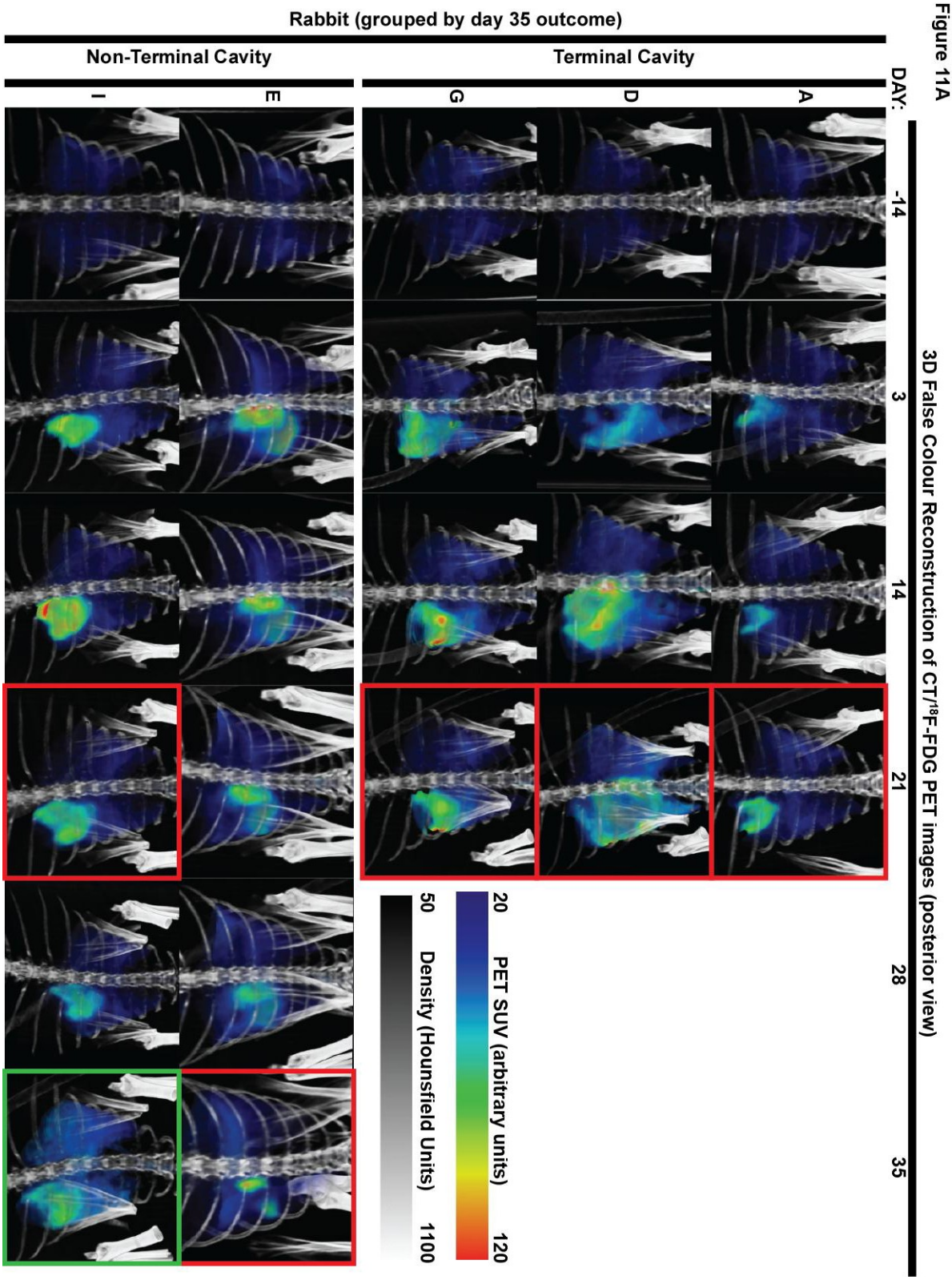
3D False Colour Reconstruction of CT/18F-FDG PET images (posterior view)
DAY:
-14
3
14
21
28
35
Rabbit (grouped by day 35 outcome)
Terminal Cavity
Non-Terminal Cavity
A
D
G
E
I
PET SUV (arbitrary units)
20
120
Density (Hounsfield Units)
50
1100

Figure 11B

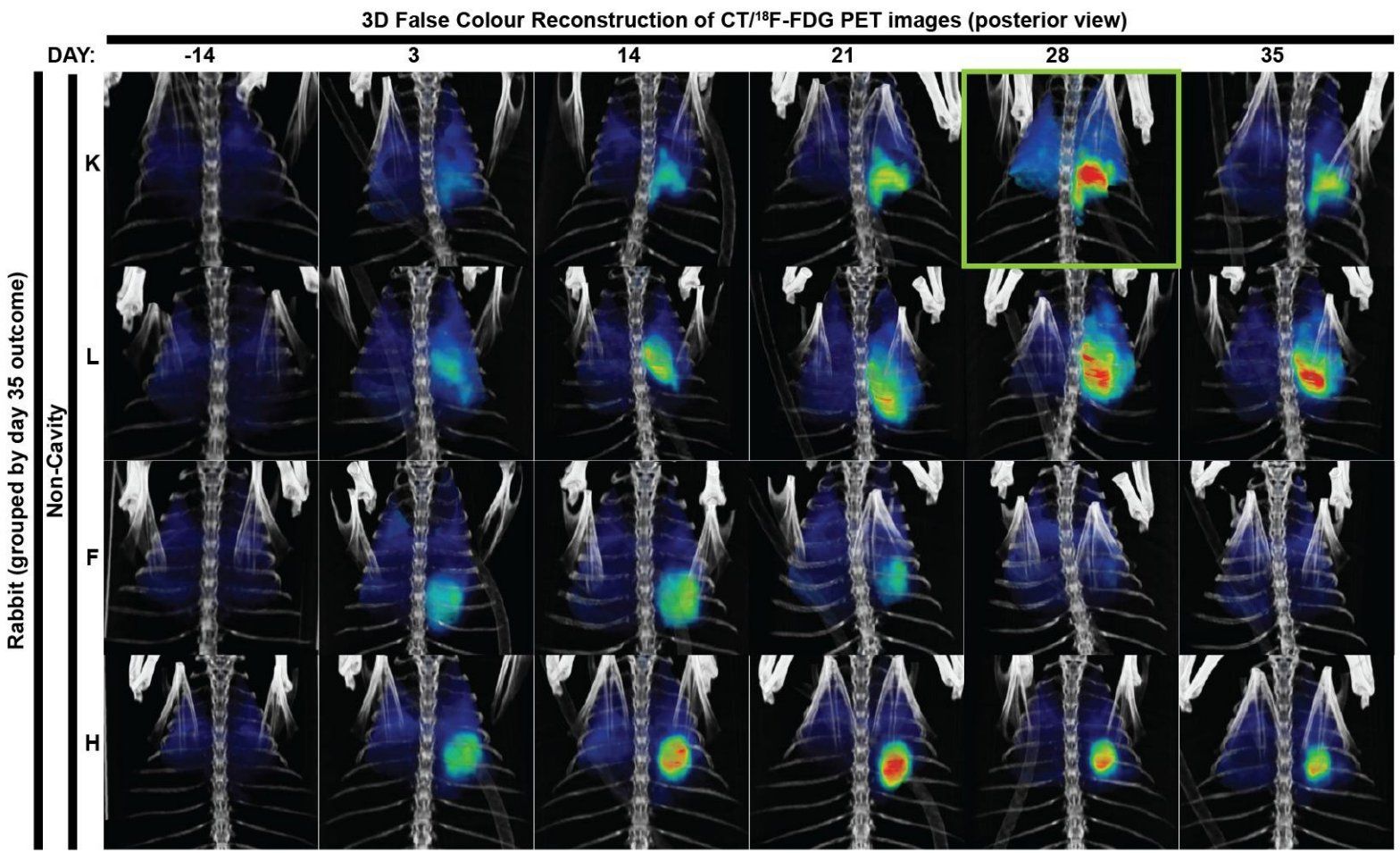

Figure 11. Despite similar sensitisation and infection procedures, multiple outcomes were observed: 3D reconstructions of merged CT/^{18}F-FDG imaging demonstrate variable lesion progression. Red boxes indicate where cavities were observed. Green boxes indicate images where uptake is a relative estimate because tracer injection was only partially successful. Disease progression is seen over the first 28 days in all animals except F which showed decreased ^{18}F-FDG uptake from day 14 to day 21. At day 35, 3 distinct phenotypes were identified: Terminal cavities and Non-terminal cavities **(A)**, and Non cavitary disease **(B)**. *(SUV - Standardised Uptake Value)*.

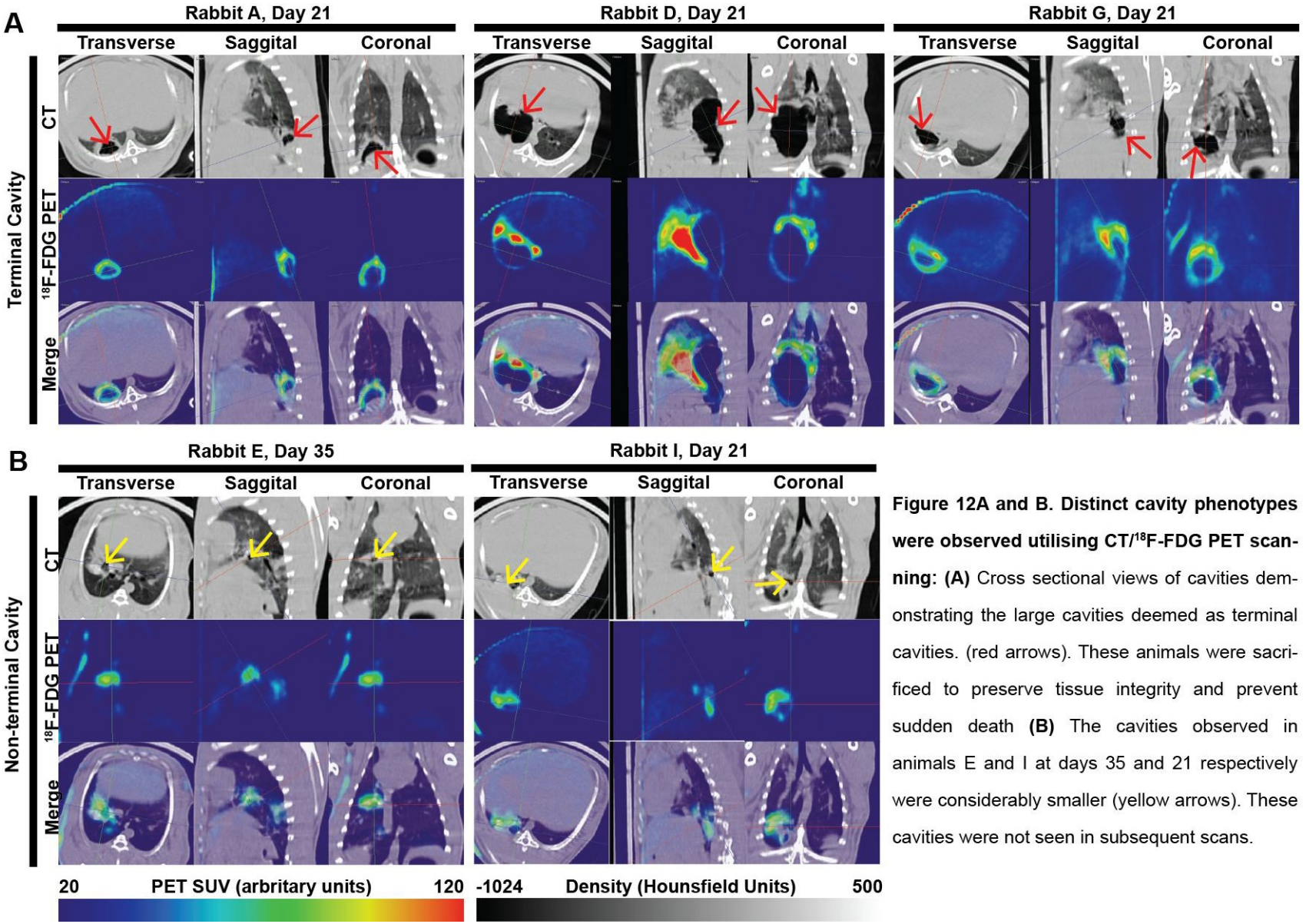

Figure 12A and B. Distinct cavity phenotypes were observed utilising CT/^{18}F-FDG PET scanning: (A) Cross sectional views of cavities demonstrating the large cavities deemed as terminal cavities. (red arrows). These animals were sacrificed to preserve tissue integrity and prevent sudden death **(B)** The cavities observed in animals E and I at days 35 and 21 respectively were considerably smaller (yellow arrows). These cavities were not seen in subsequent scans.

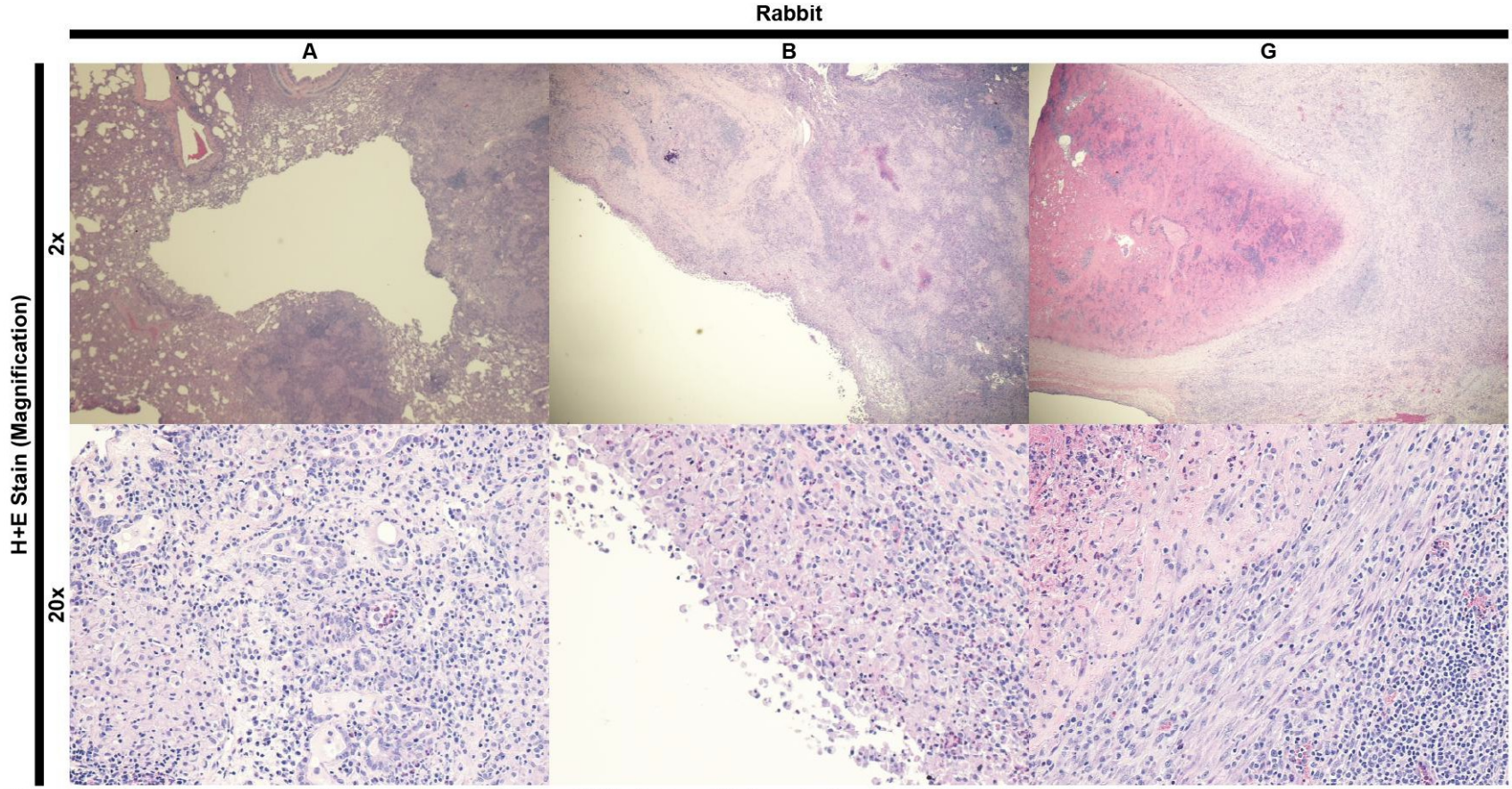

Figure 12C. H+E staining of the lesions dissected from rabbits A, D and G (terminal cavities): Rabbits D and G demonstrate a clear cavity interface; G with significant necrotic debris still in place. Each animal shows that the infiltrate surrounding the lesions consists largely of epithelioid macrophages. Rabbits D and G demonstrate a fibrous cuff, with mononuclear cells external to the fibrous cuff and a number of epithelioid macrophages on the inner surface of the cuff.

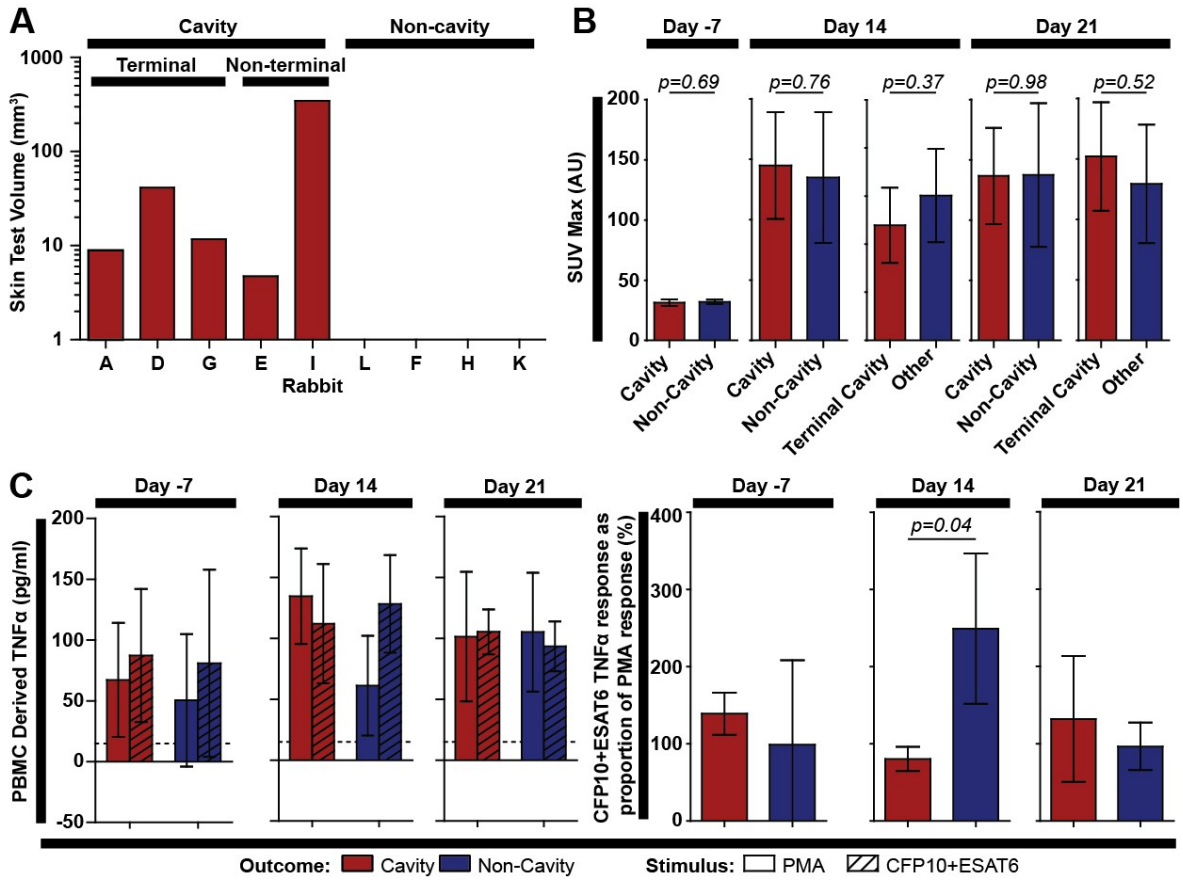

Figure 13. PPD-TST positivity is associated with a cavitary response to *M. tuberculosis* infection in rabbits: (A) All animals that had a positive response to PPD went on to develop cavities. **(B)** SUVMax values did not correlate with or predict cavity formation or type. Cavity animals were compared to non-cavity animals, and terminal cavities were compared to all other animals (other). **(C)** TNFα secretion from isolated PBMCs stimulated with *M. tb* antigens was measured by ELISA. A comparison between 3 animals with terminal cavities and 3 infected animals without cavities was made. The time-points assessed were 14 days after sensitisation (day -7) and 14 days and 21 days post infection. The cells were stimulated with either a combination of mycobacterial proteins (CFP10+ESAT6) or PMA as a positive control. The threshold of detection was 15pg/ml (dotted line). TNFα secretion did not change significantly with either time or condition (*by two-way ANOVA*). At day 14 the response to CFP10+ESAT6 as a proportion of the PMA response was significantly greater in the animals that did not cavitate (*student t-test p=0.04, Two-way ANOVA comparing all results from all time points-Bonferroni multiple comparisons post-test p<0.05*). (CFP-10 - culture filtrate protein 10; ESAT-6 - early secretory antigenic target 6; PMA - phorbol 12-myristate 13-acetate).

PPD-TST was positive prior to infection in all animals which later formed cavities. PPD-TST was negative in those that did not form cavities (figure 13A). Cavity formation was not associated with increased inflammation as measured by ^{18}F-FDG PET activity (figure 13B). This suggests a specific relationship between PPD sensitivity and cavity formation. In an attempt to understand the specific immune mechanisms involved, cytokine levels in supernatants from stimulated peripheral blood

mononuclear cells (PBMCs) were examined (figure 13C). The PBMCs were stimulated with phorbol 12-myristate 13-acetate (PMA) or a combination of culture filtrate protein 10 (CFP10) and early secretory antigenic target 6 (ESAT6) (both antigens used in IGRAs). PBMCs isolated at 3 time points were examined. A comparison was made at each time point, between 3 animals which developed terminal cavities, and 3 which had negative PPD-TSTs prior to infection, (and did not develop cavities). Interferon gamma (IFNɣ) could not be detected using available reagents, however, TNFα was detected. Although TNFα responses were not significantly different at any time point or between outcomes, it was noted that at day 14 the relative response of the cells to *M. tb* specific antigens when compared to their respective PMA control was significantly greater in animals which did not develop cavities (figure 13C). This indicates that antigen-specific TNFα responses were greater in rabbits which did not form cavities. Clearly, further investigation would be required to confirm the precise mechanisms involved, however, this preliminary evidence allows for the speculation that TNFα responsiveness may unexpectedly reduce tissue destruction.

To assess the long term outcome of these initial responses to *M. tb* infection, the surviving animals were followed for a further 105 days and subjected to CT/^{18}F-FDG PET scanning on day 140 (figure 14).

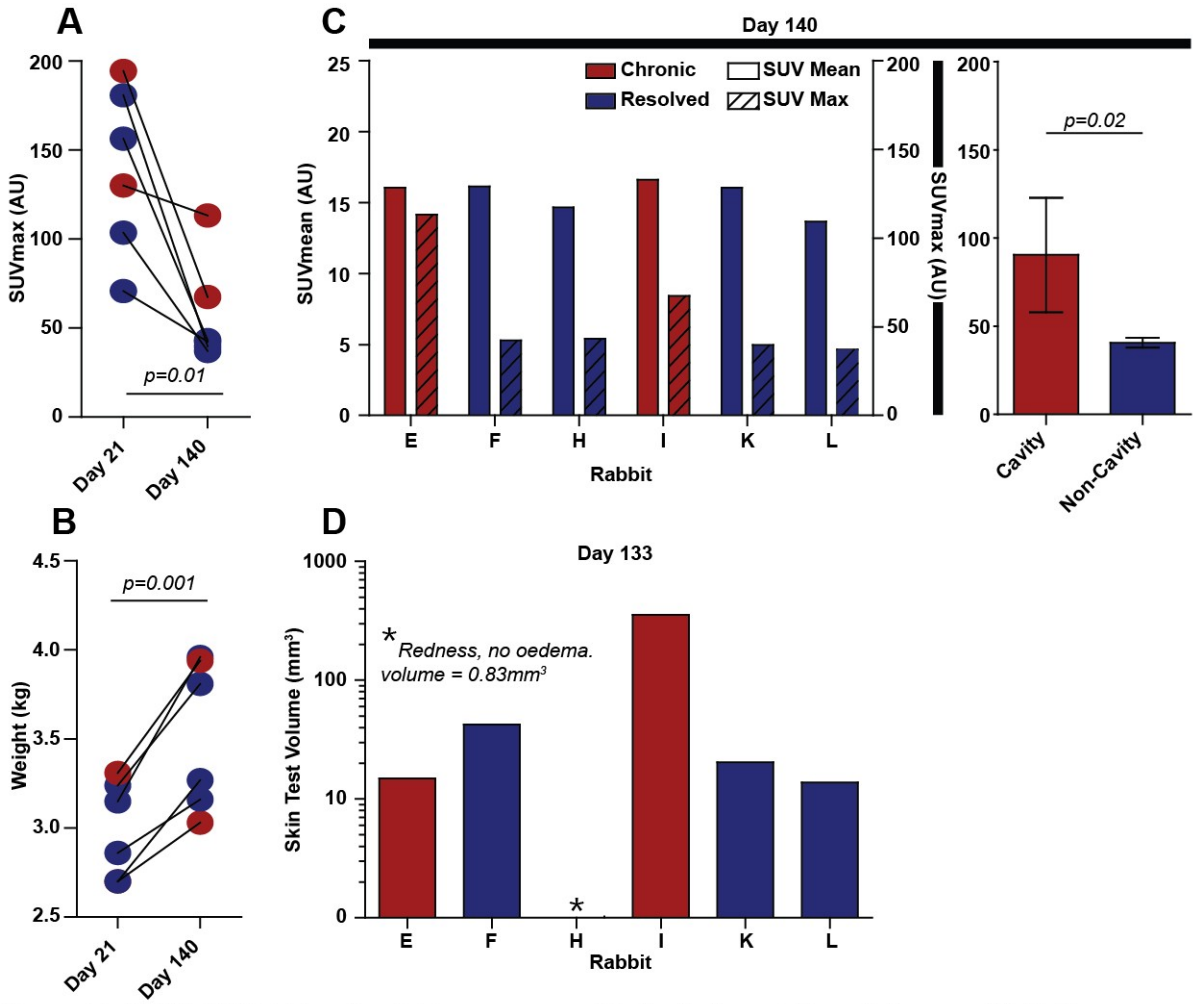

Figure 14. CT/^{18}F-FDG PET and weight measurement indicated resolution of disease: (A) SUVmax measurements demonstrate that there is a clear reduction in ^{18}F-FDG uptake between day 21 and day 140. **(B)** Animals continued to put on weight during this period. **(C)** SUVmean (left y-axis) values for the lung window at day 140 show that overall uptake was similar in all animals. SUVmax values (right y-axis) are statistically significantly higher in those that had cavities, suggesting an ongoing disease process. **(D)** All animals converted to skin test positivity by day 133, although rabbit H had an extremely limited response with no swelling. *(p-values calculated by paired student's t-test in A and B and unpaired student's t-test in C).*

PPD-TSTs were conducted at day 133, by which time all animals had some reaction, although the response in rabbit H was minimal, with some reddening and no oedema (figure 14D). All animals appeared to be resolving disease by subjective CT and PET observations (figures 15 and 16) and also by quantitative ^{18}F-FDG PET uptake measurements (figure 14A). Overall health appeared to improve as indicated by continued increases in weight (figure 14B). Animals without cavities appeared to be devoid of any identifiable sign of disease (Figure 16). However, animals which had formed cavities

still had disease as classified by both subjective CT/^{18}F-FDG PET observations (figure 15). SUVmax measurements confirmed these subjective observations (figure 14C).

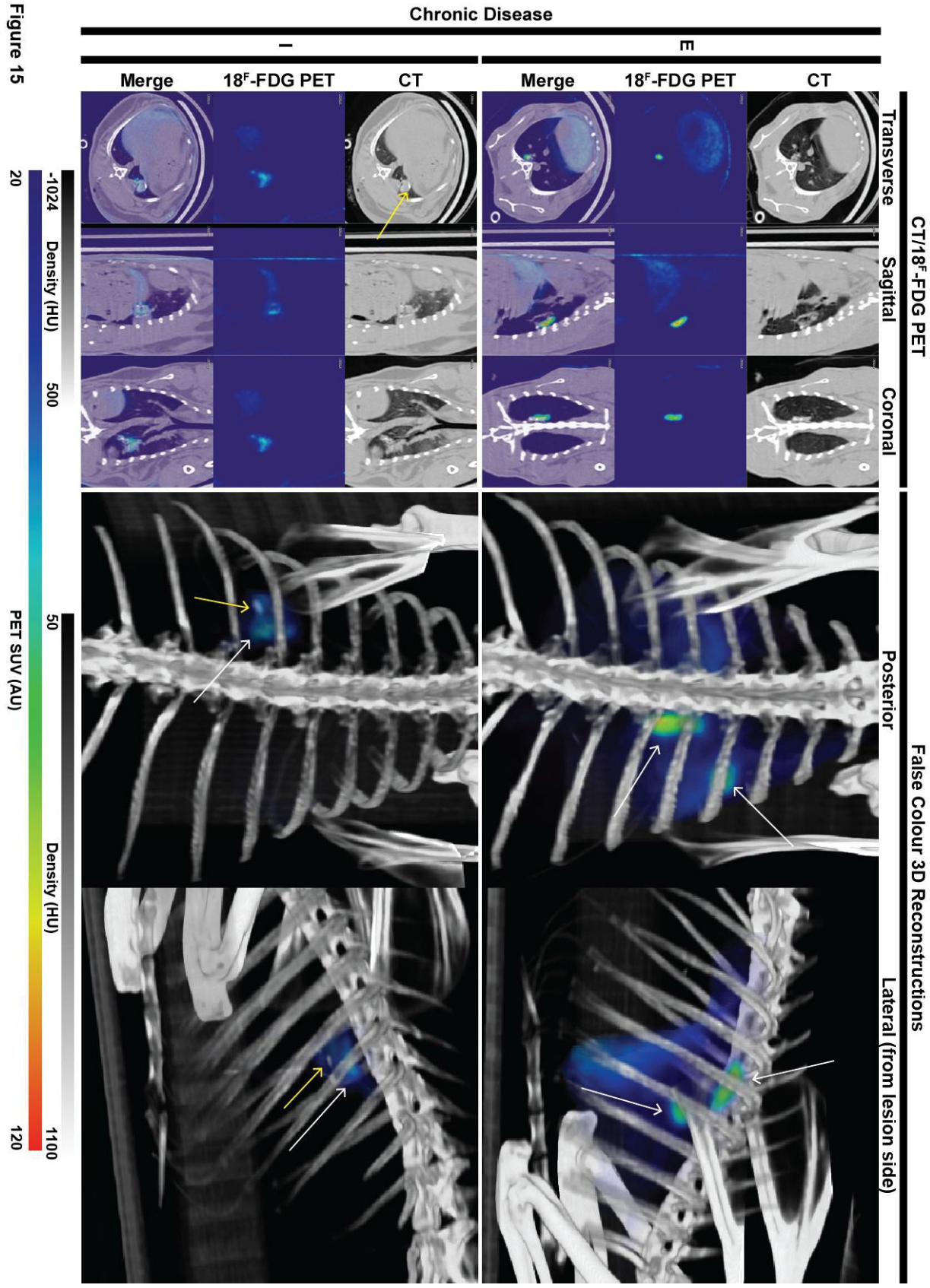
Chronic Disease
–
+
Merge
18F-FDG PET
CT
CT/18F-FDG PET
Transverse
Sagittal
Coronal
False Colour 3D Reconstructions
Posterior
Lateral (from lesion side)
-1024
Density (HU)
500
20
PET SUV (AU)
50
Density (HU)
1100
120

Figure 15

Figure 15. Animals defined as having chronic disease at day 140: These animals demonstrated localised ^{18}F-FDG PET uptake consistent with ongoing inflammation at the site where infection took place (white arrows). CT changes consistent with ongoing disease co-localised to the point of infection. CT changes consistant with lesion calcification were also noted in rabbit I (yellow arrows). *(AU; Arbitrary units, HU; Hounsfield units).*

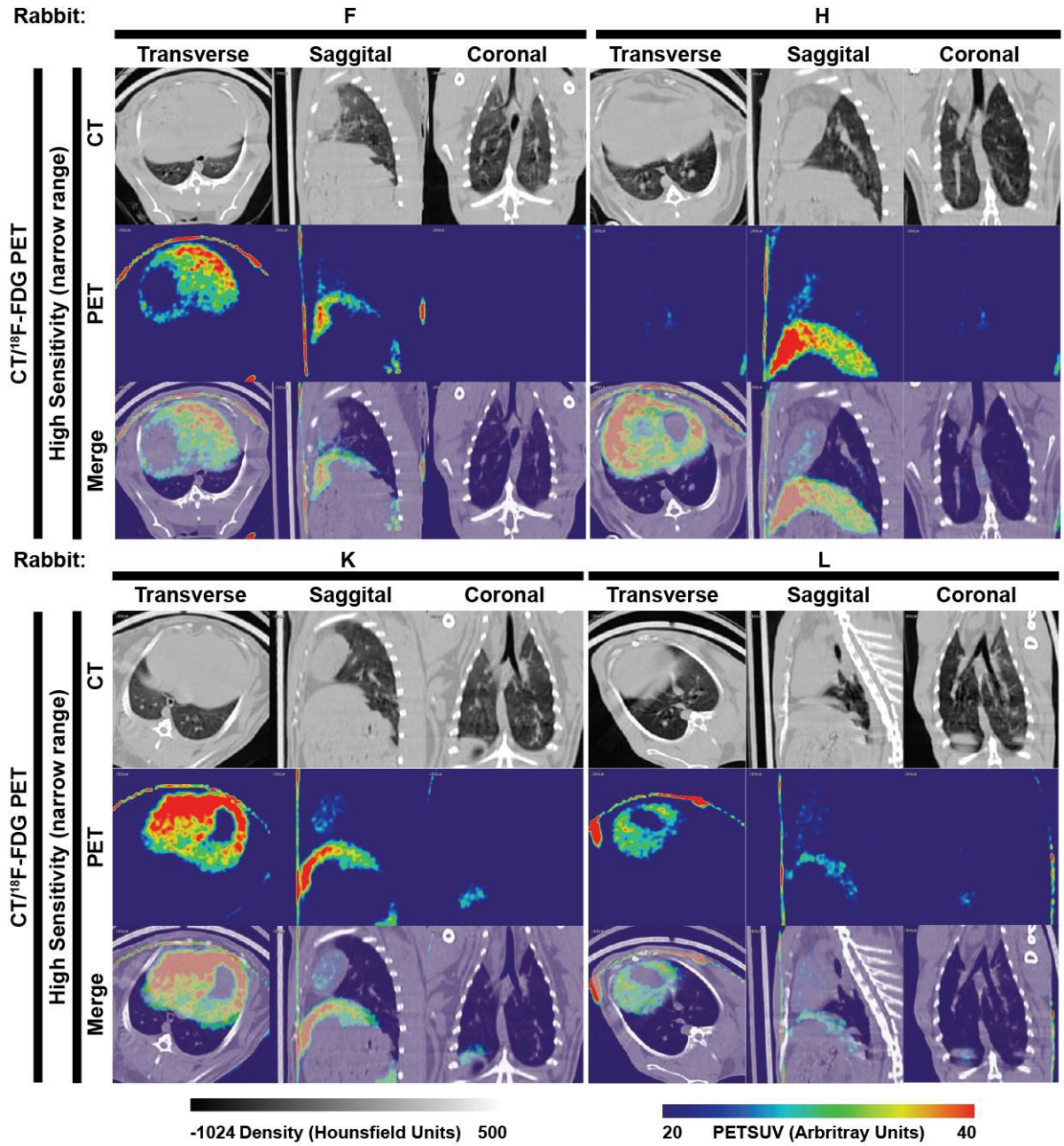

Figure 16A: Slices through regions where lesions were previously identified, in animals defined as having resolved disease by day 140: Rabbits F, H, K and L had no signs of active disease at day 140, there were no distinguishable lesions in the lung field.

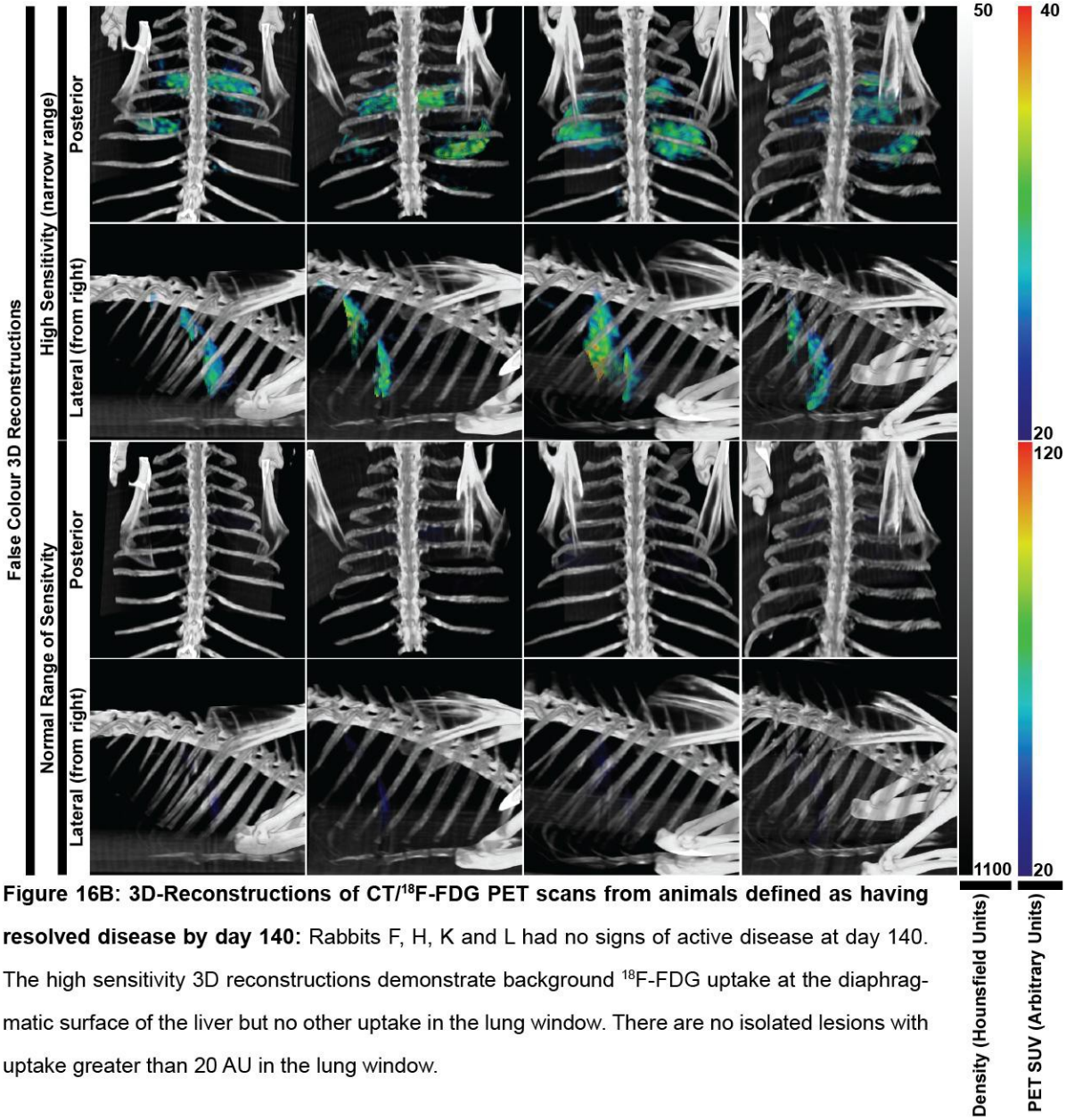

Figure 16B: 3D-Reconstructions of CT/^{18}F-FDG PET scans from animals defined as having resolved disease by day 140: Rabbits F, H, K and L had no signs of active disease at day 140. The high sensitivity 3D reconstructions demonstrate background ^{18}F-FDG uptake at the diaphragmatic surface of the liver but no other uptake in the lung window. There are no isolated lesions with uptake greater than 20 AU in the lung window.

In those animals with chronic infection, lesions remained at the original site of infection (figure 15). Interestingly, in animal E, where two distinct lesions developed, both continued to have significant ^{18}F-FDG uptake, even though only one lesion was at the site of the previous cavity. This allows for the speculation that the cavity itself is not the predisposing factor to chronic disease. Instead it suggests that the factors that predispose to cavity formation also predispose to disease reactivation. This observation lends credence to the idea that not only did PPD-TST positivity indicate a predisposition to cavity formation, but that PPD responsiveness itself increases the risk of chronic disease in rabbits.

Having identified that 4 out of the 6 animals appeared to have resolved disease (figure 16), the question remained as to whether these animals had cleared infection. To answer this, the animals were then immunosuppressed with high-dose dexamethasone. It has been demonstrated by Subbian *et al.* that the pulmonary bacterial burden can fall to levels that are not detectable by culture of rabbit lung, and that subsequent immune suppression for can increase bacterial burden to an extent where bacillary burden is detectable (156). After 4 weeks of immune suppression the animals were allowed 4 weeks to reconstitute their immune systems. After this recovery period disease was again assessed by CT/^{18}F-FDG PET (figure 17) and the whole lung cultured to determine bacterial burden, with the exception of a small region (<5% of total mass) which was excised for histological analysis. In 4 out of 6 animals substantial bacterial burdens (~10^4 CFU per lobe) were found (figure 18A). Bacilli were cultured from the site where primary infection took place, but not any other site (except in rabbit H which had approximately 1x$10^{3.4}$ CFU in the right middle lobe – the lobe adjacent to where the infection took place). The total number of CFU was similar in these animals. No bacilli were cultured from the lungs of rabbits F and K. Histopathological changes associated with TB were identified only in those rabbits from which bacteria could be cultured (figure 19). The lesions in rabbits' I and E appeared more necrotic than those seen in L and H; in-keeping with the hypothesis that necrosis is a component of active disease; whereas granuloma formation may be associated with disease containment (but not necessarily eradication). The threshold of detection for bacteria was estimated to be 20 CFU per lobe. Interestingly, only 2 of the 4 animals with detectable bacterial burden demonstrated disease by CT/^{18}F-FDG PET (figure 18).

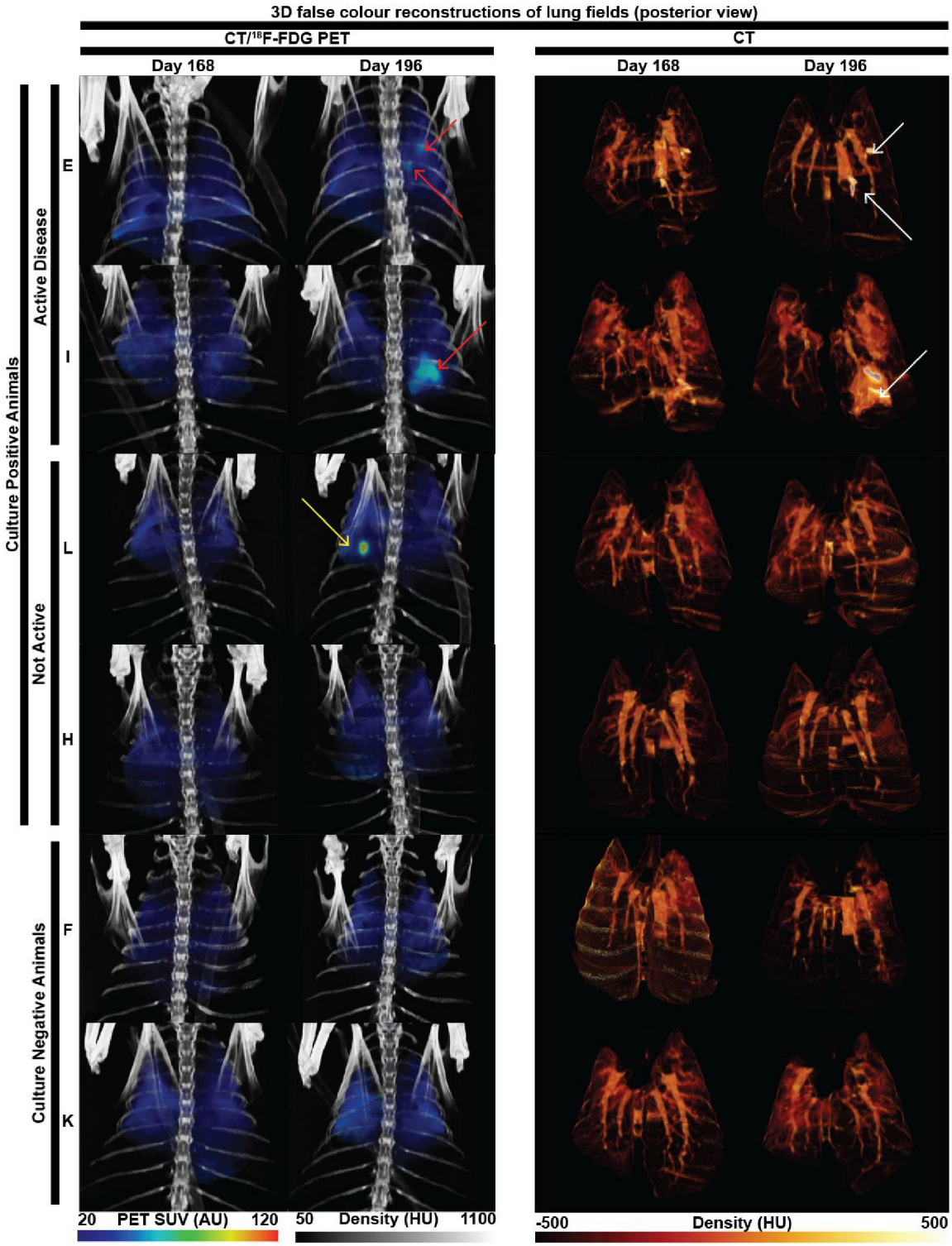

Figure 17. Immunosuppression with high-dose dexamethasome led to varied outcomes as defined by CT/^{18}F-FDG PET: ^{18}F-FDG PET and CT false colour reconstructions demonstrating sites of increased density (white arrows) which correlate with regions of increased ^{18}F-FDG uptake (red arrows). Rabbit L developed a lesion not observable by CT, which showed extremely high ^{18}F-FDG uptake (yellow arrow, SUVmax=175 AU) - no bacteria were culturable from this site, and no pathology was identified at necropsy (figure 18). *(AU; Arbitrary units, HU; Hounsfield units).*

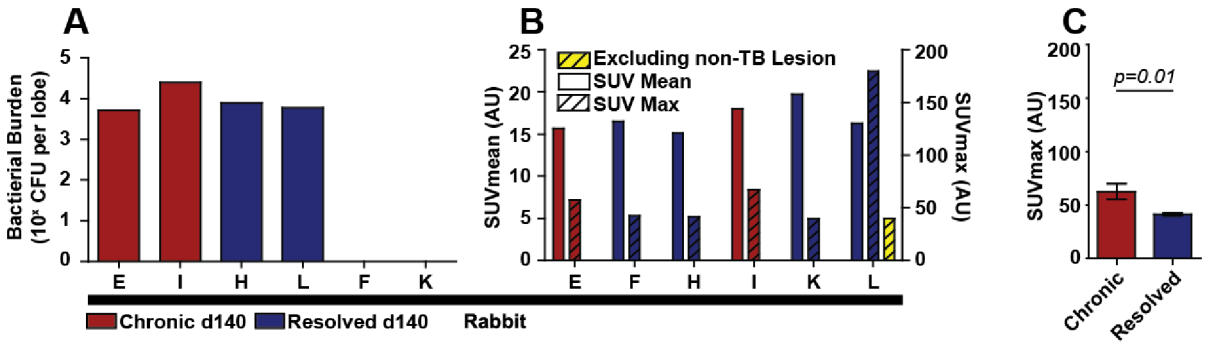

Figure 18. Immunosuppression with high-dose dexamethasome led to varied degrees of reaction as defined by bacteria burden and CT/^{18}F-FDG PET uptake: (A) On day 196, (28 days after the end of dexamethasone treatment) animals were sacrificed and all lung lobes weighed and colony counts enumerated; the lower right lobe, to which the original incolum was delivered, is displayed culturable bacilli and are shown here. All other sites were culture negative, except for the right middle lobe of rabbit H which had bacteria ($10^{3.48}$). The estimated threshold of detection was 20 CFU ($10^{1.3}$) per lobe. **(B)** SUVmean and max values demonstrate similar overall uptake, this overall uptake was not significantly influenced by high local uptake as demonstrated by SUVmax values. Rabbit L had very high localised uptake (figure 18), however, no bacteria were grown from this lobe, and no tuberculous pathology was found by histological analysis; this lesion was excluded from future analyses. **(C)** Excluding rabbit L (see B) from the analysis demonstrates that the SUVmax levels in rabbits E and I was significantly greater than in Rabbits F,H and K (*p=0.01 by student t-test*). *(AU; Arbitrary units)*.

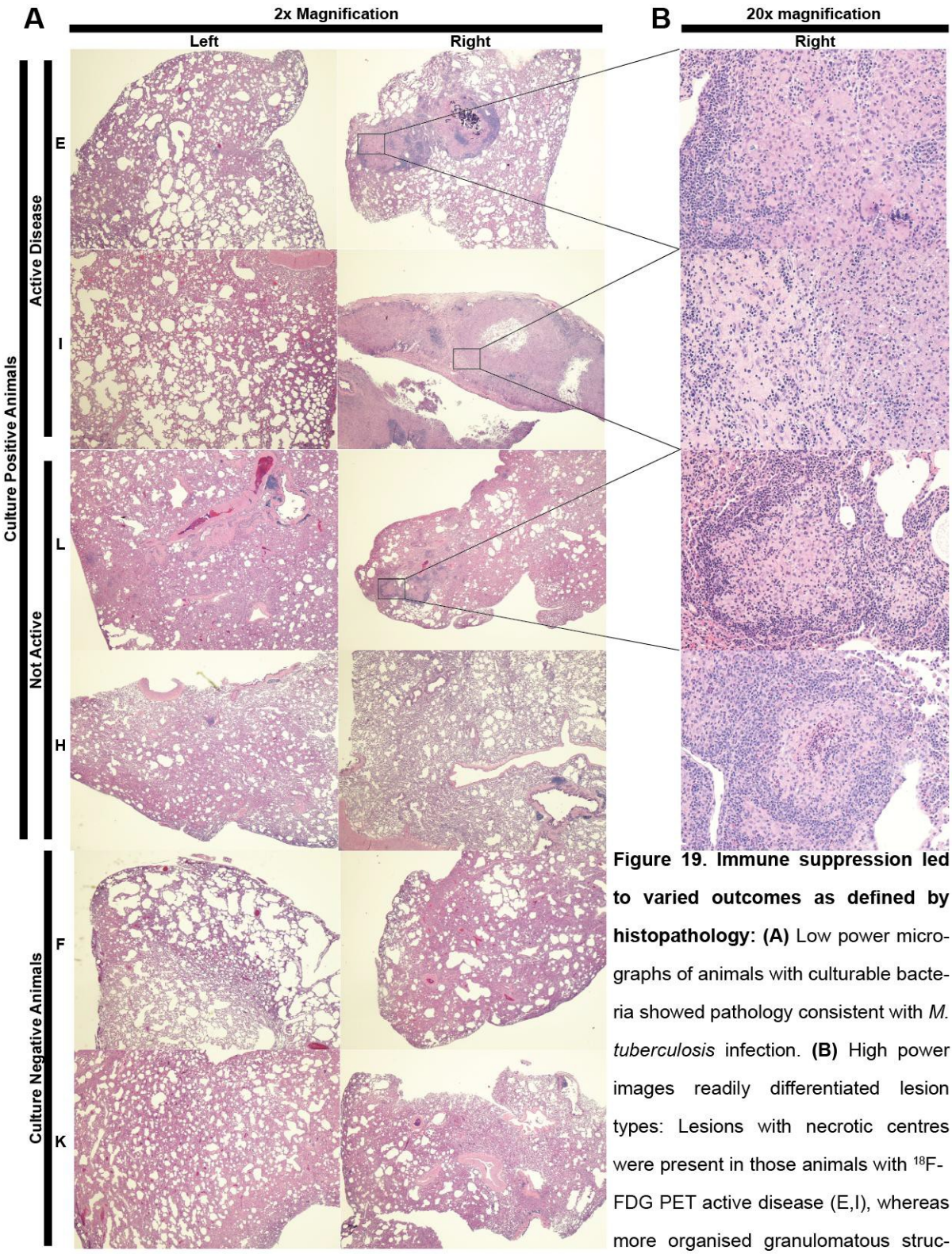

Figure 19. Immune suppression led to varied outcomes as defined by histopathology: (A) Low power micrographs of animals with culturable bacteria showed pathology consistent with *M. tuberculosis* infection. **(B)** High power images readily differentiated lesion types: Lesions with necrotic centres were present in those animals with ^{18}F-FDG PET active disease (E,I), whereas more organised granulomatous structures were observed in those with culturable bacteria but no visible signs of disease by CT/^{18}F-FDG PET (L,H). Culture negative animals did not show tuberculous pathology (F,K).

This study proved highly informative. First, it demonstrated a clear link between PPD-TST positivity and cavity formation. It indicated that there was a predisposition in certain rabbits to PPD-TST positivity, and hence a predisposition to developing the immune response associated with cavity formation. Second, it showed that tissue destruction in the form of cavity formation was associated with significantly slower resolution of disease, and relatively limited TNFα responses to *M. tb* antigens early during infection. Whether slowed resolution is the result of cavities themselves, or is the result of a dysfunctional immune response that concurrently drives cavity formation is presently unknown. Finally, the different clinical states of the animals (i.e. increased ^{18}F-FDG uptake and CT changes consistent with infection), despite equal bacterial burden, supports the idea that active disease in rabbits, like humans, is dependent not only on bacterial burden but also host-responsiveness. Although this study is very small, the data indicates that altered host-responses, resulting from previous exposure to mycobacterial antigens may predispose *M. tb* infected individuals to active disease.

Because PPD-TST reactivity predisposed strongly to cavity formation the sensitisation regimen was altered to enhance PPD-TST responses.

3.6. PPD-TST positivity is induced in rabbits with high-dose sensitization and reliably leads to cavity formation: A 70 day model of *M. tuberculosis* cavity development

To further examine the relationship between PPD-TST positivity and cavity formation in rabbits, an attempt was made to induce very high levels of sensitivity to mycobacterial antigens by increasing the sensitising dose of heat-killed bacteria 10-fold (from 10^7 to 10^8 heat-killed CFU per injection).

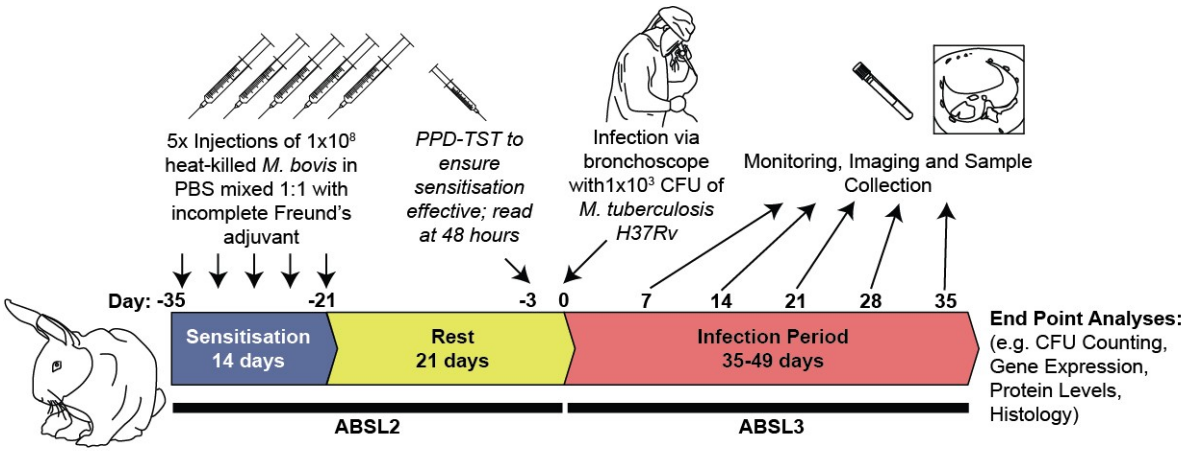

Figure 20. A model of tuberculosis in which cavitation is reliably produced in 28 days: Sensitisation is achieved by delivering 5 0.2ml injections containing 10^8 heat-killed CFU of *M. bovis ravenel* in incomplete Freund's adjuvant over 14 days. Animals are then allowed 21 days to develop immune responses after which 0.1ml of PPD (5 tuberculin units) was administered. Successful sensitisation is confirmed by any induration of PPD-TST response. Infection with 10^3 CFU of *M. tuberculosis H37Rv* is performed under bronchoscopic guidance and the animals are monitored longitudinally.

Unsurprisingly, all rabbits in this cohort became PPD-TST positive. The degree of response was variable, but universally some degree of oedema developed by 48 hours post PPD-TST administration (table 3, figure 21). 10^3 CFU of *M. tb H37Rv* were delivered via bronchoscope into the right or left lower lobe of the lung (figure 23) and the animals randomly assigned to necropsy at either 5 or 7 weeks post-infection (figure 20).

Rabbit	Dimension 1 (mm)	Dimension 2 (mm)	Thickness (mm)	Impression	Volume (mm^3)
A	6.4	8.0	0.2	+	42.89
B	9.6	9.1	1.0	+	219.56
C	6.0	5.5	1.0	+/-	138.24
D	12.0	13.1	0.5	++	658.48
E	5.6	5.6	0.8	+/-	65.68
F	13.3	12.9	0.6	++	574.94
G	8.9	8.2	1.0	+/-	183.42
H	10.3	10.4	0.1	++	448.70
I	3.4	2.7	0.1	+/-	3.85
J	5.8	5.4	0.1	+/-	13.12
K	7.9	6.8	0.3	+/-	67.51
L	12.3	14.4	2.1	++	1558.03

Table 3. Sensitvity to PPD can be achieved by using a very high dose sensitisation regimen of 5 injections containing 10^8 heat-killed M. bovis in incomplete Freund's adjuvant: 0.1ml of PPD (5TU) was administered intradermally and monitored for 72 hours. Responses at 48 hours are documented above. PPD reactivity occured in all animals, a high degree of variability in reactivity was noted between animals despite identical treatment.

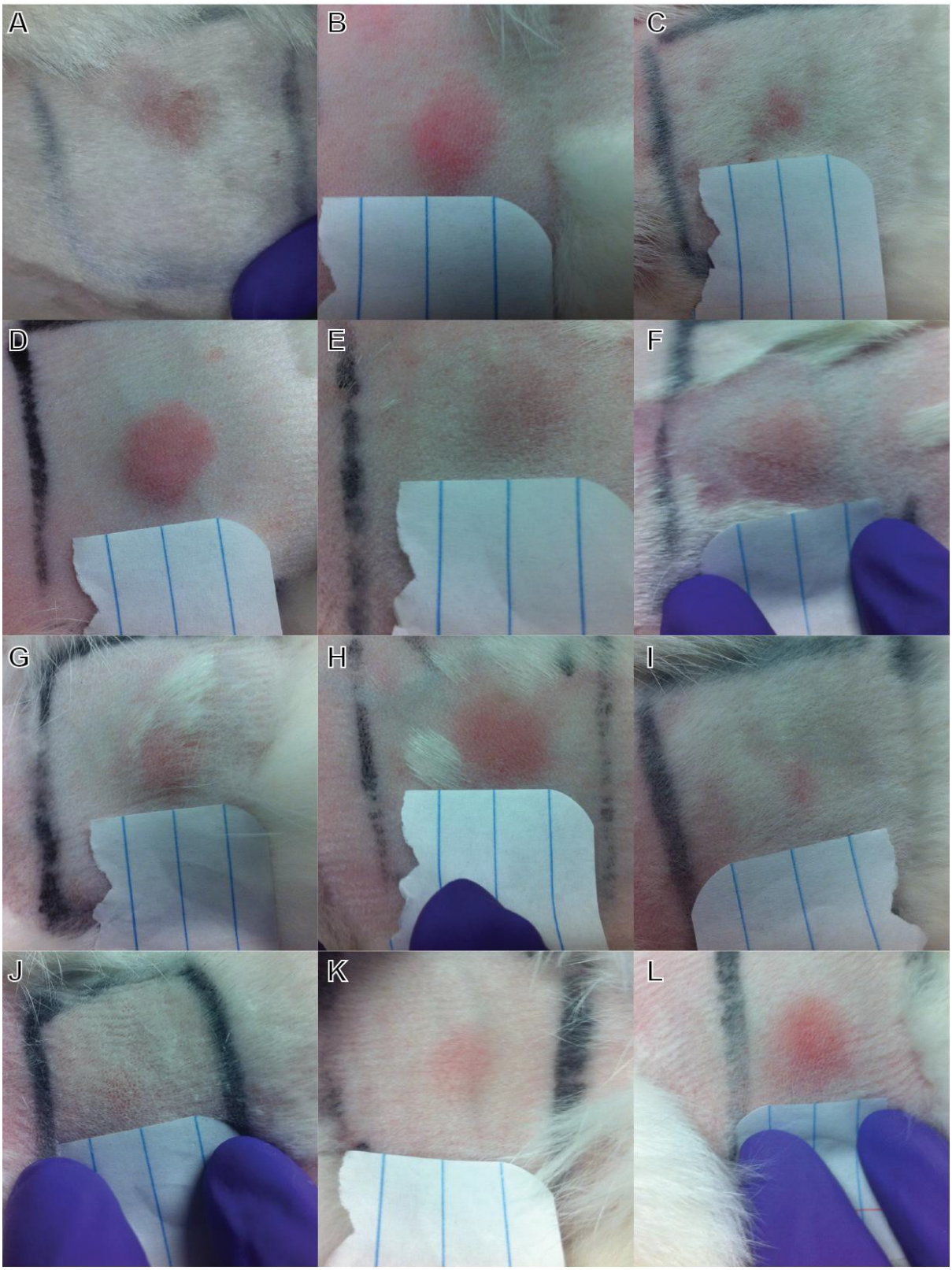

Figure 21. Images of positive PPD results: There is significant variability in the appearance of skin tests. Raised red lesions are seen in all animals - although the degree of inflammation varies significantly. Each letter is the rabbit reference number. *(Lined paper is 8.89mm ruled)*.

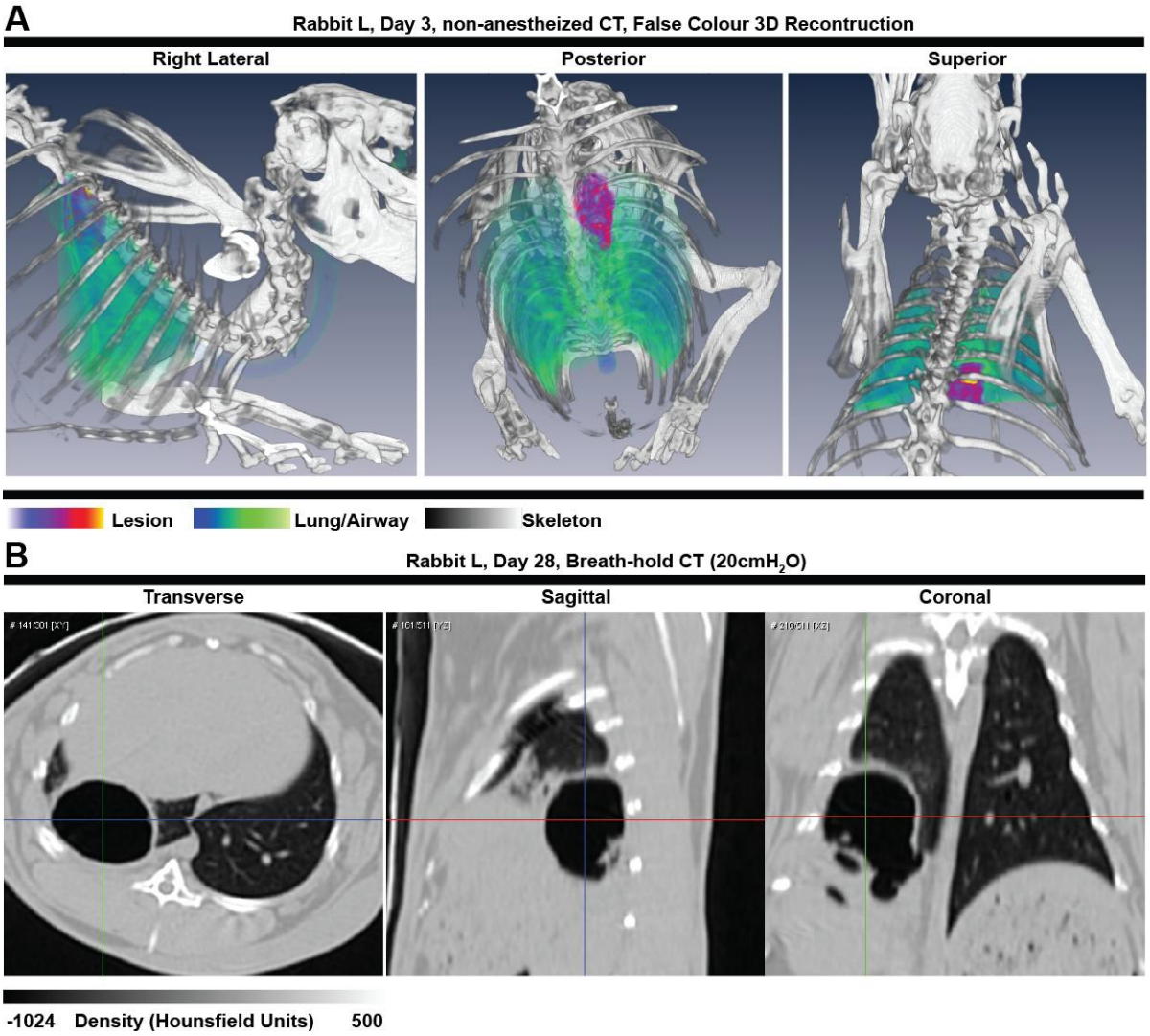

Figure 22. Novel non-anaesthetised and breath-hold *in vivo* imaging procedures allow for detailed imaging analysis: (A) Scan of a naturally positioned, non-anaesthetised animal demonstrating apical location of lesion. **(B)** Representative CT slices from rabbit L at day 28 showing a large cavity in the right lower lobe - the site at which the bacteria were implanted. Breath-holding removes breathing artefacts.

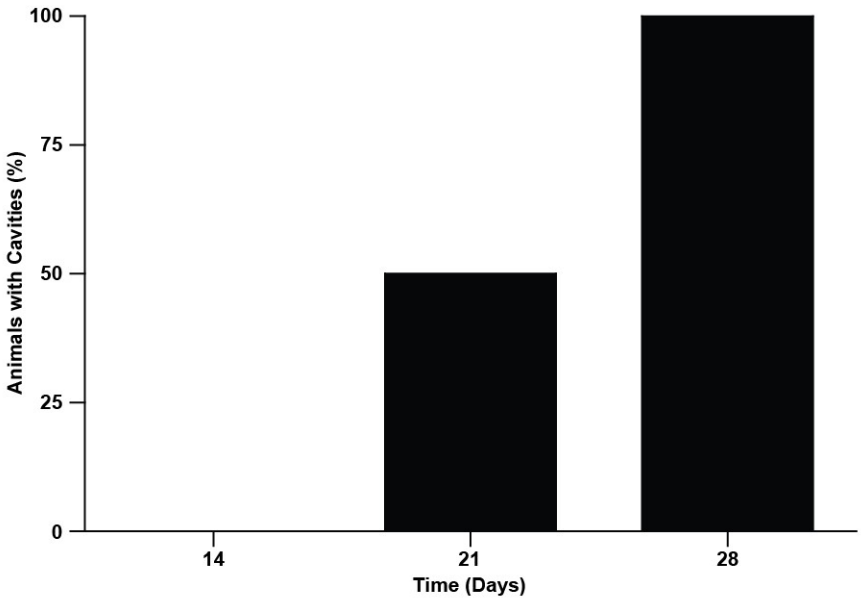

Figure 23. PPD positive animals all developed cavities within 28 days: Cavity formation, as defined by CT imaging, had occurred in 50% of animals by day 21 and all animals by day 28.

All animals developed extensive cavities within 28 days; as identified by breath-hold CT imaging (figure 22), which remained identifiable at necropsy (figure 23). This technology is described in the methods (section 2.1.2.5.) and in section 4.6.

This study showed that cavities occurred in all rabbits with PPD-TST positive reactions and supports the hypothesis that PPD-TST positivity is essential in rabbits for the generation of cavities. It also demonstrates for the first time a model of cavity development in which trials of therapeutics could be assessed for their effectiveness in cavitary disease. The tissue destructive phenotype, which is the most common gross pathology observable in active TB, has never been directly included in preclinical trials of drugs or vaccines, despite being the site where the highest bacterial burdens are located during active TB.

3.7. Characterisation of a 70 day model of *M. tuberculosis* cavity development by *in vivo* imaging, gross pathological, histological and bacteriologic methods

As a result of the study above a significant number of closely related matched samples (12) were generated. It was therefore possible to investigate the pathogenesis of *M. tb* infection in the PPD-TST positive animal. For the first time, with a high degree of accuracy, the structural changes that occur during cavity formation in this model were monitored. This was achieved using a custom-built ventilator, which allowed for BSL-3 containment combined with pulmonary pressure control (see section 4.6 for further details).

3.7.1. *In vivo* breath-hold CT findings

Cavity formation is an extremely rapid process. In this model, infection is followed by an infiltrative process. There is a reduction in infiltrates over the first 14 days (as assessed by non breath-hold images), but increased localised density as a more clearly defined lesion becomes apparent. The next observation is a progressive increase in this density, which occasionally increases in volume. Next, this tissue erodes; often nearly the entire apparently consolidated region is lost, leaving a dense surrounding ring. Finally the cavity appears to reduce in size, accompanied in surrounding regions by increases in consolidation and infiltrate (figure 24).

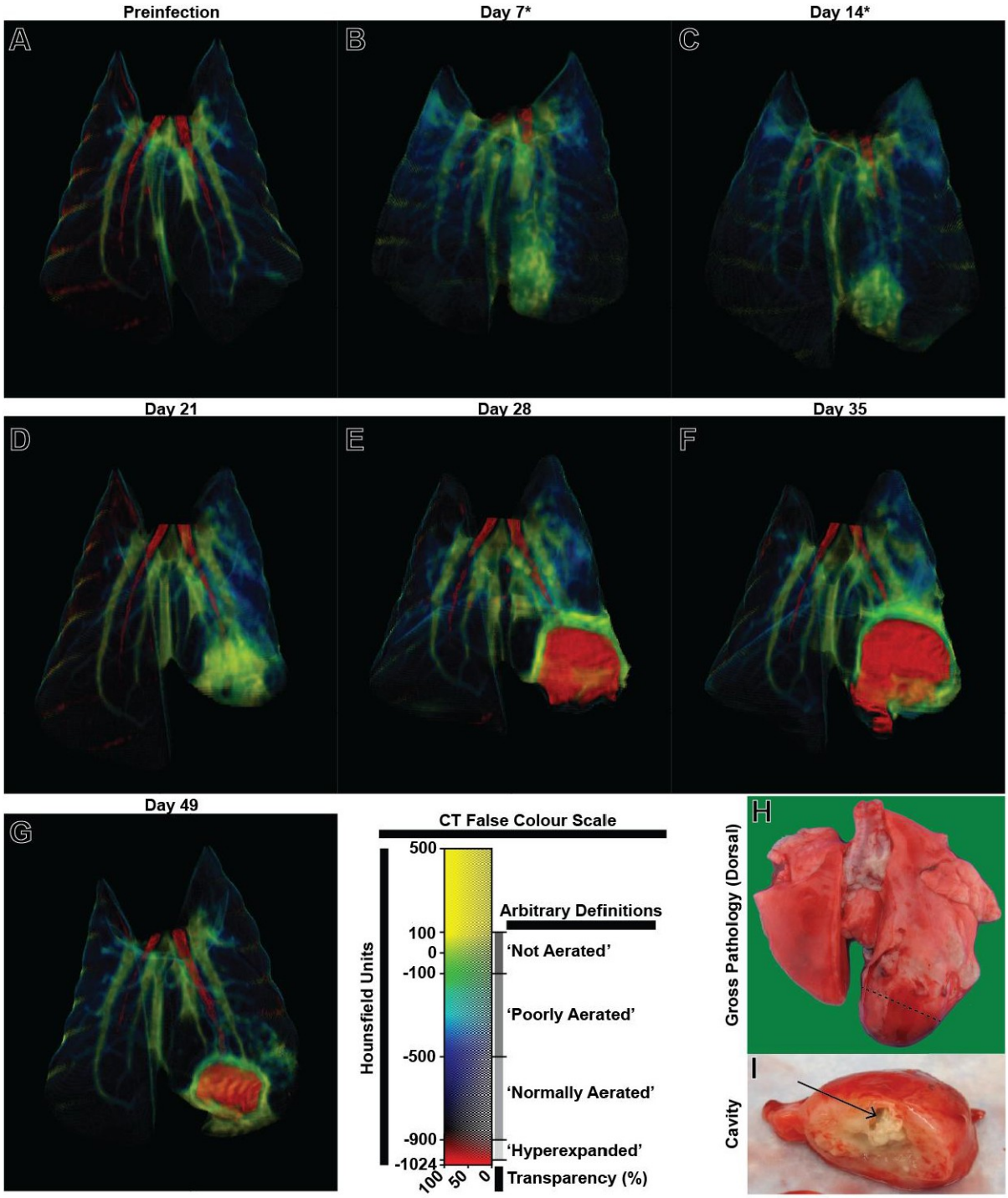

Figure 24. Example of cavity formation and progression: (A-G) False coloured 30 reconstructed CT scans at 1OcmH O (except* taken without anaesthesia) demonstrate the dynamic cavity forming process (dorsal views are shown). Initially the infiltrated region is small. Between day 7 and day 14 infiltrates become more localised. At day 21, a large highly dense infiltrate is seen. Between day 21 and 28 the entirety of this region is replaced by a cavity, which is surrounded by a highly dense region. The cavity is enlarged at day 35. By day 49 the size of the lesion has drastically been reduced and infiltrates are seen in the adjacent region. (H) Posterior view of resected lungs from this animal. (I) Cut section through cavity region (dotted line in H) demonstrating cavity and surrounding necrosis. Healthy tissue is relatively under-represented in such images,as it collapses after the lung is removed.

Because scans from day 21 through 49 were conducted utilising the breath-hold technique (section 4.6), more subtle observations of the pathology surrounding cavity formation during this period were recorded. 20cmH_2O of pressure allow for the identification of regions of density as small as 1-2mm in diameter. This was of particular interest, as increased infiltrates appear after cavity formation in distal regions of the lung (Figure 25). This suggested that cavity formation was associated with intra-pulmonary dissemination.

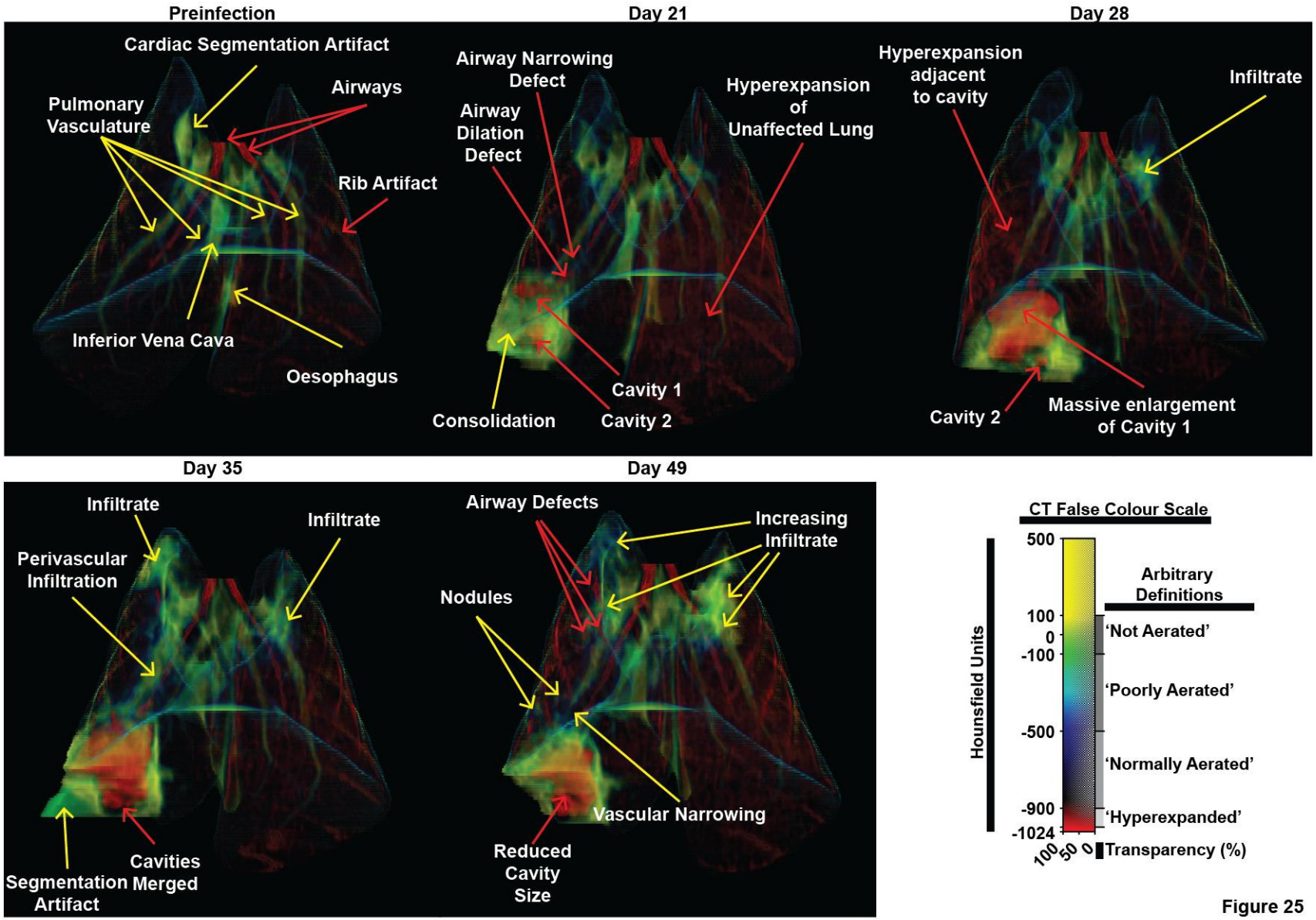
Preinfection
Cardiac Segmentation Artifact
Airways
Pulmonary Vasculature
Rib Artifact
Inferior Vena Cava
Oesophagus
Day 21
Airway Narrowing Defect
Airway Dilation Defect
Hyperexpansion of Unaffected Lung
Consolidation
Cavity 1
Cavity 2
Day 28
Hyperexpansion adjacent to cavity
Infiltrate
Cavity 2
Massive enlargement of Cavity 1
Day 35
Infiltrate
Infiltrate
Perivascular Infiltration
Segmentation Artifact
Cavities Merged
Day 49
Airway Defects
Increasing Infiltrate
Nodules
Vascular Narrowing
Reduced Cavity Size
CT False Colour Scale
Hounsfield Units
500
100
0
-100
-500
-900
-1024
Arbitrary Definitions
'Not Aerated'
'Poorly Aerated'
'Normally Aerated'
'Hyperexpanded'
100
50
0
Transparency (%)

Figure 25

Figure 25. False colour CT reconstructions highlight common changes during disease progression in set-pressure (20cmH_2O) breath-hold images: A number of normal findings are observed within specific ranges of interest in the preinfection scan: the airways appear red (hypodense) and vasculature appears in the yellow/green range (dense). There are two principal artefacts; one arising from the challenge of segmenting at the cardiac border and a second from rib shadowing into the lung field. The first artefact causes dense regions corresponding to cardiac tissue being placed accidentally into the lung field. The rib artefact causes rib shaped regions of apparent hypodensity (red) adjacent to the actual rib location. At day 21 the site of infection consists largely of dense regions, and in this rabbit, small cavities are observed within this region. Additionally, airway defects proximal to the region of disease are noted; there is proximal narrowing and distal dilation. The contralateral lung appears hyperinflated - and is more inflated than the affected lung. At day 28 an infiltrate is observed in the left upper lobe of the lung. The cavity has dramatically changed in structure, with one cavity expanding dramatically and apparently displacing the infiltrate surrounding it. At day 35 the cavity has again changed in shape. Perivascular infiltrates are seen in the right lung. There is an increase in the amount of infiltrate in left upper lobe and new infiltrates in the right upper lobe. At day 49 infiltrative densities have increased. Distinct nodules are noted adjacent to the cavity, and new airway dilation defects are seen in the left upper lobe in the vicinity of the infiltrates that appeared a day 35. The infiltrates are now more extensive. The lumen of the cavity has decreased in size. *All scans are to scale, with a pressure of 20cmH_2O being applied via a custom built, breath-hold apparatus. The view was standardised by identifying the sterno-spinal axis using this to dictate the z axis, the sternum formed the vertical (y) reference and the posterior portion of the ribs were used to identify the horizontal (y) axis. Orthographic projections are presented.*

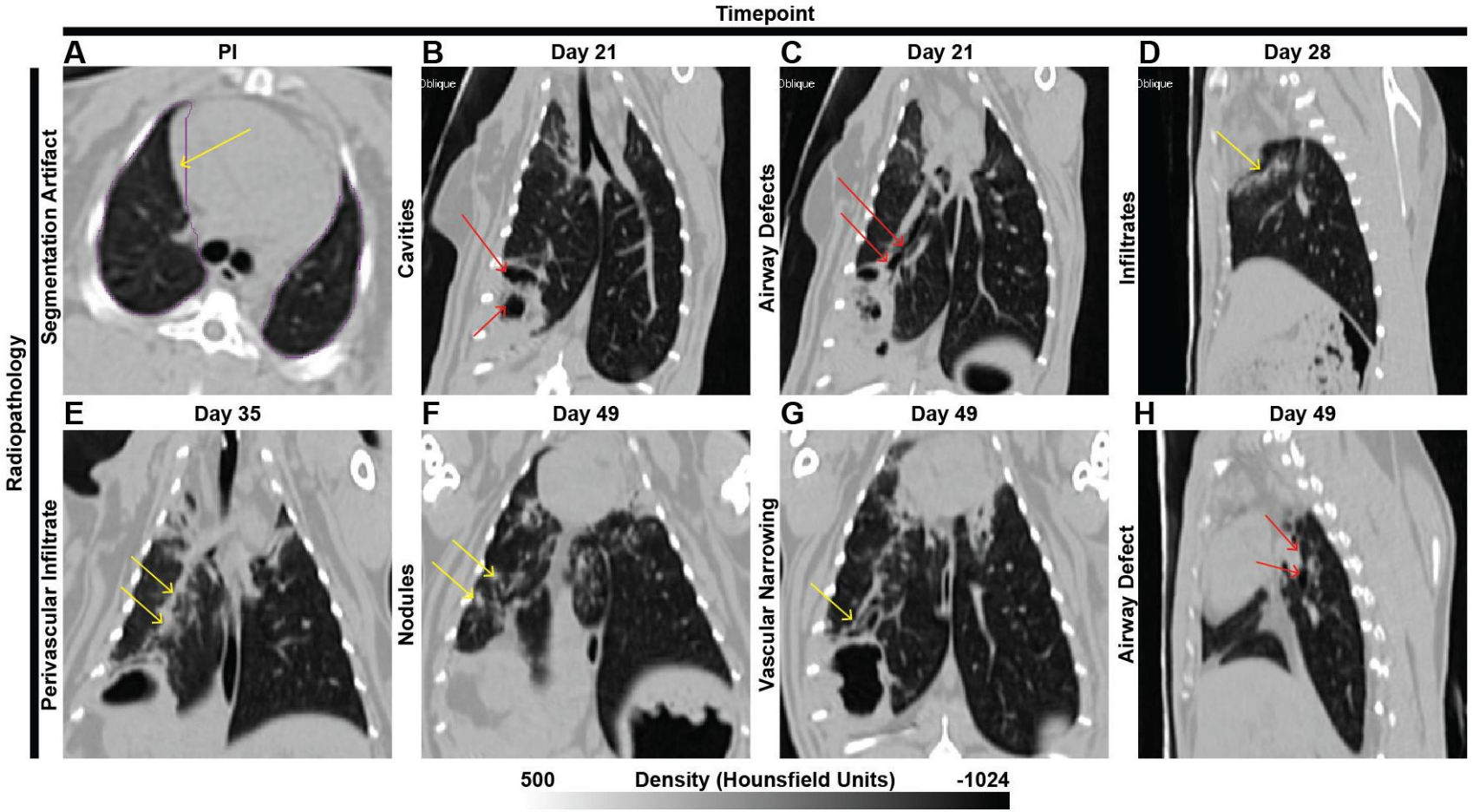

Figure 26. Traditional CT slices demonstrating pathologies and artefacts identified in 3D false colour reconstructions: (A) Cardiac border artefact: transverse section showing dense regions *(yellow arrow)* corresponding to cardiac tissue mistakenly placed into the lung filed *(purple line)* during semi-automated segmentation. **(B)** Cavities identified at day 21 *(red arrows). Coronal section.* **(C)** Airway defects proximal to the region of disease are noted. There is a stricture proximal to a dilation in the airway *(red arrows). Coronal section.* **(D)** At day 28 an infiltrate is observed in the left upper lobe of the lung *(yellow arrows). Sagittal section.* **(E)** Perivascular infiltrates *(yellow arrows). Coronal section.* **(F)** Distinct nodules are noted adjacent to the cavity *(yellow arrows). Coronal section.* **(G)** A distinct narrowing of the pulmonary vasculature *(yellow arrow). Coronal section.* **(H)** Dilation of the bronchiole tree in the left upper lobe in the vicinity of the infiltrates *(red arrows). Sagittal section.*

The changes in lung parenchyma were quantified over time (figure 27). The amount of tissue recruited was calculated by comparing the density measurements at two separate pressures at which breath-hold manouvers were performed (191). By monitoring tissue density (as measured by hounsfield units; HU) and evaluating tissue mass, as opposed to volume, an estimate of functional tissue could be established (section 4.8). This analysis demonstrated a decrease in functional tissue following infection, but also that functional tissue was lost between day 21 and day 35, indicating a measurable progression of disease. Cavities can be considered a space occupying lesion where gas exchange is not occuring, changes in the size of the cavity most likely reflect the health of surrounding tissue, and the ability to preferentially inflate these regions in comparison to the cavity (figure 27).

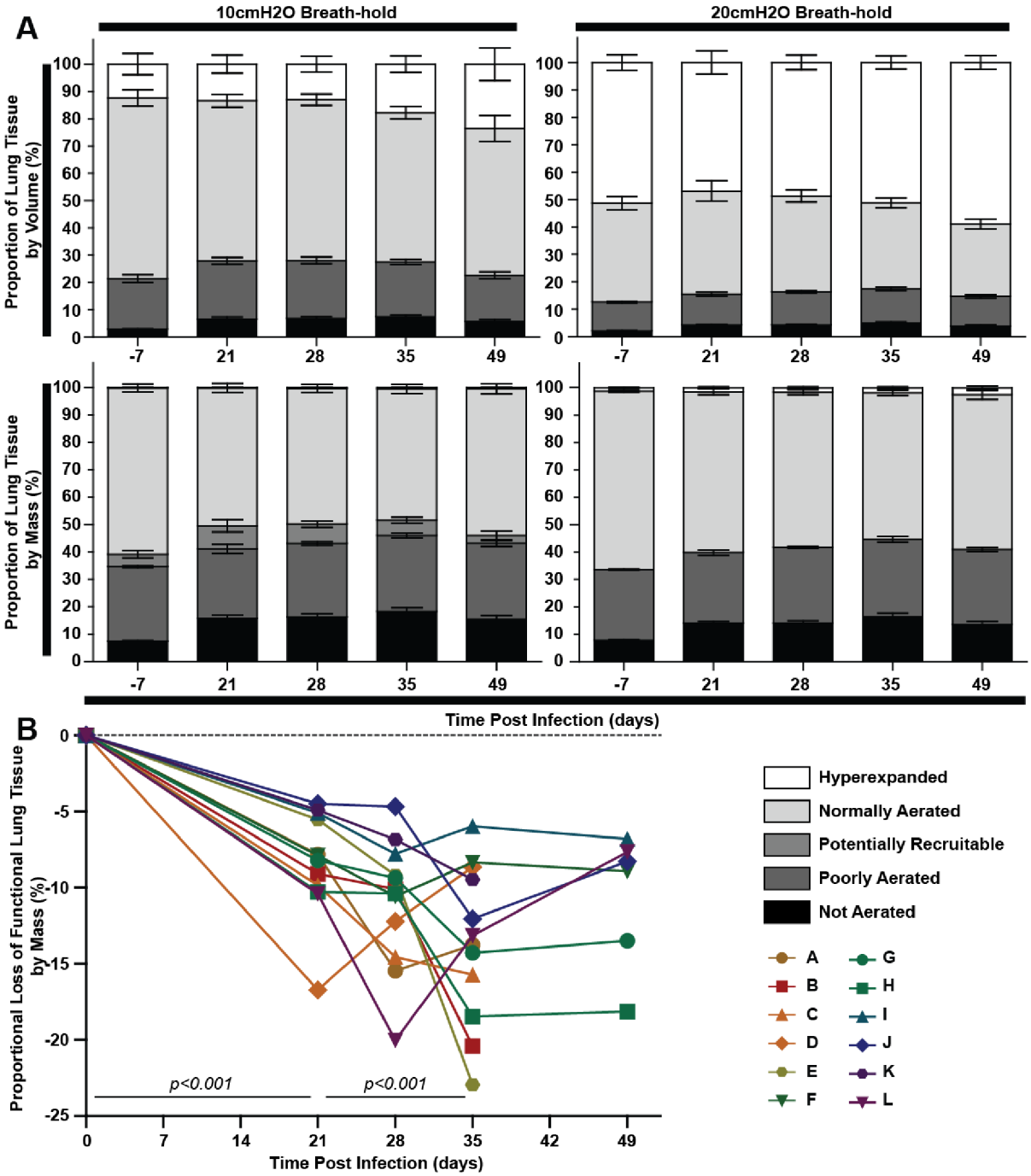

Figure 27. Signature zones can be used to quantify disease progression: (A) Quantification of regions by accepted density definitions reveals an increase in low density and high density regions (i.e. hyperexpanded and not aerated zones). This is accompanied by a reduction in normally aerated regions. This occurs at all inflation pressures, when either the volume of tissue or mass of tissue is measured. The proportion of lung tissue by mass can be used to evaluate which tissue is recruited during inflation from 10 to 20cmH_2O. This allows for both the mass of normally aerated and potentially recruitable tissue to be evaluated in a 10cmH_2O breath-hold. **(B)** Adding the potentially recruitable and normally aerated tissue masses together, gives the proportion of the lung made up functional tissue. The proportion of functional tissue is significantly reduced post infection, and also decreases as disease progresses. *(Statistics calculated by repeated measures ANOVA with Tukey post-test).*

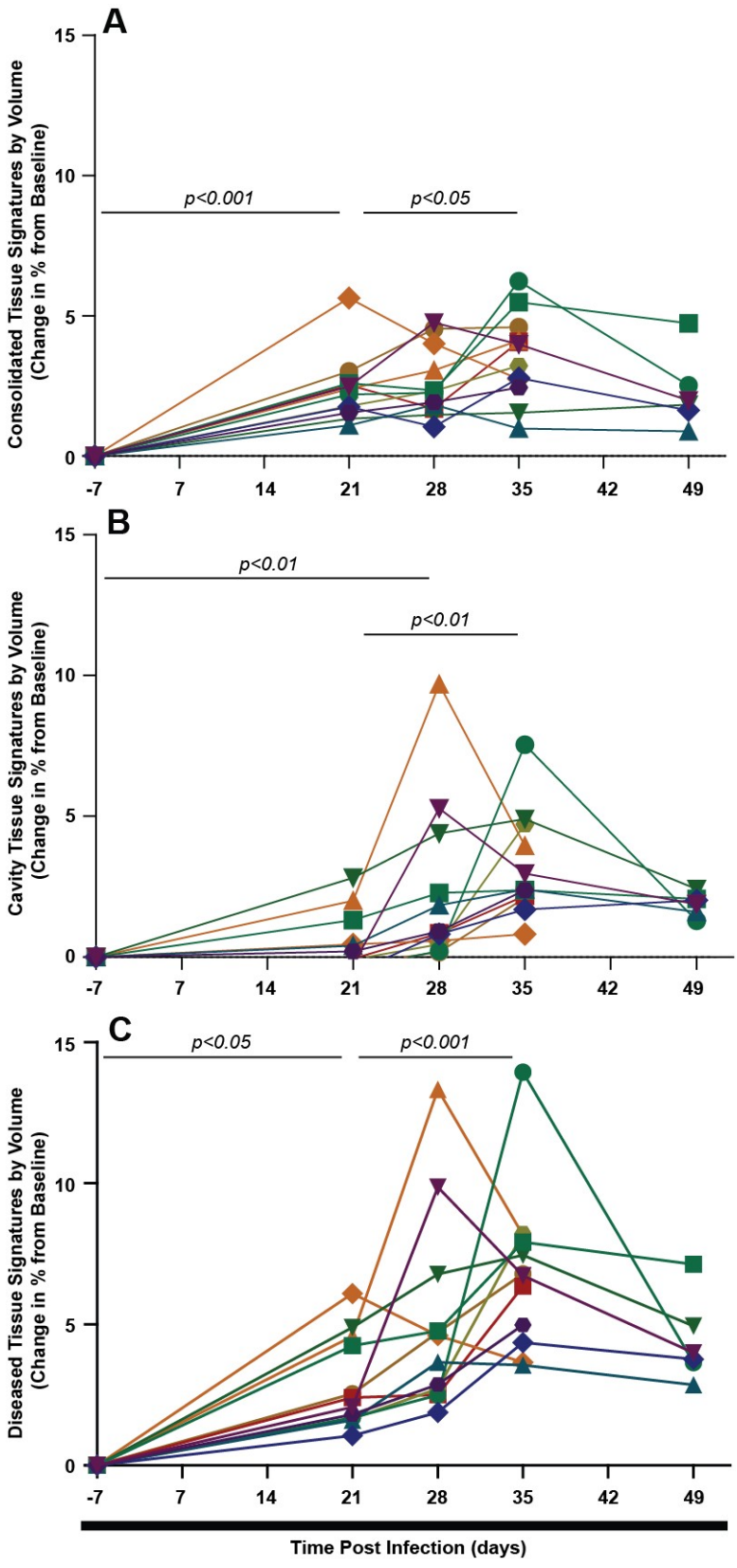

Figure 28. Signature zones can be used to compile simple quantitative analyses for disease progression: (A) Consolidated tissue zone (HU -184 to +156) increases as a proportion of the lung region in all animals post infection **(B)** The cavity specific zone (-1024 to -917) increases only when cavities occur (in 6 animals at day 21 and all 12 animals by day 28). **(C)** By combining cavity and consolidated disease zone scores, a single metric of total affected lung by volume, which is normalised by inflation pressure per individual animal, is generated. The volume of diseased tissue as a proportion of total lung volume is maximal by day 35, having shown significant and substantial increase over the preceding 14 day period. *(Statistics calculated using repeated measures ANOVA with Tukey post-comparison test*).

As expected, progressive infection is associated with progressive change in quantifiable CT observations. Importantly, these measurements may be useful for investigating changes after administration of therapeutic interventions.

3.7.2. Gross pathology correlates with *in vivo* imaging and is associated with bacterial burden

Breath-hold CT observations correlate very closely with gross pathology observations, and also with bacterial burden (figure 29). Infiltrative pathologies are seen in both the scans and photographs at the experimental endpoints. More than 99% of the bacterial burden is located within the lobe containing the cavity (figure 28 and 29). Interestingly, bacterial dissemination to the spleen were observed in 5/6 animals at day 35 and only 1 animal sacrificed at day 42. This fits with the proposed concept of early bacterial dissemination put forward by Volkmann *et al.* (111). The reason for clearance for these early disseminated organisms by week 7 is unclear. This may indicate a change in immune status from a situation in which bacterial dissemination to the spleen can occur, to a situation where this dissemination is prevented. There was no concordance between pulmonary and splenic bacterial burden.

Figure 29A

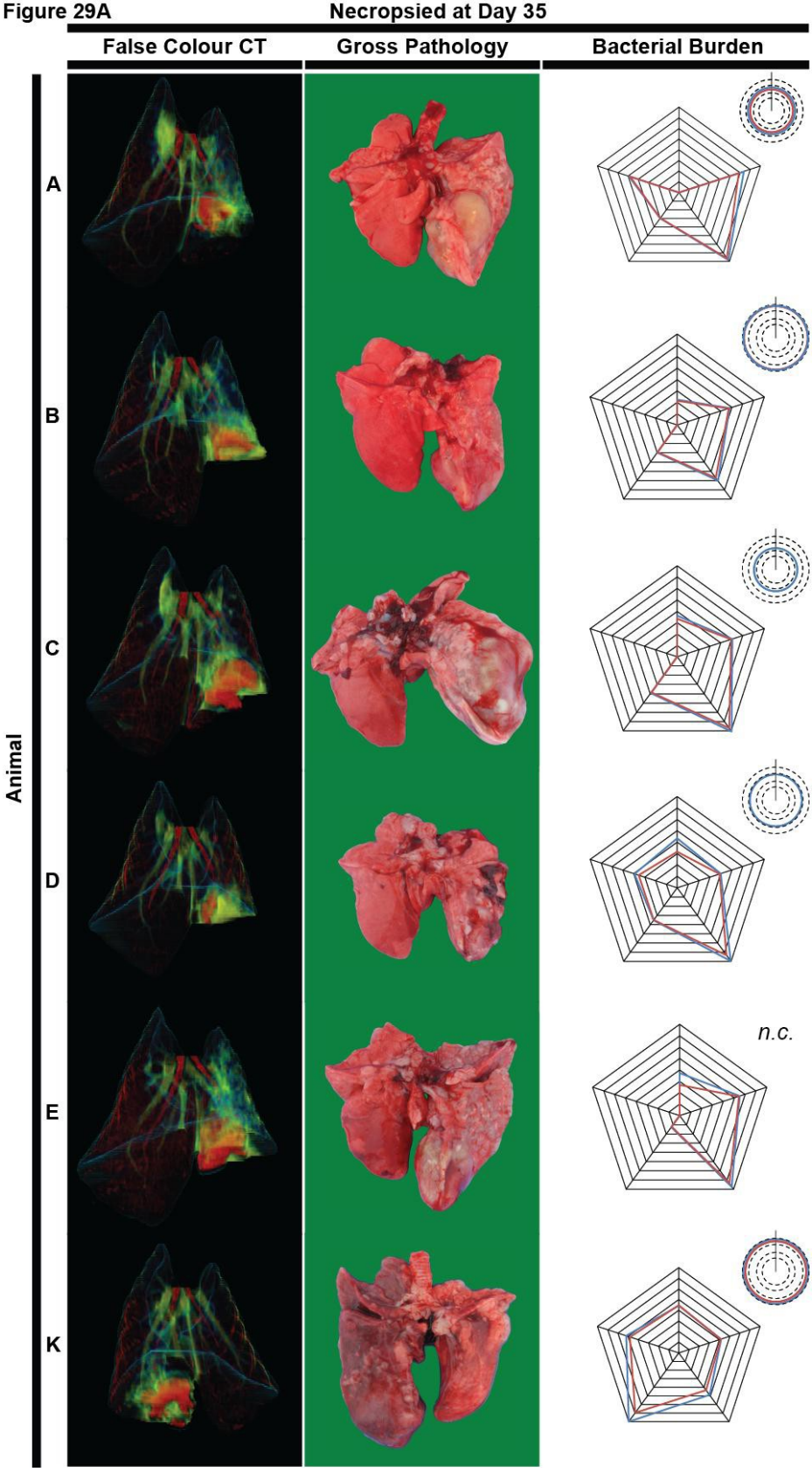
Necropsied at Day 35
False Colour CT
Gross Pathology
Bacterial Burden
Animal
A
B
C
D
E
K
n.c.

Figure 29B

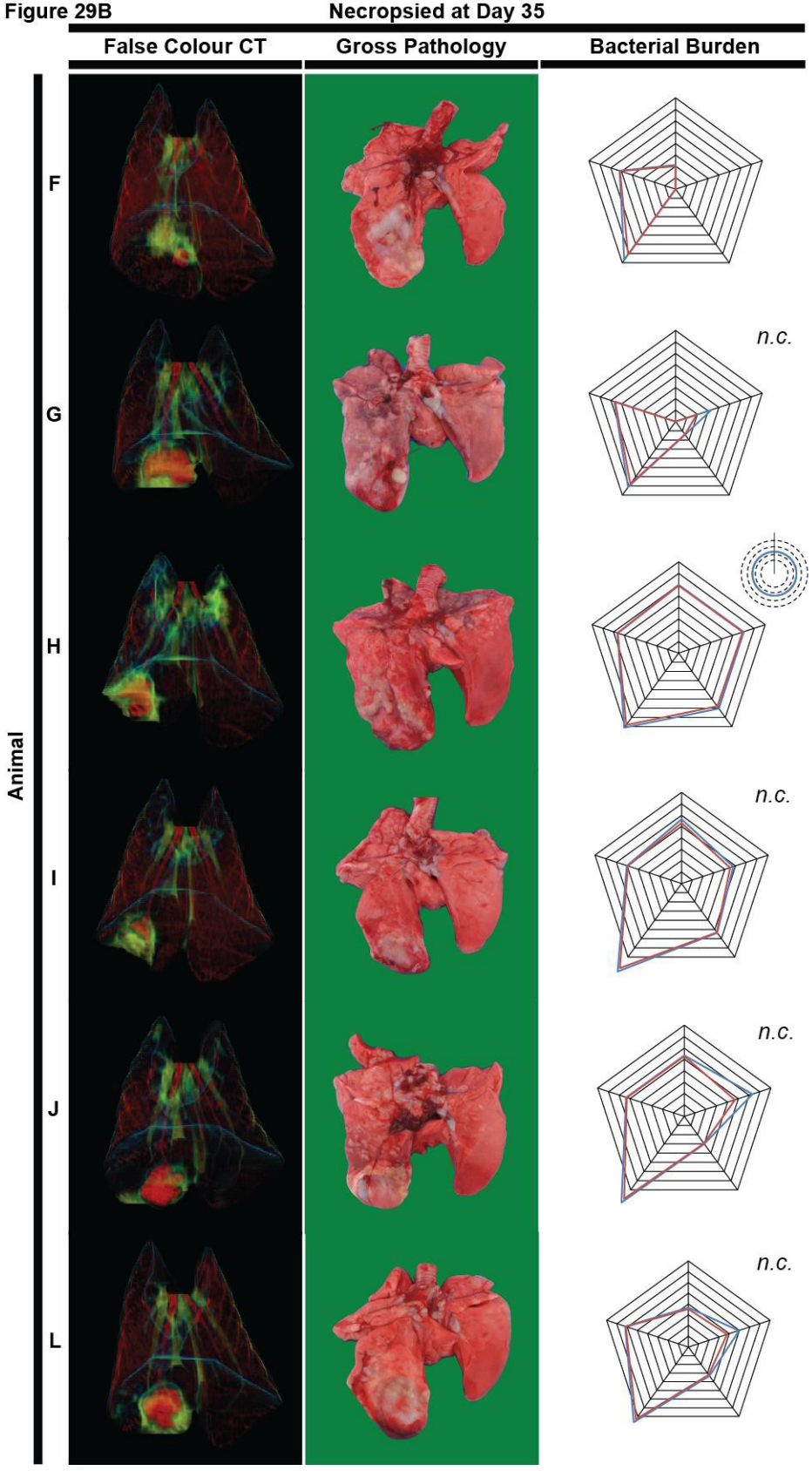
Necropsied at Day 35
False Colour CT
Gross Pathology
Bacterial Burden
Animal
F
G
H
I
J
L
n.c.
n.c.
n.c.
n.c.

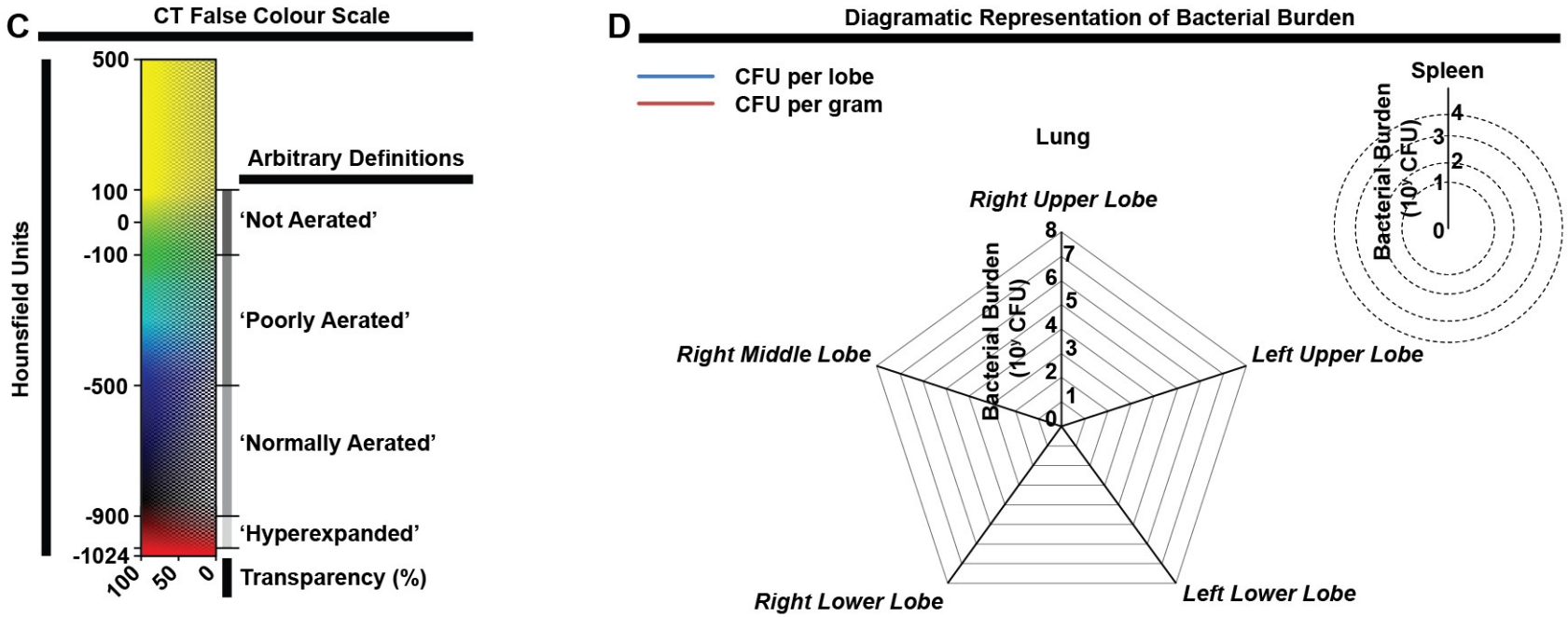

Figure 29. CT observations correlate with gross pathology and CFU data: (A+B) Pathology as observed by CT correlates to gross pathology, and bacterial burden, an explanation of the diagrammatic representation of bacterial disease is shown in (D). **(C)** The legend for false colour CT reconstructions. This scale highlights regions of consolidation (-100 to +100HU green to yellow) and low attenuation i.e. cavities or hyperexpansion (-1024 to -900; red). **(D)** The legend for diagrammatic representation of bacterial burden in A. Each spine represents a lobe, and each gradation along that line away from the centre is a log increase in bacteria burden. Red lines are calculated CFU per gram, and blue lines represent CFU per lobe. Splenic burden is shown by plotting a circle with a radius which is representative of the logarithm of the CFU cultured. *Threshold of detection ~20CFU. (n.c. none cultured).*

3.7.3. Bacterial burden in the affected lobe is highly concentrated at the cavity surface

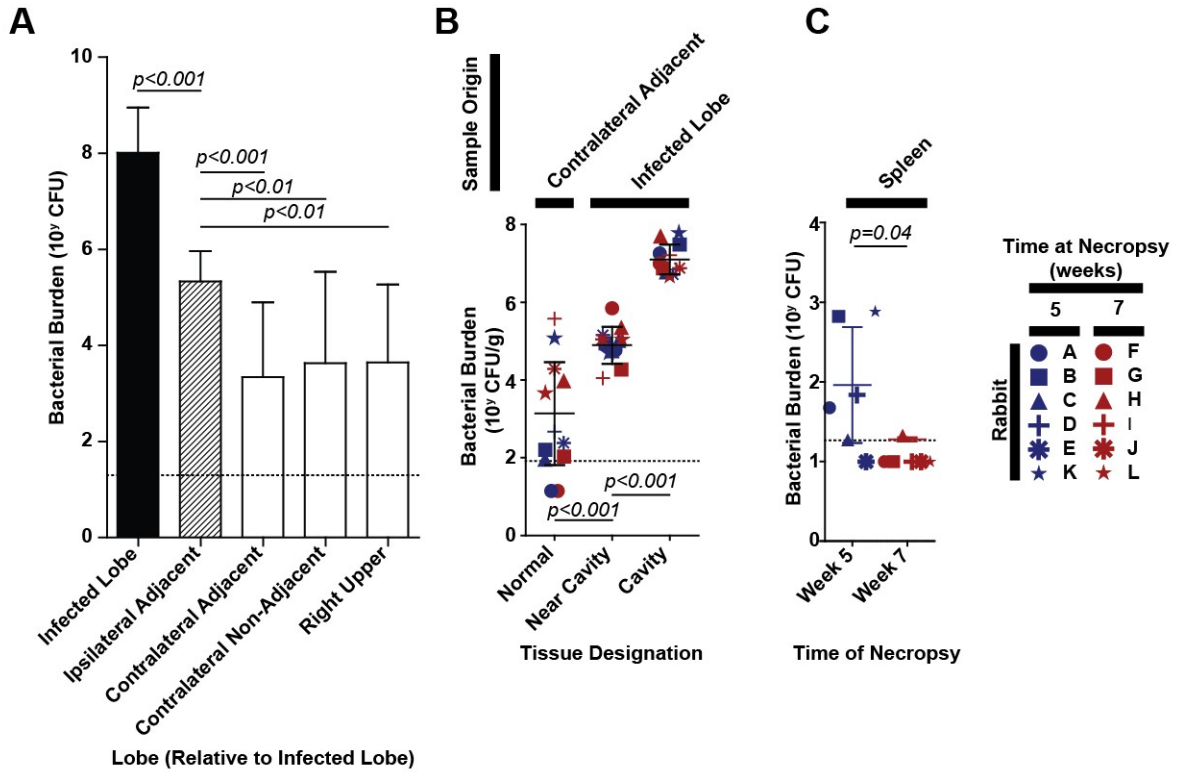

Figure 30. The distribution of bacterial burden in cavitary rabbits: (A) Distribution of bacteria within the lungs of infected animals by site in relation to site of infection. The infected lobe contains the vast majority of the bacterial burden, the lobe with the next highest bacterial burden is the lobe most closely associated with the infected lobe - the ispsilateral lobe adjacent to it. **(B)** 3mm Punch biopsies (x6 per animal) were taken from the grossly visible pathologies within the lung. Cavity wall biopsies demonstrate that the vast majority of the bacterial burden in the infected lobe is found at the cavity wall itself, as opposed to the tissue surrounding the cavity but from the same lobe. The regions adjacent to the cavity still contain considerable burdens of bacteria (10^4-10^6), however, this represents an approximately 150 fold reduction from the burden in the cavity wall itself. In comparison normal tissue excised from the contralateral lobe contained far fewer bacteria then the regions adjacent to the cavity. *The limit of detection in these assays was calculated to be $10^{1.9}$ CFU per sample and statistics were calculated by one-way ANOVA with Tukey multiple comparisons post-test.* **(C)** Bacterial burdens in the entire spleen were calculated by homogenising >90% of the organ by weight and plating 5% of the final volume. Bacteria were detected in 5/6 animals at day 35 and only 1/6 at week 7. The burdens were significantly different *(student t-test). Threshold of detection is represented by the dotted lines. Where bacteria were undetectable the threshold of bacterial burden was assumed to be equal to the threshold of detection (in place of zero CFU) to calculate statistical significance. These data are plotted below the threshold of detection in the graphs.*

Biopsies from the affected lung lobes were taken. These were used to assess the bacterial distribution within the affected lobe. This demonstrated that the vast majority of the bacterial

burden in the affected lobe was present at the cavity surface and not in the surrounding inflammatory tissue (figure 30).

3.7.4. Histopathological analysis demonstrated human-like disease, including high bacterial burden within the cavity, granuloma formation and erosion into the airways

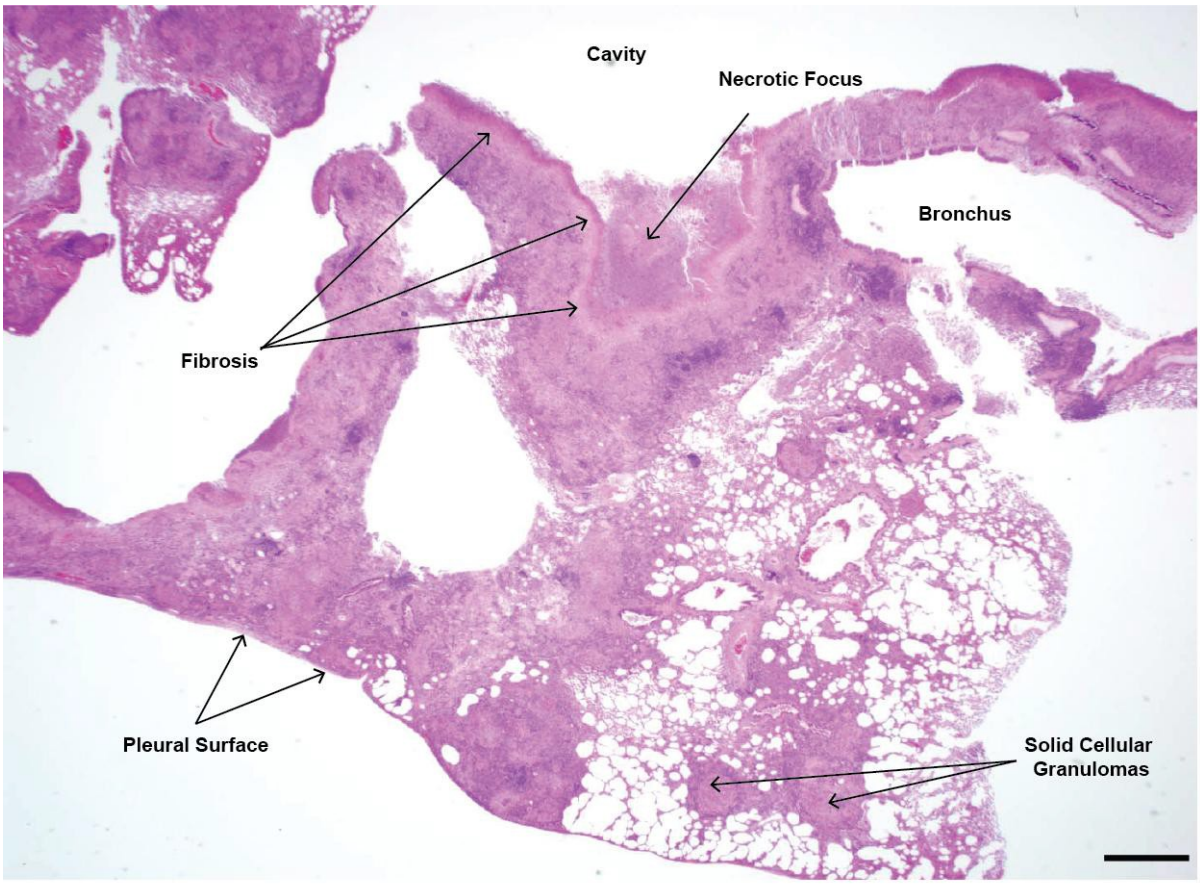

Figure 31. Haematoxylin and eosin stained section demonstrates multiple human-like TB pathologies: The Cavity region surrounds and is contiguous with the bronchus. Adjacent to the bronchus, the epithelium is denuded and the bronchial wall is necrotic. Cellular debris is present in the airway lumen. The cavity contains a central core of necrotic cellular debris surrounded by a loose fibrous capsule. Distal to the cavity, there are numerous variably-sized solid cellular granulomas that often coalesce to form extensive areas of granulomatous pneumonia. *Scale bar = 1mm.*

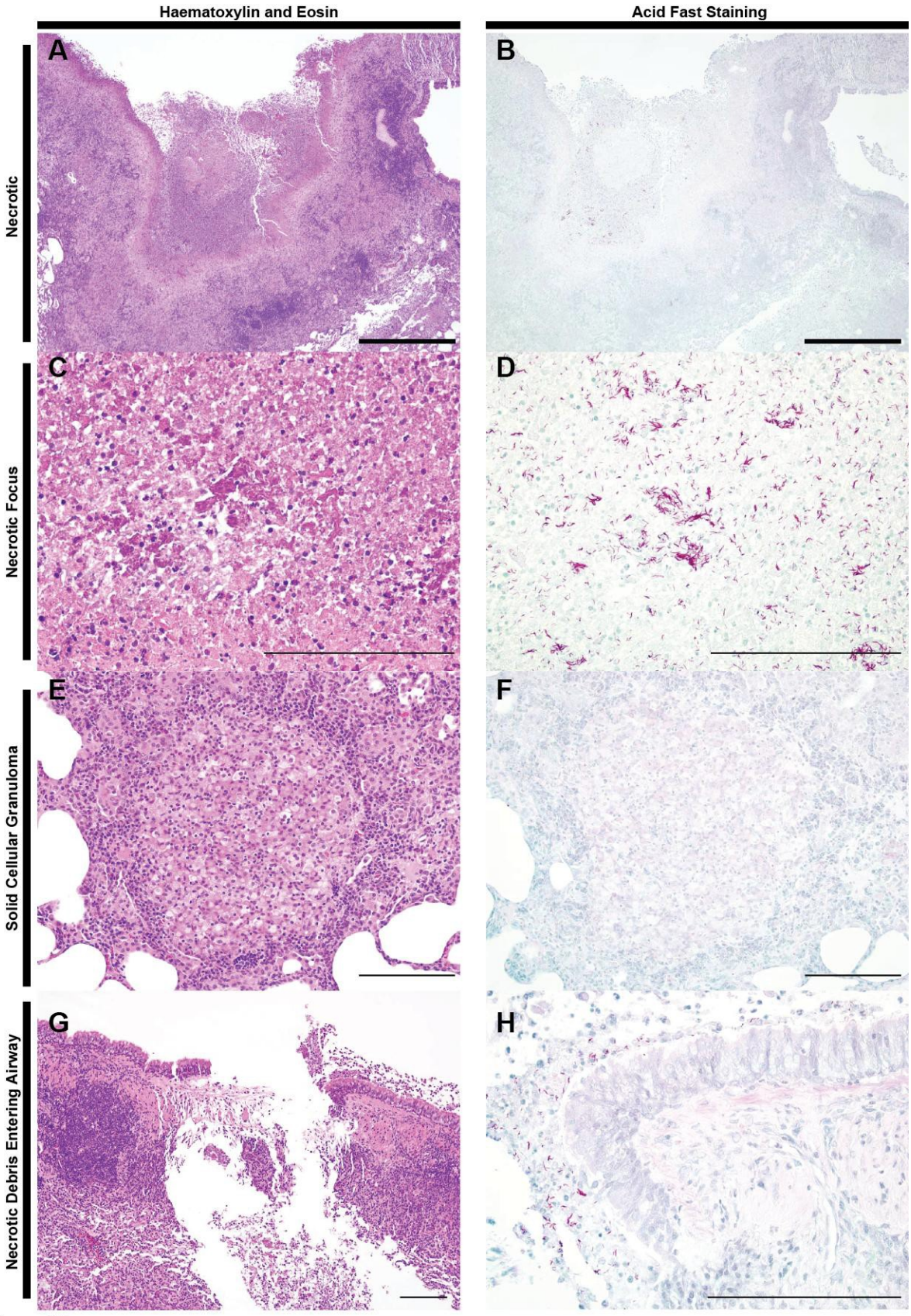
Haematoxylin and Eosin
Acid Fast Staining
Necrotic
Necrotic Focus
Solid Cellular Granuloma
Necrotic Debris Entering Airway
A
B
C
D
E
F
G
H

Figure 32

Figure 32. Haematoxylin and eosin stained sections demonstrates multiple human-like TB pathologies: **(A-D)** The edge of cavity showing a large area of caseous necrosis surrounded by a rim of fibrosis (pale pink border); large numbers of acid fast organisms are present within the necrotic debris. **(E-F)** Small solid granulomas consist of a core of large, foamy appearing macrophages surrounded by a thin rim of lymphocytes admixed with few heterophils. Only rarely are organisms seen within these granulomas. **(G-H)** In this area of the bronchus, the epithelium is denuded and the bronchial wall is necrotic. Cellular debris is present in the airway lumen. Large numbers of acid fast bacilli are present within the necrotic cavitary debris and within the airway debris. *(Scale: thick bar=1mm, thin bar = 200uM)*.

Specimens taken from the regions of interest demonstrated a full complement of human-like pathologies (figure 31 and 32).

3.7.5. Summary

The disease processes surrounding cavity formation in this model are similar in a number of ways to human TB. First, there is cavity development – a phenotype not reliably produced in any other model but present in the majority of active TB cases. The pathology seems to be similar to the descriptions of cavity development by RL Hunter (73); there are changes in the proximal airway (figure 25 and 26) and the cavity arises from an infiltrative lesion, with subsequent granuloma formation in adjacent tissues. There are also infiltrative changes subsequent to cavity development – indicating a dissemination event, or continuous dissemination, corresponding to cavity formation (figure 25 and 26). As in humans, there are extremely high bacterial burdens within the cavity itself, and apparent containment of disease in the rest of the animal (figure 29, 30 and 32). None of the animals lost weight during the 49 day period, and the animals appeared grossly healthy; suggesting that this extensive pathology is not highly symptomatic (in this early stage) – however, longer term studies would be required to see if disease progressed or resolved in these animals. Whether the model could be extended to explore chronic disease depends on whether these large cavities can sustain infection in a host which is globally resistant to infection.

Although the model is highly artificial, it is as a result highly reproducible. The immense power that *in vivo* imaging adds in the form of virtual necropsy is only briefly touched on here, although the correlations are remarkable. It is clear from these studies that this technology means that relatively

small numbers of animals could be used to examine how therapies can affect cavity development and associated disease progression, and also how current and novel therapies act in this environment and how this action is involved in the development of resistance.

This model uniquely recapitulates the most common form of active tuberculosis which is disease in the immunocompetent individual with global immunity to *M. tb* but local immune failure.

4. Novel Technologies for Assessing Pathology in Rabbits

There are a number of challenges involved in working with rabbits (170). Not least amongst which is the expense and technical expertise required to work in this model. Whilst the methods described below are largely based on methods that previously existed, each required special adaptation for use under BSL-3 conditions and some are entirely conceptually novel within the field. This chapter aims to provide the reader with insight into how the methods used in section 3 and 5 were developed, and also act as a reference for future model users.

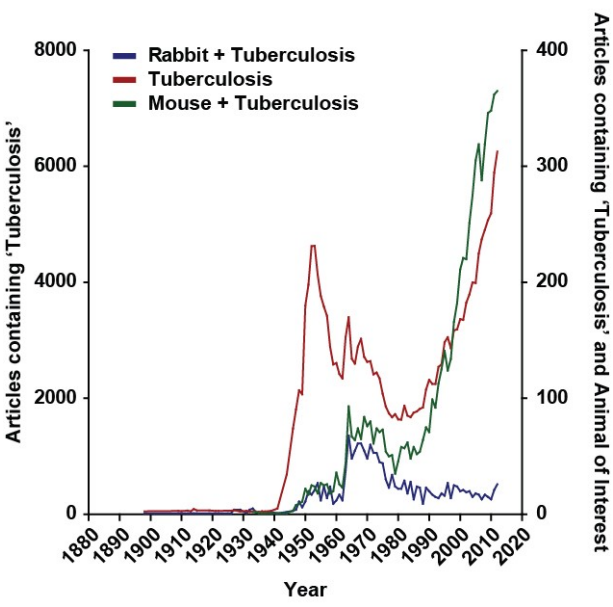

Figure 33. PubMed articles relating to tuberculosis and rabbit usage shows the fall from favour of the rabbit model: Using the results by year tool on PubMed (www.ncbi.nlm.nih.gov) gives an impression of the increased relative use of mice and reduction in the use of rabbits for TB research. 'Tuberculosis' containing references are plotted against the left y axis (red line), and of these the number containing rabbit (blue line) and mouse (green line) are plotted against the right y axis. Rabbit research declined with all tuberculosis research during the 1970s, but never increased when interest in the field was renewed in the late 1980s.

The rabbit has fallen from favour in tuberculosis research (figure 33), despite its obvious relevance to human disease (74, 75, 155). The reasons for this become clear when you consider the scale of performing a drug study in these animals: Prior to beginning this thesis, a study proposed at looking at an anti-cavity therapy would require a model in which 100 days of infection, 39 days of sensitisation and highly variable outcomes must be accommodated for. If 3 time-points were used, and 6 animals per treatment are required, 36 animals would be needed. Each animal weighs 3.5 to 5kg and this means that a study requiring 10mg/kg of drug would require at a minimum of 72g of

drug for just these 18 data points. An equivalent sized study in mice would require only 360mg of drug – i.e. the same volume of drug would allow for 200 times more data points. This is without including the tribulations of animal housing, reagent and tissue storage and the scheduling of studies. Rabbit studies are both logistically difficult to manage, but also costly and technically challenging. With no promise of positive results, they are also a daunting investment of time and money for academics.

This chapter outlines how the use of simple technologies, applied to the model described in the previous chapter, can be used to simplify rabbit research, putting it in reach of more investigators. This is achieved by describing methods which can be used with limited technical expertise and commonly available resources. The biosafety element of working with pathogenic *Mycobacteria* species is foremost in the design of the strategies developed. Some investigations into the infectiousness of rabbits were performed, and the data presented here is indicative that these animals are minimally infective, however, it must be noted that the studies were performed in a manner aiming to quantify whether culturable bacilli were exhaled under normal conditions, and do not exclude the potential risk of infection.

4.1. Delivering a reproducible infectious inoculum:

Although simple, aerosol infection techniques are not reproducible. For each aerosolised infectious delivery in mice, 5 mice are required to evaluate what the infectious bacterial burden in any given experiment is. This is because machines such as the commonly used glas-col nebuliser, are variable in their ability to aerosolise and distribute bacteria.

Following from Nedeltchev *et al.* (168) we utilised a bronchoscopic infection technique (also used by Lewinsohn *et al.* for infection of cynomologus macaques(192)). A known volume of bacteria are delivered under direct bronchoscopic guidance to the lower lobe of the lung. To confirm that this method is a reliable, a study was conducted to evaluate both the volume of liquid delivered in this manner as well as the bacterial number (figure 34). This study established that bacterial delivery via simple catheters made from luer-stubs and TE-50 tubing could be used to deliver measured amounts of bacteria.

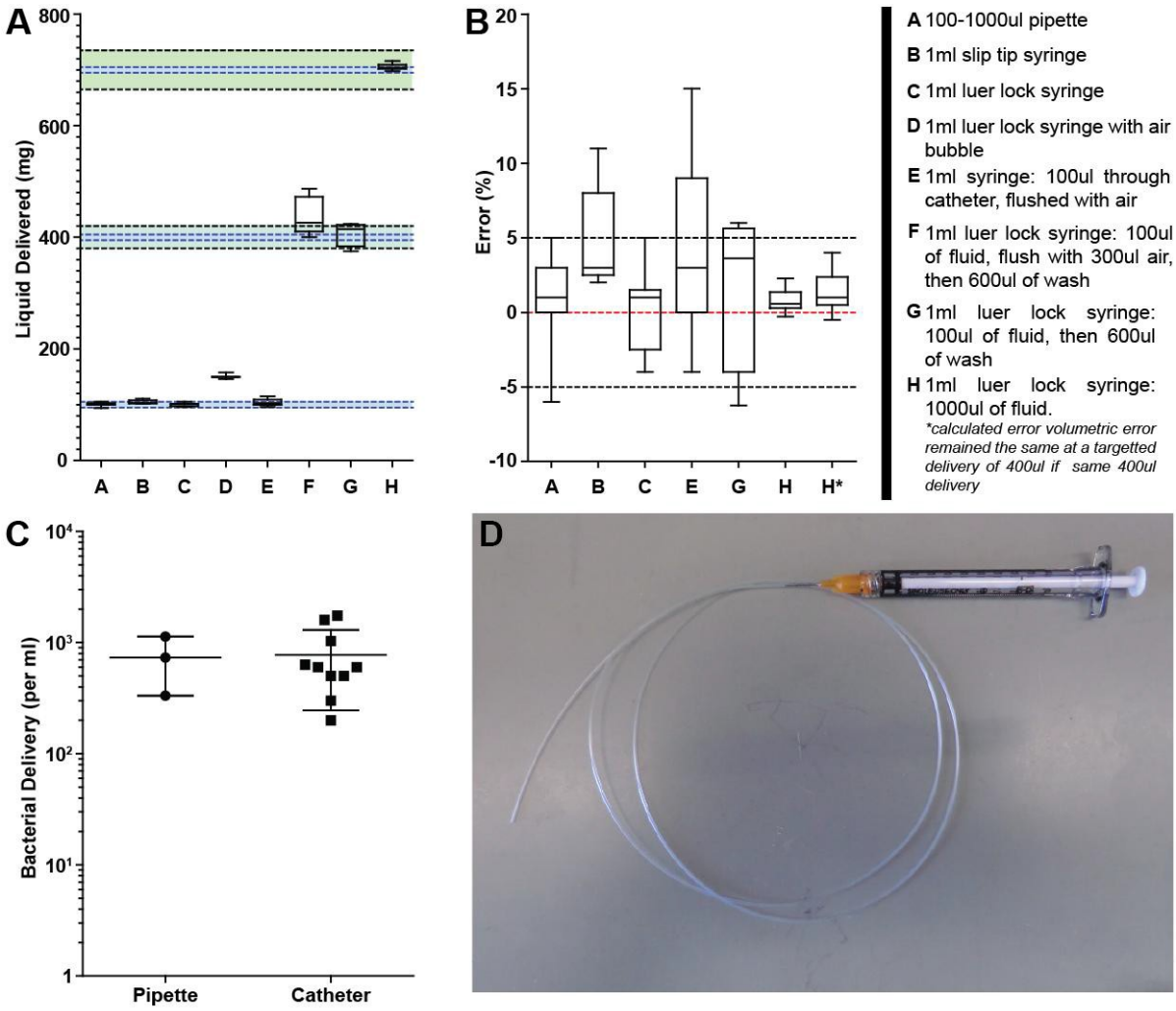

Figure 34. Inoculum delivery via a catheter is highly reliable: In order to determine if the technique being utilised to deliver the infectious inoculum was accurate, a series of tests were performed comparing the delivery of liquids with various syringes and catheters and a 100-1000 ul pipette. **(A)** The syringes performed equally well to a pipette in delivering various quantities of liquid onto a microbalance. The Luer lock syringe appeared to produce a smaller variance than the slip tip syringe, and was then utilised to compare the delivery of liquids through the catheter. Of the 4 scenarios tested, delivery of a known volume through an air free system outperformed any permutation of flushing with air or a secondary liquid 'wash'. *Blue dotted lines represent +/-5ul and black dotted lines represent +/-5% errors. Error bars represent range and boxes interquartile range. 10 repeats of each measurement were made. A-E target 100ul, F-G target 400ul, H target 700ul.* **(B)** The percentage error for each technique was calculated - this demonstrates clearly the reduced error in using an air-free syringe catheter system for delivery. The error in the delivery of 400ul of liquid is less than +/-5%. *Midline represents the mean with whiskers representing the range. Red line indicates target value.* **(C)** The air free catheter technique was tested for delivery of the inoculum into PBS which was subsequently diluted for plating on 7H11 solid agar. The system had a similar error to direct pipetting of bacteria. *Error bars represent standard deviations.* **(D)** Photograph of catheter system containing Luer lock syringe, Luer lock stub and catheter tubing.

4.2. Arterial line for blood sampling

Blood is the most readily available fluid in clinical settings, it is routinely taken for diagnosis and monitoring of a huge number of conditions and changes in composition indicate the immune, chemical and physiological status of the subject. In rabbits, blood is taken from either the marginal ear vein or central ear artery. Many researchers utilise blood withdrawal techniques with no anaesthesia. In our experience, this is highly stressful and painful to the animal and results in unknown effects on the animals' physiology. Complete anaesthesia easily facilitates blood withdrawal and volumes of up to 20-30mls. This volume is appropriate for complex analysis such as flow cytometry. Anaesthesia is an appropriate solution if the animal is sedated for other reasons (for example imaging procedures); however, wherever possible it is preferable to avoid the potential complications of anaesthesia or the confounding effects of anaesthetic drugs. Additionally, during pharmacokinetic studies repeated samples must be taken, and so a method for repeated withdrawl without repeated needle sticks was developed. This method allows for an indwelling ear catheter which we have maintained for 72 hours with no significant signs of ear damage or inflammation.

The animal is anesthetised using ketamine, xylazine and acepromazine (as per methods). The ear is shaved and sterilised. Using a standard 22 gauge IV catheter, the central auricular artery is canulated. At this time blood can be retrieved. The hub of the catheter can then be capped using a Clade device. Blood can be drawn through the device, and if warranted a heparin lock can be placed. For prolonged placement, heparinisation is suggested – this is challenging as rabbits metabolise heparin rapidly (193). The catheter can be secured in place and kept from the conscious rabbit by securing the ears to each other. When blood withdrawal is required the first 1ml can be drawn and discarded to remove any residual heparin, and a second draw is then made of the required volume whilst the animal is lightly restrained. Covering the eyes of the animal can facilitate placement in a non-anaesthetised animal.

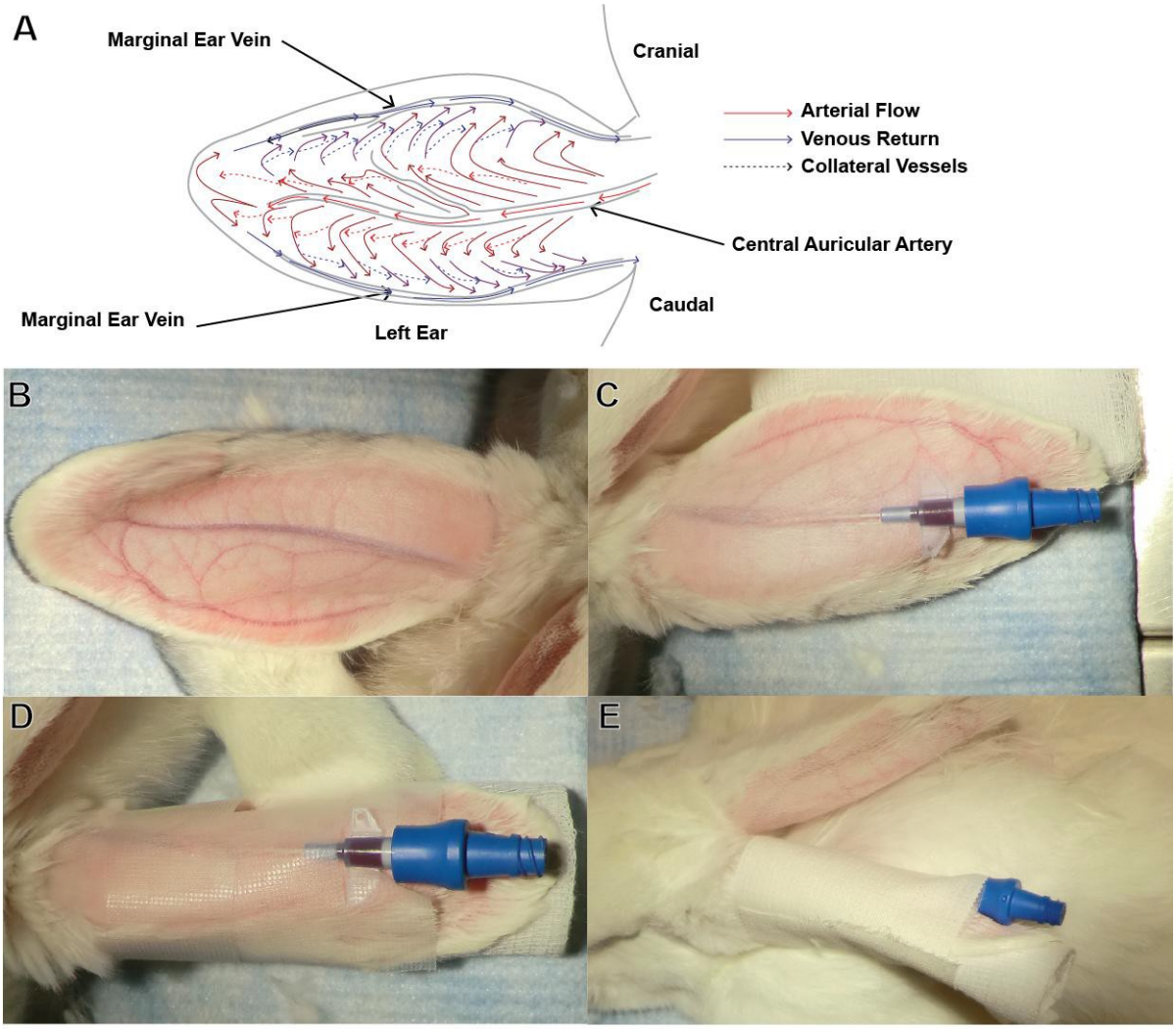

Figure 35. Placement of an auricular arterial catheter: (A) Rabbit ear anatomy. The artery is centrally located and blood flow is from this central artery to the peripheral veins. There is a good collateral supply so obstruction of the vessels can be tolerated. **(B)** The ear is prepared by shaving the entire surface and disinfecting with 70% ethanol or clinical disinfectant such as betidine. **(C)** The canula (22 gauge 3/4 inch in length) is inserted at a shallow angle (15°), taking care to ensure the finger tips are distal to the catheter tip. After fully inserting the catheter, the sharp is withdrawn and disposed directly into a sharps container. Light pressure applied to the artery proximal to the canula can prevent excess bleeding. At this point a syringe can be used to draw blood directly or a Clade device can be fitted as shown. **(D)** The catheter is then secured in place over a roll of gauze **(E)** The canula is secured so that only the top of the Clade device is accessible. If necessary, an Elizabethan collar can be used, or the ears can be secured to each other to prevent the rabbit dislodging the catheter.

4.3. Accurate drug delivery in rabbits

Delivering accurate amounts of drug to large animals is not always a straight-forward task. A number of studies have used oral gavage. However, the physical strength of rabbits means they may injure themselves or the investigator during such procedures (194). Stress may have confounding effects during investigations of inflammation as rabbits have strong adrenocorticoid responses (195, 196). This can be controlled for by sham treating control animals, but may add a complicated variable to experiments. Syringe feeding has been also been used to treat animals, but is only appropriate when unpleasant tasting drugs can be masked by fruit flavourings or sweeteners. Accurate delivery of drug is challenging when syringe feeding, as there is no guarantee that the entire amount of drug will enter the oral cavity, or that the animal will swallow it. A further problem with oral drug administration is that antibiotics are reported to have dramatic effects on the gut flora, and as a result, bacterial overgrowth syndromes are common in lagomorphs (197).

The following strategies were developed:

i) Nasogastric tube placement; for accurate delivery of oral drug doses (figure 36)

ii) Peripherally Inserted Central Catheters (PICC); for long-term IV drug delivery (figure 37)

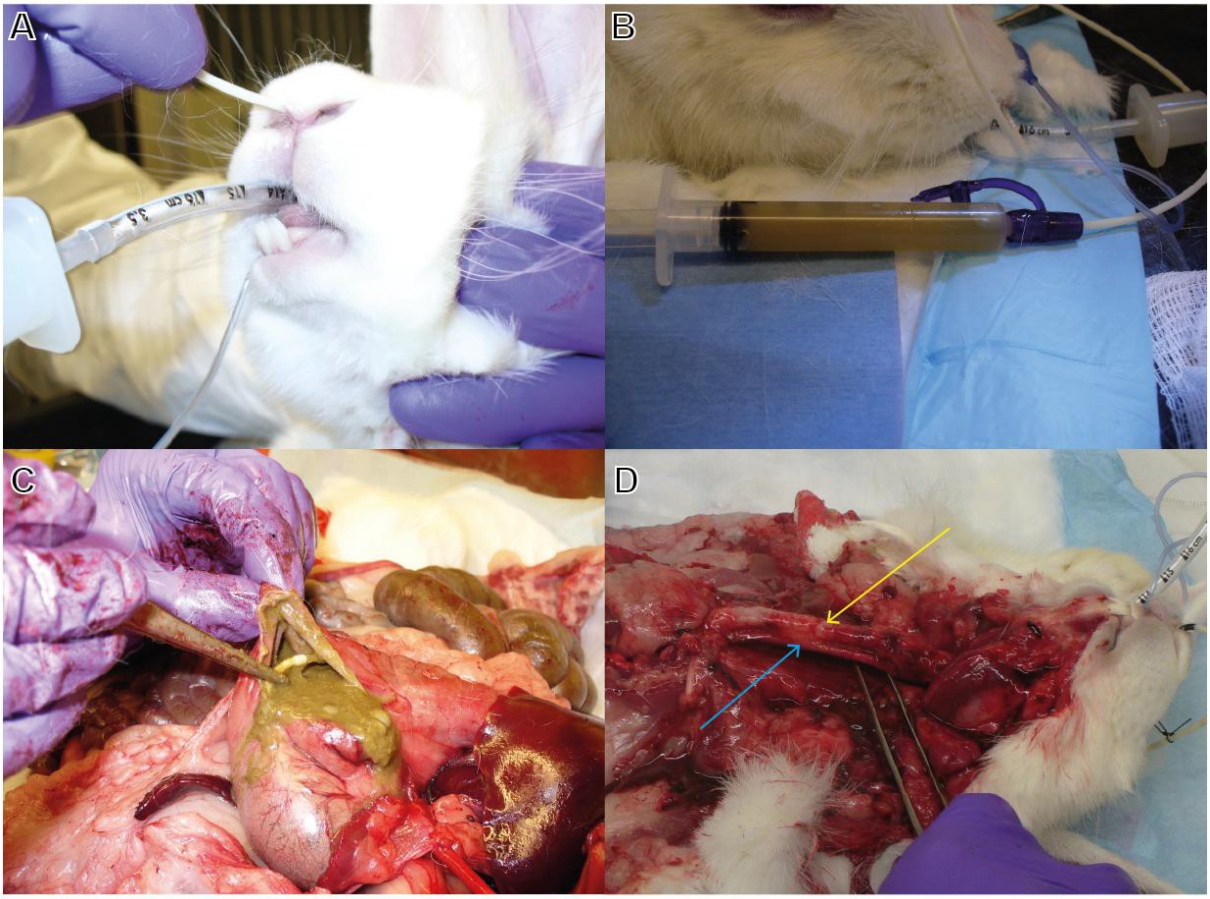

Figure 36. Nasogastric (NG) tube placement in the rabbit: (A) Endotracheal tube placement is necessary to ensure oesophageal placement of the NG tube in an anaesthetised rabbit. An 8-French NG tube is lubricated with a water-based lubricant and then placed into the nare of the rabbit, placement is facilitated by inserting the tube upwards towards the roof of the nasal cavity. **(B)** After advancement (the distance from the tip of the nose to the lowest rib is appropriate) placement is confirmed by aspiration of stomach contents, this can be challenging and so flushing with 15ml of water may be required. **(C)** Correct placement in the stomach confirmed at necropsy. Note at the bottom right of the image that the diameter of the NG tube is places tension on the oesophagus. **(D)** Rabbits can continue to feed with the NG tube in place, however, long term placement (3-days or more) caused discomfort and the rabbits became lethargic and withdrawn. (Yellow arrow shows the endotracheal tube in place, the blue arrow indicates the position of the nasogastric tube).

Two animals underwent nasogastric (NG) tube placement, as described in (198), except that placement was performed under anaesthesia. The animals were monitored for 48-72 hours. NG tube placement appeared highly distressing for the animals; they became lethargic, hunched and ungroomed. Faecal output was reduced, as was dietary intake. 1 tube blocked after 48 hours despite regular flushing with water. The use of smaller tubes may reduce the stress of placement, but are more liable to blockage. This method may be suitable for accurate oral drug delivery in the short

term (24-48hours), but longer term placement is inappropriate. This method may allow for accurately timed and volumetrically reproducible oral dosing for PK studies. Some articles suggest repeated gavage using this technique is feasible, however, our experience calls into question the broad application of this technique (194, 198).

Since IV delivery is the most reliable manner in which to deliver accurate levels of drug, studies were conducted to assess the ease of placement of peripherally inserted central lines – a technique which has been shown to be feasible but costly (199). Utilising commercially available fine tubing, a simple catheter stud, and a through needle delivery system we generated a simple, safe and clean technique for placement of central line catheters in rabbits (figure 37).

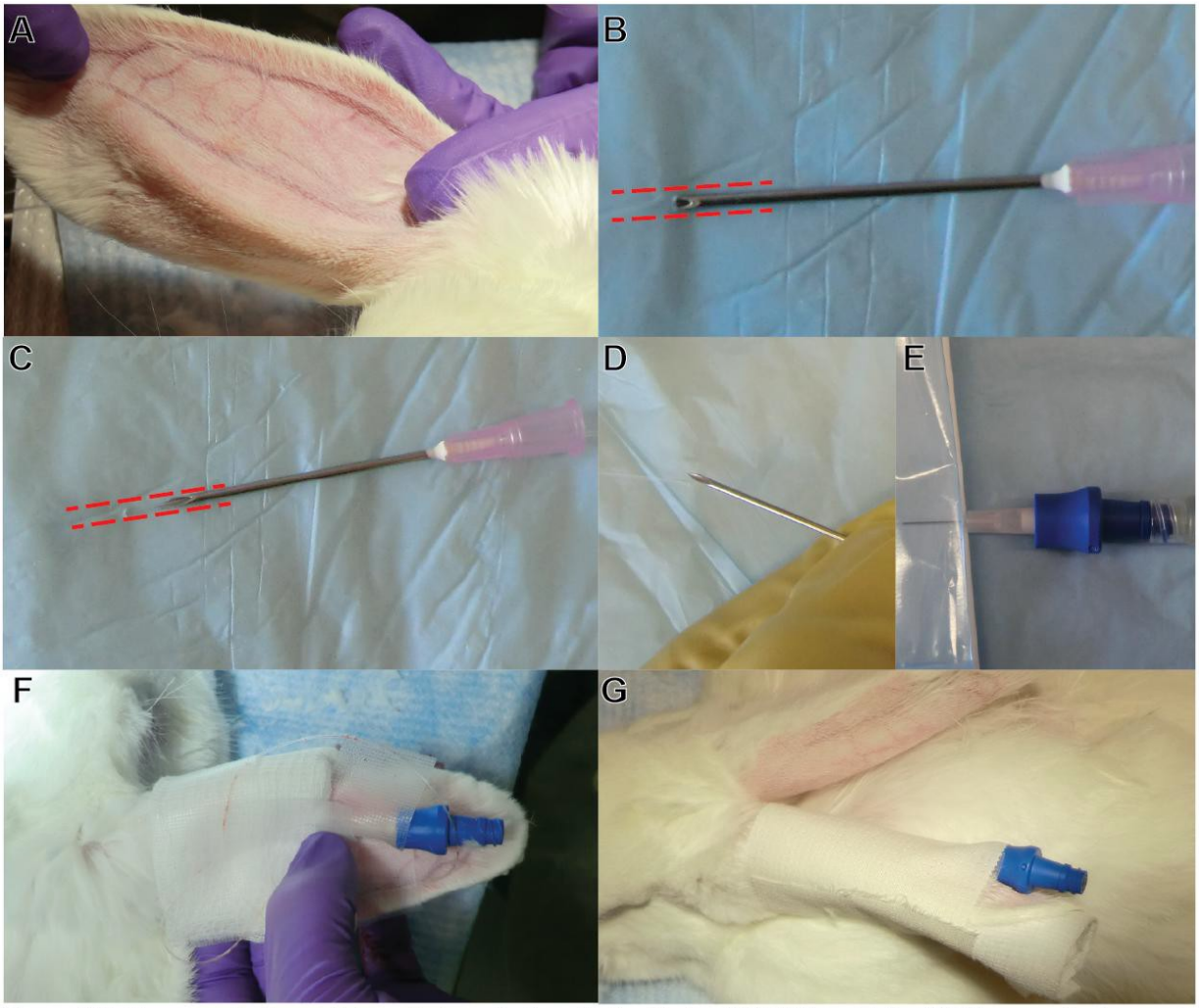

Figure 37. Placement of a peripherally inserted central catheter (PICC) in rabbits: (A) The marginal ear vein is manually dilated by obstruction the proximal portion and sterilised with betadine, and sterile technique should be used for the remainder of the insertion. **(B)** An 18G needle is used to guide the catheter into the ear vein. **(C)** A preheparinised catheter (30cm) is advanced to a depth of 25cm. **(D)** The 18G needle can be removed. **(E)** The catheter stub is put in place, with heparinised Clade attachment. Blood is drawn back until visible to confirm placement, and also to ensure complete removal of air bubbles. A heparin lock is then applied. **(F)** The catheter can be secured with tape, ensuring that there is some slack within the line which allows visualisation of blood withdrawal and flushing.

2 rabbits underwent PICC line placement as described above, alongside simultaneous arterial catheterisation. The PICC lines remained patent for 72 hours and allowed for hazard free administration of heparinised saline. We also demonstrated that if necessary blood could be drawn from the PICC line – however the fine gauge of the line is liable to cause haemolysis, and so this may not be a suitable method for blood sampling in some conditions.

4.4. Urine withdrawal techniques

Urine is perhaps the most easily available sample in the clinical setting, and so has great potential as a matrix from which to extract biomarkers. It is also a convenient sample to handle, although its high salt content often means sample processing is required prior to assessment.

Using a technique adopted from (170) manual urine can be reliably achieved. An anaesthetised rabbit is placed in dorsal recumbence, the bladder is manually palpated by identifying the pubic synthesis and moving in a superior direction (usually about 5-10cm). By applying a firm constant pressure from the superior aspect of the bladder in the direction of sacrum, urine can be expelled and collected in a 50ml conical tube (figure 38). On average between 1-5mls can be consistently collected, and often as much as 20mls is easily available.

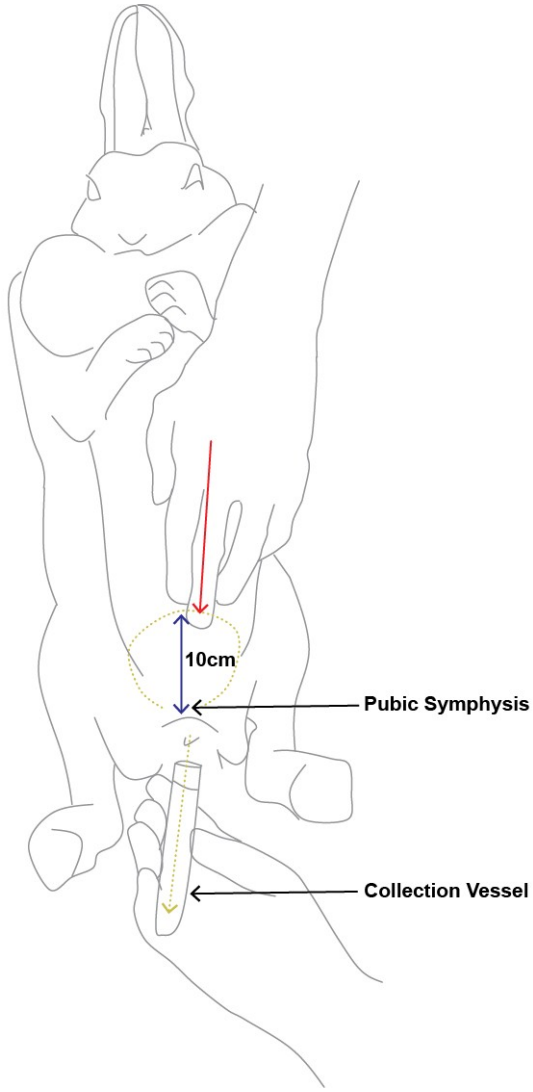

Figure 38. Manual urine expression in rabbits: Urine is expelled from the bladder (dotted line) of an anaesthetised rabbit by placing firm pressure (red arrow) from the apex of the bladder in the direction of the sacrum. The bladder apex can be palpated approximately 10cm above the pubic symphysis. Urine can be collected in a receptacle, and if mid stream urine is required, the initial 1ml can be discarded. 5ml can be consistently collected, although volumes of up to 150ml have been collected.

Alternatively catheterisation allows for cleaner sample collection, and more reliable delivery, but requires more equipment and time, and runs the risk of traumatic injury to the urethra (170). Metabolic cage collection protocols are also available (170), but were not necessary during the trials conducted.

4.5. Computed tomography (CT) of rabbits

CT scanning can provide high resolution structural imaging of rabbit anatomy. The information collected during CT scans of rabbits has primarily been used to correlate PET readings with structural information (such as organ position and bone structure) (165). In this context, reproducibility and detailed structural information are not important.

Since the pathologies of interest in TB are often identifiable on CT scans – use of CT to assess pathology in a longitudinal manner was assessed. A number of challenges had to be overcome in order to achieve accurate, reproducible and comparable scans:

i) Breathing artefact: CT scans utilising the clinical scanners commonly available in hospital settings take anywhere from 4-20 seconds to cover a 20cm window (approximately the size of the inflated rabbit lung); during this time both cardiac and respiratory motion can cause movement artefacts within the images. Rabbits average between 30-60 breaths per minute, and so there is nearly always motion present within scans.

ii) Lack of normalisation: Even if the motion artefact were prevented, a problem in comparing the scan from one time point to the next arises because the period of the breathing cycle during which the scan is taken may be different.

iii) Scanning of BSL-3 pathogen infected animals: The majority of researchers do not have access to expensive scanning machinery in dedicated BSL-3 facilities; however, it is becoming increasingly common to have scanning facilities in adjoining BSL-2 facilities or machines that are accessible in clinical settings. In order to be financially viable, the Center for Inflammation and Infection Imaging Research (CI3R) at Johns Hopkins is a fine example of how temporary biosafety enclosures can be utilised to contain BSL-3 pathogen infected animals safely in a BSL-2 laboratory (134, 135). However, this requires that all systems are fully sealed with the exception of HEPA filtered gas exchange.

iv) Pulmonary collapse during anaesthesia. Respiratory support is not commonly used in

BSL-3 laboratory rabbit anaesthesia, due to the challenges of intubating and operating ventilator support safely in the BSL-3 environment. As a result, raised peak end expiratory pressures (PEEP) are not used. Since muscular tone is decreased during anaesthesia lung collapse occurs and can appear as consolidation (as observed during this study).

There are a number of options for dealing with respiratory motion during CT acquisition. Dynamic scanning can be used to acquire a series of low dose CT images over time, and facilitate observations of motion, or construct visual averages of moving objects. However, this requires newer generations of scanners – which were not available at the facility in which this research took place (or indeed widely available). Another option is a respiratory gating strategy, whereby scans are designed to synchronise with breathing cycles. Respiratory monitoring equipment and an interface between the scanner and monitoring equipment is required for this to occur (200). Again, such facilities were not available. Another option would be to use a ventilator system that minimised lung movement during scan acquisition, such as high-frequency ventilation, however, these systems would require development of novel protocols as well as purchase and service expenses. The use of paralytics and full ventilation could also be used, but is extremely difficult to justify in animal research, as paralytics may prevent the animal from responding if anaesthesia is insufficient – a situation tantamount to performing an intervention in fully conscious animal. Instead, the natural tolerance of rabbits for high carbon dioxide (201) was used to justify developing modified technique, previously used in infants (202) to breath-hold animals during scanning (section 4.5.1.).

4.5.1. Development of a breath-hold scanning technique for use in BSL-3 pathogen infected rabbits

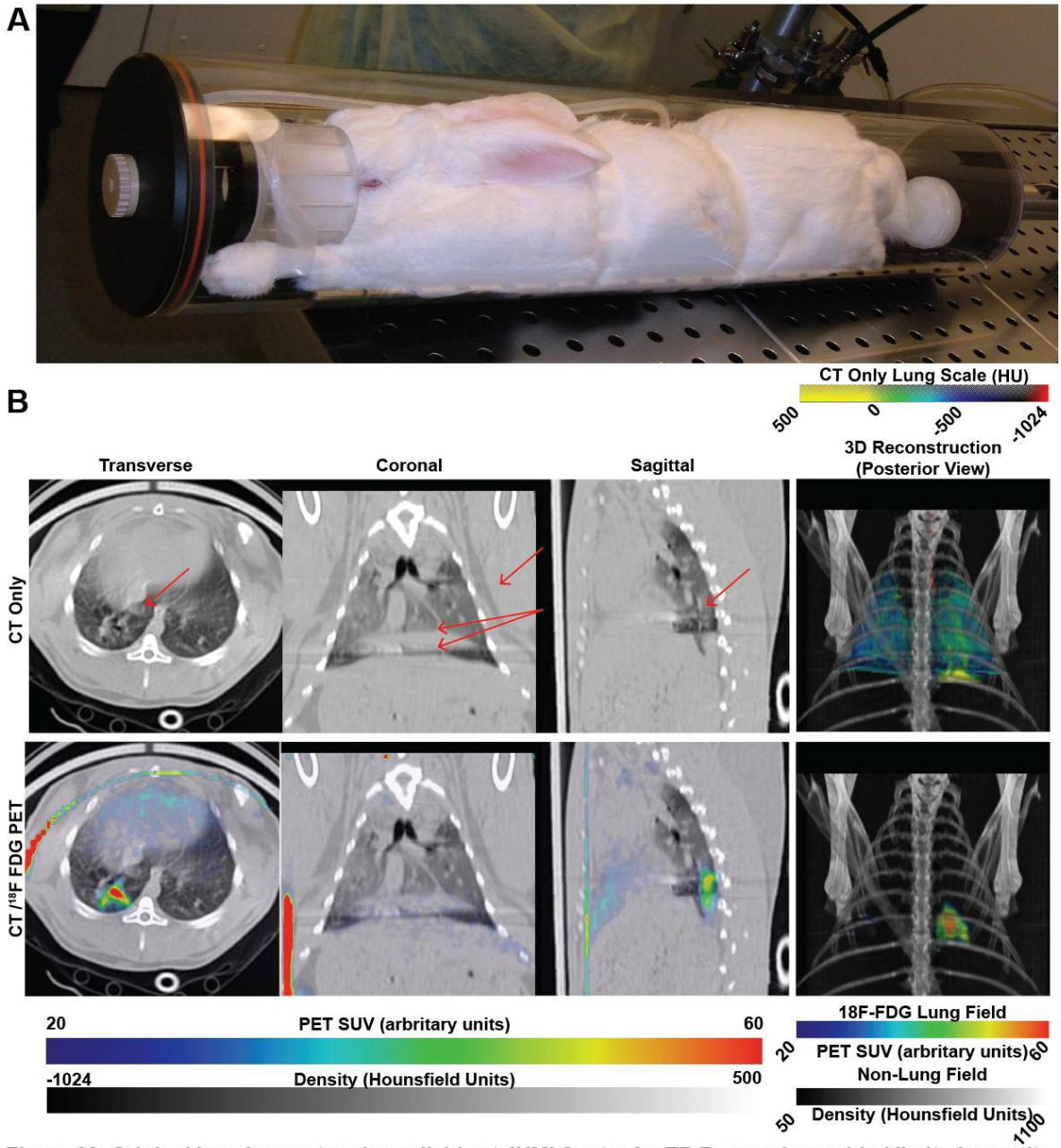

Figure 39. Original imaging protocols available at JHMI Center for TB Research provided limited quantitative data due to artefacts: (A) A custom built imaging chamber (Minerve) was purchased for the imaging of rabbits. The chamber comprised a Perspex cylinder with o-ring sealed end caps with ports for anaesthesia delivery and heated-gas. A CT/^{18}F-FDG PET scan takes approximately 60 minutes to complete. **(B)** The CT images slices demonstrated large respiratory artefact (red arrows). Co-registration of CT/^{18}F-FDG PET was achieved by manual alignment of the images. Because the PET shows positron emission over a 45 minute period, and hence the entire breathing cycle, whereas the CT image represents the lung location at one fraction of the respiratory cycle the CT/PET relationships are approximate. This is particularly troubling when attempting to distinguish pulmonary from extra-pulmonary uptake at the border of the liver and heart.

A number of ventilators which utilise either pressure or volume based breath-hold techniques are available. Two main systems, the Harvard Apparatus 'Inspira Advanced Safety Single Animal Pressure/Volume Controlled Ventilator (ASPV-IH)' and the SciReq 'Flexivent', are both suitable for the task of breath-hold ventilation, but cost $10,000 and $50,000 respectively. Additionally both systems require professional maintenance, and are not easily decontaminated using common anti-tuberculocidal products. A trial of the ASPV-IH demonstrated that breath-holding could dramatically improve image quality:

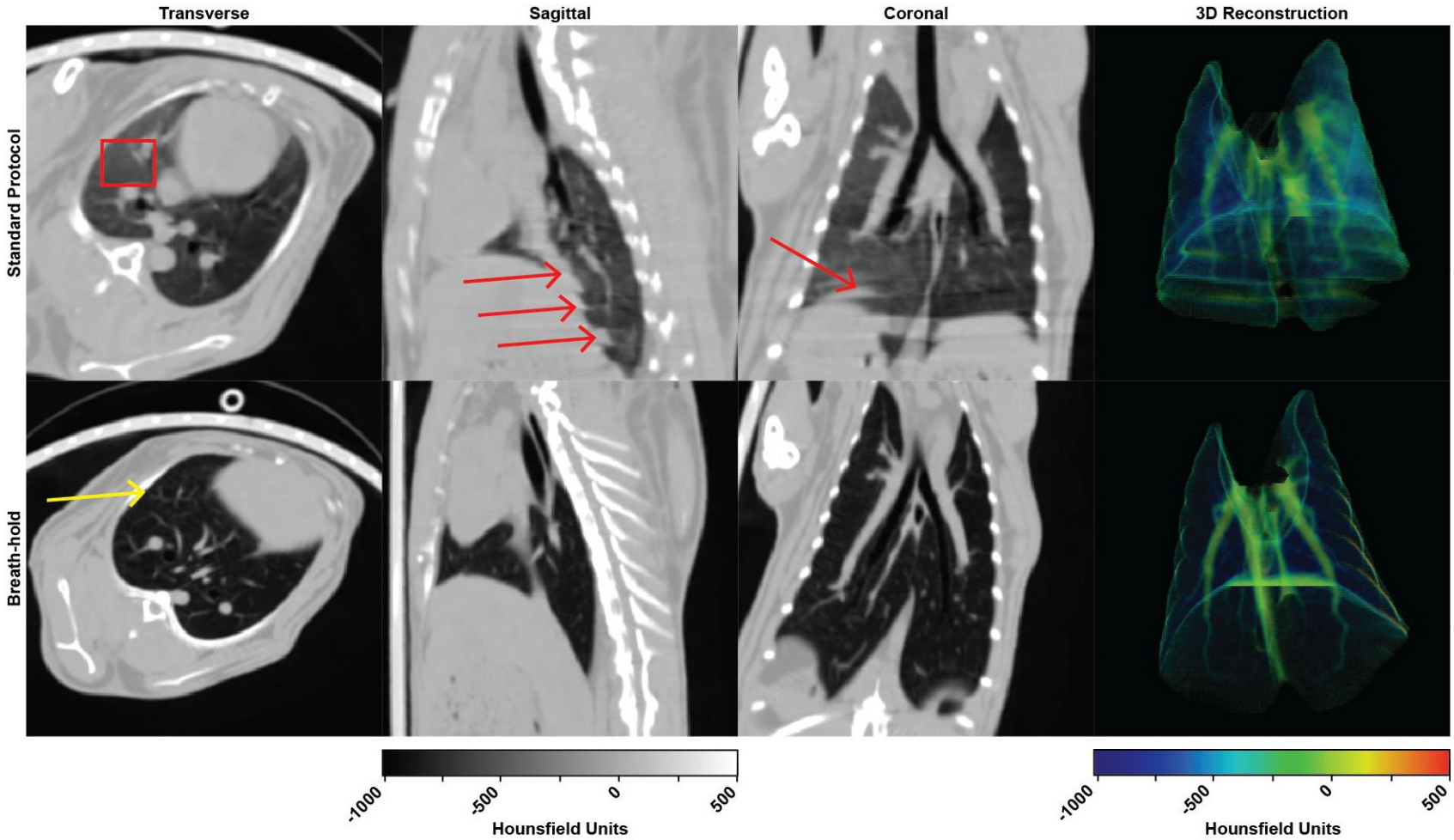

Figure 40. Breath-hold scanning vastly improves CT image quality: Using a Harvard Apparatus 'Inspira Advanced Safety Single Animal Pressure/Volume Controlled Ventilator (ASPV-IH)' we subjected a rabbit to a breath-hold scan. When compared to the standard protocol one can see an enormous improvement in image quality. Areas of blurred density (red square) are no longer present, and z-stacking inconsistencies (red arrows) are completely removed. Detailed vascular structure was revealed.

On the basis of the quality of image provided it was apparent that breath-hold imaging could vastly improve identification of structures and had great potential. Unfortunately, the commercially available system could not be modified in a manner which allowed safe ventilation of BSL-3 pathogen infected animals. A custom built bio-container which allowed for manual breath-holding at set pressures was designed and manufactured (figures 41 and 42).

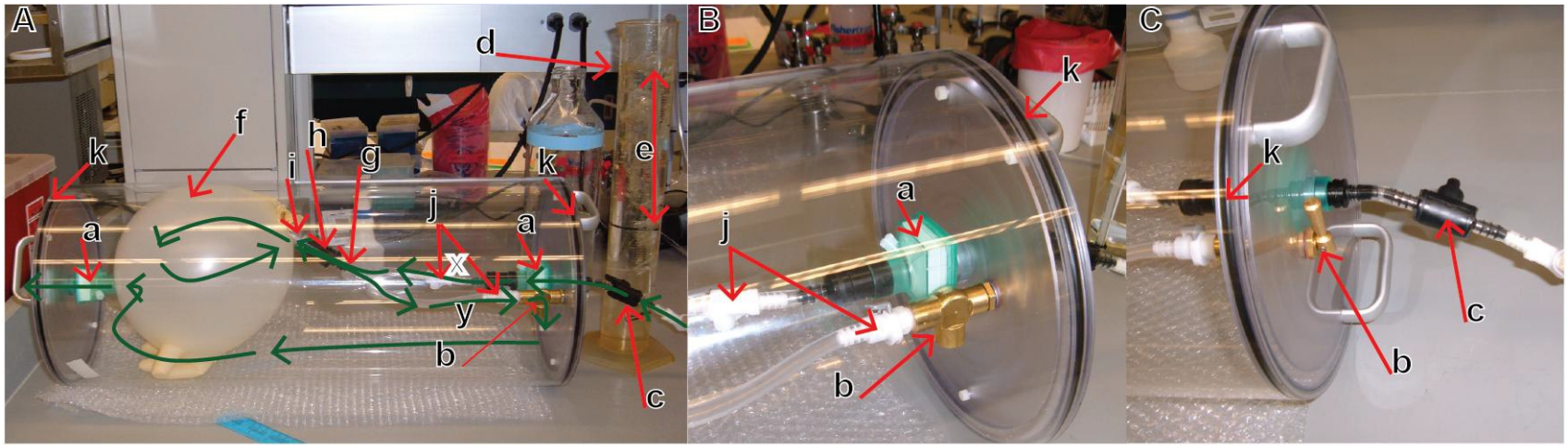

(a) HEPA grade low-resistance filter (b) Panel-mount valve (c) In-line valve (d) Water-column (e) Depth determines water pressure (f) Glove to simulate rabbit lung (g) Y-connector (h) Endotracheal tube adapter (i) Endotracheal tube (j) Quick-release tube connections (k) O-ring sealed endcap (x) Inspiratory Limb (y) Expiratory limb (green arrows) Gas flow

Figure 41. A simple breath-hold setup designed to enhance image quality whilst safely maintaining BSL-3 containment: (A) Image of container with components labelled (a-k). Gas is delivered through an inline valve. All points where gas can enter and leave the cylinder are HEPA filtered in order to prevent transmission of bacteria, even in the case of gas failure. O-ring sealed endcaps allow for removal of transfer of animals within the BSL-3 laboratory. The expiratory limb (y) of the circuit contains a panel mounted valve that allows the valve to be operated from outside the cylinder. Closing the expiratory valve allows the pressure to rise to the depth of the water set in the column (e). In the final version of the chamber L-tubes were placed immediately adjacent to the panel mount valve and inward filter which allowed the end of the endotracheal tube to be located adjacent to the end cap - allowing maximal space for the animal to be positioned. **(B)** Detail of internal surface of endcap. **(C)** Detail of external surface of endcap.

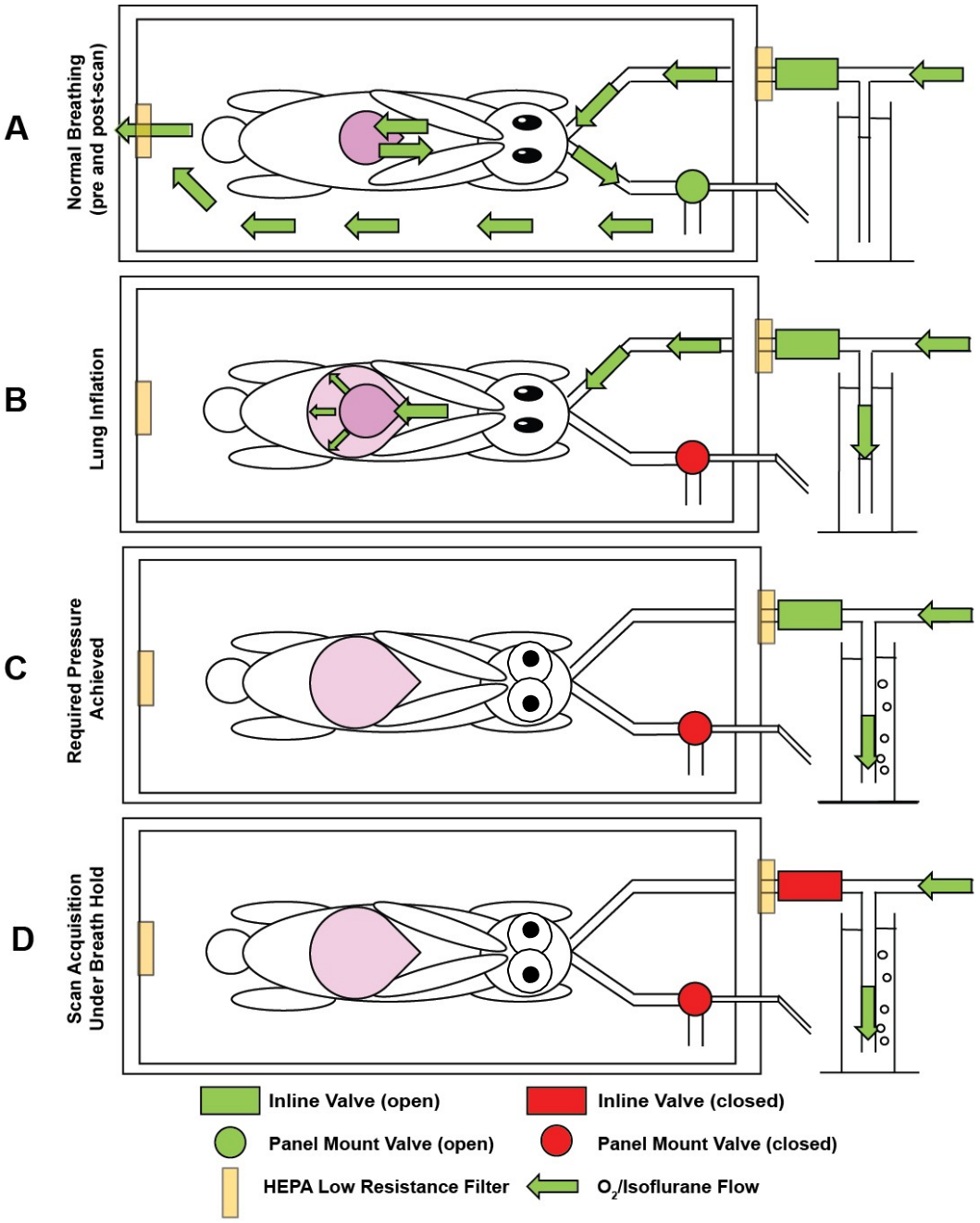

Figure 42. The breath-hold procedure: (A) During transport and placement for the scan the animal is allowed to breath normally. The oxygen/isoflurane mix is delivered at a constant rate of $3lmin^{-1}$. **(B)** To initiate inflation the panel mount valve (in the expiratory limb) is closed. This causes the pressure in the lung to rise and so it inflates. The pressure building in the circuit drives down the column of water. The depth of this water dictates the maximum reachable pressure. **(C)** When this pressure is reached, bubbles appear in the column and the inline valve can be closed **(D)**. This maintains pressure in the rabbit lung and prevents movement - the CT scan is acquired at this point. Release of both valves immediately after scan acquisition restores normal flow and pressure.

This system allowed for breath-hold scanning of rabbits at matched pressures. The total cost for manufacture was $132.50 for the acrylic tubing, $102.50 for the endcaps, $30 for the valve, $2 per

filter and $0.50 per feet for the tubing. To modify the existing chamber to allow combined breath-hold and PET imaging a cap was built for less than $100. The system is easily utilised, and customisable by the insertion of further ports for either monitoring equipment, or sampling devices (figure 41 and 42).

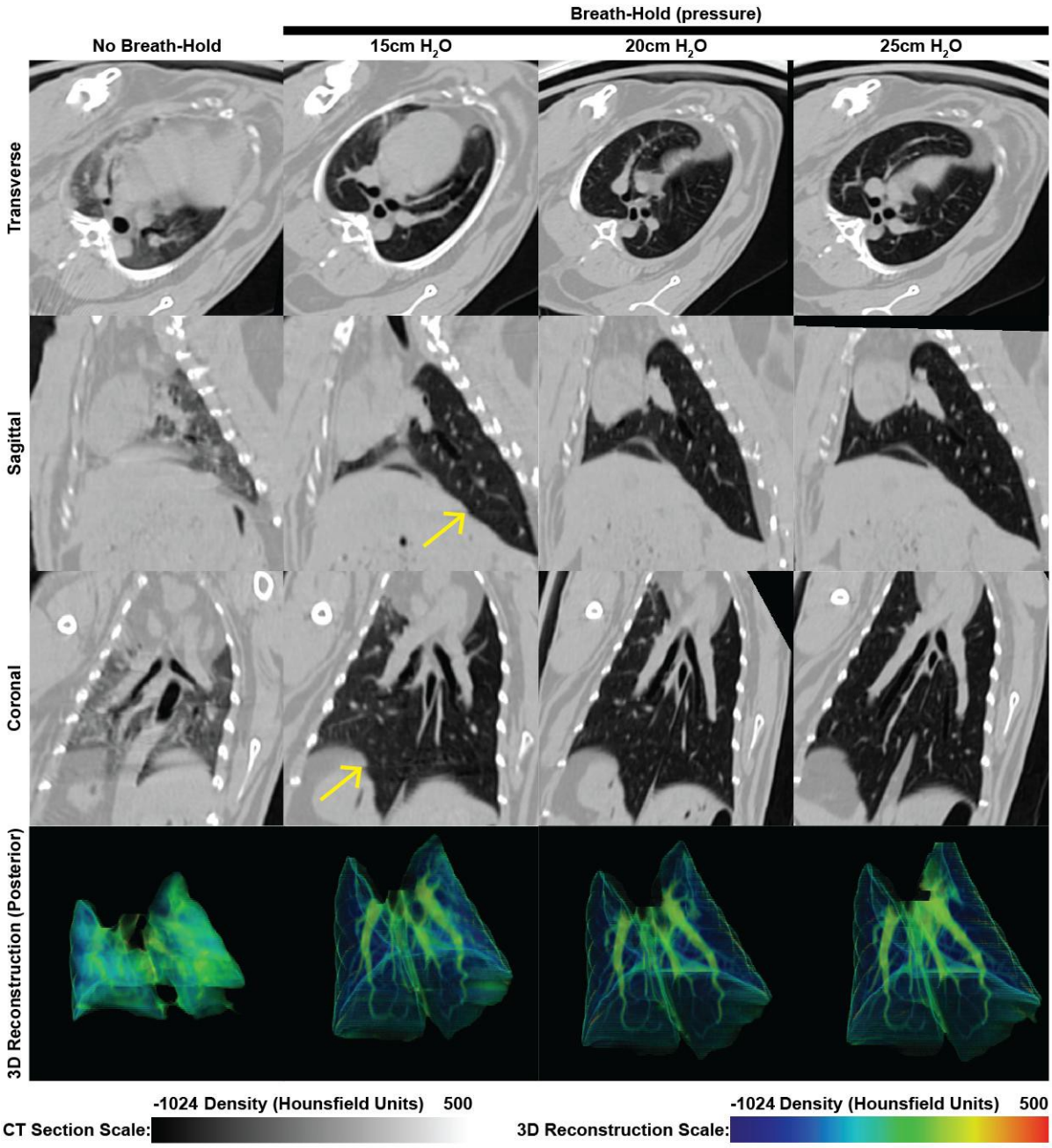

Figure 43. Breath-holding using custom designed device significantly improved image quality, and allowed for set pressure breath holds: Representative CT slices are displayed above. Compared to no breath-hold, all breath-hold images at every pressure tested offer significant improvement in image quality. A small amount of motion artefact is noted in the 15cmH_2O (yellow arrow). The remaining images, although not artefact free (there is a motion artefact generated by uneven flooring in the imaging facility, a problem which was subsequently corrected), are dramatically more informative than the non-breath hold images.

Initial trials demonstrated that breath-holds at 10-25cmH_2O of pressure were well-tolerated and provided different information (figure 43). At the writing of this thesis more than 100 scans of infected animals have been performed, with no adverse events recorded.

4.5.2. Non-anaesthetised imaging of rabbits

On the CT acquisition system used scanning of the rabbit takes approximately a minute for the entire body length, and reconstruction takes 5-10 minutes. The majority of time during scan days is taken by anaesthesia and recovery of the animal. Because anaesthesia poses a risk to animal health and experimental outcomes, methods for scanning of non-anaesthetised animals were investigated. A low-stress, and safe procedure that allowed for capture of informative, high-quality CT scans of rabbits was developed (figure 44).

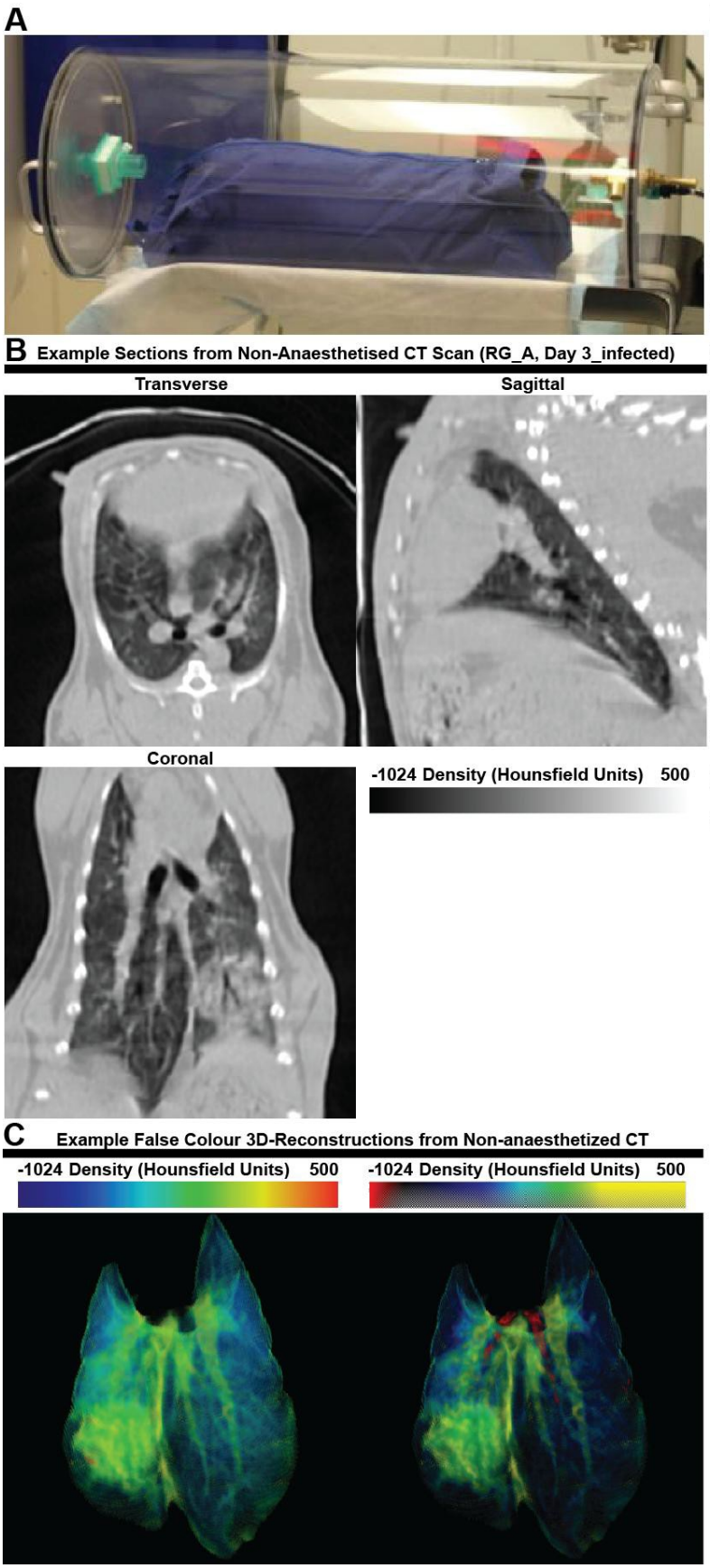

Figure 44. Non-anaesthetised rabbit imaging provides informative and high-quality scans: (A) Photograph of soft restrained animal in imaging chamber. **(B)** CT scans show some degree of breathing artefact and improved lung inflation. This occurs because of enhanced muscle tone in non-anaesthetised animals and rapidly provides very informative images. **(C)** 3 dimensional image reconstructions show that the overall artefact is minimal and key structures are visible. The colour scale on the right highlights regions of density (yellow/green) which include the vasculature as well as an area of consolidation located at the site of infection. The hypodense regions (red) are the airways.

The reproducibility of these scans was compared to breath-hold images by segmenting the lung volume (figure 47) and assessing the distribution of densities within the scan (figure 45). This demonstrated that the variations between scans were very small, suggesting that such scanning methodology was safe and reproducible.

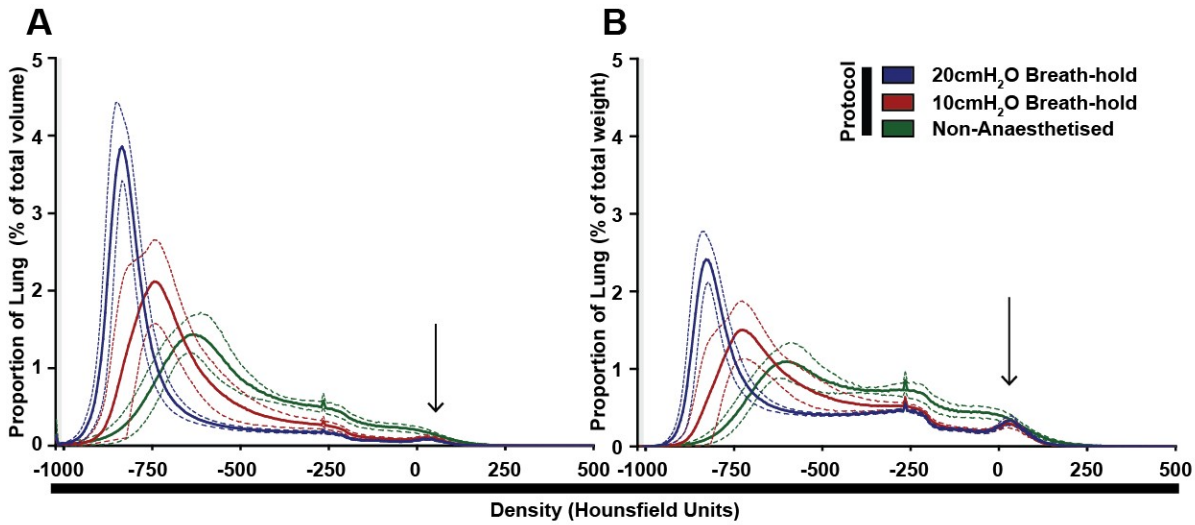

Figure 45. Quantification of various scanning protocols demonstrating reproducibility of high pressure breath holds and smoothing of peaks without breath-holding: (A) Histograms showing the frequency of voxels with a given density as a proportion of all voxels in non-anaesthetised animals, as well as breath-hold scans at 10 and 20cmH_2O. 20cmH_2O scans show small standard deviations and two-distinct peaks; a large peak at -850 HU and a much smaller peak at 50 HU. As expected the distribution of densities is more variable in the 10cmH_2O breath-hold scans however, two peaks are still observed; the low density peak now at around -750 HU and the smaller high-density peak unmoved. The non-anaesthetised scan shows small standard deviations, but the peak at 50 HU is lost (black arrows). This is the density at which lung vasculature and consolidation are observed. The loss of this peak in the non-anaesthetised scans most likely occurs because, during respiratory motion, small dense areas are measured as they move through multiple less dense areas. This effect results in a false observation of a large region of lower density, instead of a region of normal density with a localised very dense area. **(B)** These histograms use each voxel measurement to calculate the weight of tissue in that voxel, the y-axis is used to indicate what proportion by weight these voxels make up of the total lung weight. These graphs therefore represent the mass of tissue at each density. This highlights the fact that the low density changes account for a substantial portion of the lung mass (0.5%) of the total lung mass. This method better demonstrates the significance of these high density changes than volume based assessment. *(n=54 for scans at 10 and 20cmH_2O scans, and n=24 for non-anaesthetised scans, solid lines represent the mean and dotted lines represent standard deviations)*.

Image quality was also subjectively compared, non-anaesthetised images could be used to accurately quantify changes, but this method outperformed anaesthetised scans where breath-

holding was not used. Non-anaesthetised scans do not match the clarity of images when breath-holding was applied (figure 46).

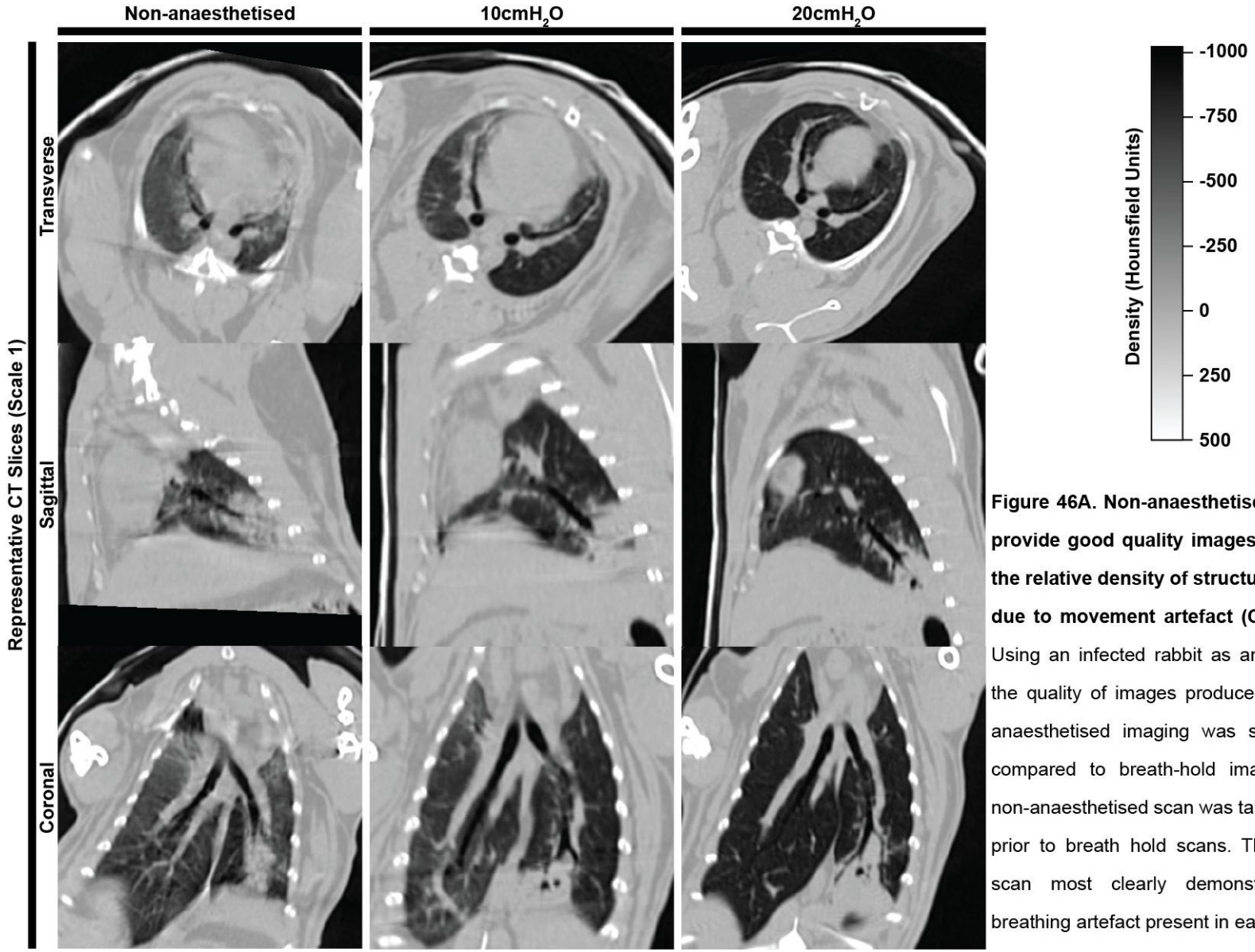

Figure 46A. Non-anaesthetised images provide good quality images, however the relative density of structures varies due to movement artefact (CT slices): Using an infected rabbit as an example, the quality of images produced by non-anaesthetised imaging was subjectively compared to breath-hold imaging. The non-anaesthetised scan was taken 14 day prior to breath hold scans. The coronal scan most clearly demonstrates the breathing artefact present in each scan.

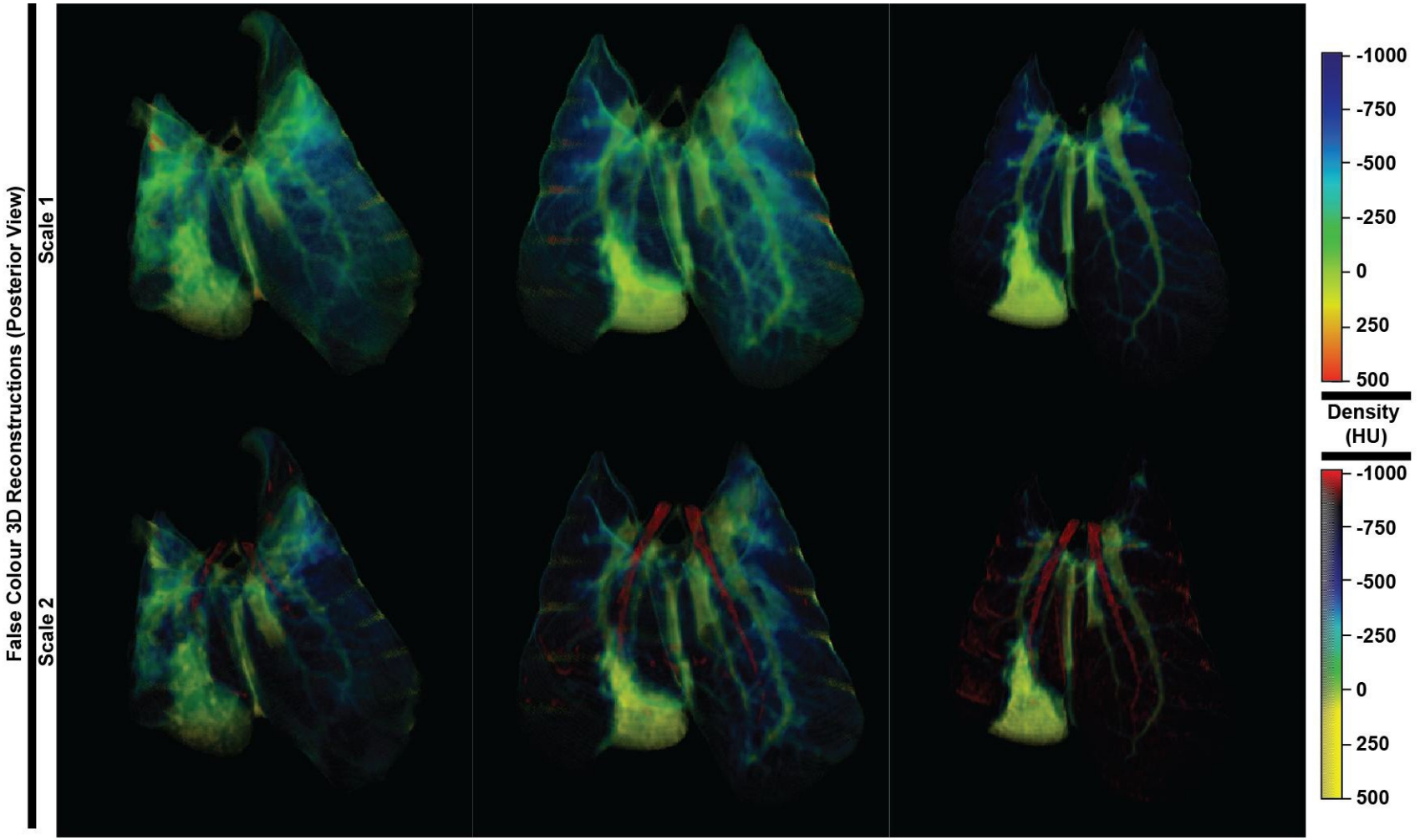

Figure 46B. Non-anaesthetised images provide good quality images, however the relative density of structures varies due to movement artefact (3D reconstructions): Increased attenuation, that may be consolidation, in the right lung at 10cmH_2O (3D reconstructions) is resolved by inflation to 20cmH_2O. The increased inflation allows for complete resolution of the vasculature and the lesion (lower left lobe).

4.6. Segmentation of CT images

In order to quantify images, two general methods are used; scoring systems and quantification. Scoring systems are inherently subjective; this can be compensated for by utilising multiple readers, blinded to the information in the study. When one considers the cost of a trained radiologist's time, and that many imaging studies may have 4-5 timepoints and as many as 30 animals, the cost of such analysis is beyond the capabilities of most research laboratories. Additionally, there are also only a few experts in laboratory animal anatomy, and almost none with familiarity of specific pathologies in diverse models. Quantification can be unbiased – but is extremely challenging, especially when considering the identification of pathologies that are complex in nature.

The most common quantitative methods are those applied to Positron Emission Tomography (PET) scanning. The emission of positrons from a trapped radiotracer is counted – and the location of the origin of these counts is used to generate a 3-dimensional 'uptake' scan. Because the amount of tracer injected into the animal can be measured accurately, the uptake value can be standardised by its distribution to generate standardised uptake values (SUVs). These values take into account the amount of tracer injected and the volume of the animal. Such scans require co-registration onto a structural scan, such as a CT, in order to localise uptake. PET scans take significant periods of time (anywhere from 20 minutes to several hours depending on the isotope being used). Co-registration is relatively straightforward in stationary organs; however, within the lung, motion is inevitable. Although strategies were developed to reduce motion artefact, a strategy for taking scans representative of the average breathing cycle has not been developed. As a result, in the images presented in this thesis (as in all work where CT scans are not dynamically acquired with the PET scan), the area of uptake is only approximately relative to the CT image.

Quantification of CT images themselves is often on a case-by-case basis, for example, monitoring the change in the size or number of lesions. This process is normally carried out using trained radiologists. An alternative to this is to use 'computer vision' to detect and segment images completely automatically (203). Technologies are being developed, and a cavity and airway

segmentation strategy was developed as part of this project (204). For the work presented here, a semi-automated segmentation technique, which allowed for isolation and measurement of the lung-field was developed (figure 47). This method which used commercially available tools (Amira), allowed for objective quantification of density changes within the lung field, as well as the generation of reconstructions of this isolated field. These reconstructions also allow for improved subjective assessment. The process takes approximately 15 minutes per scan (figure 47 and 48).

Step 1: Contiguous selection of region in density -1024 to -200 HU using a space filling tool isolates the lung from outside tissue in addition to gas bubbles in the stomach and the airways. Large vasculature within the lung is excluded.

Step 2: Enlarging the volume by 3 pixels in all directions.

Step 3: Holes within the segmented region are filled, this means all vasculature is included.

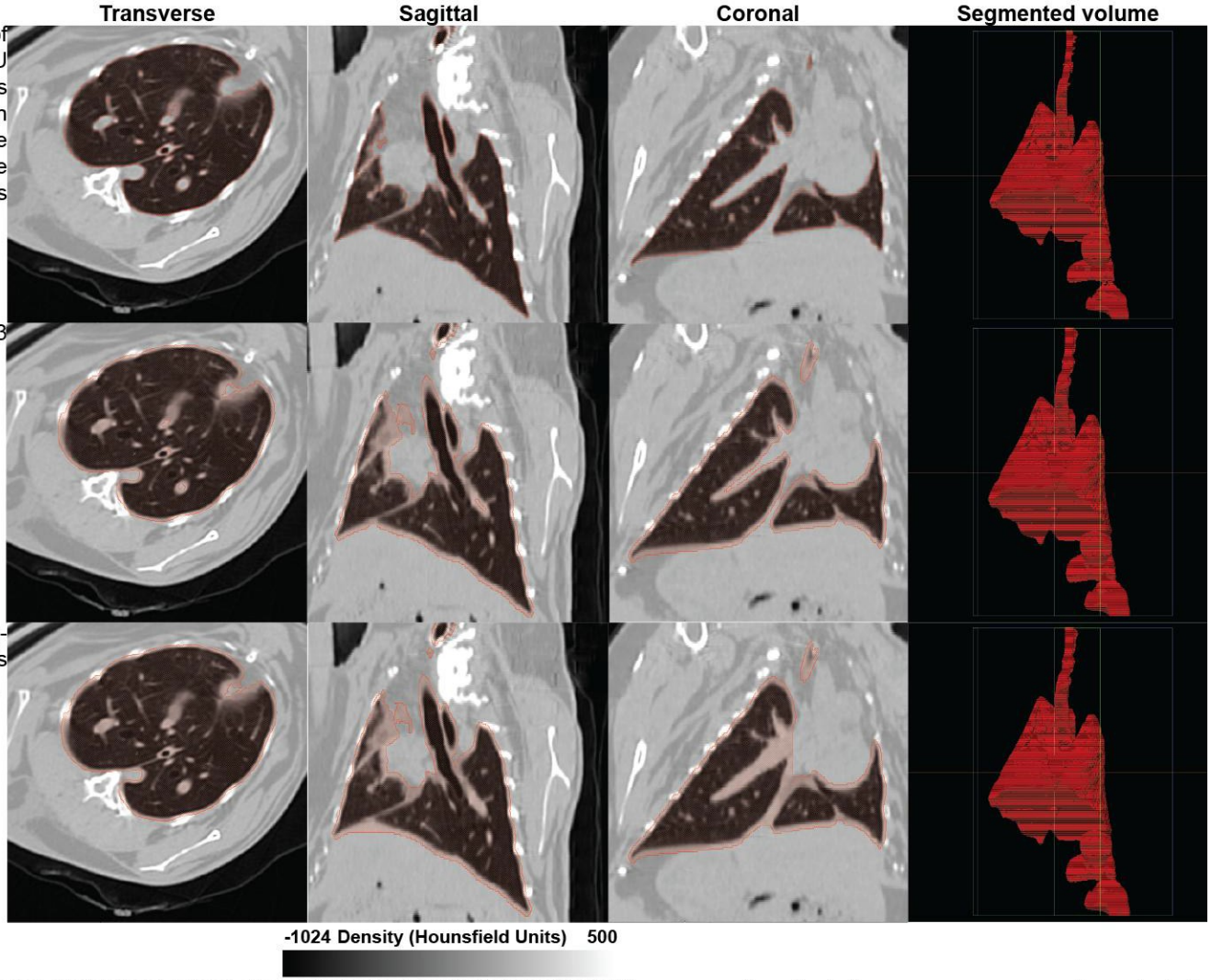

Figure 47. A simple, semi-automated, watershed based space filling segmentation method: The process described above uses common software tools to accurately segment lungs (even when disease is present) in a timely manner (approximately 15 minutes), with limited subjective bias. Red shaded zones indicate the segmented region. *(HU, Hounsfield Units), continued overleaf (part 1).*

Step 4: Regions which link non-lung regions to the lung are manually removed - followed by a space-filling tool for removal of contiguous non-lung regions.

Step 5: A smoothing algorithm is applied to the entire shape to correct for deviations during the manual removal of sections.

Step 6: If dilated, the oesophagus is removed with a space-filling tool in the range of -1024 to -800 HU.

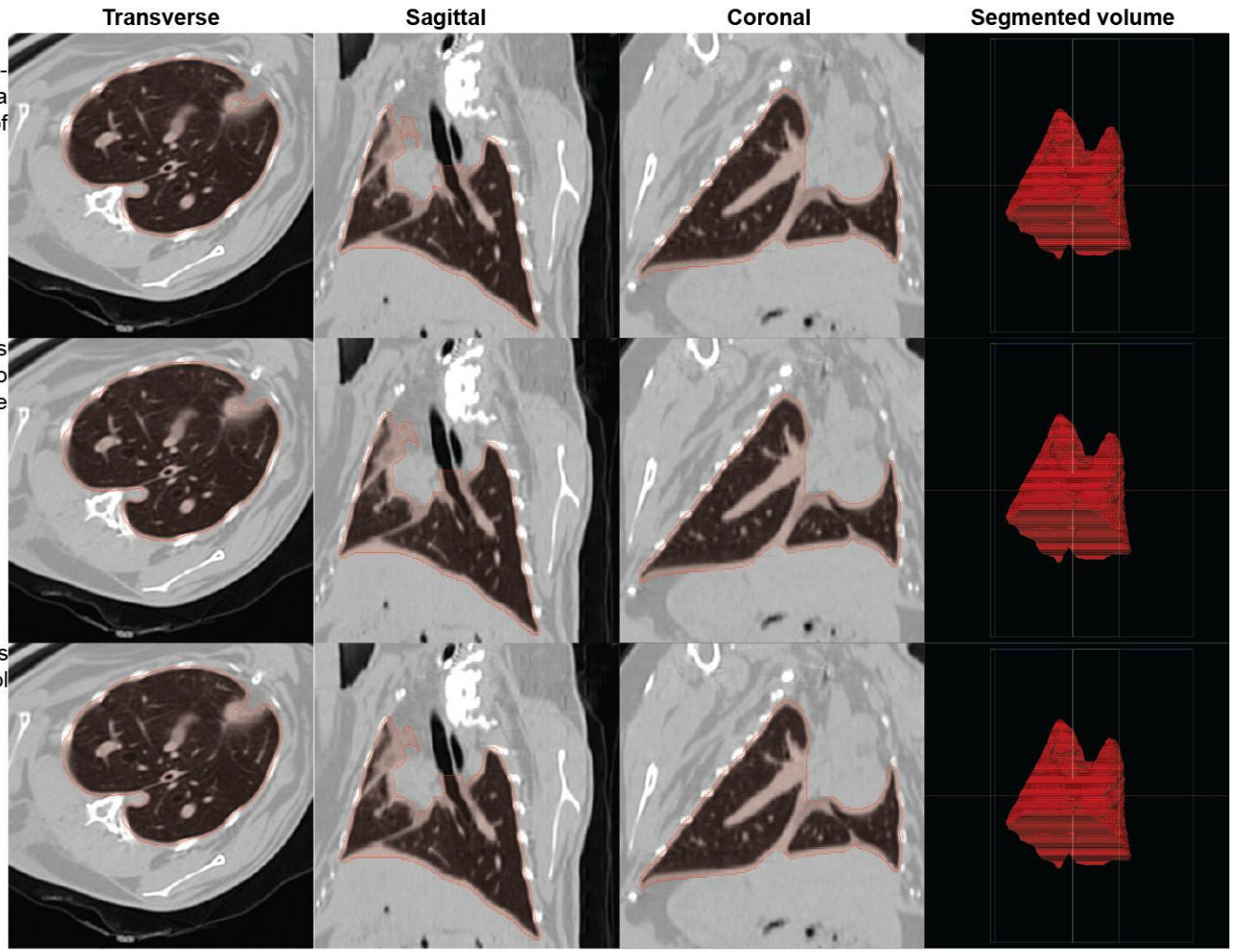

Figure 47. A simple, semi-automated, watershed based space filling segmentation method. *(Part 2).*

Step 7: The selection is eroded by 3 pixels in all directions, leaving an accurately selected lung field.

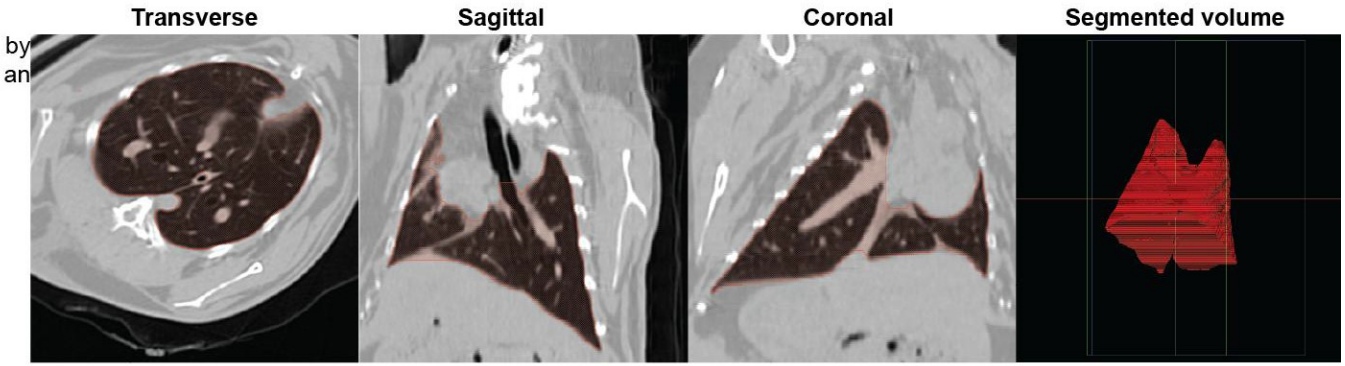

Figure 47. A simple, semi-automated, watershed based space filling segmentation method. *(Part 3).*

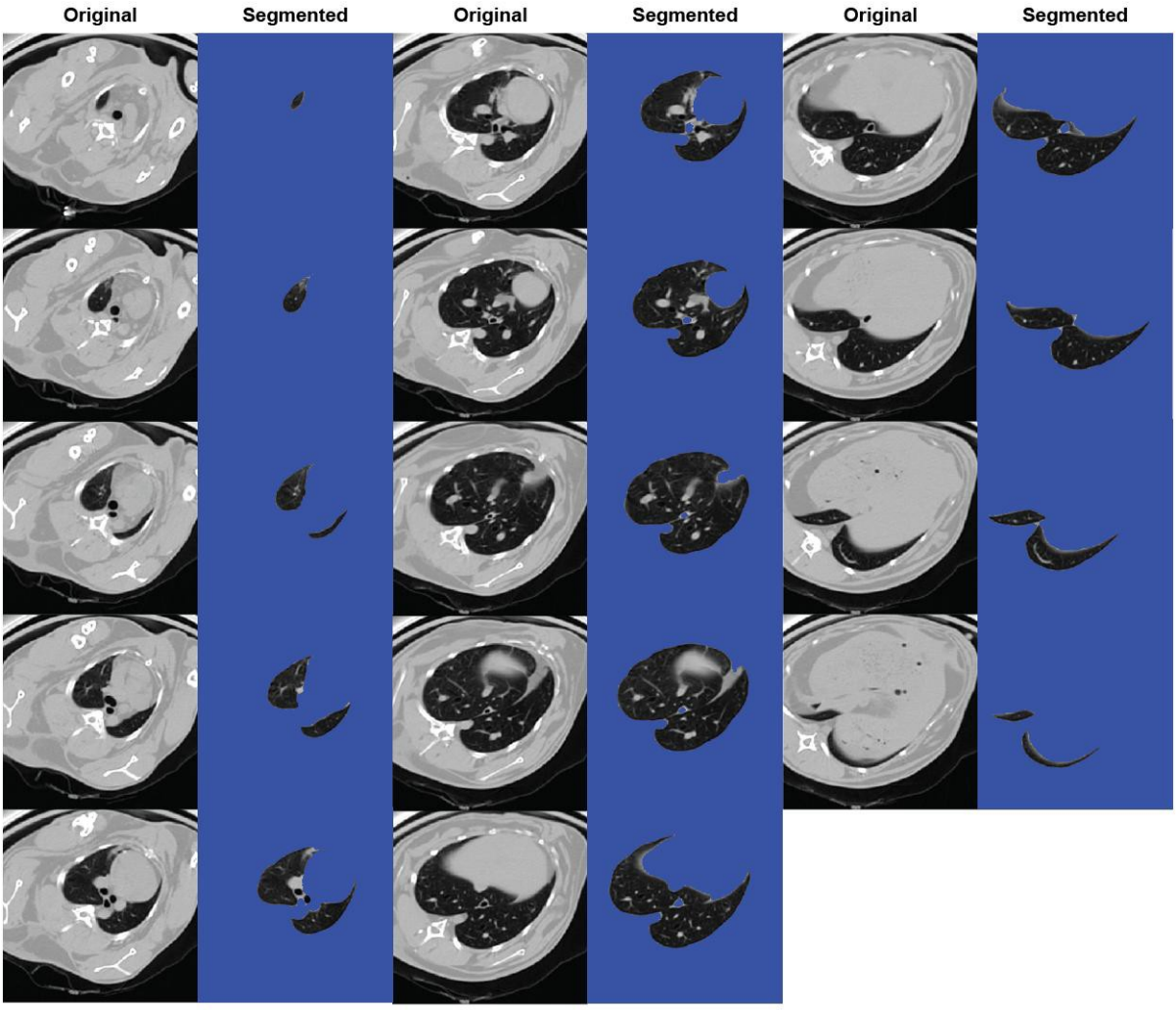

Figure 48. Result of semi-automated lung segmentation: Using the method described in figure 47, lung windows were isolated. 14 representative slices are shown. The lung window is effectively isolated, inclusive of the vasculature. Isolation of this region allows for quantitative measurements of the densities within in it and also for quantification of local change in uptake co-registered PET scans. *Representative transverse sections laid out craniocaudally from top to bottom, then left to right.*

4.7. Identification of regions of interest in CT scans:

Having developed a method for set pressure breath-holding of animals during scans (figures 41, 42 and 43), and a way to reliably segment the lungs (figure 47 and 48), the identification of regions of interest was attempted by comparing scans at different pressures, before and after infection. These data were also used to make basic estimate of lung compliance. More complex studies were beyond the realm of this thesis – but the proof of principal that relatively simple technologies can be used to generate quantitative information in a non-biased manner, demonstrates that such types of evaluation could be used to assess the effect of therapeutics in this model.

4.7.1. Lung density changed in a reproducible manner when inflated to controlled pressures

First, the reproducibility of breath-hold scans was assessed. This was achieved by segmenting the lung window and counting the number of voxels (3-dimensional pixels) that fall within a given density range (figure 49).

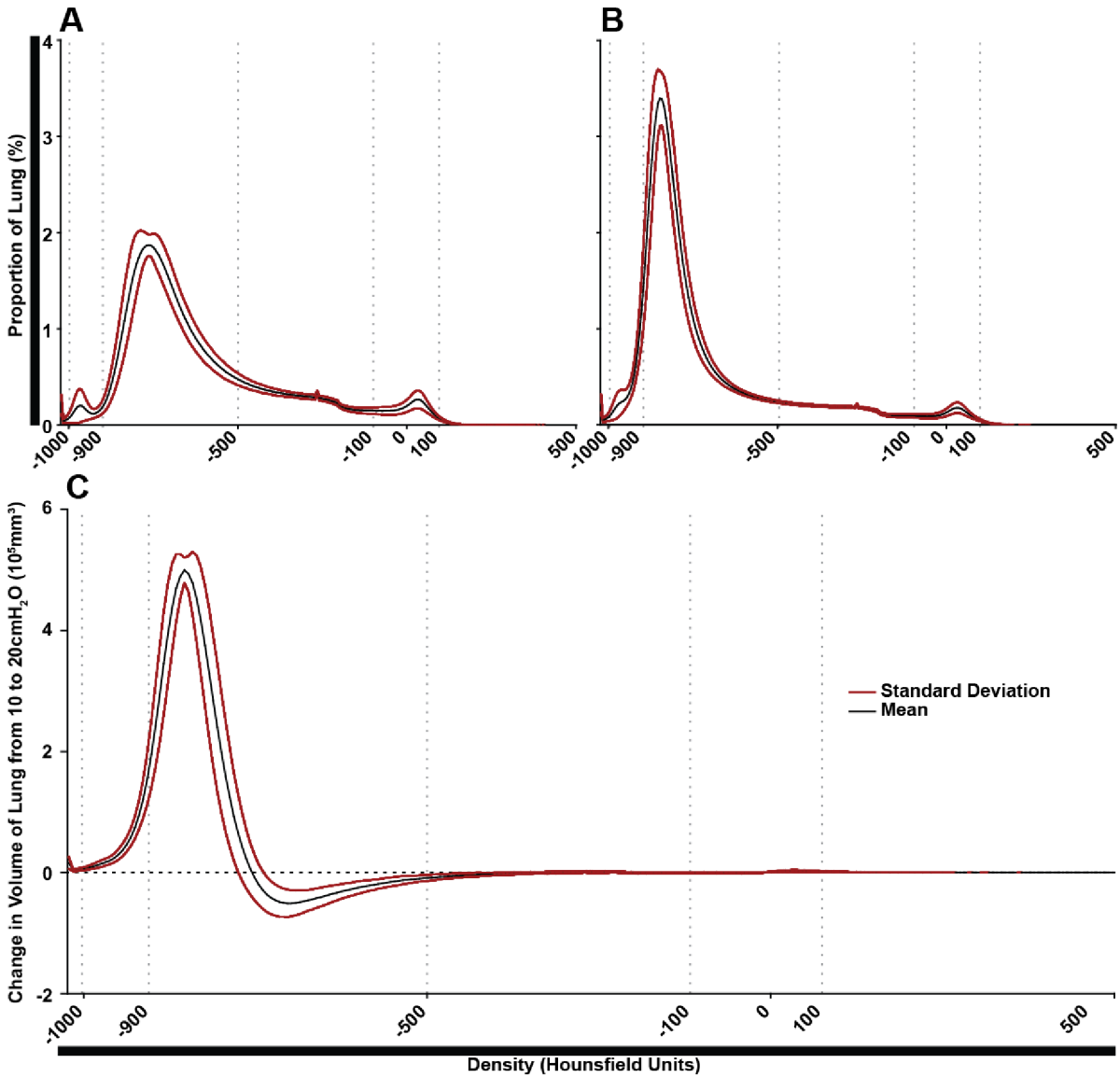

Figure 49. Comparing the change in tissue density between 10 and 20cmH_2O scans: These graphs represent changes in tissue at a given density when comparing breath-hold scans at 10cm with 20cm H_2O of pressure. In A and B, the x-axis represents a given density, and the y-axis is the volume of that density as a proportion of the total lung volume. In C, the change in volume of a given density is shown on the y-axis. Dotted lines represent standard cut-off values for lung tissue types in CT scans. **(A)** Distribution of densities in the lung window averaged across 54 breath-hold scans in healthy and infected animals. Scans taken at 10cmH_2O. The majority of the lung volume is represented by densities between -900 and -500 Hounsfield Units. **(B)** Using the same animals as in 'A', scans at 20cmH_2O were assessed. The majority of the lung still falls into the -900 to -500 window, but now the peak is shifted towards -900 and there is a reduction in proportional volumes towards -500. **(C)** As expected there is an increase in the volume of lung with a low density as shown by the peak between -1022 and -754 (peak -853). There is a decrease between -754 and -321 (peak -703) indicating that the recruitment of this region affords the inflation of the less dense region.

4.7.2. The reproducibility of CT scan changes corresponded to specific pathologies

Figure 49 shows that the biggest change in volume of a given density occurred in the range -1022 to -754 (the peak at -853) when lungs were inflated from 10 to 20cmH_2O of this region at these pressures. There was a reduction in the volume of a large range of denser tissues (-754 to -321) suggesting that the expansion in the low density peaks occurred as a result of recruitment from this region. The absence of any change below -450 suggest strongly that there is no recruitment of this at these pressures. These data indicate that compliant, functional lung tissue lies in the range of -500 to -925 HU in a rabbit CT scan. This is in-keeping with human CT findings where the arbitrary designations for lung tissue are (i) -1000 to -900; hyperexpanded, (ii) -900 to -500; normally aerated (iii) -500 to -100; poorly aerated and (iv) -100 to 100; not aerated (191).

Next the data was analysed to assess whether specific changes occurred after infection. To do this, lung density from preinfection scans was compared to each time point after infection (figure 50).

4.7.3. Identifying changes which correspond to pathology

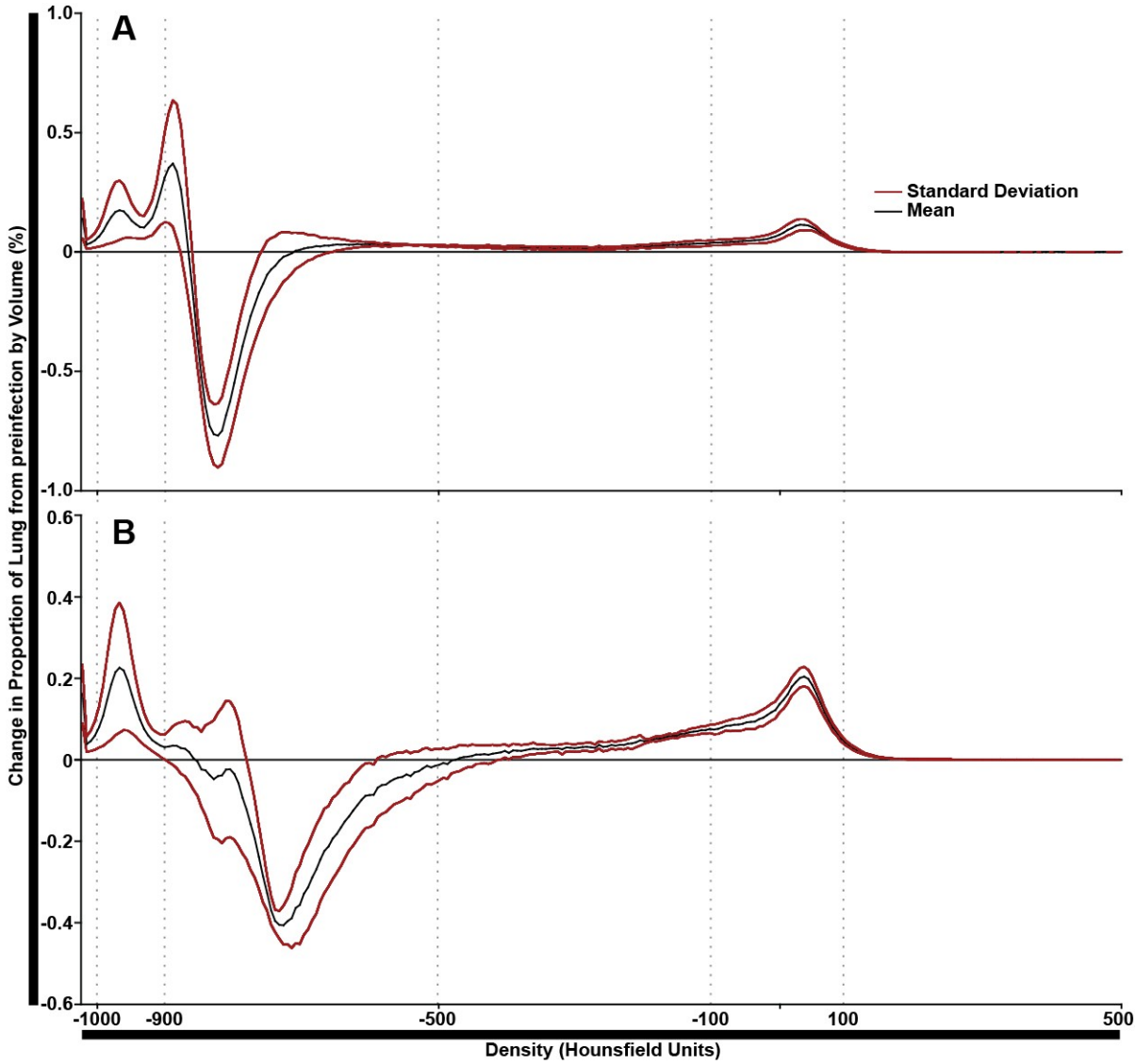

Figure 50. Comparing tissue density distribution before and after infection reveals a distinct pattern of change: These graphs represent changes in the proportion of tissue at a given density when comparing post-infection scans to preinfection scans at different pressures of breath-hold. This is calculated by taking the proportion of lung at a given density post infection and subtracting the proportion of lung at that density pre-infection (n=42). **(A)** 20cmH_2O: At this pressure there is a large reduction in densities between -866 and -712 HU (Peak -823). 54% of this reduction is compensated by an increase between in regions -712 and 272 HU, (Peak 29.19) and 46% is compensated by an increase between -1022 and -866 (Peak -967 HU; 90% -1015 and -883HU). **(B)** 10cmH_2O: At this pressure there is a reduction in tissue which corresponds to tissues with a density of -856 to -475.3 (peak -727). 28% of this reduction is compensated for by an increase between -1022 and -856 (peak -967). The remaining 71% increase is distributed over an increase between -475 and 497 (peak 35.19).

A distinct pattern of change was observed after infection (figure 50). There was an increase in the proportion of tissue at high density and very low density tissue. There was a concurrent decrease in

the ‘normally aerated’ tissue (-900 to -500 HU). These changes indicated that normal tissue was replaced by both low and high density changes post infection; the densities of which correspond to cavity formation (very low density), hyper-expansion (low density) and consolidation (high density). As shown in figure 50, the change in the low density peak in 20cmH_2O scan is bimodal. The 10cmH_2O scan shows only a singular peak which corresponds with the lowest density peak of the 20cmH_2O scan. It was hypothesised that the very low density peak was the result of cavity formation and that the slightly less dense peak was the result of hyperexpansion. To test this, cavity and non-cavity animals from a single time point were assessed (figure 51).

4.7.4. Understanding how cavity tissue and hyperexpanded tissue differ

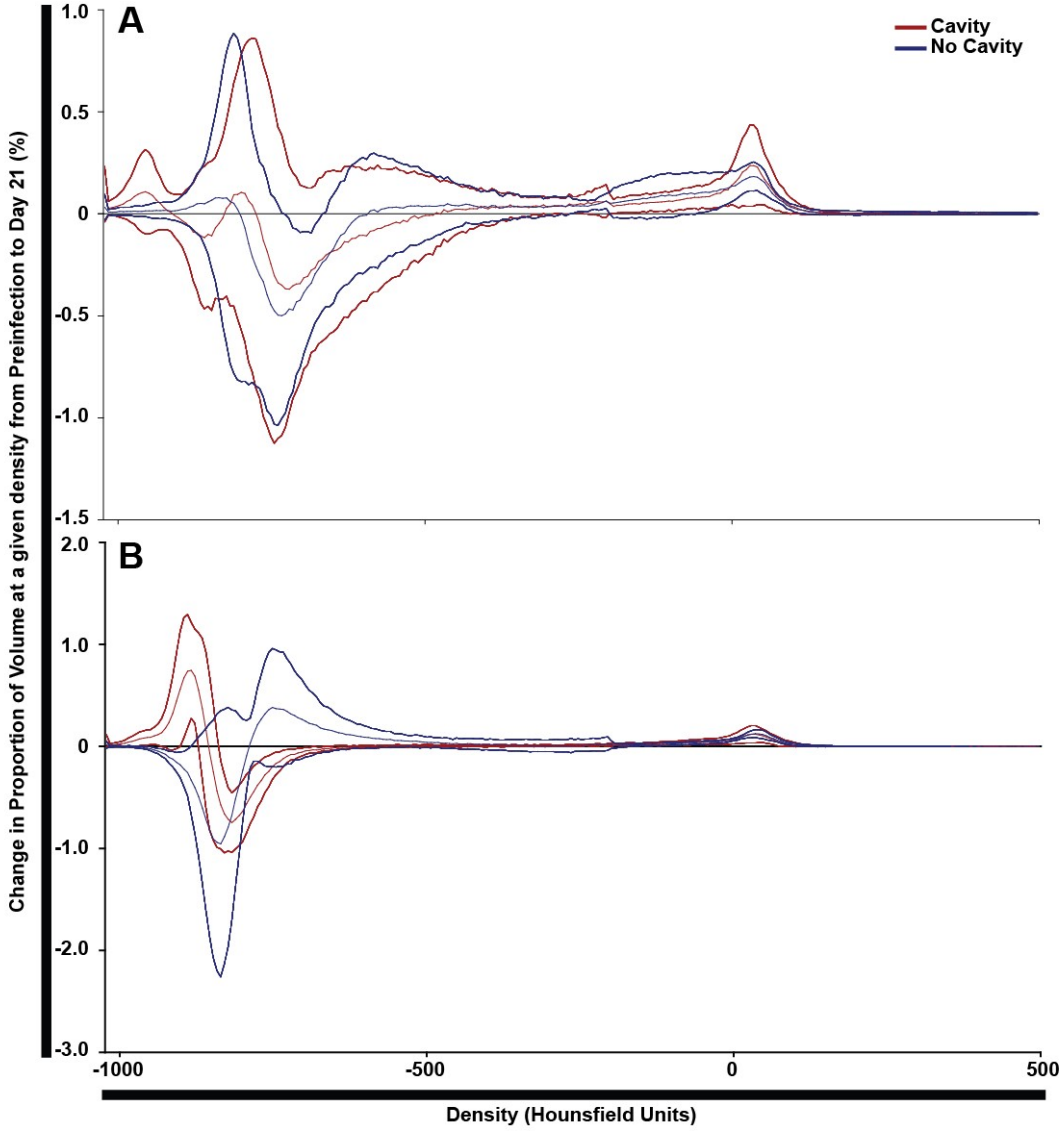

Figure 51. Comparing tissue density distribution in cavity vs non-cavity animals at multiple pressures reveals a cavity signature separate from hyperexpansion: These graphs represent changes, from baseline, in the proportion of tissue at a given density of 6 animals at day 21, against changes, from baseline, in 6 animals without cavities at day 21. The errors are large due to animal to animal variation, as expected with such a small data set. **(A)** 10cmH_2O: At this pressure two peaks occur in cavity animals, compared with one in non-cavity animals, found in low density regions (Cavity -1022 to -918HU and -829 to -769HU, non-cavity -1022 to -801HU). **(B)** 20cmH_2O: At this pressure a singular positive peak is seen in each group (cavity: -1022 to -855HU, peak -883HU, non-cavity: -789 to 263HU, peak -751HU). The apparent increase in volume of low density regions in animals with cavities suggests an increased compliance, but this is confounded by the fact the cavity may be contributing to this increase in the number low density voxels. *(Thin lines=mean, thick lines=standard deviations)*.

By comparing the 10cmH_2O scans of cavity to non-cavity animals at a single time point, a cavity signature (-1022 to -918HU) was distinguished from a hyperexpansive (-829 to -796HU) signature

(figure 51). There was no increase in the cavity region when observing non-cavity animals. In the 20cmH_2O scan, hyperexpansion occurred in those animals with cavities. Non-cavitary animals showed a reduction (from preinfection) in hyperexpanded zones. These data suggested that the 20cmH_2O scan could be used to demonstrate newly hyperexpanded regions, and that these are identifiable by a threshold values within the scan.

This was tested by segmenting the lung tissue from surrounding tissue in the scans, and then segmenting various regions by their relative density. It was shown that the region -1024 to -917HU corresponded to major airways and cavities (figure 52). Since the major airways do not change significantly in volume during the experiment, changes in this region were strongly associated with cavity formation. The region from -917 to -855HU represents hyperexpanded, but not cavity containing tissue. This hyperexpansion occurs in all regions except the directly infected area, suggesting that the lung compensates for the affected region mechanically.

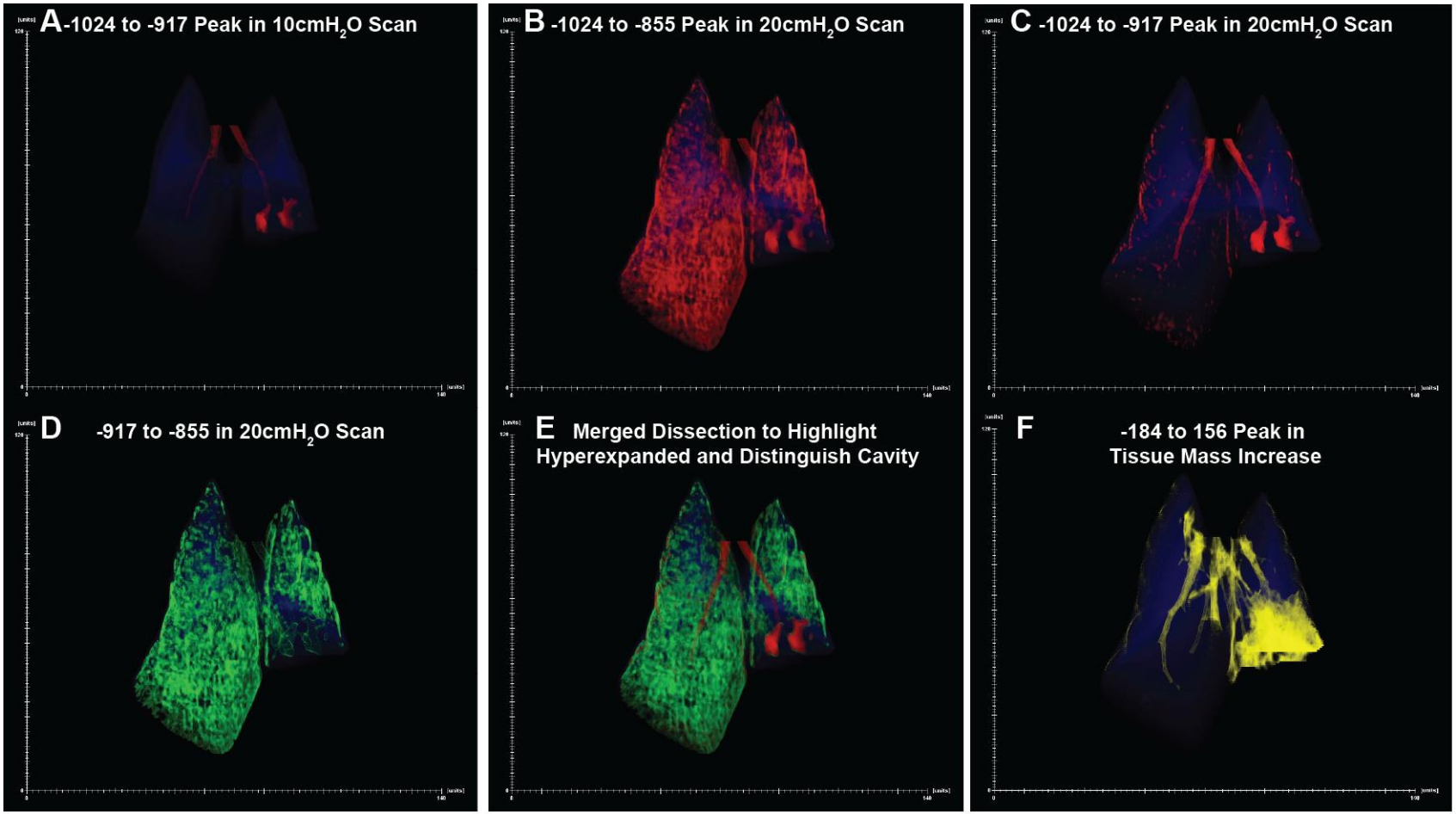

Figure 52. Histogram identified signature zones allow for rapid rendering of pathologies using a false-colour reconstruction: The changes identified by histogram analysis (figures 49, 50, 51 and 53) were utilised to define zones of interest. **(A)** The low density change from figure 51 is rendered in the 10cmH_2O scan. **(B)** As expected the low density peak in figure 51 corresponded to both cavities and hyperinflated regions. **(C)** The cavity signature in figure A is better at identifying the cavity than the range in B. **(D)** Subtraction of C from B gives the region of hyperexpansion; and allows rendering of hyperexpansion and cavity to be defined in the 20cmH_2O shown in **E**. **(F)** The tissue with high density identified in figure 54 corresponds to consolidation, which, in this case, surrounds the cavity.

4.7.5. High density changes in rabbit CT scans and their correlation with pathology

Next the high density peak (-184 to 53HU) was examined. Conceptually, one must remember that a CT density results from the given proportion of a tissue to air within a voxel. As such, an increase in regions of density can reflect either an increase in the amount of tissue at a given density, or an increase in the amount of air in the same mass of tissue. With dense tissue, the interest is not in the amount of aeration, but instead the increase in actual tissue mass resulting from infiltration of the airspace and fibrosis, CT density readings converted into tissue mass. This took place using the simple equation (191):

$$Tissue\ mass = \left(1 - \frac{CT}{1000}\right) \times Volume$$

Where the CT number is the density of a voxel in Hounsfield units, and volume is the number of voxels containing this density. This equation is derived from the fact that water has a density of 0HU and air of -1000HU and the assumption that a voxel with a density between 0HU and -1000HU are composed of a proportion of tissue (that has a density equal to water) and air.

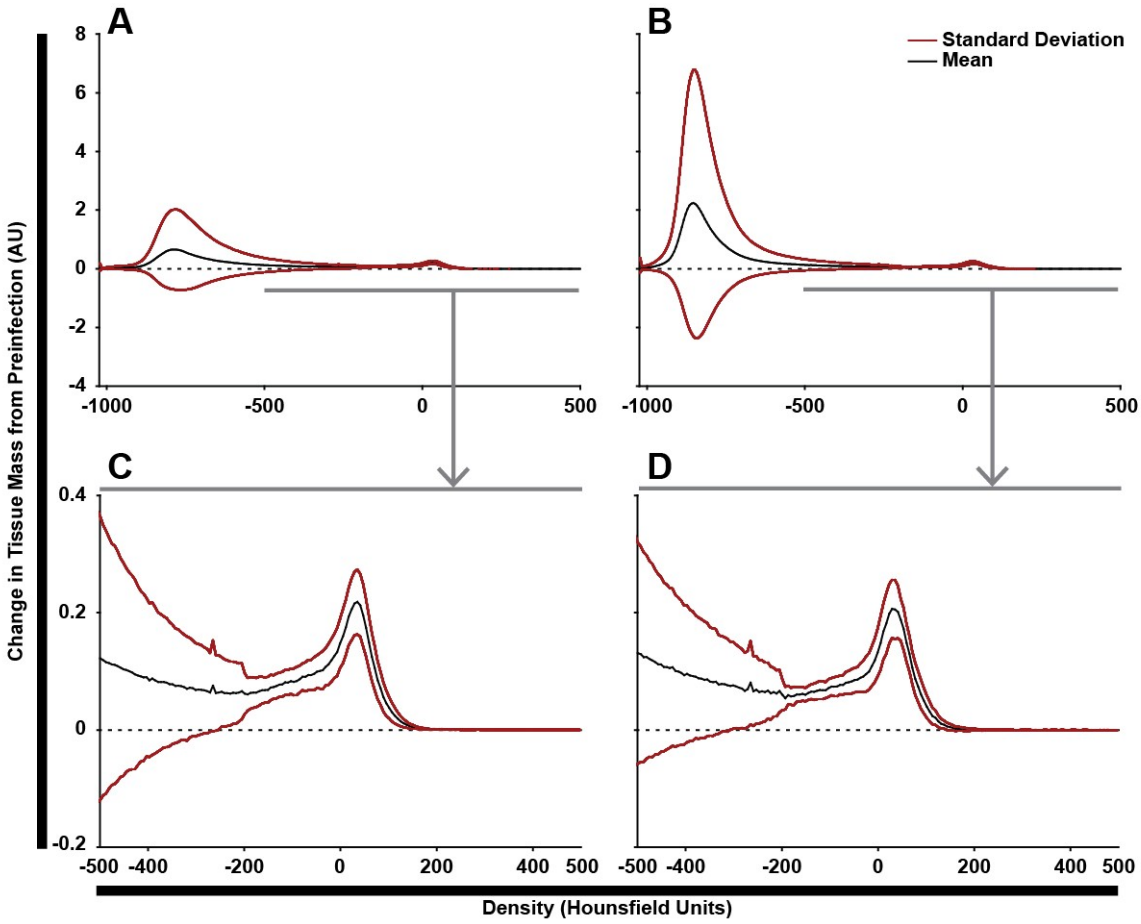

Figure 53. Comparing changes in tissue density distribution by mass after infection reveals a significant increase in the mass of high density tissue: These graphs represent changes in tissue, by weight, at a given density, when post infection scans are compared to baseline, preinfection scans *(n=42)*. There is an increase in tissue mass at all densities suggesting overall increase in lung mass; but this is only consistent in high density regions. **(A)** 10cmH_2O: Substantial variations in mass distribution are seen at low densities. **(B)** 20cmH_2O: A similar pattern in mass variation is seen with high pressure scans. **(C)** Zooming on the high density peak shows that a highly reproducible change in mass accounts for the peak in mass of tissue at just over 50 HU. **(D)** The same region highlighted in C, shows increased abundance in the 20cmH_2O scan.

This analysis revealed a small but significant increase in the abundance of high-density tissues (figure 53). Since there was an increase in mass of all tissue densities post infection, the proportional increase in each zone was compared (figure 54).

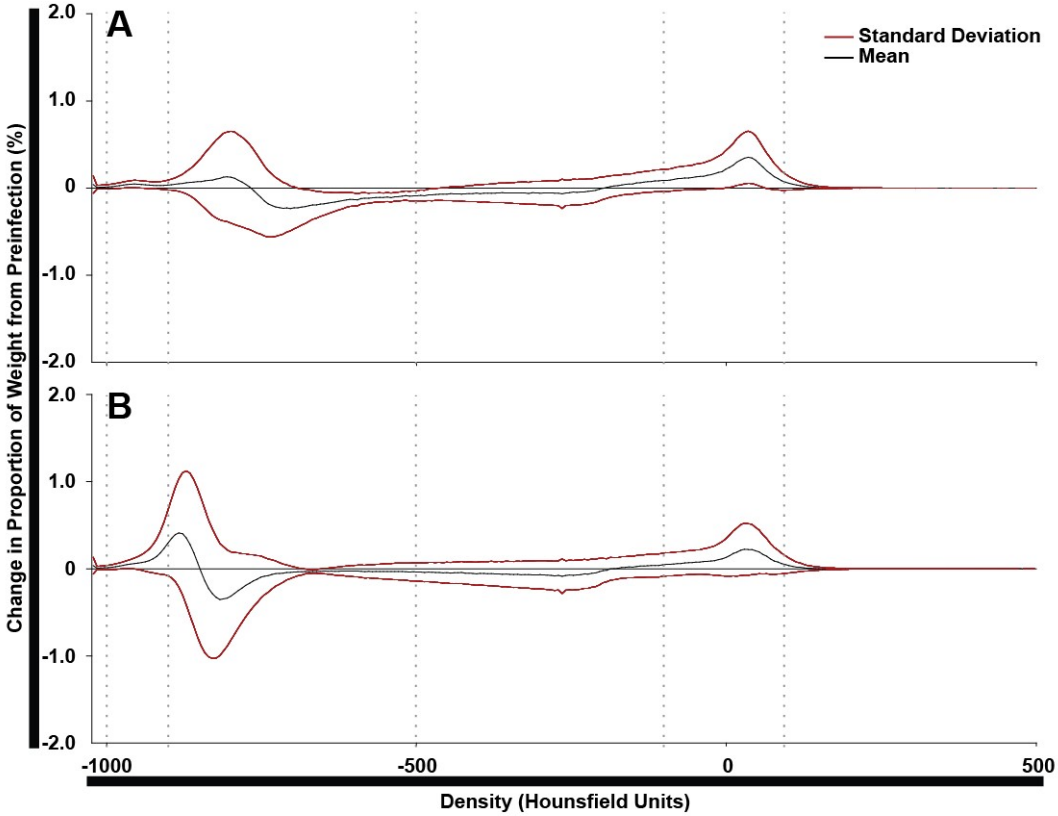

Figure 54. Comparing tissue density distribution by proportional tissue mass pre and post infection reveals an increase in the proportional mass of high density tissue: Since there was an increase in lung mass pre and post infection, the changes were normalised to total lung mass *(n=42)*. These regions are therefore regions where we would expect to observe disease related change. **(A)** 10cmH_2O: The principal high density peak lies between -197 and 213 HU, (peak 35 HU). **(B)** 20cmH_2O: At this peak the principal high density peak lies at 29 HU (-184 to 156).

Analysing the proportional changes showed that a subset of the regions with density between -200 and 200 Hounsfield units increased as a proportion of the entire lung mass. This region; -184 to 156, corresponds with vasculature and consolidated tissue (figure 52). As with the cavity signature, this information was used to generate a false colour scale and map the region. This confirmed that the increase in proportion of this region correlated with the regions of consolidation.

4.7.6. Visual representation of pathological changes

Regions of consolidation, hyperexpansion and cavitation were identified. By combining all this information, a 3D colour map that highlights these pathologies was generated. When combined with the segmentation method, this allows for rendering of pathology within the lung field which complement the quantitative information (figures 27 and 28) produced.

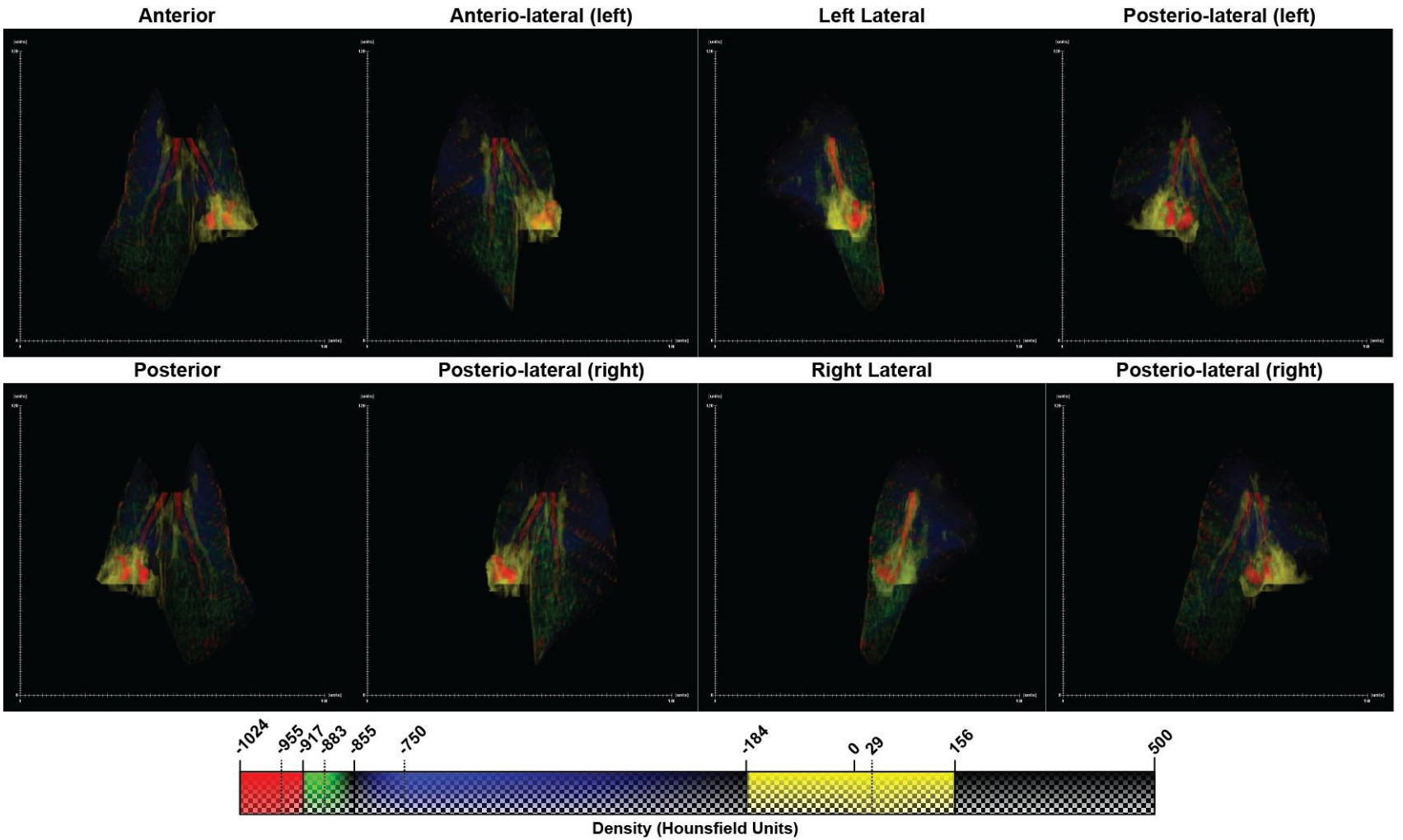

Figure 55. A merged colour map allowing for simultaneous visualisation of zones that change post infection: A 3-dimensional colour map can be used to display regions where the novel signatures appear. By adding a degree of transparency to each layer, with maximum opacity corresponding to the region where change was greatest these regions which change in a quantifiable manner can also be mapped.

This map successfully rendered major changes, but did not allow for rendering of more subtle pathologies, which occur in densities that did not necessarily change in overall volume, but may have changed in distribution (figure 55). For example, tissue with a density of -300 units is found distributed throughout the lung, and may not change in absolute or relative amount during infection. However, despite the absence of an overall change, changes in distribution of this density would indicate pathological change (i.e. nodule development). As a result, the scale was modified to allow clearer representation of disease pathology (figure 56).

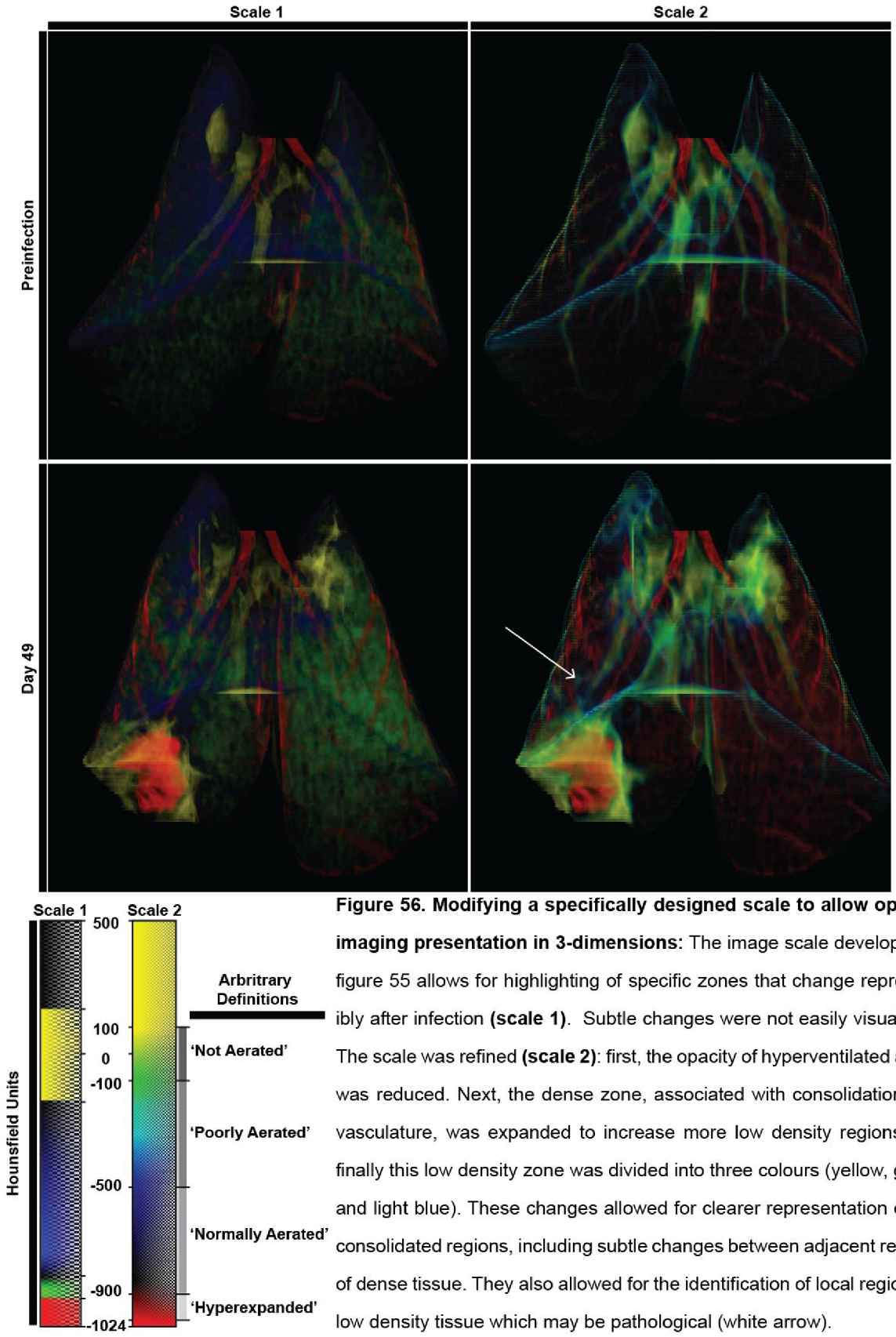

Figure 56. Modifying a specifically designed scale to allow optimal imaging presentation in 3-dimensions: The image scale developed in figure 55 allows for highlighting of specific zones that change reproducibly after infection **(scale 1)**. Subtle changes were not easily visualised. The scale was refined **(scale 2)**: first, the opacity of hyperventilated areas was reduced. Next, the dense zone, associated with consolidation and vasculature, was expanded to increase more low density regions and finally this low density zone was divided into three colours (yellow, green and light blue). These changes allowed for clearer representation of the consolidated regions, including subtle changes between adjacent regions of dense tissue. They also allowed for the identification of local regions of low density tissue which may be pathological (white arrow).

4.8. Assessing transmission from rabbits

Cavity formation is associated strongly with bacterial transmission (184, 185). Preliminary studies were conducted to investigate whether transmission could be modelled using the rabbit as a source. Animal to animal transmission of *M. bovis* has been demonstrated by Lurie (205). However, this required large amounts of bedding to be added to the cages, and though the bacteria appeared to be inhaled, it could not be established if infection could was being expelled via the respiratory tract. A series of experiments were conducted in order to investigate if rabbits exhaled virulent *M. tb* in the presence of cavitary lung disease.

4.8.1. Bacterial collection using hydrophobic HEPA grade filters

First, the breath-hold chamber was modified to allow placement of a filter in the expiratory limb of the respiratory circuit (figure 57). After exposure, the filter was removed, rinsed in 40ml of PBS and 0.05% tween and plated on selective 7H11 plates (500ul per plate; 12 plates per filter). 12 animals were used for this experiment. Filters were cultured from all animals, 6 animals had not yet developed cavities at the first time point, and 6 animals had cavities. The procedure was repeated 7 and 14 days later, at which point all animals had cavities. Filter exposure lasted for approximately 45 minutes.

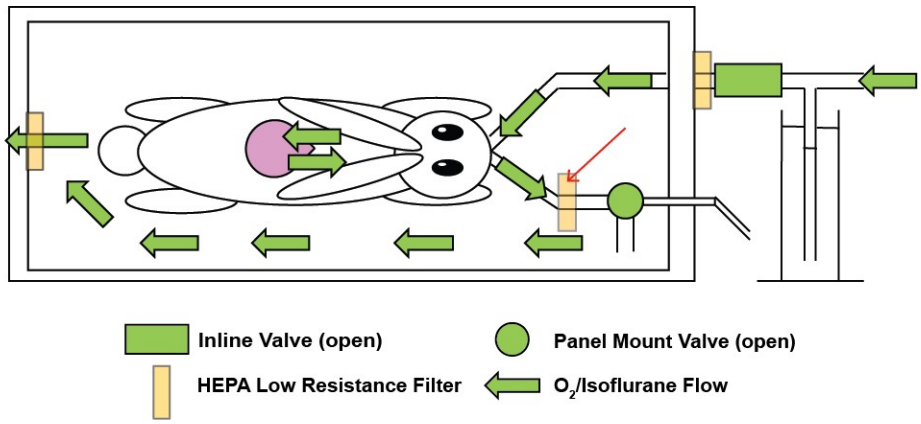

Figure 57. Modified breath-hold setup to allow for isolation of exhaled bacteria: An additional hydrophobic filter was added to the breath-hold chamber (red arrow). This should have allowed for the collection of exhaled bacteria. A constant flow of $3lmin^{-1}$ Oxygen was delivered with 1% isoflurane, in order to force exhaled air through the distal filter, which was located at a distance approximately 3cm from the mouth of the rabbit.

No colonies were found on any plates. This suggests that large amounts of viable bacteria were not exhaled by rabbits, however, a number of alternative explanations for this observation are possible. Technically, there are a number of problems with this experiment. *M. tb* may not survive in exhaled droplets for a long time; since the droplets would theoretically be collected on the filter and then exposed to high concentrations of unhumidified oxygen, containing 1% isoflurane for up to 45 minutes, which may lead to desiccation (although the ability for *M. tb* to survive on surfaces for periods of up to six months is well documented). Secondly, the bacteria may become trapped in the filter. The filter membranes are hydrophobic and extraction was performed with very mild detergent (0.05% tween 80) which may not release bacteria. Attempts were made to develop a protocol to homogenise filters, but none were successful (data not shown). Also, one would expect that the hydrophobic nature of the filters should mean that droplets containing bacilli should be found on the surface and not embedded in the membrane.

This experiment by no means demonstrates that rabbits do not exhale bacteria. Conceptually, exhalation of bacteria may be dependent on specific mechanics (for example coughing) – and although the animals were subject to significant changes in respiratory pressure, the rapid airflow generated by coughing was not recapitulated. Bacterial entry from the parenchyma, into the airway, may be sporadic, for example if it coincides with cavity formation. If this were the case, in a singular event, many millions of bacteria may be simultaneously released, rather than a constant stream of bacteria. It should be noted however, that filters on the expiratory circuits of rabbits with cavities were exposed for a total of 36 hours – and that the absence of any culturable bacteria strongly suggests that rabbits in general are not highly infectious.

4.8.2. Bacterial collection using gelatin filters

A second experimental setup using only 3 animals yielded identical results. This time air was sampled directly onto a gelatin filter, using a commercially available bacterial sampling device (Sartorius MD8 Air Sampler). In this experiment all animals had cavities and were between 42-49 days post infection. The concept was that the gelatin collection method would reduce the risk of

desiccation. This method of capturing aerosolised *M. tb* has been used to assess the prevalence of aerosolised *M. bovis*, did not yield any culturable bacteria from badger sets (206). The machine was modified to ensure sampling of all exhaled gas (figure 58).

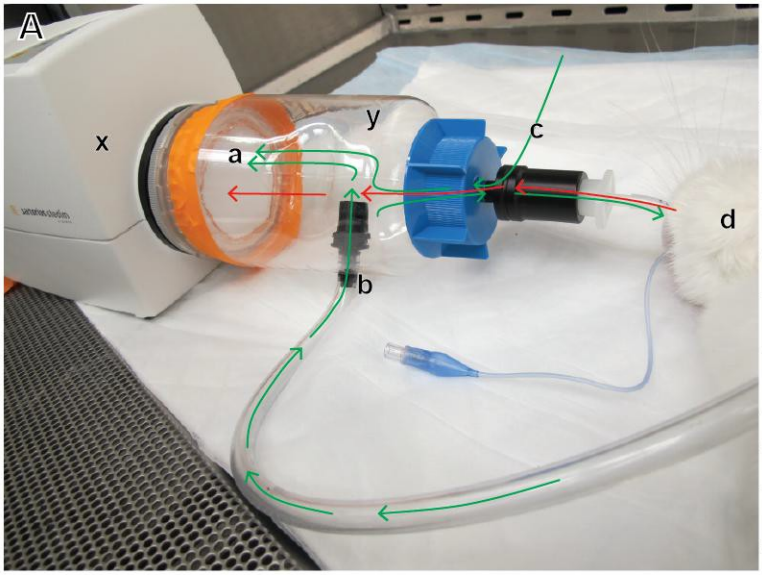

Figure 58. Direct breath-sampling: (A) This device was used to examine exhaled breath from rabbits, with cavities, 49 days after infection. Exhaled breath from intubated animals is collected on the gelatin filter (a) attached to the vacuum source (x). The chamber (y) allows for pressure equalisation and prevents direct negative pressure on the rabbit lung. After 15 minutes of sampling, the filter was placed onto agar, and another filter put in place. **(B)** Diagram of operation of device.

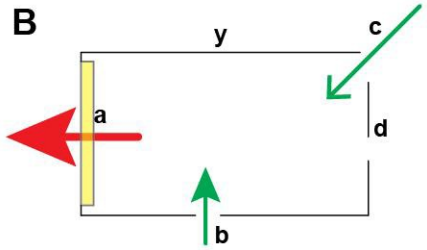

At rest: Gas is being drawn into the air sampling device (a), simultaneously oxygen is delivered into the chamber (b). To prevent a excess negative pressure being placed on the animals respiratory tree, a vent was placed (c). The gas flow at *a* = *b*+*c*, meaning that pressure remains atmospheric within the sampling chamber.

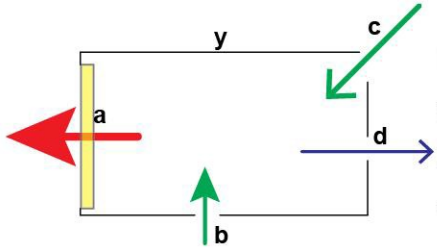

Inspiration: When the animal inhales, it generates a negative pressure which draws gas from the chamber into the respiratory tree. The increase in outflow is matched by an increase in gas flow at c. Flows: *a*+*d* = *b*+*c*.

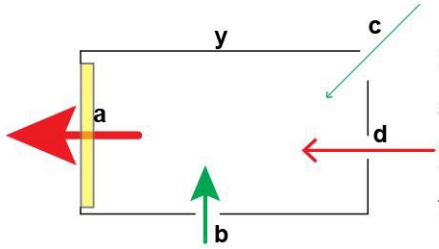

Expiration: When the animal exhales, pulmonary elastic recoil forces air into the chamber (d). Flow into the chamber increases at d, and is balanced by reduced flow at c. As long as d+b<a all gas being removed from the cylinder exits via a. *a*+*d* = *b*+*c*.

4.8.3. Rabbit to guinea-pig transmission

Simultaneously to these experiments a 'natural' transmission study was designed to see if guinea-pigs could be used as sentinels for the detection of exhaled viable bacteria. Since as few as 10 bacteria can establish progressive disease in the guinea pig it was thought that animal co-housing could demonstrate if sporadic infectious events occur (146, 207). A custom caging setup was used to prevent direct animal contact, and maintain animal well being (figure 59). A rabbit with extensive cavities disease was housed with a guinea pig for 8 weeks. At the end of this period the guinea pig was sacrificed and the entire lung homogenised in 12ml of PBS. The entire volume was plated on selective 7h11 agar (500ul per plate). No bacteria were grown from the guinea pig lung.

Figure 59. A custom designed cage setup to allow for rabbit to guinea-pig transmission challenges: A divider was secured between the rabbit and guinea pig. This prevents direct contact, but allows air flow. The direction of air flow is from the rabbit side of the cage (image right) to the guinea pig (image left) although this flow is not entirely linear. Theoretically, two guinea-pigs could be housed at the same time as the rabbit. Daily clearance of faecal debris from the rabbit side of the cage is required. The rabbit maintains access to water and food, and a water bottle is put in place for the guinea pig as well as a food trough. **(A)** Inside Cage **(B)** Cage Door.

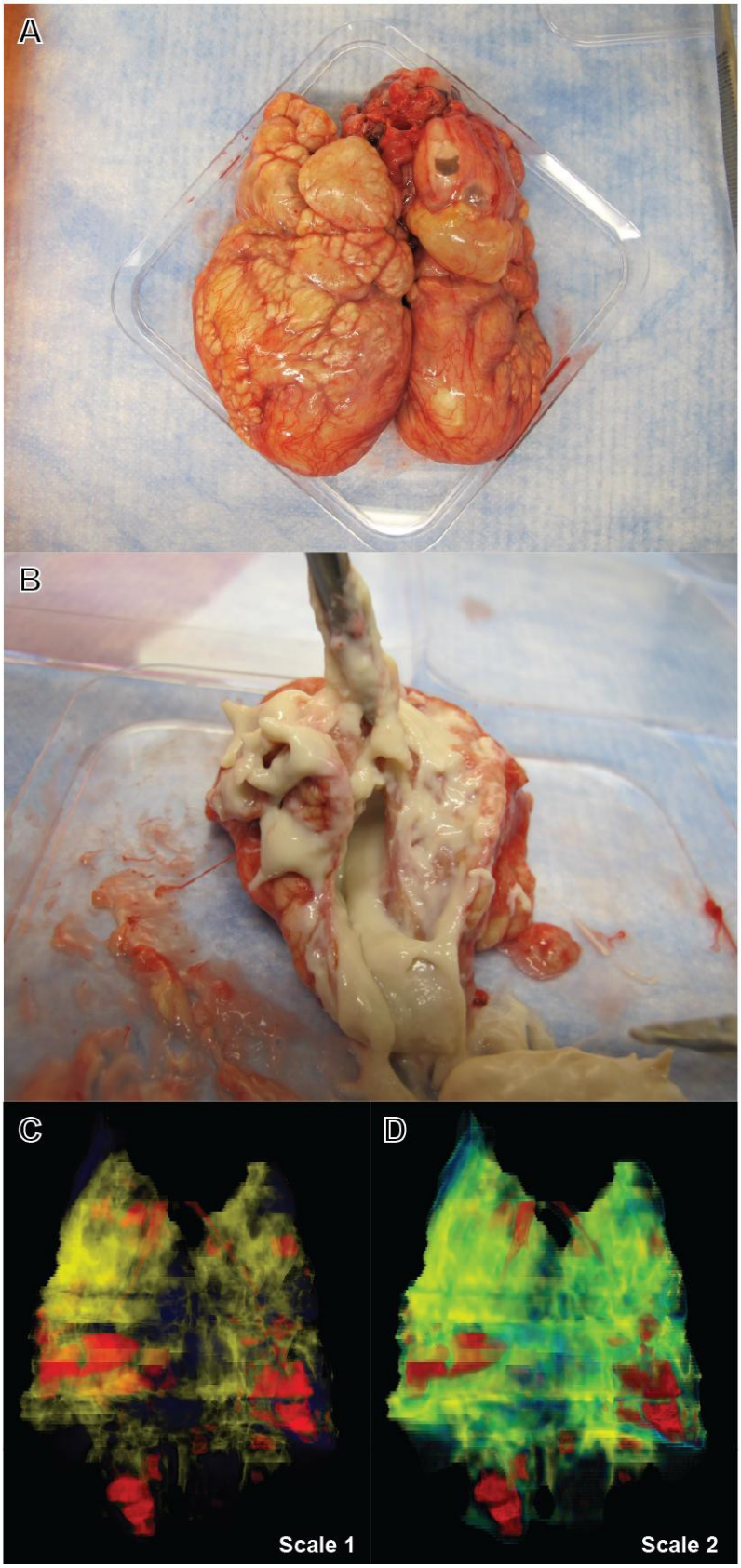

Figure 60. Co-housed rabbit lungs showed extreme pathology: The infected animal used for the transmission experiment showed extreme cavitary pathology. The animal had been infected 30 weeks previously with H37Rv. An aerosol infection was used, and the animal failed to contain infection - developing instead a progressive cavitary disease. **(A)** Posterior view of the lungs **(B)** Extensive caseous necrosis. Despite extensive disease, no bacteria were isolated from the guinea pig lungs. **(C and D)** At the initiation of the co-housing period, the rabbits were CT scanned, and extensive cavitation (red regions) and consolidation (yellow/green) was present .

It should be noted that whilst this experiment does not exclude the possibility of animal to animal transmission, it suggests that it would be at best a rare event. A number of technical improvements

could be made to enhance the chance of transmission. First, air flow in the caging could be reduced. High air-turnover has been demonstrated to reduce the risk of contracting *M. tb* infection in man (24). Secondly, larger numbers of animals could be used. Thirdly, a method to induce coughing could be developed – procedures such as nebulised citric acid have been used to induce this response in rabbits (208, 209). This modification would probably best be applied to direct bacterial collection on filters; although a design for a chamber which allowed for coughing and airflow from a rabbit to guinea-pig could be used.

It should be remembered that a practical transmission model would allow quantitative assessment the effect of interventions in preventing transmission. Since the mechanism of transmission is exhalation of aerosol droplets, an ideal model would recapitulate this process in a quantifiable and predictable manner. Currently this model does not readily demonstrate this; however, since reliable cavity formation is possible (figure 23), and cavities are strongly associated with TB transmission (184, 185), safely trialled anti-cavity therapies could be translated to human studies, without the proof that they prevent transmission in the animal model, but with the expectation that this may a beneficial result of treatment in humans.

4.9. Summary

This work, though very simplistic in nature, provides entirely novel options in assessing outcomes in rabbit experiments. By combining multiple biological samples and high quality CT images, we can see that virtual necropsy is possible, and hence reduce animal and drug usage, allowing expanded research in multiple areas. CT scanning can be used to measure levels of lung involvement and disease extent, and uniquely allows longitudinal follow-up of animals before and after interventions. Although this does not replace the need for studying animal bacterial burdens, it also gives previously undetectable, quantitative and highly clinically relevant information about the extent of lung involvement. There is also potential for comparison of disease to any marker in biological fluids, rudimentary detail of regional compliance of the lung and the ability to compare, for the first time within the same animal, these details over time. A few simple modifications could greatly improve the power of the tools developed here. Automated radiology techniques could allow for non-biased image analysis, with rapidly availability of results. Advanced respiratory monitoring using devices such as the SciReq Flexivent in combination with CT imaging could be used to examine the detailed mechanical properties of the lung during infection (210, 211). The techniques described here are easily modifiable to other large animal species.

The application of these technologies to the 70 day model of TB described in the section 3.8 of this thesis mean that trials involving drugs aimed at targeting cavity formation are possible using 1 group of animals in the control and treatment arm. As a result of this work, a short-duration, highly relevant model of TB cavity formation is available for investigating novel therapies in the context of human-like pathology.

5. Molecular Characterisation of the Rabbit Cavity Model of Tuberculosis

Tissue destruction is an important process in active tuberculosis (TB). The molecular mechanisms are poorly understood. Since destruction of the collagen ECM is central to the process, collagen degrading enzymes are likely involved (84, 85, 171). The model was investigated to better understand the molecular similarities and differences between what is known about human disease and the rabbit model.

Because MMPs, especially MMP-1, have been identified as potential targets for anti-cavitary therapy in TB (53, 54, 84, 85, 105, 107, 109-111, 114-118, 171), the investigations focussed primarily on these enzymes. Elkington *et al.* proposed a selective inhibitor of MMP-1 may be able to mediate cavitary pathology, however, have not been able to perform preclinical trials of the drug in a relevant animal model (109). Since the newly developed rabbit model described in section 3.8 of this thesis closely resembles the pathological phenotype of TB, we sought to investigate whether there were molecular correlates of human disease. Having confirmed a number of molecular correlates, we then investigated if this model could predict unidentified mediators of ECM degradation in man. Cathepsin K was predicted and confirmed as a potential mediator, via identification in a whole transcriptome screen, and was subsequently confirmed as being associated of tissue destruction in TB.

5.1. Selection of reference genes for quantitative real time polymerase chain reactions

Since quantitative real-time polymerase chain reactions (qRT-PCR) had not been utilised for the assessment of rabbit pulmonary tissue infected with *M. tb* at the initiation of this thesis, the first step in assessing the gene expression was to establish suitable reference genes (although publications with rabbit gene expression from granuloma expression have since been published, the process of reference gene analysis was not published (156, 167)). A vast number of strategies have been used to identify reference genes (172). Conceptually, the idea of a reference gene is that by comparing expression of genes of interest to a known reference gene, for which expression does not change in the conditions of interest, the relative expression of the gene of interest can be determined. Since the principal focus of this study was to identify whether genes of relatively high expression (i.e. the MMPs) matched findings observed in human cells and samples, an exhaustive search for stable reference was not conducted, instead, a small panel of potential reference genes were identified from the literature (212), and primers designed according to the available rabbit reference genome (oryCun2 [GCA_000003625.1]).

Potential reference genes identified are listed below (table 4)

Primer ID	Sequence	Target	Direction
NCA0127	CTGAACCCCAAGGCCAACC	Rabbit Beta actin	Forward
NCA0128	AGAGGCGTACAGGGACAGC	Rabbit Beta actin	Reverse
AKP001	GGCATCGTGACCAACTGGGA	Rabbit Beta Actin (2)	Forward
AKP002	CCGGCGTGTTGAACGTCT	Rabbit Beta Actin (2)	Reverse
AKP013	GTTCAACACGCCGGCCATGT	Rabbit Beta Actin (3)	Forward
AKP014	AGCGCGTAGCCCTCGTAGAT	Rabbit Beta Actin (3)	Reverse
AKP021	GTTCAACACGCCGGCCATGT	Rabbit Beta Actin (3)	Forward
AKP022	AGCGCGTAGCCCTCGTAGAT	Rabbit Beta Actin (3)	Reverse
AKP025	CGCTTCCGTTGCCCCGAG	Rabbit Beta Actin (4)	Forward
AKP026	GCCGCCCGACAGCACCGT	Rabbit Beta Actin (4)	Reverse
AKP171	CGATCATGAAGTGCGACGTGG	Rabbit Beta Actin (5)	Forward
AKP172	TCTTCATGGTGCTGGGCG	Rabbit Beta Actin (5)	Reverse
NCA0129	TTGTTCCCCTGCCTGGAGT	Rabbit B-2 Microglobulin	Forward
NCA0130	GATGAAACCCAGATAC	Rabbit B-2 Microglobulin	Reverse
AKP027	TGCTCGCGCTAGTCTTGTTCCC	Rabbit B-2 Microglobulin (2)	Forward
AKP028	TCTGGGGCGGATGAAACC	Rabbit B-2 Microglobulin (2)	Reverse
AKP193	ACGCCCAATGATAAGGAT	Rabbit B-2 Microglobulin (3)	Forward
AKP194	CCTCCATGCTGTTGATTA	Rabbit B-2 Microglobulin (3)	Reverse
AKP219	TCCATGTTTTCTGTACTTCTGG	Rabbit B-2 Microglobulin (4)	Forward
AKP220	AACTATGGATTCCCACCC	Rabbit B-2 Microglobulin (4)	Reverse
NCA0131	CGTCTTCACCACCATGGAG	Rabbit GAPDH	Forward

NCA0132	CAATCTTGAGAGAGTTGTC	Rabbit GAPDH	Reverse
AKP003	AAGTGGATGTTGTCGCCA	Rabbit GAPDH (2)	Forward
AKP004	ATGGCCTTCCCGTTGATG	Rabbit GAPDH (2)	Reverse
AKP017	AAGTGGATGTTGTCGCCA	Rabbit GAPDH (2)	Forward
AKP018	ATGGCCTTCCCGTTGATG	Rabbit GAPDH (2)	Reverse
AKP041	TTCCAGTATGATTCCACCCACG	Rabbit GAPDH (3)	Forward
AKP042	CACTTGATGTTGGCGGGA	Rabbit GAPDH (3)	Reverse
AKP177	CAAGAAGGTGGTGAAGCAGGC	Rabbit GAPDH (4)	Forward
AKP178	GCCCCAGCATCGAAGGTAGA	Rabbit GAPDH (4)	Reverse
NCA0133	GCTCGAGATGTGATGAAGG	Rabbit HPRT1	Forward
NCA0134	GTCATAGGAATGGATCTATC	Rabbit HPRT1	Reverse
AKP005	AATCATTACGTCGAGGAC	Rabbit HPRT1 (2)	Forward
AKP006	ATAATCCAGCAGGTCAGC	Rabbit HPRT1 (2)	Reverse
AKP033	AAGTTCTTTGCTGACCTGCTGG	Rabbit HPRT-1 (3)	Forward
AKP034	CATCTCCACCGATTACTTT	Rabbit HPRT-1 (3)	Reverse
AKP045	GCTCGAGATGTGATGAAGGAGA	Rabbit HPRT-1 (4)	Forward
AKP046	TCCCCTGTTGACTGGTCATTAC	Rabbit HPRT-1 (4)	Reverse
NCA0135	CAAGAGCCTGACCAACGAC	Rabbit HSP-90	Forward
NCA0136	TCAAACAGGTCAAACG	Rabbit HSP-90	Reverse
AKP179	CTCCCAGAACCGCAAGAAGC	Rabbit HSP-90 (2)	Forward
AKP180	TGGTCCTTGGTCTCACCTGTGA	Rabbit HSP-90 (2)	Reverse
AKP181	ACGAAGTTCGAGAACCTCTGCA	Rabbit HSP-90 (3)	Forward
AKP182	CCGTACGTGCTTGTGACGATG	Rabbit HSP-90 (3)	Reverse
AKP031	TGCCGTCAACAACACTCTCACA	Rabbit GUSB	Forward
AKP032	TCCCGCGTAGTTGAAGAAGTCA	Rabbit GUSB	Reverse
AKP195	TTTCCATGGGGTCAACAAGCAC	Rabbit GUSB (2)	Forward
AKP196	TGCATCACCTCCTCCGCAT	Rabbit GUSB (2)	Reverse
AKP197	TGCGCCGGGACAAGAATCA	Rabbit GUSB (3)	Forward
AKP198	TGGTCACAAAGGTCACGGGC	Rabbit GUSB (3)	Reverse
NCA0139	GGTTCCTGCTTTCACAGG	Rabbit PPIA	Forward
NCA0140	CATCCTCGAACTTCTCTC	Rabbit PPIA	Reverse
AKP029	CTGAGCACCGGAGAGAAAGGA	Rabbit PPIA (2)	Forward
AKP030	ATAGATGGACTTGCCGCCGG	Rabbit PPIA (2)	Reverse
AKP173	CCCAACACAAACGGCTCCCA	Rabbit PPIA (3)	Forward
AKP174	TGCTGGTCTTGCCGTTCTCG	Rabbit PPIA (3)	Reverse
AKP175	GGTTCCTGCTTTCACAGG	Rabbit PPIA (4)	Forward
AKP176	CATCCTCGAACTTCTCTC	Rabbit PPIA (4)	Reverse
AKP035	CTCTGCTACGCGATGGTTGCTA	Rabbit TFRC	Forward
AKP036	TCCGCGTTTTCTGACTGCTC	Rabbit TFRC	Reverse
AKP199	TCCAGACGATTTCCAGAGAGGC	Rabbit TFRC (2)	Forward
AKP200	CAGCACGTTGTTCACAGTGAGC	Rabbit TFRC (2)	Reverse
AKP201	TGCTGCTTTCCCTTTCCTTGCT	Rabbit TFRC (3)	Forward
AKP202	CCCGGGCCATTTTGTTCA	Rabbit TFRC (3)	Reverse
AKP037	TGGGTCTGTCATCCTGCTGG	Rabbit PGK-1	Forward
AKP038	TTGGCTGGTTCCGCTTTA	Rabbit PGK-1	Reverse
AKP203	TTGGTCGGGCGAAGCAGATTGT	Rabbit PGK-1 (2)	Forward
AKP204	TCTCCACCGCCGATGATGGT	Rabbit PGK-1 (2)	Reverse
AKP205	AGTCCGTTGTCTTGATGAGCCA	Rabbit PGK-1 (3)	Forward
AKP206	GGGCCCACACAATCCTTTAAGA	Rabbit PGK-1 (3)	Reverse
AKP039	GCAGCAGTGTCGTCCGCAAA	Rabbit ALAS	Forward
AKP040	CCACTGGGGTCCTCTCCGT	Rabbit ALAS	Reverse
AKP207	TGTGGCCAACGACTCAACCC	Rabbit ALAS (2)	Forward
AKP208	CGTCGTTGTGGCGGAAGATGTA	Rabbit ALAS (2)	Reverse
AKP209	GAATTGGTGATCGGGACGGAGT	Rabbit ALAS (3)	Forward
AKP210	TGAAGATGAAGCCAGCCGC	Rabbit ALAS (3)	Reverse
NCA0137	TGGACCTGGTGGTTCAC	Rabbit PBGD	Forward
NCA0138	TGAAAGACAACAGCATCGCAG	Rabbit PBGD	Reverse

AKP211	AGTGCTATCATCCTGGCTGTGG	Rabbit PBGD (2)	Forward
AKP212	TCGAACTTCCACTCCCAGGG	Rabbit PBGD (2)	Reverse
AKP213	AGGAGTCTGGAGTCTGGATGGC	Rabbit PBGD (3)	Forward
AKP214	TCCTCGTGGAATGTTCCGG	Rabbit PBGD (3)	Reverse
AKP015	GAATGAGTCCACTTTAAATC	Rabbit 18S rRNA	Forward
AKP016	GATCCAACTACGAGCTTT	Rabbit 18S rRNA	Reverse
AKP215	CAGTTATGGTTCCTTTGGTCGC	Rabbit 18S rRNA (2)	Forward
AKP216	AGGCTGACCGGGTTGGTTT	Rabbit 18S rRNA (2)	Reverse
AKP217	GCAAGACGGACCAGAGCGAA	Rabbit 18S rRNA (3)	Forward
AKP218	GTCATGGGAATAACGCCGC	Rabbit 18S rRNA (3)	Reverse

Table 4. Potential reference gene primers for qRT-PCR.

From this list primers, those pairs which had an average efficiency of 1.8 to 2.2 (as evaluated by Ramakers linear regression method (172)) and generated products with a singular melt point, were used to establish reference gene stability in 5 paired RNA isolates from cavity wall grossly normal tissue. The following primers demonstrated reproducible products and efficient reactions (table 5).

Primer ID	Sequence	Target	Direction
AKP025	CGCTTCCGTTGCCCCGAG	Rabbit Beta Actin (4)	Forward
AKP026	GCCGCCCGACAGCACCGT	Rabbit Beta Actin (4)	Reverse
NCA0129	TTGTTCCCCTGCCTGGAGT	Rabbit B-2 Microglobulin	Forward
NCA0130	GATGAAACCCAGATAC	Rabbit B-2 Microglobulin	Reverse
AKP041	TTCCAGTATGATTCCACCCACG	Rabbit GAPDH (3)	Forward
AKP042	CACTTGATGTTGGCGGGA	Rabbit GAPDH (3)	Reverse
AKP005	AATCATTACGTCGAGGAC	Rabbit HPRT1 (2)	Forward
AKP006	ATAATCCAGCAGGTCAGC	Rabbit HPRT1 (2)	Reverse
AKP181	ACGAAGTTCGAGAACCTCTGCA	Rabbit HSP-90 (3)	Forward
AKP182	CCGTACGTGCTTGTGACGATG	Rabbit HSP-90 (3)	Reverse
AKP031	TGCCGTCAACAACACTCTCACA	Rabbit GUSB	Forward
AKP032	TCCCGCGTAGTTGAAGAAGTCA	Rabbit GUSB	Reverse
AKP029	CTGAGCACCGGAGAGAAAGGA	Rabbit PPIA (2)	Forward
AKP030	ATAGATGGACTTGCCGCCGG	Rabbit PPIA (2)	Reverse
AKP035	CTCTGCTACGCGATGGTTGCTA	Rabbit TFRC	Forward
AKP036	TCCGCGTTTTCTGACTGCTC	Rabbit TFRC	Reverse
AKP037	TGGGTCTGTCATCCTGCTGG	Rabbit PGK-1	Forward
AKP038	TTGGCTGGTTCCGCTTTA	Rabbit PGK-1	Reverse
AKP207	TGTGGCCAACGACTCAACCC	Rabbit ALAS (2)	Forward
AKP208	CGTCGTTGTGGCGGAAGATGTA	Rabbit ALAS (2)	Reverse
AKP213	AGGAGTCTGGAGTCTGGATGGC	Rabbit PBGD (3)	Forward
AKP214	TCCTCGTGGAATGTTCCGG	Rabbit PBGD (3)	Reverse

Table 5. Reference gene primers for qRT-PCRs to establish reference gene stability.

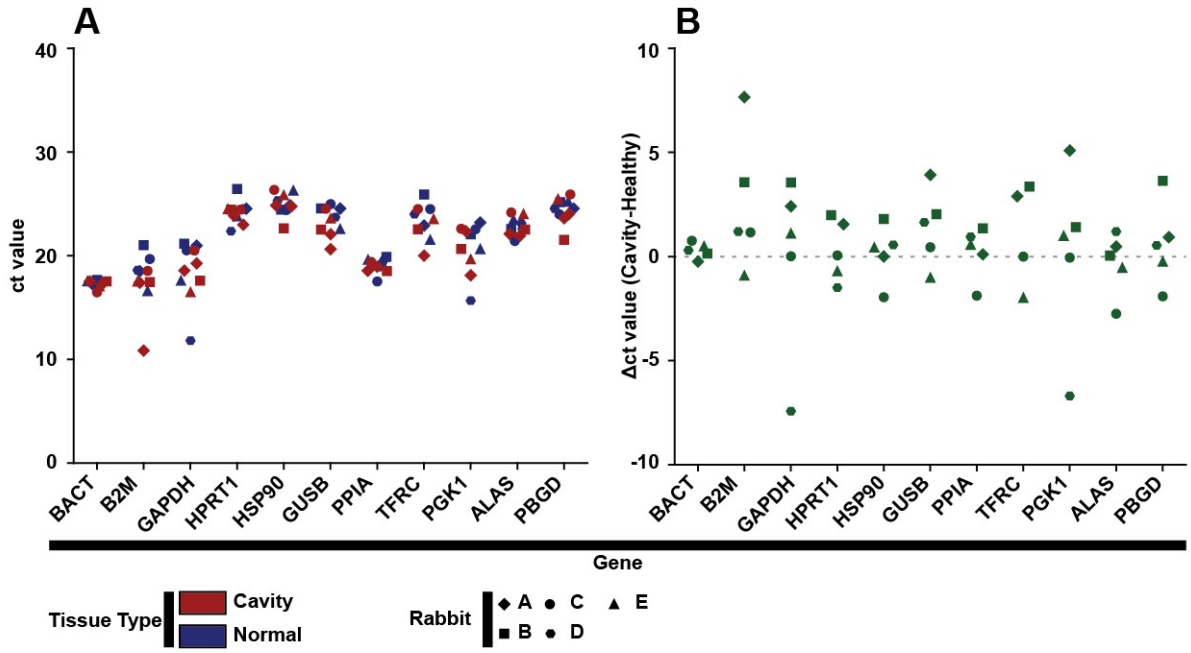

Figure 61. Reference gene selection: 11 potential reference genes were identified from the literature. RNA was isolated from paired cavity and non-cavity samples. RNA concentration was evaluated utilising a Nanodrop and normalised to 12.5ng/ul prior to cDNA conversion. Samples were subjected to qRT-PCR, and ct values calculated. **(A)** A variety of ct values were obtained for nearly all genes, with variation being most limited in BACT. **(B)** There was little change in BACT expression independent of the tissue state. The next most stable gene was PPIA.

Having identified BACT and PPIA were clearly the most stable genes (figure 61), it was decided that these should be used as reference genes. GAPDH was included in all experiments as there is a precedent for its use in comparing RNA from *M. tb* infected rabbit lungs (156, 163, 167). Subsequently, multiple primers for each of the MMPs mapped in the rabbit genome as well as the 4 TIMPs were selected

5.2. Selection of MMP primers for qRT-PCR

Below is a list of primer pairs that were trialled for each identifiable MMP in the rabbit genome (Table 6).

Target	Forward Primer ID	Forward Primer Sequence (5' → 3')	Reverse Primer ID	Reverse Primer Sequence (5' → 3')	Product Size (bp)	
					gDNA	cDNA
MMP-1	NCA0212	CAACTCTGGAGTAATGTCACACC	NCA0213	GAACATCCCCTCCAATGC	408	172
MMP-2	NCA0214	GCAATACCTGAACACCTTCTACG	NCA0215	TATAGTTGGCCACATCC	179	179
MMP-3	NCA0216	GCTCATGCTTATGCACCTGG	NCA0217	TACATCAGCGCTTCAGGGTTGG	1720	167
MMP-7	NCA0218	AGGAGATGCAGAAGTTCTTTGG	NCA0219	TCTGGAAGTCCACTTCGG	143	143
MMP-8	NCA0220	ATTTTATTTCCCTGTTCTGGCC	NCA0221	TTCATAGCCATTCAGAGC	696	122
MMP-9	NCA0222	ACCTGTTCCGCTATGGTTACACC	NCA0223	TGGAATTTGCCCACGTCC	181	181
MMP-10	NCA0224	CTACAACACCTTCACAGACCTGGC	NCA0225	GCATCGAAGGACAAAGCC	373	177
MMP-11	NCA0226	GACCTTCACTGAGGTGCATGAGG	NCA0227	TTGGGGAAGAAGGCATGG	207	123
MMP-12	NCA0228	TCAAGTATGGAGCGATGTGACC	NCA0229	TCCAATACCAGGTCCAGGC	248	163
MMP-13	NCA0230	CTCATTCTGAAGTTGAAAAGGC	NCA0231	TCAAATGGGTAGAAGTCGC	584	148
MMP-14	NCA0232	CAAAGCAACAGCTTCAGCC	NCA0233	TCATGGTGTCTGTATCGG	3829	172
MMP-15	NCA0234	AGATGCAGCGCTTCTACGG	NCA0235	TTGGCTTTCACGTGCACC	654	118
MMP-16	NCA0236	CAAGGAAAAATGACAGGCC	NCA0237	AAAACAAACATCTCACGGC	130	130
MMP-17	NCA0238	ACGCAAGAGGAACTGTCCAAGGC	NCA0239	TTGTTCCACTTGGTCGG	519	185
MMP-19	NCA0240	AAGGACCTCAGGTCTTCAGGC	NCA0241	GGGTCTTCTGATTGAAGG	1342	159
MMP-20	NCA0242	AGCTACAAGCGTTCTTTGGC	NCA0243	GGAAGAGACGATAGTTCGC	114	114
MMP-21	NCA0244	GATGATGACGAACACTTCACACCG	NCA0245	ACCAGTCCAACTCGAACGC	404	169
MMP-24	NCA0246	CTGAAGCTCCATTTTCCCAGG	NCA0247	TTGTCTGATCCAGCACGC	3110	168
MMP-27	NCA0248	CAAAGAGCCTTGATGTTCC	NCA0249	ATCCTGTGTCACAGGCATGG	832	160
MMP-28	NCA0250	TACAAGCAGCACCTCTCCTACCG	NCA0251	CTTGGAAGAAGGTGAGGC	172	172
TIMP-1	NCA0264	TGTCTGCTCTGCACACTTCGGC	NCA0265	GCAGGTTTGGAATCAGGGGC	-	120
TIMP-2	NCA0266	CGGAGAAGAACATCAACGGG	NCA0267	CCAGAAACTCCTGCTTGGGG	111	111
TIMP-3	NCA0268	AAGCCTCTGAGAGTCTCTGTGGCC	NCA0269	TCCACGAAGTTGCACAGCCC	475	112
TIMP-4	NCA0270	ACACTCAGAGAATGATCCGG	NCA0271	CACCACAGAGAGAAGAGTCA	544	114
MMP-10(2)	NCA0274	ATGAACCATCTTGTCCTC	NCA0275	CCTTCTTTTGTGAGGTTG	809	143
TIMP-3(2)	NCA0278	CTCTGAGAGTCTCTGTGG	NCA0279	TAGCGATAGTTCAGC	522	159
MMP-3(2)	AKP007	GAGCCTCAAGGGATGCAGA	AKP008	AGCCAAGGAACTTCTGCA	649	156
MMP-9(2)	AKP009	GTGACGCCACTCACCTTCAC	AKP010	TCGTCGAAGTGGGCATCTCC	399	167
MMP-14(2)	AKP011	CACTGTCAGCTGCCATTG	AKP012	TCGGACATTGGCCTTGAT	414	146
MMP-1	AKP023	CAACTCTGGAGTAATGTCACACC	NCA0213	GAACATCCCCTCCAATGC	408	172
MMP-1	AKP043	CCCTGAAGATGATGAAGCAACC	AKP044	ACATCTGCCCTTGACAGGTCTG	234	142
HPRT-1	AKP045	GCTCGAGATGTGATGAAGGAGA	AKP046	TCCCCTGTTGACTGGTCATTAC	-	191
MMP-2	AKP047	AGCCCAAGTGGGACAAGAATCA	AKP048	TTCGAGAAAACCGCAGCGG	916	138
MMP-3	AKP049	AGGTGATACGCAAGCCCAGGTG	AKP050	CAATGGCAGCATCAACAGCA	241	150
MMP-7	AKP051	TACTCACCACTCCCAAGCAGCC	AKP052	CCACAAGTTGAAAGCCTTTGCC	218	135
MMP-8	AKP053	TCCTTGCCCATGCCTTTCAGCC	AKP054	TGAGCGAGCCCCAAGGAAT	4478	145
MMP-9	AKP055	ACGTCAGGGGCATCCAGCAT	AKP056	GGTAGTGGGGTGCTCGGAGG	1095	146
MMP-10	AKP057	GGAGGTGATACGCAAGCCCA	AKP058	GCATCTCTTGGCAGATCTGGTG	226	144
MMP-11	AKP059	GTCACGCCACTGACCTTCACTG	AKP060	CCCCAGGCCCATCAAAGG	190	106
MMP-12	AKP061	CTCGATGTGGAGTGCCTGATGT	AKP062	GCTTCATGTCTGGAGTGT	1049	111
MMP-13	AKP063	TCCTCGAACACTCAAATGGTCC	AKP064	GGCCTTTTCAACTTCAGA	1052	91
MMP-14	AKP065	TTCGATGGCGAGGGTGGCTT	AKP066	GCTCATGCACAGCCACCAGG	646	148
MMP-1	AKP067	ACCTTCCCAAAATCCCAGTCAG	AKP068	GATTTGCCCGCATGTAGAACC	1979	137
MMP-1	AKP069	ATTGACGCTGCTGTTTCTGAGG	AKP070	CCTTGTTTCCAATTCCTGGGA	1991	148
MMP-2	AKP071	CCGCAGTGATGGCAAGATGTG	AKP072	GGGCTGCCACGAGGAACA	1789	107

MMP-2	AKP073	GACATCAAGGGCATTCAAGAGC	AKP074	GCGATGCCATCGAAGACGAT	1177	134
MMP-3	AKP075	TCTCAAGATGATGTGGATGGCA	AKP076	AGTGCTGATTGCATCGAAGGAC	337	153
MMP-3	AKP077	TGGCCATCTCTTCCTTCAGCA	AKP078	TGCTTCTTGGGTAACCAGCTTG	878	130
MMP-7	AKP079	AGGAAACACACTGGCTCACGC	AKP080	CCAAGTTCATGAGTTGCCACGT	2183	135
MMP-7	AKP081	CCACAGTGGGAACAGGCTCA	AKP082	CCAGTTATAGGCAGGCCAAAGA	3114	128
MMP-8	AKP083	CAAGCACGTTTTCACTCCCTCA	AKP084	TGGTGGCAGCATCAAAGG	2260	138
MMP-9	AKP085	ACCGCCAGCTACGACAAGGA	AKP086	TTGCCCAGGAAGACGAAGG	429	119
MMP-9	AKP087	TCGCCGAGATAGGGAACAAGC	AKP088	GTCGGCGATGAGGAAGGG	224	104
MMP-10	AKP089	TACCCAAAAGACATCCACACCC	AKP090	TCGCTCCATAGACTGGCTGC	1173	147
MMP-10	AKP091	GCACGAAGGAGAGGCTGACA	AKP092	AACATCTCCATAAAGCCCAGGC	557	130
MMP-11	AKP093	GGACACCAATGAGATAGCACCG	AKP094	GCGCAGCCTCCACACAAA	237	130
MMP-11	AKP095	TGAGAGCCAGCAACCGACAG	AKP096	TGAGAGCCAGCAACCGACAG	865	92
MMP-12	AKP097	CCCATGCCAAAACCTGACAATC	AKP098	ACGGACACTGGTCGTTGAACTC	1313	150
MMP-12	AKP099	CCTGGGCTTCCCTGACTTTGTG	AKP100	TCAGCTTGGGATAACCAGCATC	1941	143
MMP-13	AKP101	ACTCATTGCTGGTCCCTGCC	AKP102	TCCCGCAGGATTCAGAGGA	212	120
MMP-13	AKP103	GAAGACCCCAACCCTAAACACC	AKP104	AGCTCTGCATCCACCTGCTGAG	763	149
MMP-14	AKP105	CTGCCTGCGTCCATCAACA	AKP106	AGCCTCGTCAAACACCCA	216	90
MMP-14	AKP107	GATCGATGCCGCTCTCTTCTG	AKP108	CGCTGTCCACTGCCCTGA	522	101
MMP-15	AKP109	GCGGGGAGATGTTCGTGTTC	AKP110	AAACGGCCATCTTGGCGCTC	410	148
MMP-15	AKP111	TTCGACGCCGATGAGCCC	AKP112	ATCCACTGGTAGAACGGCGC	471	149
MMP-15	AKP113	GCTACCCCAAGCCCATCAGTGT	AKP114	GCGCTCGTTGTCGAATTTCC	1178	128
MMP-16	AKP115	AACAGGACAGAAGTGGCAGCAT	AKP116	CATCAAAGGCACGGCGAA	4939	107
MMP-16	AKP117	AGCACTGGAAGACGGTTGGAT	AKP118	AATACTGCTCCGTTCCGC	103	103
MMP-16	AKP119	GGACTTTATGGGCTGTGATGGA	AKP120	GGCCAAGATGCAGGGAATGAC	142	142
MMP-17	AKP121	CGCACCAGCGACCACAAGAT	AKP122	GCCGCGGGTATCCTTCCT	3379	88
MMP-17	AKP123	TCTCCAAGGCCGACCACAA	AKP124	GGCCTCGTCGTCATCAAA	123	123
MMP-17	AKP125	ATTGGGCTGGGCCATGTTG	AKP126	GGACACAGACTCCCGTACACCA	1335	144
MMP-19	AKP127	GGCCCTCATGGCTCCTGTCTAT	AKP128	TGGGCAGCTCTGTCTCTTCTTC	527	140
MMP-19	AKP129	GAATCGGATCGAGCCTAACCTG	AKP130	TTGGGGTAGCGGCTGAAGTC	295	129
MMP-20	AKP131	TGAAAGGGATCCAGGCGTTGTA	AKP132	TCCCAGCATCGTCACAGCA	2250	140
MMP-20	AKP133	CATGCATTTGCACCTGGAGAAG	AKP134	TTCATGAGCAGCGACCGT	908	111
MMP-21	AKP135	AATGCAGCCCAACTACACTCCC	AKP136	CCTCCCCAAACTGGTTTCTCTC	1225	149
MMP-21	AKP137	GTCAACAGGAACCAAGTGCCG	AKP138	AGAAGAGCGAGCCGTGCG	133	133
MMP-24	AKP139	CCGTAGGCGGAGAAACAAGC	AKP140	TCAAAGGCCTGGCGAATAGC	1576	135
MMP-24	AKP141	CCAAGGGGCCTTCATCAGCAAA	AKP142	TGCAGCCCATCCAGTCACG	2595	137
MMP-27	AKP143	GCACTGGAAGTATGGAGCAACG	AKP144	TGACGAGGACATCGGCCA	201	133
MMP-27	AKP145	CAAATCCATCCATACGCTCGGC	AKP146	CCATGGTTTGGGTCATCTCATC	729	137
MMP-28	AKP147	AGGTGGCAGCAGACGGCAAT	AKP148	TCTCCAGCACCGACTCCCTT	669	140
MMP-28	AKP149	CACAACGATGGGCTGGGCAA	AKP150	AGCACCACGAACAGGTTGCG	2474	149
TIMP-1	AKP151	GTGGGGGCTCCAGAAGTCAATC	AKP152	TGCCCCAAGGCGTCAAAT	631	92
TIMP-1	AKP153	ACTCCCACAAATCCCAGAACCG	AKP154	CGGAACGTTGAGAGAAGCTCAG	404	129
TIMP-1	AKP155	GCCCGGACAGACGCTAGAGAAT	AKP156	TGAGGTGGGACACAGGTGCA	1002	116
TIMP-2	AKP157	AGGTGGACTCTGGGAACGACA	AKP158	CGGGGCCTTTGAACATCT	1128	89
TIMP-2	AKP159	CTGGACGTGGGAGGCAAGAA	AKP160	GGTTCAGGCTCTTCTTCTGCGT	5747	153
TIMP-3	AKP161	ACGCCTTCTGCAACTCCGACAT	AKP162	ACGTGGGGCATCTTGGTGA	-	139
TIMP-3	AKP163	AGAATGAGTGCCTTTGGACCG	AKP164	TGCAGTAGCCGCCCTTTT	99	99
TIMP-4	AKP165	TTAGAAGCCAACAGCCAGAAGC	AKP166	GGCTTTCCCTCTGCACCAAG	2982	127
TIMP-4	AKP167	GCTGTTGCTGCGGCTGCT	AKP168	ACGTGCTGCTGGGGGTGC	87	87
EMMPRIN	AKP183	TGAAGAAGTCGGAGCACGCC	AKP184	TGGGAGCCGTTCTGGATGAC	-	136
EMMPRIN	AKP185	GCTGGCTGAAAGGGAAGGAA	AKP186	TTGCCAAACCTGTCGTCC	-	91
EMMPRIN	AKP187	CGGAGCTGCACATCAAGGAC	AKP188	CCACGATGCCCAGGAAGG	-	150
TIMP-1	AKP189	GGCCTTCTGCAACTCCGA	AKP190	TGCCCCAAGGCGTCAAAT	1857	126
MMP-9	AKP191	CGCCAGCTACGACAAGGACA	AKP192	AAGTGGTGGCACACCAGAGG	-	-
CTSK	AKP221	TGGGGACTCAAGGTTCTGCTG	AKP222	CCCAAATTAAACGCCGAGAGA	1589	148
HO1	AKP223	TGAAGGAGGCCACCAAGGA	AKP224	TCCAGGGCCACGTAGATGTG	2124	136

HO1	AKP225	CAGCTTGCCCCAGGATTTGTC	AKP226	TGGTACAGGGAGGCCATCACCA	972	147
HO1	AKP227	ATCGCCAGCGCCACCAAGTT	AKP228	GCAGCTCCTGCAACTCCTCAA	1215	148

Table 6. Primer pairs trialed prior to qRT-PCR analysis.

From these primers, those that most reliably produced a single peak under melt-curve analysis, and an efficiency of between 1.8 and 2.2 by Ramaker's linear regression analysis (172) were selected to carry out preliminary analysis of MMP expression in cavity vs non-cavity tissue (table 7):

Amplicon Description	Forward Primer ID	Forward Primer Sequence (5' ⊠ 3')	Reverse Primer ID	Reverse Primer Sequence (5' ⊠ 3')	Product (bp)	Size
					gDNA	cDNA
PPIA	AKP025	CTGAGCACCGGAGAGAAAGGA	AKP026	ATAGATGGACTTGCCGCCGG	246	123
GAPDH	AKP041	TTCCAGTATGATTCCACCCACG	AKP042	CACTTGATGTTGGCGGGA	229	122
β-actin	AKP005	CGCTTCCGTTGCCCCGAG	AKP006	GCCGCCCGACAGCACCGT	234	147
MMP-1	AKP067	ACCTTCCCAAAATCCCAGTCAG	AKP068	GATTTGCCCGCATGTAGAACC	1979	137
MMP-2	AKP071	CCGCAGTGATGGCAAGATGTG	AKP072	GGGCTGCCACGAGGAACA	1789	107
MMP-3	AKP077	TGGCCATCTCTTCCTTCAGCA	AKP078	TGCTTCTTGGGTAACCAGCTTG	878	130
MMP-7	AKP081	CCACAGTGGGAACAGGCTCA	AKP082	CCAGTTATAGGCAGGCCAAAGA	3114	128
MMP-8	NCA0220	ATTTTATTTCCCTGTTCTGGCC	NCA0221	TTCATAGCCATTCAGAGC	696	122
MMP-9	AKP087	TCGCCGAGATAGGGAACAAGC	AKP088	GTCGGCGATGAGGAAGGG	224	104
MMP-10	AKP089	TACCCAAAAGACATCCACACCC	AKP090	TCGCTCCATAGACTGGCTGC	1173	147
MMP-11		UNDETECTED				
MMP-12	AKP061	CTCGATGTGGAGTGCCTGATGT	AKP062	GCTTCATGTCTGGAGTGT	1049	111
MMP-13	AKP101	ACTCATTGCTGGTCCCTGCC	AKP102	TCCCGCAGGATTCAGAGGA	212	120
MMP-14	AKP107	GATCGATGCCGCTCTCTTCTG	AKP108	CGCTGTCCACTGCCCTGA	522	101
MMP-15	AKP113	GCTACCCCAAGCCCATCAGTGT	AKP114	GCGCTCGTTGTCGAATTTCC	1178	128
MMP-16	AKP119	GGACTTTATGGGCTGTGATGGA	AKP120	GGCCAAGATGCAGGGAATGAC	142	142
MMP-17	AKP121	CGCACCAGCGACCACAAGAT	AKP122	GCCGCGGGTATCCTTCCT	3379	88
MMP-19	AKP127	GGCCCTCATGGCTCCTGTCTAT	AKP128	TGGGCAGCTCTGTCTCTTCTTC	527	140
MMP-20		UNDETECTED				
MMP-21	NCA0244	GATGATGACGAACACTTCACACCG	NCA0245	ACCAGTCCAACTCGAACGC	404	169
MMP-24	AKP141	CCAAGGGGCCTTCATCAGCAAA	AKP142	TGCAGCCCATCCAGTCACG	2595	137
MMP-27	AKP145	CAAATCCATCCATACGCTCGGC	AKP146	CCATGGTTTGGGTCATCTCATC	729	137
MMP-28		UNDETECTED				
TIMP-1	AKP189	GGCCTTCTGCAACTCCGA	AKP190	TGCCCCAAGGCGTCAAAT	1857	126
TIMP-2	AKP157	AGGTGGACTCTGGGAACGACA	AKP158	CGGGGCCTTTGAACATCT	1128	89
TIMP-3	AKP161	ACGCCTTCTGCAACTCCGACAT	AKP162	ACGTGGGGCATCTTGGTGA	47989	139
TIMP-4	NCA270	ACACTCAGAGAATGATCCGG	NCA0271	CACCACAGAGAGAAGAGTCA	544	114

Table 7. Primer pairs used preliminary analysis qRT-PCR analysis.

This preliminary data is shown in figure 62.

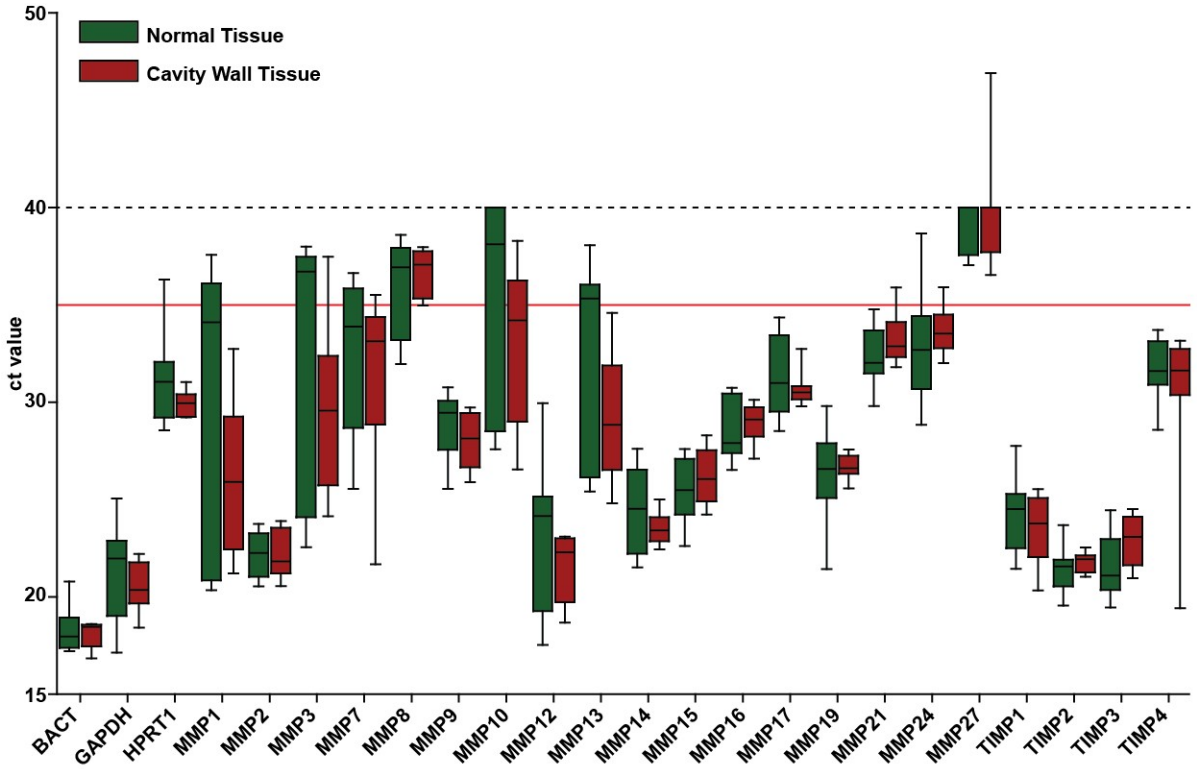

Figure 62. Preliminary qRT-PCR data comparing gene expression of all identifiable MMPs and TIMPs: ct values are shown. These give an approximate indication of transcript abundance. MMPs-1, -2, -4,-9,-12, -13, -14, -15, -16, -17, -19 and TIMPs-1, -2, -3 and -4 were detectable. Boxes range from the 25th to 75th percentile with whiskers demonstrating the range. Results below 35 cycles (red line) are considered unreliable, 40 cycles is the limit of detection.

This preliminary data, which is not intended to be used to draw conclusions about expression, was used instead to refine the assays for future experiment but also allowed for several conclusions to be drawn. Most importantly, although primers had previously shown amplification of certain MMPs, the primers did not regularly amplify product for a number of amplicons: MMP-8, MMP-10 and MMP-27. Very low levels of MMP21 and 24 were detected. MMPs -1, -2, -3, -7, -9, -12, -13, -14, -15, -16, -17 and -19 and TIMPs -1,-2,-3 and -4 were detected reliably detected in cavity samples. Of these, only MMP-9, -12, -14, -15, -16, -17 and -19 and the TIMPs were detected in normal tissue.

5.3. Preliminary evaluation of MMP expression

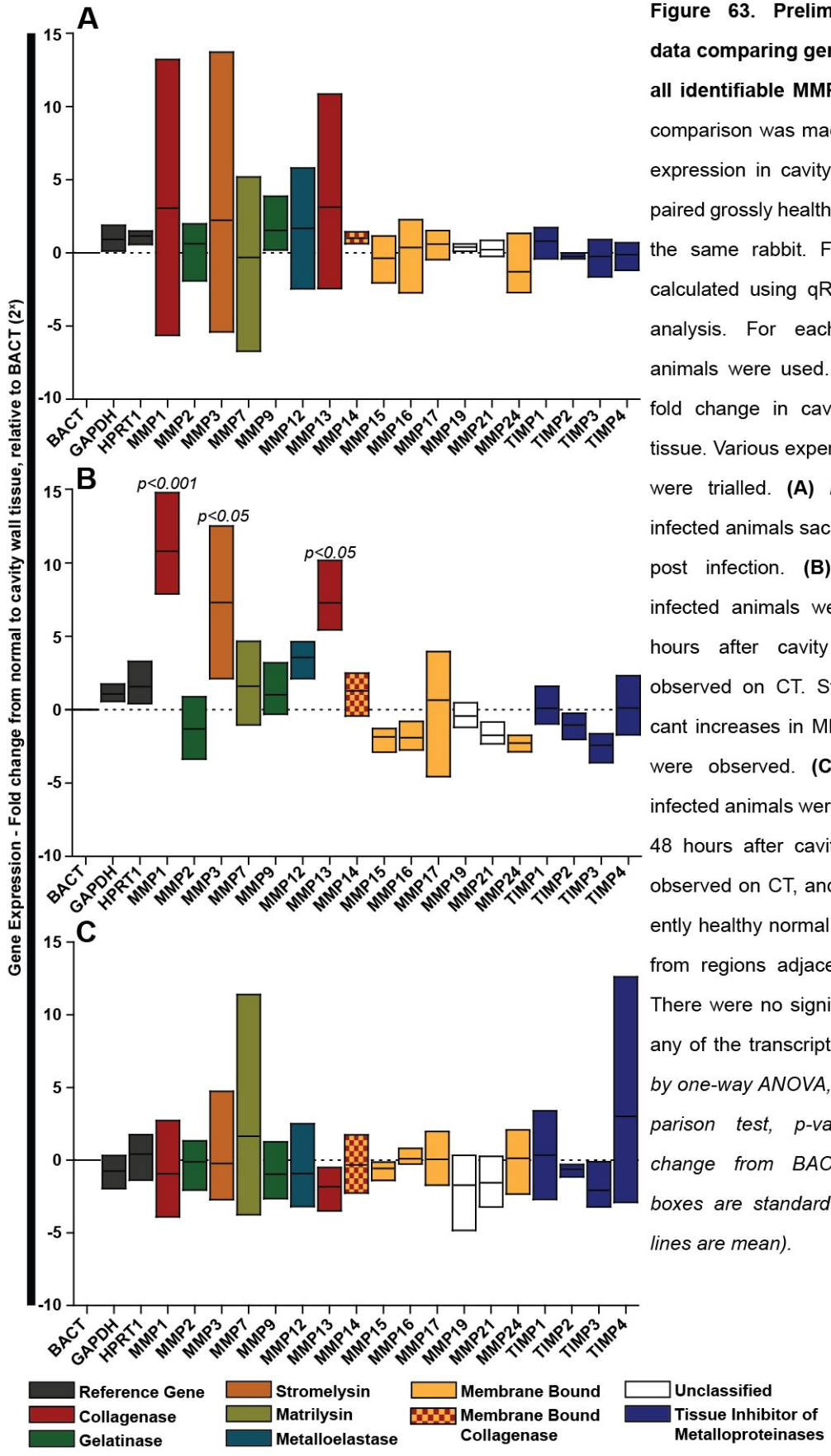

Figure 63. Preliminary qRT-PCR data comparing gene expression of all identifiable MMPs and TIMPs: A comparison was made between gene expression in cavity wall tissue, and paired grossly healthy lung tissue from the same rabbit. Fold change was calculated using qRT-PCR and **ΔΔ**ct analysis. For each experiment 3 animals were used. Data represents fold change in cavity over 'normal' tissue. Various experimental protocols were trialled. **(A)** *M. tb CDC1551* infected animals sacrificed at 6 weeks post infection. **(B)** *M. tb H37Rv* infected animals were sacrificed 48 hours after cavity formation was observed on CT. Statistically significant increases in MMP-1, -3 and -13 were observed. **(C)** *M. tb H37Rv* infected animals were again sacrificed 48 hours after cavity formation was observed on CT, and this time apparently healthy normal tissue was taken from regions adjacent to the cavity. There were no significant changes in any of the transcript levels. *(statistics by one-way ANOVA, Tukey post comparison test, p-value quoted for change from BACT fold change; boxes are standard deviations, midlines are mean).*

Different experimental modalities and dissection techniques were used in each of these preliminary studies. The primary observation from these data is that there is significant variation in the expression levels of genes in rabbit tissue, and that the method of dissection can make a significant difference in attempting to define these differences. Figure 63B demonstrates that when tissue is dissected from the cavity immediately after cavitation and compared to tissue from distant sites, MMP-1, -3 and -13 are highly upregulated. Figure 63C demonstrates that the expression of MMPs remains constant between closely related but normal tissue as compared to cavity wall tissue, and suggests that either the imprecise dissection method confounds results, or the adjacent tissue grossly healthy tissue may have a similar pattern of MMP and TIMP expression to cavity tissue.

Having established that the dissection technique used in figure 63B was most ideally suited for examining differences in gene expression between affected and unaffected tissue; we went on to further examine these tissues by RNA-Seq – a non-biased, next-generation whole-transcriptome sequencing approach, that allows for determination of the concentration of each RNA species within a sample.

5.4. RNA-Seq analysis of cavitary lung tissue, non-cavitary infected lung tissue, and uninfected lung tissue

RNA was isolated from lung tissue from animals infected with *M. tb* immediately after cavity formation (as identified by CT). Cavity wall was paired with healthy RNA from each of 3 rabbits, a comparison was also made between the three healthy tissue samples and tissue from uninfected rabbit lung. The mRNA was sequenced on the ABI Solid platform, and mapped to the oryCun2 (GCA_000003625.1) sequence. More than 17000 transcripts were mapped.

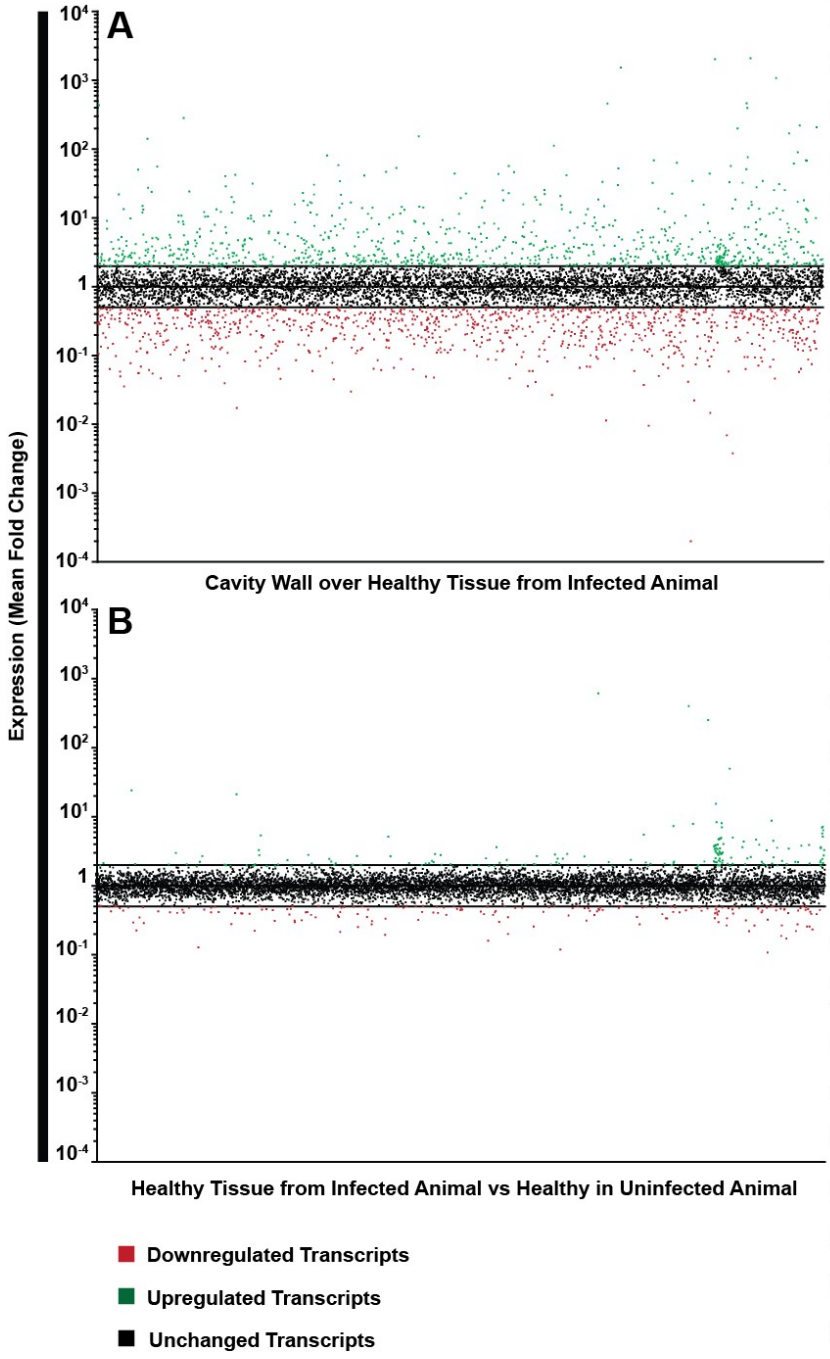

Figure 64. RNA-Seq reveals large changes in gene expression between pathological and non-pathological tissue, with relatively limited change between infected but non-pathological tissue and uninfected controls: (A) RNA was extracted from infected rabbit lungs. Cavity wall sites (x3) were compared to paired grossly healthy tissue to give a fold change in expression of each gene. The mean fold change was calculated and plotted. 2088 transcripts changed significantly, 1410 by greater than 2 fold. 615 protein coding transcripts were upregulated, and 795 were downregulated. **(B)** The same healthy tissue as above was compared to uninfected control tissue, fold change was calculated by taking the mean expression of each gene in each tissue type and calculating fold change. Only 133 transcripts changed significantly by greater than 2 fold. 86 were protein coding; 27 of which were upregulated, and 59 were downregulated.

The transcriptome analysis suggested 2 main things. First, that the expression pattern in these animals is relatively reproducible; as shown by the large number genes which differed significantly between healthy and cavity tissue but not between similar tissue types in different animals. Second, that healthy tissue from infected animals is very similar to uninfected tissue, as shown by the limited fold change across all genes assessed (figure 64). The remaining analysis was conducted by making comparisons between paired infected cavity and non-cavity tissues.

To better understand the nature of the genes involved, pathway analysis was performed using the 'Consensus Pathway Database' (CPDB) (213, 214). This allows for investigation of enrichment and over representation analysis of a number of different pathway reference sources. Amongst these, KEGG (Kyoto Encyclopedia of Genes and Genomes) pathways are perhaps the most commonly used when assessing disease processes. The KEGG database is a collection of manually curated pathways, which 'represent our knowledge on the molecular interaction and reaction networks' for multiple processes (215, 216). 48 pathways were found to be significantly enhanced in cavity vs non-cavity tissue. Genes involved in the response to tuberculosis in man were highly enriched; more genes associated with this process were enriched than from any other mapped process (figure 65). A second pathway database, Reactome, was used to further assess the genes involved. Reactome is also an open-source, open access, manually curated and peer-reviewed database (217-219).

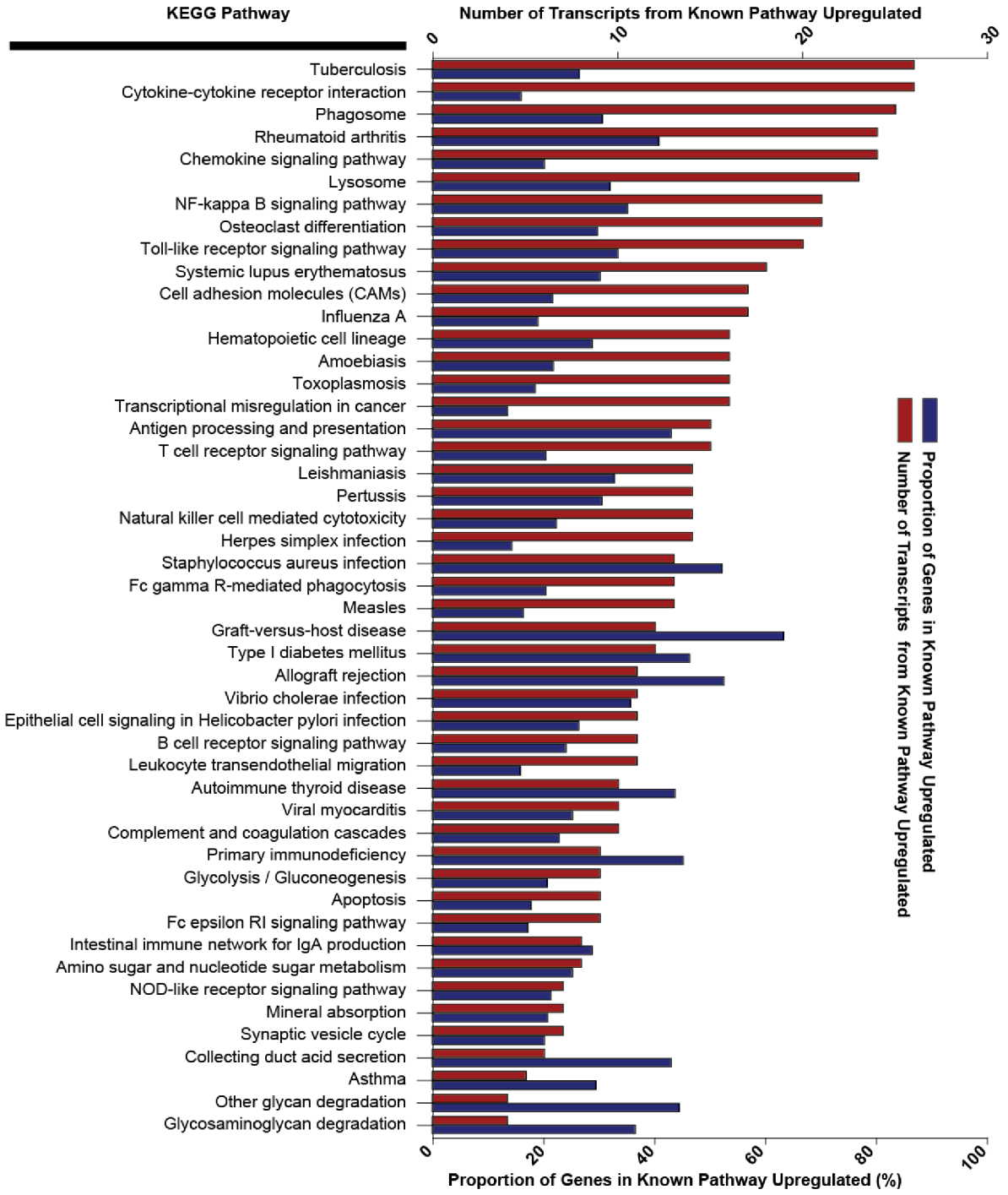

Figure 65. Analysis of pathways upregulated in KEGG database: All genes with homologous human genes were assigned to KEGG pathways of human processes. Pathways that were enriched for significantly upregulated genes (i.e. fold change >2 and $p<0.05$ *Wilcoxin signed-rank test*) are displayed above. Although only a small proportion of most pathways were involved, their relative involvement compared to all other pathways, is assessed as part of the analysis. The greatest number of genes changed in pathways associated with the human responses to tuberculosis. There were also a very high proportion of genes known to be involved in graft-versus-host disease seen in cavity tissue.

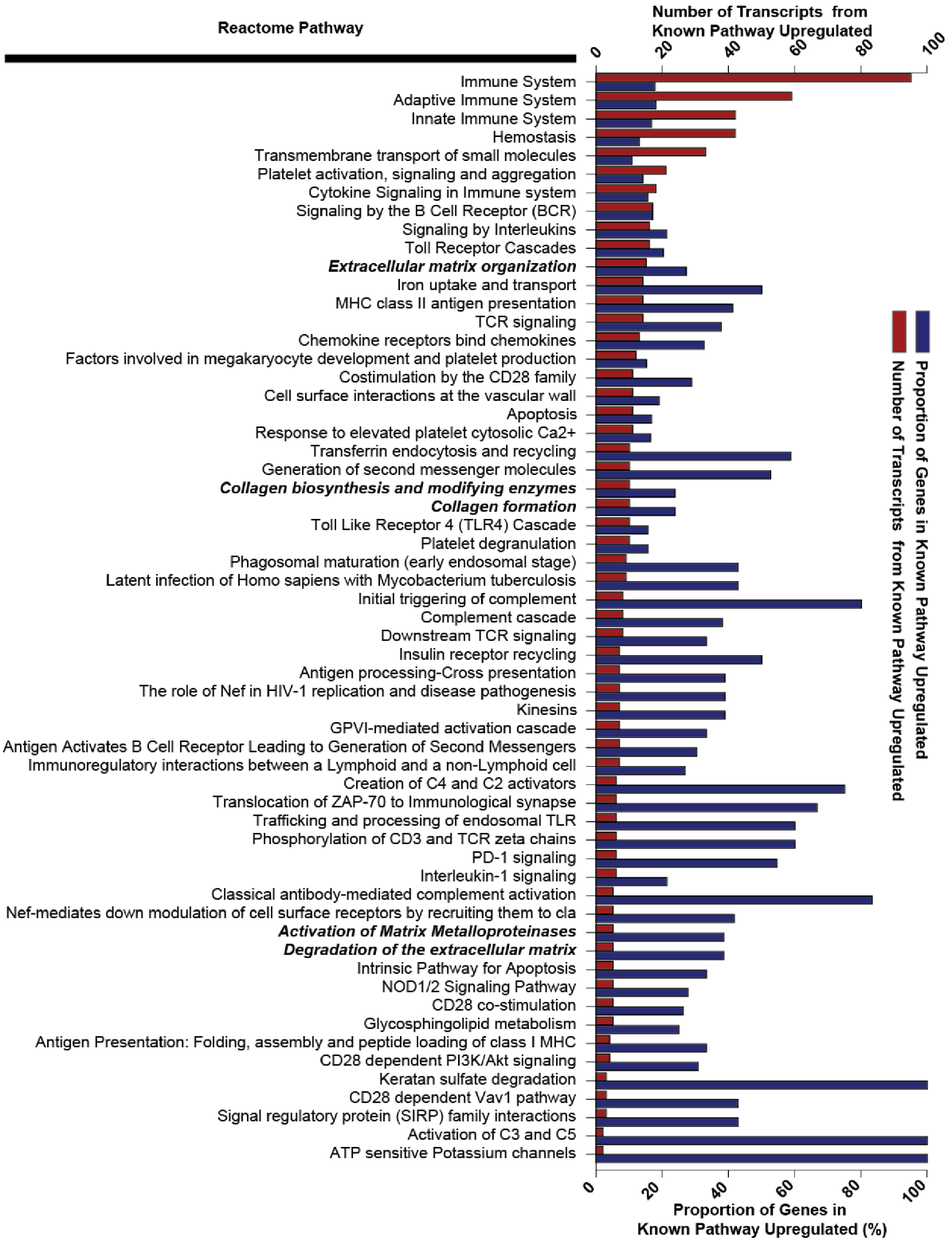

Figure 66. Analysis of pathways upregulated in REACTOME database: All genes with homologous human genes were assigned to REACTOME pathways of human processes. Pathways that were enriched for significantly upregulated genes (i.e. fold change >2 and $p<0.05$ *Wilcoxin signed-rank test*) are displayed above. The greatest number of genes changed in pathways associated with 'immune processes'. There was also substantial involvement of known genes in complement pathways, as well as matrix metalloproteinase activation, as well as both specific T cell mediated and Innate Immune mechanisms. Again pathways known to be involved in responses to *M. tuberculosis* were enriched in the cavity as compared to the non-cavity tissue.

Using two separately curated databases to assess this data set independently suggested that many genes involved in human reponses to *M. tb* were found to change in this infection model (figure 65 and 66). Clearly pathway analysis is of limited practical value, especially when there are limited data sets, and limited correlation (presently) between rabbit and human databases. However, the data presented above is a useful summary of the types of gene expression changes seen within the tissue. Making strong claims based on such data is inappropriate, but does facilitate description of general changes. Such curated databases are subject to editor bias, as well as field bias.

These general changes show a strong involvement of immune repsonses to infection, complement activation, and a degree of auto-inflammatory activity. Finally, a number of pathways related to ECM turnover are described. This was of great interest given the hypothesis that such processes may be therapeutically targetable (84, 109, 118, 171), but previously have not been identified models of disease where therapeutic trials could occur.

Because the process of collagen turnover does not have a well-curated pathway, the RNA-Seq data was manually mined for expression of genes involved in collagen turnover. First, MMPs were identified (figure 67).

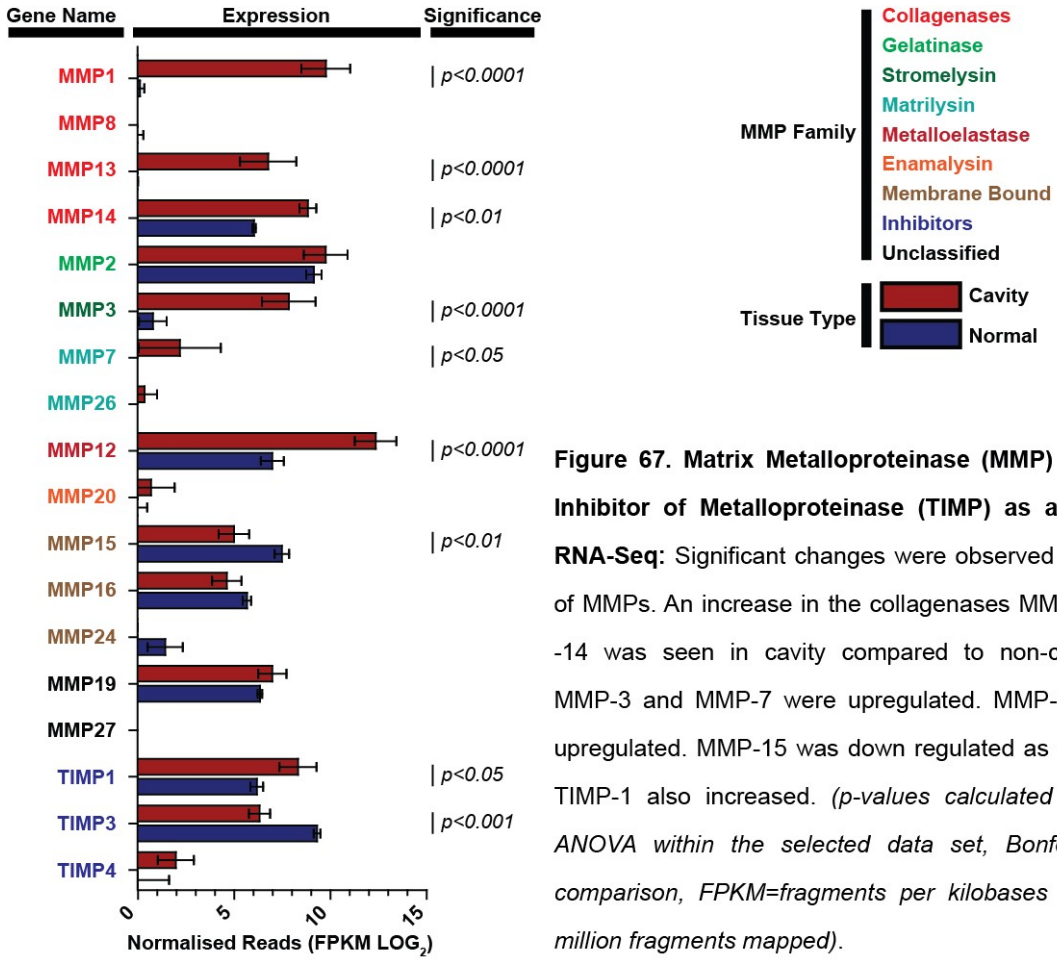

Figure 67. Matrix Metalloproteinase (MMP) and Tissue Inhibitor of Metalloproteinase (TIMP) as assessed by RNA-Seq: Significant changes were observed in a number of MMPs. An increase in the collagenases MMP-1, -13 and -14 was seen in cavity compared to non-cavity tissue. MMP-3 and MMP-7 were upregulated. MMP-12 was also upregulated. MMP-15 was down regulated as was TIMP-3. TIMP-1 also increased. *(p-values calculated by two-way ANOVA within the selected data set, Bonferroni post-comparison, FPKM=fragments per kilobases of exon per million fragments mapped)*.

As expected there was increased transcription of the collagenase members of the MMP family MMP-1, -13, and -14 (only 3 MMP-8 transcripts were detected). Additionally, there was high expression of MMP-12 (macrophage metalloelastase). Suprisingly no reads were mapped for MMP-9.

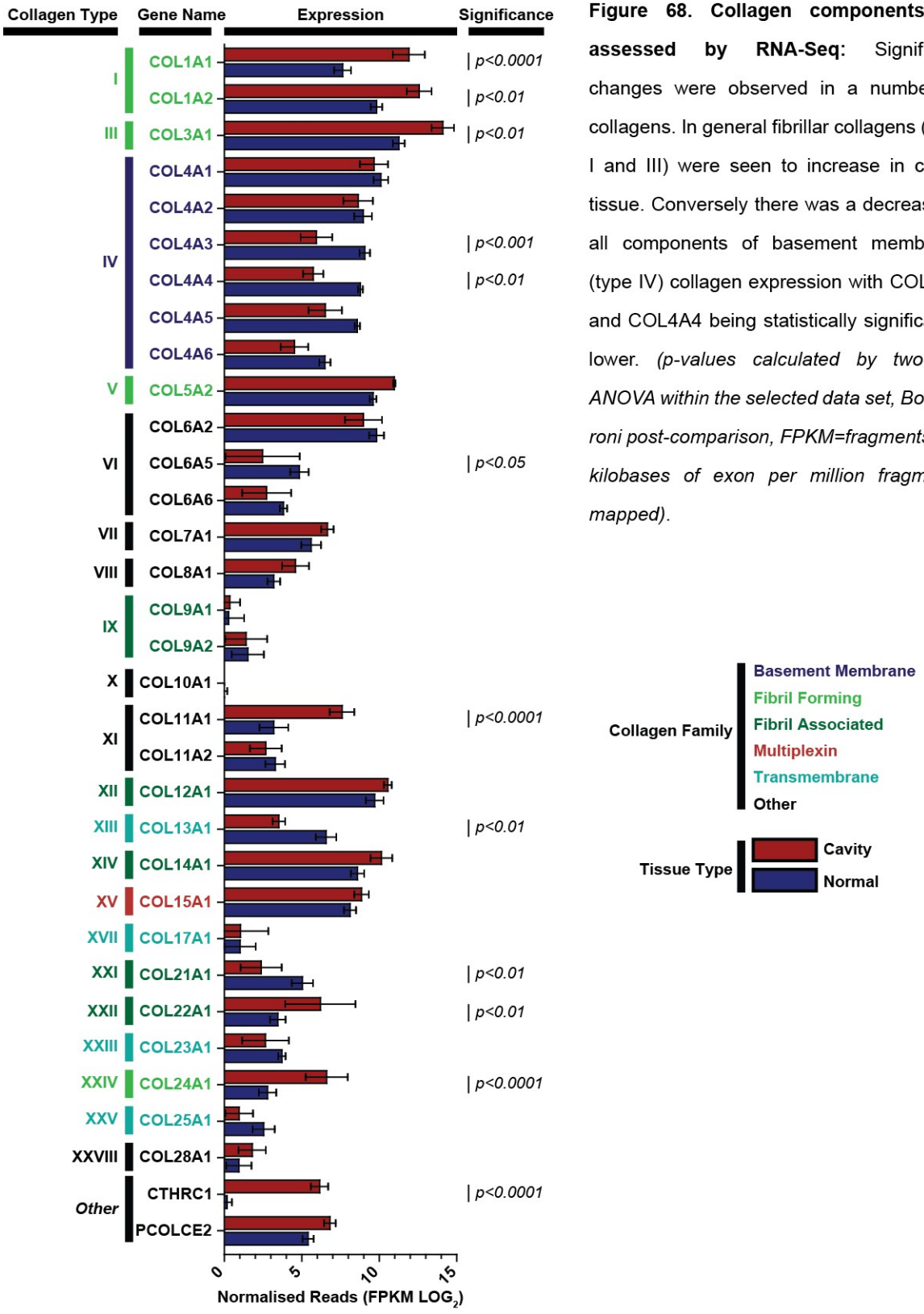

Figure 68. Collagen components as assessed by RNA-Seq: Significant changes were observed in a number of collagens. In general fibrillar collagens (type I and III) were seen to increase in cavity tissue. Conversely there was a decrease in all components of basement membrane (type IV) collagen expression with COL4A3 and COL4A4 being statistically significantly lower. *(p-values calculated by two-way ANOVA within the selected data set, Bonferroni post-comparison, FPKM=fragments per kilobases of exon per million fragments mapped).*

The strong divergence in the types of collagens expressed between apparently normal and cavitary tissue was unexpected. Increases in fibrillar types I and III collagen are associated with fibrotic

processes, but the decrease in expression of all mapped components of type IV collagen, suggest that maintenance of the basement membrane ECM is disrupted.

Next, peptidases were identified by Gene Ontology (GO) number (GO:0008233) (220), in an attempt to identify other matrix regulating proteases that may be upregulated in cavity as compared to normal tissue.

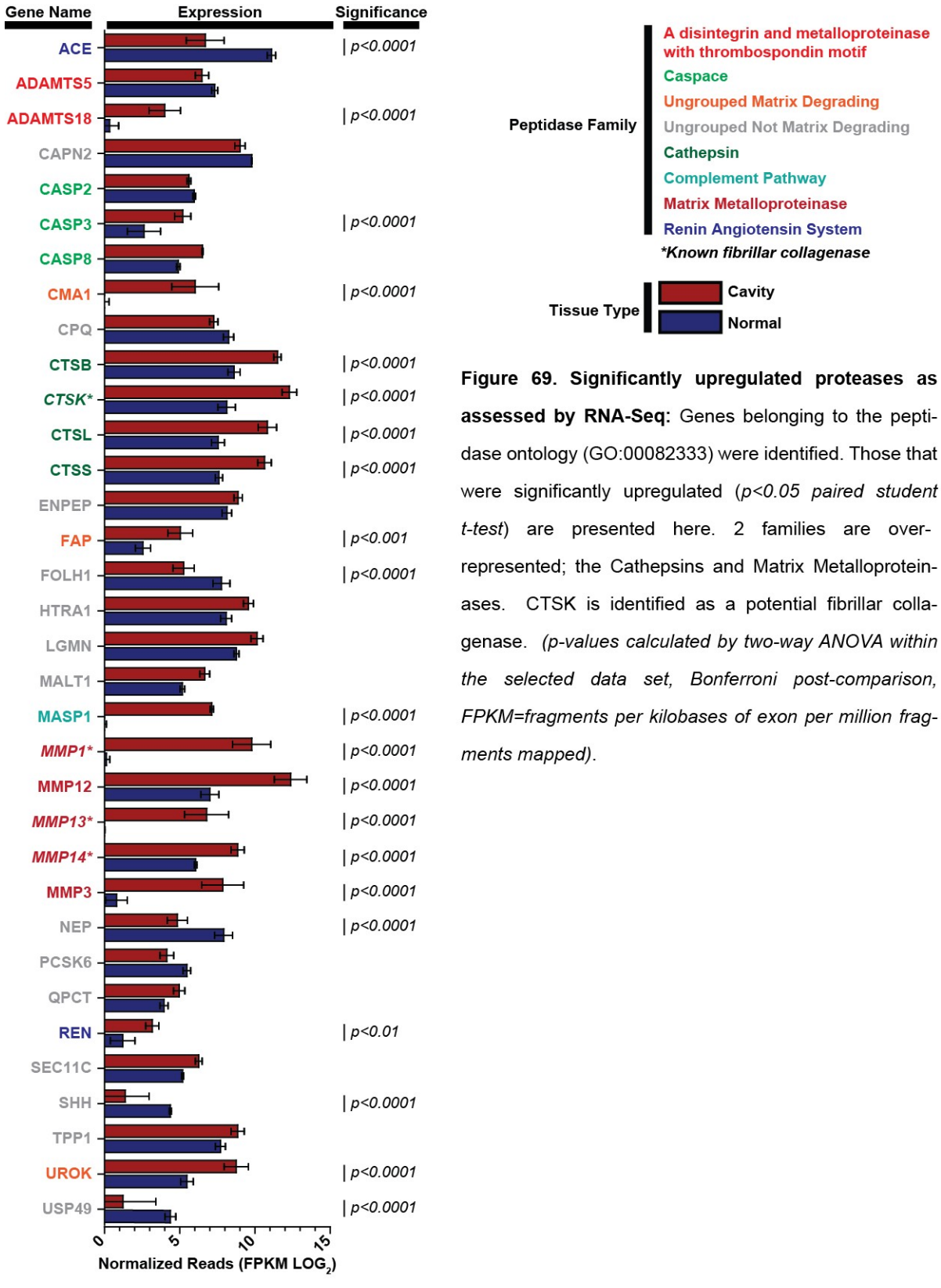

Figure 69. Significantly upregulated proteases as assessed by RNA-Seq: Genes belonging to the peptidase ontology (GO:00082333) were identified. Those that were significantly upregulated (*p<0.05 paired student t-test*) are presented here. 2 families are over-represented; the Cathepsins and Matrix Metalloproteinases. CTSK is identified as a potential fibrillar collagenase. *(p-values calculated by two-way ANOVA within the selected data set, Bonferroni post-comparison, FPKM=fragments per kilobases of exon per million fragments mapped)*.

This unbiased approach also revealed signficant increases in cathepsin expression (CTS-) and caspace expression (CASP-) as well as the already discussed MMPs (MMP-). Cathepsin K (CTSK), which functions as a fibrillar collagenase at acidic pH (221, 222) was an interesting and novel finding. The

remaining proteases do not have identified collagenolytic activty (221, 222). To confirm the presence of proteolytic activity, we designed a small experiment in order to observe whether collagen degradation was occuring.

5.5. Evaluation of collagen degradation as a biomarker in the rabbit model

Having identified that collagen turnover and MMP activity were strongly associated with the development of cavities, it became rational to investigate if collagen turnover could be used as a biomarker of cavitary disease. By examining serum, plasma and urinary levels of collagen degradation products, it became clear that even with a small sample size, changes in pulmonary lung collagen are likely reflected in peripheral breakdown products (figure 70). Although only a few samples were available for this study, the data strongly indicate that collagen breakdown products are indicative of cavity specific process in *M. tb* infection of rabbits. Further investigation of this is warranted, since this may allow for a marker of effectiveness of ECM-protective therapies in TB, or may be a marker for disease severity in clinical trials.

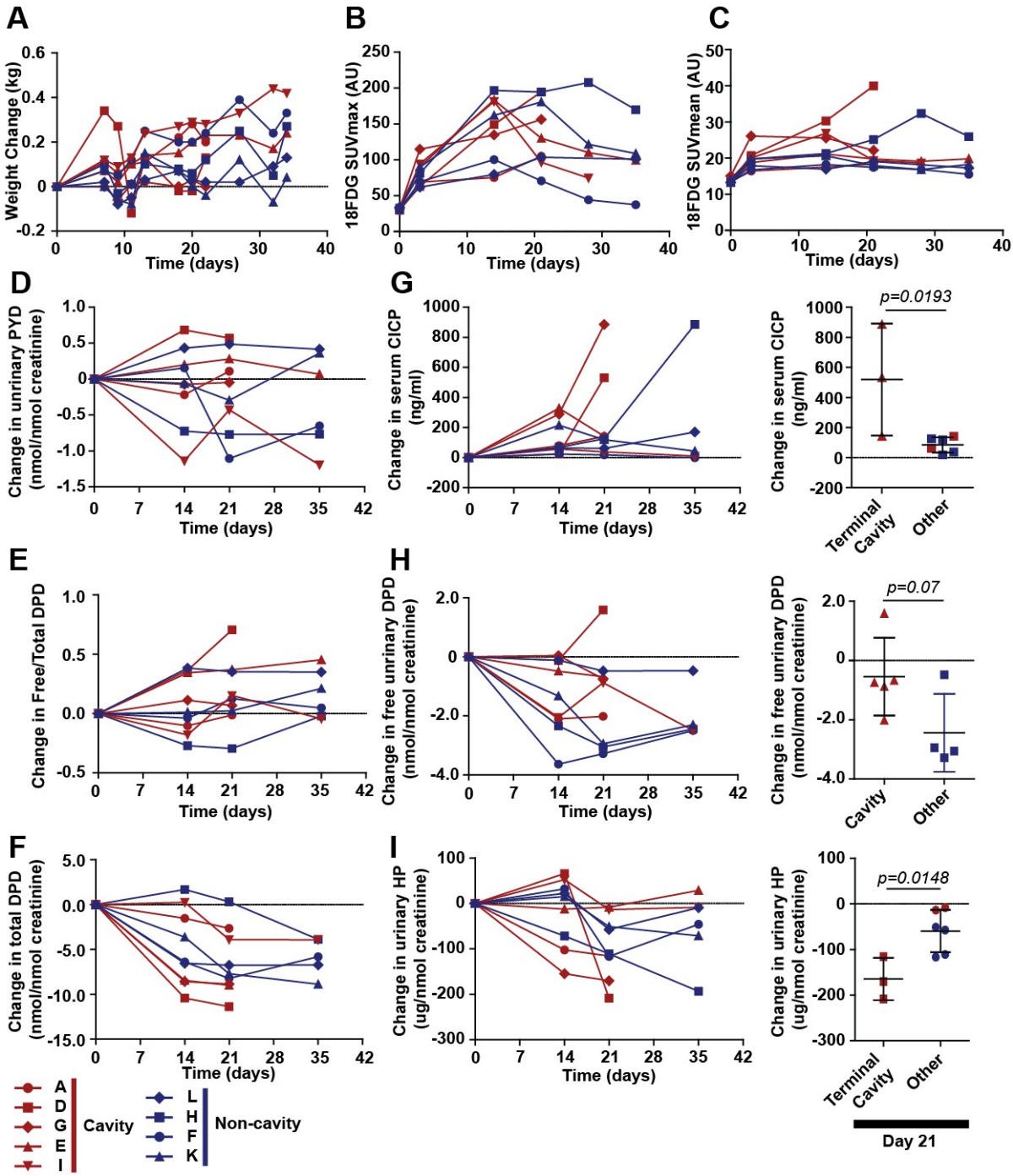

Figure 70. Collagen biomarkers outperform ^{18}F-FDG as a marker of cavitation: (A) Animal weights increase a small amount even after infection. **(B)** and **(C)** ^{18}F-FDG uptake within the lung field does not differ significantly between cavitary and non-cavitary animals; this holds true if terminal cavity animals were compared to all others. **(D)(E)(F)** Collagen cross-linking amino acids pyridinoline (PYD) and deoxypyridinoline (DPD) in urine do not change significantly over time. **(G)** Serum levels of C-terminal of type I procollagen (CICP) increased during infection. At week 3 the difference between those animals which developed extensive cavities on CT, and those that did not, reached significance. **(H)** Changes in urinary DPD were less clear but approached significance at week 3. **(I)** Urinary helical peptide (HP) was substantially reduced in those animals that developed extensive cavitation when compared to other animals which developed either no cavities or small cavities. In combination these results suggest that a perturbation in collagen metabolism coincides with cavitation; and that the degree of inflammation alone is not indicative of a more destructive phenotype. *(p-values calculated using Wilcoxin matched pairs t-test)*.

Having confirmed that collagen turnover was indeed occurring, we set out to refine the observations of gene expression changes in the rabbit model of cavitary tuberculosis, by conducting a larger scale analysis of time-matched animals, looking at differences in expression between cavity, near cavity and distant tissue.

5.6. Characterisation of collagen degrading MMPs, CTSK and TIMPs in the 70 day cavity model of tuberculosis

To characterise MMP expression in rabbit lungs, real time qRT-PCR primers were designed with an efficiency of 1.8-2.2 and their product characterized by Sanger sequencing of the amplicon.

GENE	GENE ID	GENE ID	Forward Primer	Reverse Primer
ACTB	100009272	NM_001101683.1	CGCTTCCGTTGCCCCGAG	GCCGCCCGACAGCACCGT
MMP1	100009110	NM_001171139.1	ACCTTCCCAAAATCCCAGTCAG	GATTTGCCCGCATGTAGAACC
MMP2	100009000	NM_001082209.1	CCGCAGTGATGGCAAGATGTG	GGGCTGCCACGAGGAACA
MMP3	100009111	NM_001082280.1	TGGCCATCTCTTCCTTCAGCA	TGCTTCTTGGGTAACCAGCTTG
MMP7	100357971	XM_002708573.1	CCACAGTGGGAACAGGCTCA	CCAGTTATAGGCAGGCCAAAGA
MMP8	100339790	XM_002708421.1	ATTTTATTTCCCTGTTCTGGCC	TTCATAGCCATTCAGAGC
MMP9	100008993	NM_001082203.1	TCGCCGAGATAGGGAACAAGC	GTCGGCGATGAGGAAGGG
MMP10	100101603	XM_002708561.1	GGAGGTGATACGCAAGCCCA	GCATCTCTTGGCAGATCTGGTG
MMP12	100009559	NM_001082771.1	CTCGATGTGGAGTGCCTGATGT	GCTTCATGTCTGGAGTGT
MMP13	100008685	NM_001082037.1	ACTCATTGCTGGTCCCTGCC	TCCCGCAGGATTCAGAGGA
MMP14	100009598	NM_001082793.1	GATCGATGCCGCTCTCTTCTG	CGCTGTCCACTGCCCTGA
TIMP1	100009047	NM_001082232.2	GGCCTTCTGCAACTCCGA	TGCCCCAAGGCGTCAAAT
TIMP2	100008689	XM_002723776.1	AGGTGGACTCTGGGAACGACA	CGGGGCCTTTGAACATCT
TIMP3	100008690	NM_001195682.1	ACGCCTTCTGCAACTCCGACAT	ACGTGGGGCATCTTGGTGA
TIMP4	100008691	NM_001195690.1	ACACTCAGAGAATGATCCGG	CACCACAGAGAGAAGAGTCA
CTSK	100009334	NM_001082641.1	TGGGGACTCAAGGTTCTGCTG	CCCAAATTAAACGCCGAGAGA
HO1	100008919	XM_002711415.1	ATCGCCAGCGCCACCAAGTT	GCAGCTCCTGCAACTCCTCAA

Table 8. Primers utilised for qRT-PCR analysis of MMPs, TIMPs, CTSK and HO1 in rabbit pulmonary tissue: NCBI gene references are listed, primers listed in 3' to 5' direction.

GENE	Product Sequence
ACTB	CGCTTCCGTTGCCCCGAGGCGCTCTTCCAGCCCTCCTTCCTGGGCATGGAGTCGTGTGGCATCCACGAGACCACCTTCAACTCGAT CATGAAGTGCGACGTGGACATCCGCAAGGACCTGTACGCCAACACGGTGCTGTCGGGCGGC
MMP1	ACCTTCCCAAAATCCCAGTCAGCCAGTAGGCCCACAGACCCCAAAAGTGTGTGATAGTAAACTGACCTTTGATGCTATAACCACAA TTCGGGGAGAAATAATGTTCTTTAAAGACAGGTTCTACATGCGGGCAAATC
MMP2	CCGCAGTGATGGCAAGATGTGGTGCGCGACCTCAACCAACTACGACGATGACCGCAAGTGGGGCTTCTGCCCTGACCAAGGTTA CAGCCTGTTCCTCGTGGCAGCCC
MMP3	TGGCCATCTCTTCCTTCAGCAGTGGATGCTGCATATGAAGTTATTAGCAGGGATACTGTTTTCATTTTTAAAGGAACTCAGTTCTGG GCCATTAGAGGAAATGAGGTACAAGCTGGTTACCCAAGAAGCA
MMP7	CCACAGTGGGAACAGGCTCAGGACTATCTCAAGAGATTTTATTTTCATGGCTTGAAATCAAAGGAAGTCGATAGCTTAGAAACCA GACTGAAGGAGATGCAGAAGTTCTTTGGCCTGCCTATAACTGG
MMP8	N/D
MMP9	TCGCCGAGATAGGGAACAAGCTGCATGTCTTCAAGGATGGGAGGTACTGGCGGTTCTCCGAGGGCAGTGGGCGCCGGCCGCAG GGCCCCTTCCTCATCGCCGAC
MMP10	GGAGGTGATACGCAAGCCCAGGTGTGGCGTTCCCGATGTTGGTCACTTCAGTACCTTCCCTGGCACCCCAAAGTGGACAAAAACT CACCTAACTTACAGGATTGTGAATTACACACCAGATCTGCCAAGAGATGCT
MMP12	CTCGATGTGGAGTGCCTGATGTTTATCATTTCAAAACCATGCCAGGGAGACCAGTATGGAGGAAACATTACATCACCTACAGAATC AAAAATTACACTCCAGACATGAAGC
MMP13	ACTCATTGCTGGTCCCTGCCCCTCCTCAACAGTAACGAGGATGATGATTTGTCCGAGGAAGACTTCCAGTTTGCAGAGAGCTACCT GAGATCATACTACCATCCTCTGAATCCTGCGGGA
MMP14	GATCGATGCCGCTCTCTTCTGGATGCCCAATGGAAAGACCTACTTCTTCCGGGGAAACAAGTACTACCGATTCAACGAGGAGCTCA GGGCAGTGGACAGCG
TIMP1	GGCCTTCTGCAACTCCGACCTTGTCATCAGGGCCAAGTTTGTGGGGGCTCCAGAAGTCAATCATACTACCTTGTACCAGCGTTATG AAATCAAGACAACCAAGATGTTCAAAGGATTTGACGCCTTGGGGCA
TIMP2	AGGTGGACTCTGGGAACGACATCTACGGCAACCCCATCAAGAGGATCCAGTATGAGATCAAGCAGATCAAGATGTTCAAAGGCCC CG
TIMP3	ACGCCTTCTGCAACTCCGACATCGTGATCCGGGCCAAGGTGGTGGGGAAGAAGCTGGTGAAGGAAGGGCCCTTCGGCACGATG GTCTACACCGTCAAGCAGATGAAGATGTACCGAGGCTTCACCAAGATGCCCCACGT
TIMP4	ACACTCAGAGAATGATCCGGTATGAAATCAAACAGATAAAGATGTTTAAAGGGTTTGAGAAAATCAAGGATGTTCAGTACATCTAT ACACCTTTTGACTCTTCTCTCTGTGGTG
CTSK	TGGGGACTCAAGGTTCTGCTGCTACCCGTGGTGAGTTTTGCTCTGCACCCTGAGGAAATACTGGACACCCAGTGGGAGCTATGGA AGAAGACCTACAGCAAGCAGTATAACAGCAAGGTGGATGAAATCTCTCGGCGTTTAATTTGGG
HO1	ATCGCCAGCGCCACCAAGTTCAAGCAGCTCTACCGCTCGCGCATGAACTCCCTGGAGATGACCCCCAGCGTCAGGCAGAGGGTG GTGGAAGAGGCTAAGGCCGCCTTCCTGCTCAATATTCAGCTCTTTGAGGAGTTGCAGGAGCTGC

Table 9. Sanger sequenced products from qRT-PCR reactions with the primers for MMP, TIMP, CTSK and HO1 expression analysis in rabbit pulmonary tissue: Products of the qRT-PCR reactions were first subjected to electrophoresis to determine size, prior to extraction and Sanger sequencing at the GeneWiz facility. Sequences were reassembled using Vector NTI.

These high quality primer sets were used to assess gene expression (figure 71-74).

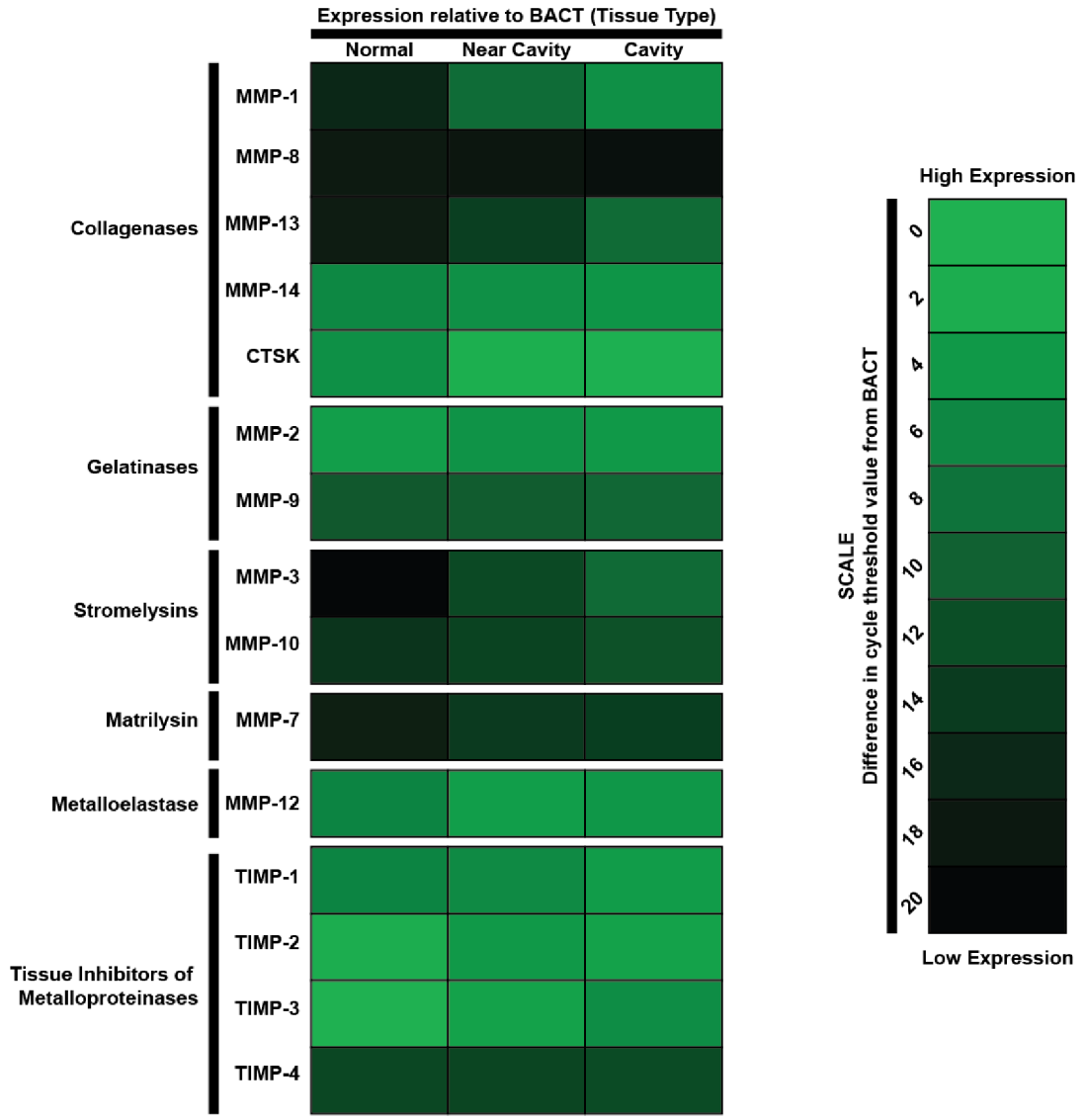

Figure 71. Approximate expression levels of key MMPs as well as CTSK and TIMPs in rabbit tissue from 3 distinct pathologies as measured by real time quantitative PCR: MMP-1, -8, -13, -3 and -7 were expressed at very low levels in normal tissue - often below the threshold of detection. However, MMP-14, CTSK, MMP-12 and TIMP-1, -2 and -3 were detected at high levels in normal tissue. TIMP-4, MMP-10 and MMP-9, were identified at relatively low levels.

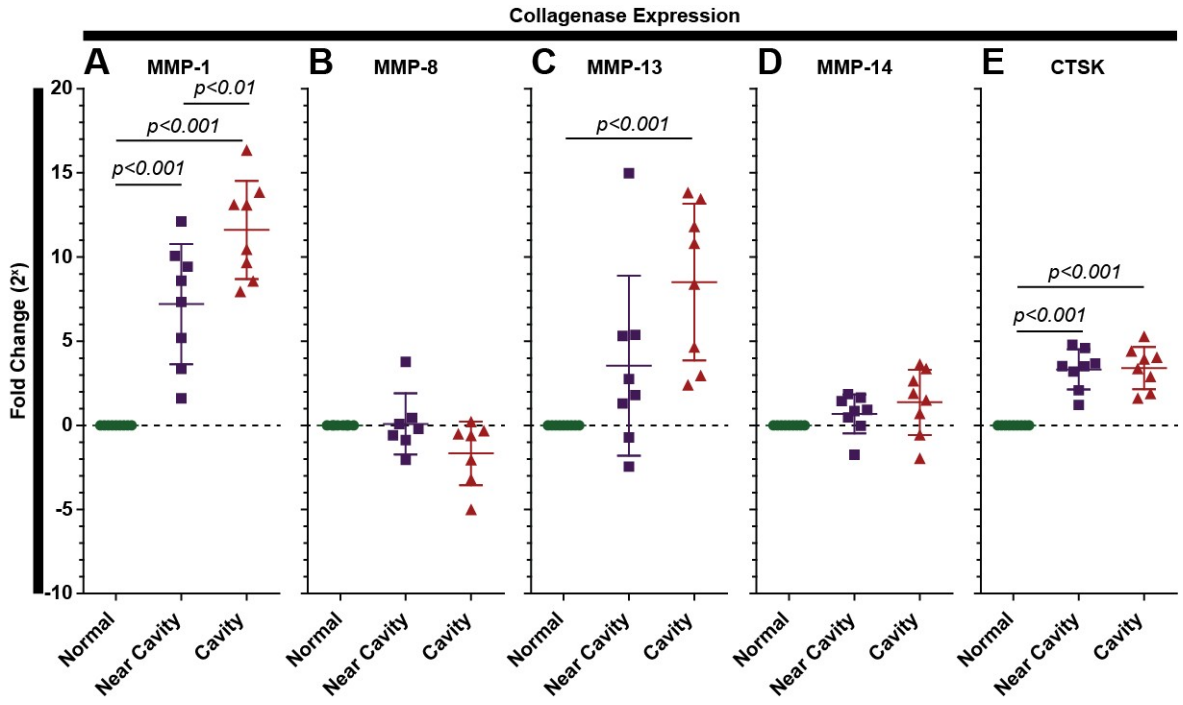

Figure 72. Relative expression of the collagenases as measured by qRT-PCR: (A) MMP-1 is significantly upregulated in all pathological tissue when compared to non-diseased tissue. Interestingly there is a significant increase in cavity wall when compared to adjacent tissue. (B) MMP-8 expression did not change. (C) MMP-13 is significantly upregulated in cavity tissue compared to normal tissue - there was an increase in 6/8 samples in near cavity tissue, however the increase was not statistically significant. (D) There was no increase in MMP-14 expression. (E) CTSK was equally upregulated in both near cavity and cavity tissue. (*p-values calculated by one-way ANOVA with Tukey post comparison*).

MMP-1, MMP-13 and CTSK were all substantially and significantly unregulated in cavity tissue as compared to infected normal tissue. MMP-8 was not detected at the transcript level, although this does not rule out is involvement, because MMP-8 is commonly stored as a protein in neutrophils (223), and so transcription may not occur at the site of activity. MMP-14 expression was relatively high in all tissue types, and a trend towards increased expression in more diseased tissue was observed, the two outlying points in the cavity and non-cavity samples, (which are not statistical outlier's by Grubb's test), result from high MMP-14 expression in the normal tissue of this animal.

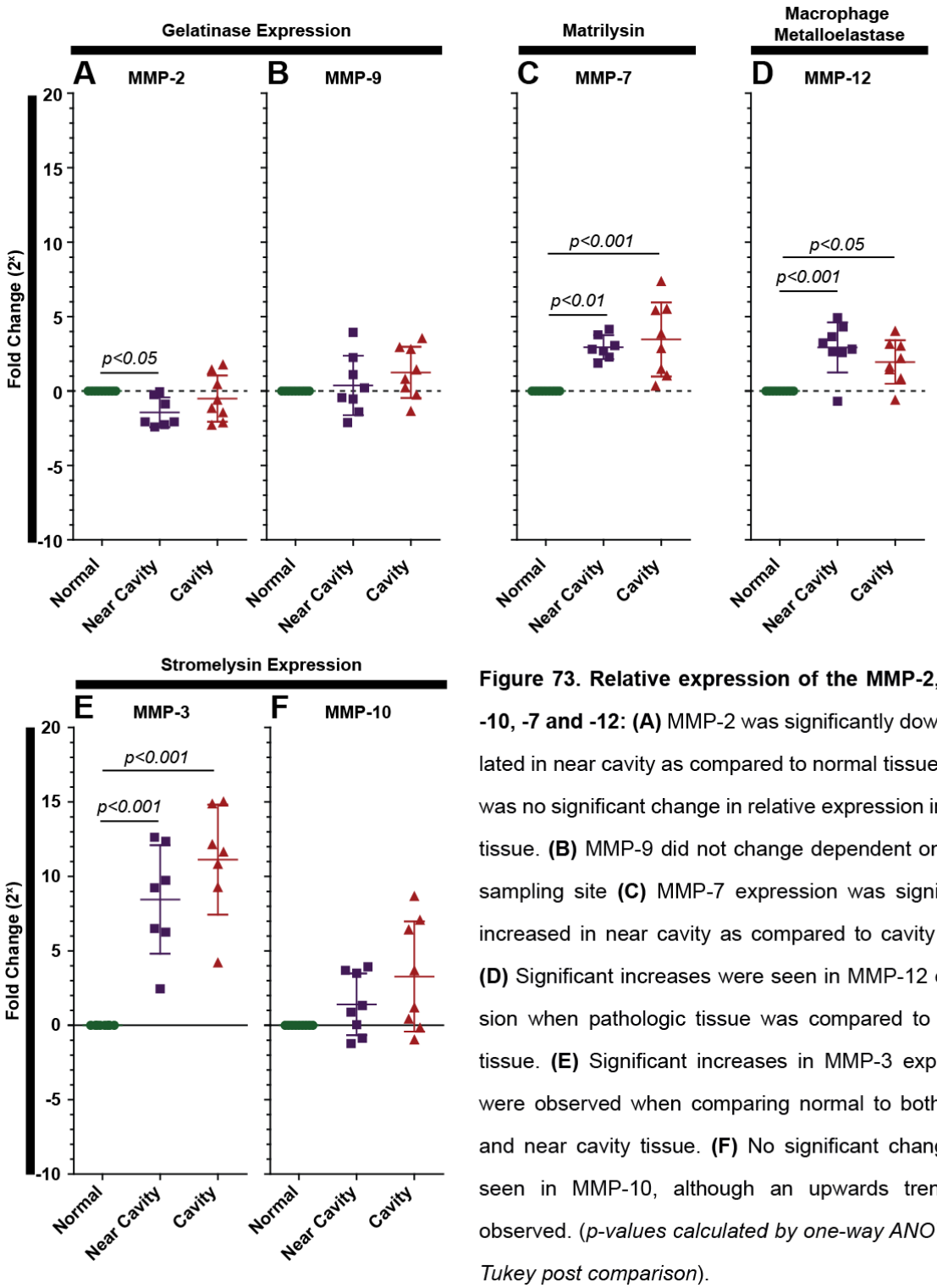

Figure 73. Relative expression of the MMP-2, -9, -3, -10, -7 and -12: (A) MMP-2 was significantly down regulated in near cavity as compared to normal tissue. There was no significant change in relative expression in cavity tissue. **(B)** MMP-9 did not change dependent on tissue sampling site **(C)** MMP-7 expression was significantly increased in near cavity as compared to cavity tissue. **(D)** Significant increases were seen in MMP-12 expression when pathologic tissue was compared to normal tissue. **(E)** Significant increases in MMP-3 expression were observed when comparing normal to both cavity and near cavity tissue. **(F)** No significant change was seen in MMP-10, although an upwards trend was observed. (*p-values calculated by one-way ANOVA with Tukey post comparison*).

Interestingly, there was no significant increase in MMP-9 expression dependent on sampling site. MMP-2 expression was statistically significantly lower in the near cavity tissue. MMP-3 showed very high expression associated with tissue pathology. MMP-10 showed an upwards trend. MMP-7 and -12 were both significantly upregulated in pathological as compared to grossly normal tissue.

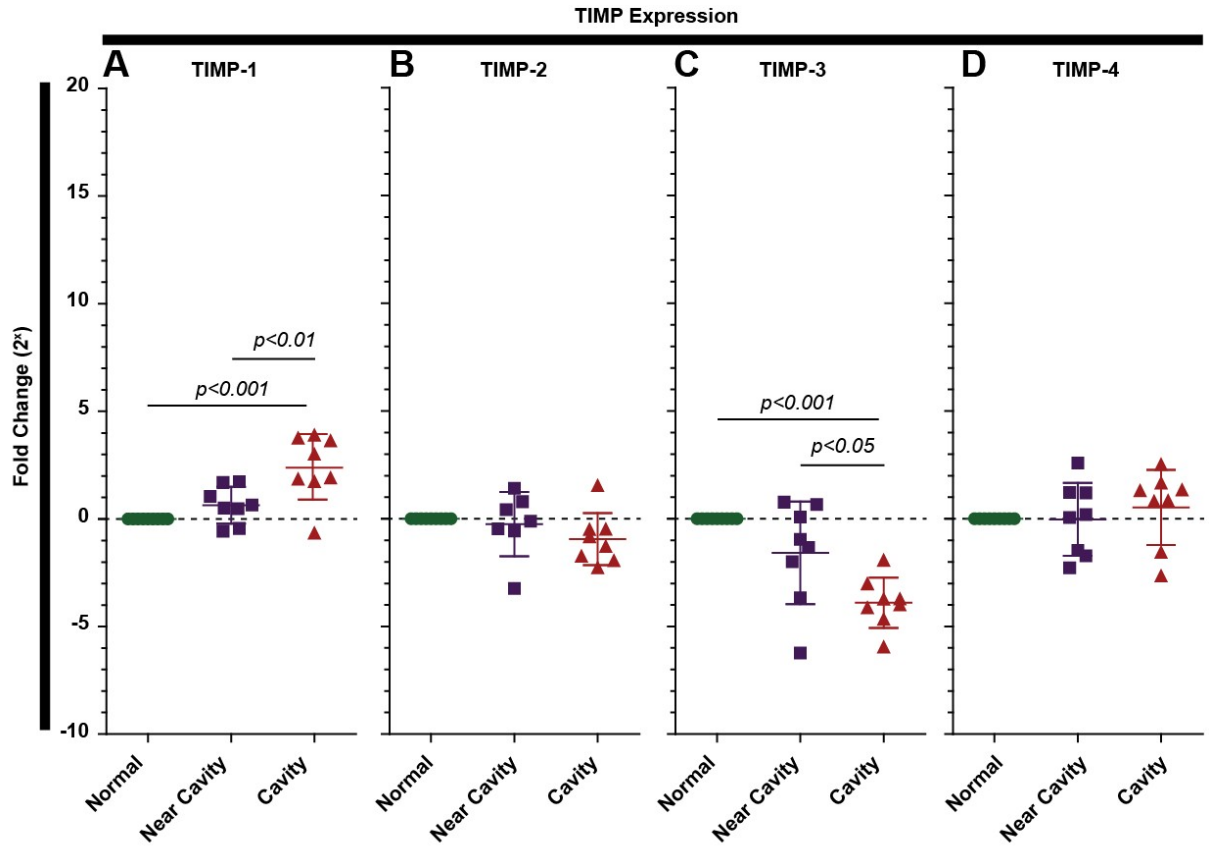

Figure 74. Relative expression of the Tissue Inhibitors of Metalloproteinases (TIMPs): (A) TIMP-1 was significantly upregulated in all cavity tissue when compared to non-diseased tissue. There was also a significant increase in TIMP-1 expression in near cavity tissue when compared to normal tissue. **(B)** TIMP-2 expression did not change. **(C)** TIMP-3 was significantly downregulated in cavity tissue when compared to normal tissue and near cavity tissue. **(D)** There was no change in TIMP-4 expression. (*p-values calculated by one-way ANOVA with Tukey post comparison*).

TIMP-1 expression was significantly increased in cavity as compared to other tissues, whereas TIMP-3 was down-regulated. TIMP-2 and -4 did not change significantly. (TIMP-4 levels were extremely low as estimated by CT value – figure 71). It is surprising that despite increases in MMPs-1, -3, -7, and -12 in near cavity tissue, TIMP's do not significantly increase. This imbalance in TIMP:MMP ratio would suggest that a collagenolytic environment occurs in infected tissue. The down-regulation of TIMP-3 is surprising. TIMP-3 is known to inhibit angiogenesis (224), and its down regulation would suggest there may be neovascularisation in this region. Although further investigation of this hypothesis is beyond the scope of this thesis, this may have ramifications for immune cell delivery and tissue hypoxia.

Since gene expression does not correlate directly with protein levels, confirmation of protein expression was sought.

5.7. MMP-1 protein levels are increased in cavity as compared to normal lung tissue from infected animals

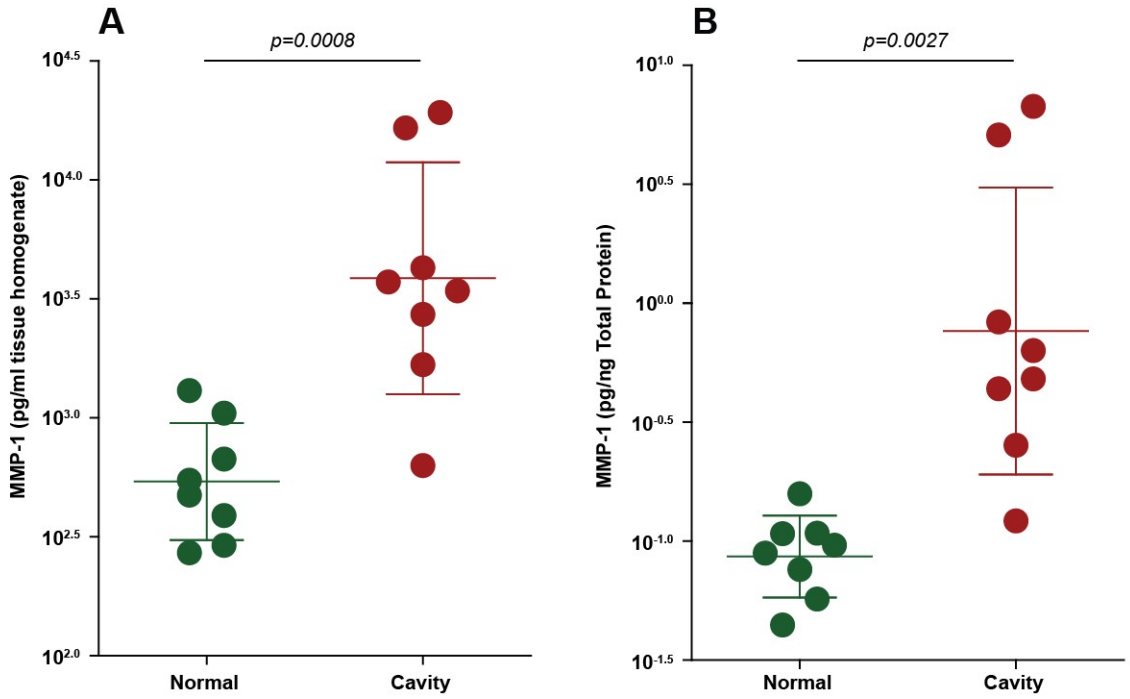

Figure 75. MMP-1 protein is significantly upregulated in cavity wall tissue as compared to healthy tissue: Equal sized biopsies from snap frozen rabbit tissue were homogenised, filter-sterilised, and measured by Enzyme Immunoassay. MMP-1 was significantly increased in cavity as compared to normal tissue by both weight normalised **(A)**, and total protein normalised **(B)**, concentrations. *(p-values calculated by student t-test, 8 biological replicates of each tissue type)*.

MMP-1 protein levels in snap-frozen, homogenized and filtered lung tissue were assayed by a commercially available ELISA. This demonstrated that MMP-1 was indeed upregulated at the protein level in cavity wall tissue as compared to normal tissue from infected animals (figure 75).

5.8. Identification of enzymatically active MMP-1 in rabbit tissue which can be inhibited by Ro32-3555, a collagenase specific MMP inhibitor

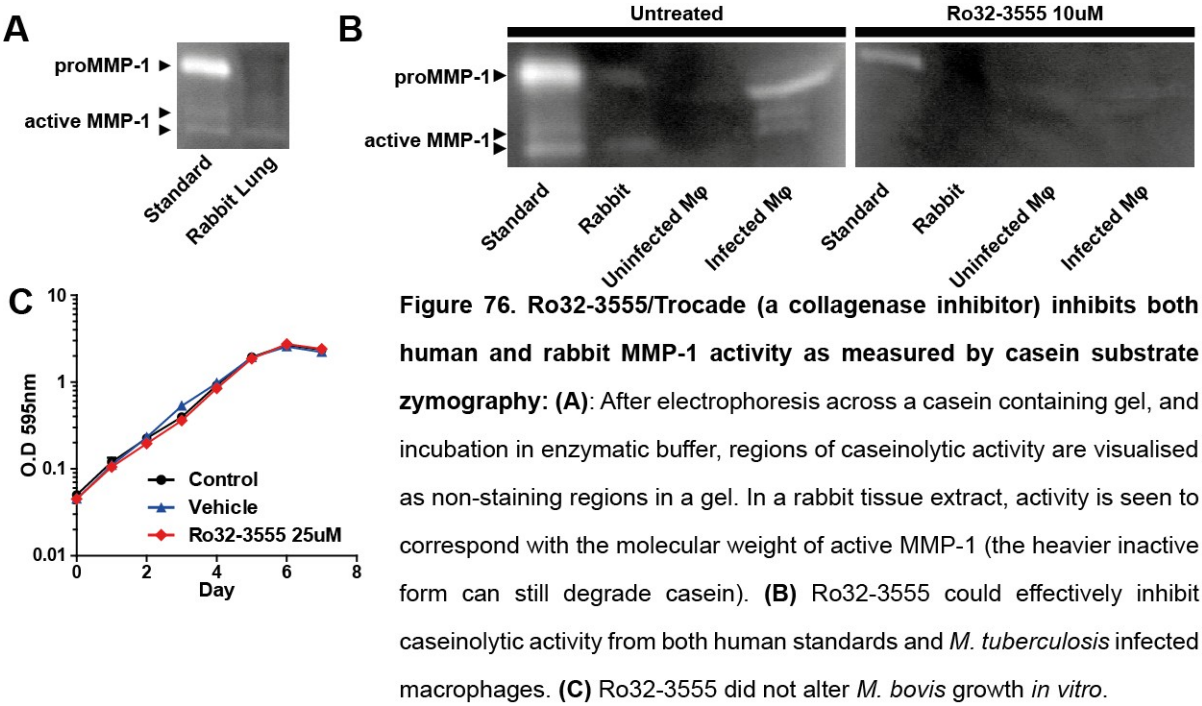

Figure 76. Ro32-3555/Trocade (a collagenase inhibitor) inhibits both human and rabbit MMP-1 activity as measured by casein substrate zymography: (A): After electrophoresis across a casein containing gel, and incubation in enzymatic buffer, regions of caseinolytic activity are visualised as non-staining regions in a gel. In a rabbit tissue extract, activity is seen to correspond with the molecular weight of active MMP-1 (the heavier inactive form can still degrade casein). **(B)** Ro32-3555 could effectively inhibit caseinolytic activity from both human standards and *M. tuberculosis* infected macrophages. **(C)** Ro32-3555 did not alter *M. bovis* growth *in vitro*.

Protein was extracted from infected rabbit lung homogenate and analysed by substrate zymography (figure 76). This method involves distribution of protein through a substrate containing gel by electrophoresis, followed by incubation in a neutral buffer, which facilitates enzymatic degradation of the substrate (225). Staining of the gel reveals enzyme activity as uncoloured regions devoid of the substrate. Enzymatic digestion of both casein and gelatin corresponding to the molecular weights of pro and active MMP-1 indicated that the protein has proteolytic activity. MMP-1 activity was challenging to visualise due to high levels of protein in the samples. MMP-1 activity could be inhibited by Ro32-3555, a collagenase specific MMP inhibitor (figure 76B). This drug completed phase III trials for treatment for rheumatoid arthritis but was withdrawn due to lack of efficacy (226, 227). The drug has potential to be trialled in the 70 day rabbit model, to evaluate the role of MMP-1 in cavity formation. Similarly, Cathepsin K is also the target of novel inhibitor, Odanacatib, which has demonstrable efficacy in man (228-233). However, cathepsin K expression had not yet been confirmed in man.

5.9. Cathepsin K is associated with TB pathology in man

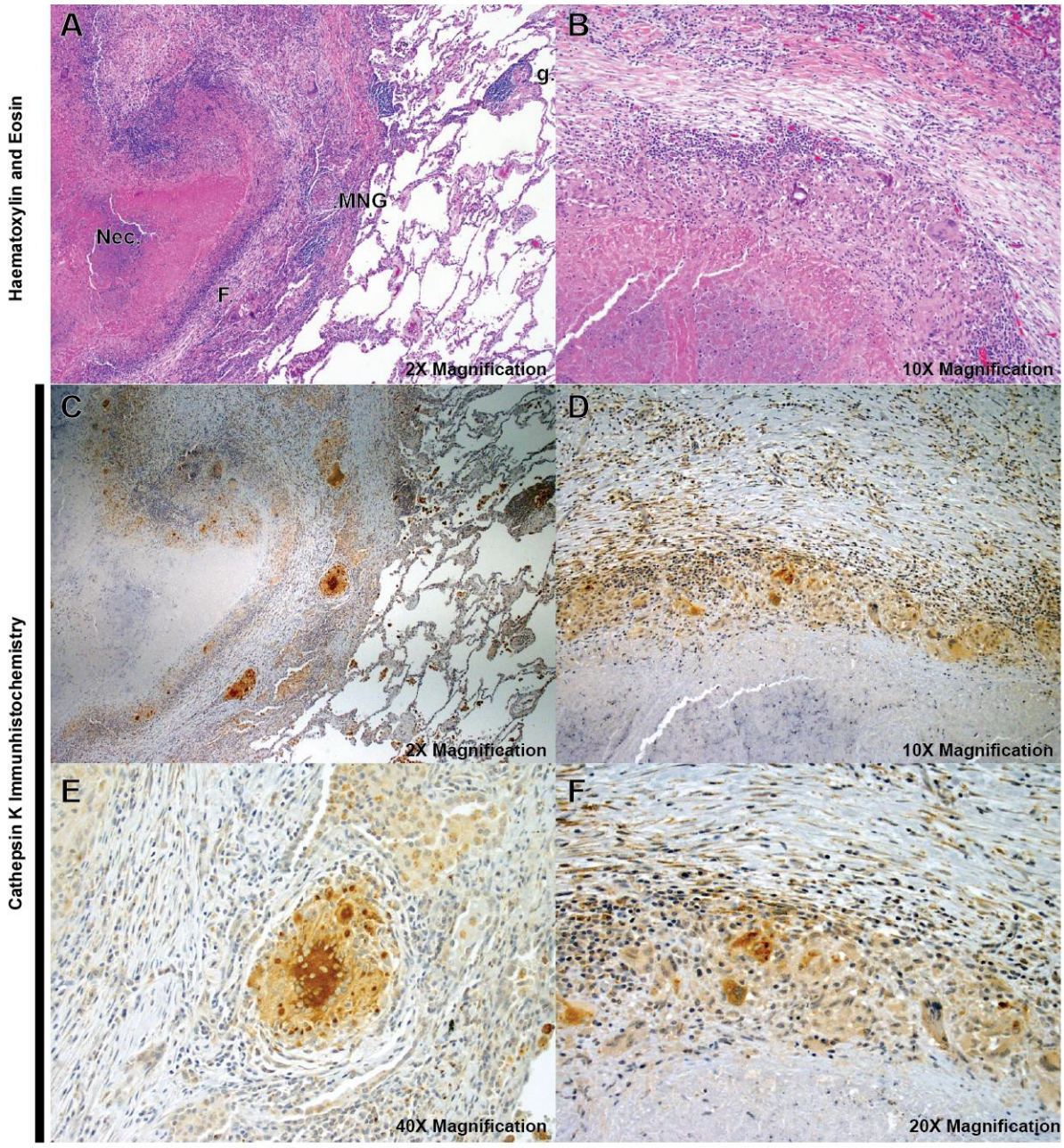

Figure 77. Cathepsin K is expressed in human pathology resulting from *M. tuberculosis* infection, localising specifically to macrophages, especially multinucleate giant cells: (A) H+E stained sections showing representative pathology from human specimens (Nec; necrosis, F; fibrous cuff, MNG; multinucleate giant cell, g; granuloma). A large necrotic lesion is visualised, with a fibrous cuff lined by epitheloid macrophages. At the top right hand side of the image a very small granuloma is found adjacent to a collection of lymphoid cells (g). **(B)** A different, extensively necrotic lesion. **(C)** Low power view of anti-cathepsin K stained tissue from A, staining localises to the multinucleate giant cells **(E)**, but also to macrophages at the periphery of the necrotic region, bordering the fibrotic cuff, where viable bacilli are most commonly localised. **(D and F)** Within the fibrotic cuff, epitheloid macrophages stain for cathepsin K. Some background staining is present.

To confirm the presence of Cathepsin K in human tissue associated with *M. tb* infection, human tissue, resected for diagnosis of suspected malignancy, and discovered instead to be TB (by pathology and acid fast staining), was stained for cathepsin K (figure 77). This demonstrated that cathepsin K was abundantly expressed and is associated with TB pathology. In particular, its expression localised to the periphery of large necrotic regions and multinucleate giant cells. These pathologies have a known association with high bacterial burdens, and this localisation suggests a specific relationship between cathepsin K expression and infection.

5.10. Summary

These studies demonstrate that MMP-1, at the transcriptional, protein and enzymatic activity level were found in the rabbit model. Both hypothesis driven, and unbiased screening approaches, identified a role for MMP-1 and collagen turnover. This reflects what is seen in human disease (99, 105, 107, 109, 110, 114). In addition to this, cathepsin K, identified by whole genome sequencing in rabbits, was shown to be associated with TB pathology, other than multinucleate giant cells (as shown very recently by Halushka *et al.* (173)). Like MMP-1, this enzyme is also easily targetable with a drug, Odanacatib, with demonstrable safety in humans even after upwards of 5 years exposure (228-233).

6. The Role of cAMP in *M. tuberculosis* Induced MMP-1 Secretion

Having identified that MMP-1 expression was present in the rabbit model of TB, further methods for targeting its secretion and activity were investigated. Whilst the drug Ro32-3555 can prevent MMP-1 activity, its failure to complete clinical trials has meant that there are no longer manufacturers of the drug. Custom synthesis is available, but it is costly to manufacture. Previous experiments suggest that pathways targeted by commonly available and cheap drugs may alter MMP-1 secretion and therefore negate such cost (116, 117).

M. tb may deregulate host cellular pathways to induce excessive MMP-1 secretion. MMP-1 secretion is substantially greater in response to *M. tb* than non-pathogenic *M. bovis BCG* (116), and this may benefit the bacteria by allowing transmission (53, 54, 109). Volkman *et al.* have shown that ESAT-6 secretion modulates MMP-9 secretion by host epithelial cells (111) but as of yet no bacterial factor has been identified that specifically upregulates MMP-1 activity. Agarwal *et al.* demonstrated that the *M. tb* gene Rv0386, which encodes an adenylate cyclase (an enzyme that converts ATP to cAMP), was required for virulence (234). They proposed that this adenylate cyclase was part of a mechanism that delivered cAMP into the host macrophage (cAMP is polarised and cannot diffuse across membranes) to alter TNFα secretion (234). cAMP synthesis is required for MMP-1 secretion during *M. tb* infection (116). It has also been observed that exogenous cAMP can augment collagenase secretion from lipopolysaccharides (LPS) stimulated macrophages (235). Inhibition of COX enzymes results in decreased MMP-1 secretion that can subsequently be restored by adding dibutyryl cAMP (dbcAMP); a membrane permeable cAMP analogue (114, 117). cAMP plays this role as part of a p38 mitogen activated protein kinase (MAPK) dependent signalling cascade: p38 MAPK signalling leads to increased levels of cyclo-oxygenase (COX) enzymes which synthesise prostaglandin E_2 (PGE_2), PGE_2 accumulation leads to host adenylate cyclase activity and cAMP

production. cAMP regulates a number intracellular signalling pathways, most notably protein kinase A (PKA). We hypothesised that *M. tb* secretes cAMP to drive MMP-1 secretion. A number of readily available and safe drugs are approved for altering cAMP levels (COX inhibitors and phosphodiesterase inhibitors).

To investigate the relationship between MMP-1 and this promising, straightforward, therapeutic intervention, a series of *in vitro* experiments were designed to establish the role of cAMP in MMP-1 secretion by macrophages infected with *M. tb*.

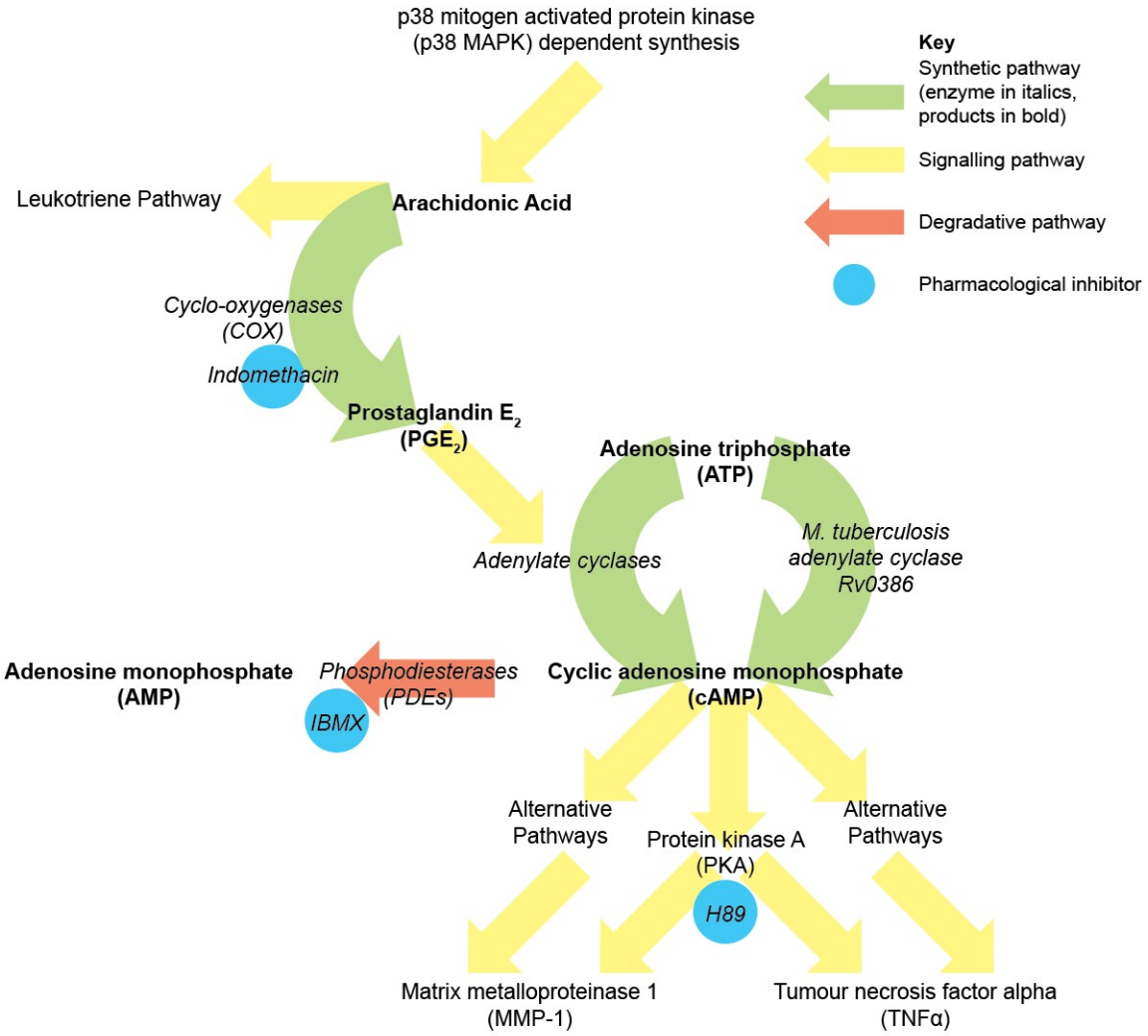

Figure 78. Simplified diagram of pathways involved in regulating MMP-1 and TNFα secretion: MMP-1 expression is regulated in cAMP dependent signalling cascade. A number of G-protein coupled receptors (GPCRs) signalling pathways, including, but not limited to, p38 MAPK, regulate arachidonic acid metabolism. Arachidonic acid is converted to a number of prostaglandins (PGEs) by COX enzymes (COX-1 and COX-2), of which PGE2 plays an important role in regulating adenylate cyclases that produce the second messenger cAMP. cAMP modulates a diverse number of host pathways, including protein kinase A. cAMP is degraded to AMP by phosphodiesterases, which can be inhibited by phosphodiesterase inhibitors such as IBMX. cAMP production plays an important role in MMP-1 secretion by human macrophages infected with TB. *M. tuberculosis* also produces cAMP, which is known to modulate host cell TNFα production, although the specific pathways involved have not been elucidated. Indomethacin is a COX-1 and -2 inhibitor, IBMX is a pan phosphodiesterase inhibitor, and H89 inhibits PKA.

6.1. Experimental protocol

Human blood monocytes were isolated by ficoll centrifugation and adhesion purification. They were then matured into macrophages. Infection was simulated either by the addition of sterile-filtered culture supernatant (TB Sup) or infection with *M. tb H37Rv* at a MOI of 1. If live infection was used, the supernatant was changed 2 hours after infection to remove any non-phagocytosed bacteria. At 72 hours cell supernatant was harvested. MMP content was analysed using either ELISA or multiplex bead-array analysis (Luminex). The data below are representative of 3 experiments and error bars represent standard deviations. We have previously observed that donor-to-donor variation leads to inter-experimental variation in absolute MMP secretion, but that changes in MMP secretion are reproducible (114, 116).

Sterile-filtered culture supernatant from logarithmically growing *M. tuberculosis* (TB Sup) was utilised to model infection in the absence of live bacteria. TB Sup contains a number of TB antigens capable of driving MMP secretion and its use means that alterations in host responses, can be investigated without confounding alterations in bacterial behaviour or growth leading to indirect alterations to host cell behaviour.

Cyclic AMP (cAMP) is not membrane-permeable, so a permeable, water-soluble analogue of cAMP, dibutyryl cAMP (dbcAMP) is used to model the effect of exogenous cAMP. The first experiment aimed to establish whether cAMP alone induced MMP-1 secretion from primary human macrophages.

6.2. Exogenous cAMP does not increase MMP-1 secretion from non-stimulated or highly-stimulated macrophages:

First, the effect of adding exogenous cAMP to macrophages with and without *M. tuberculosis*-derived stimulation was investigated. MMP-1 secretion did not increase in the presence of dbcAMP alone, which is in-keeping with previous observations (235). MMP-1 was significantly upregulated by a 1:40 dilution of TB Sup (Figure 79). This dilution was used because our group has shown that similar dilutions of supernatant from *M. tuberculosis* infected monocytes (CoMtb) drive MMP-1 secretion from primary macrophages (114). The high level of MMP-1 secretion demonstrates that this dilution of TB Sup is a very potent stimulus for the induction of MMP-1 secretion. Unexpectedly, when dbcAMP was added to this stimulus MMP-1 secretion was unchanged at low concentrations, and decreased at higher concentrations. At 10uM dbcAMP MMP-1 secretion was 50% lower than with TB Sup alone and at 50uM dbcAMP a 90% reduction in MMP-1 secretion was observed. This demonstrates that high concentrations of dbcAMP suppress MMP-1 secretion from highly stimulated macrophages.

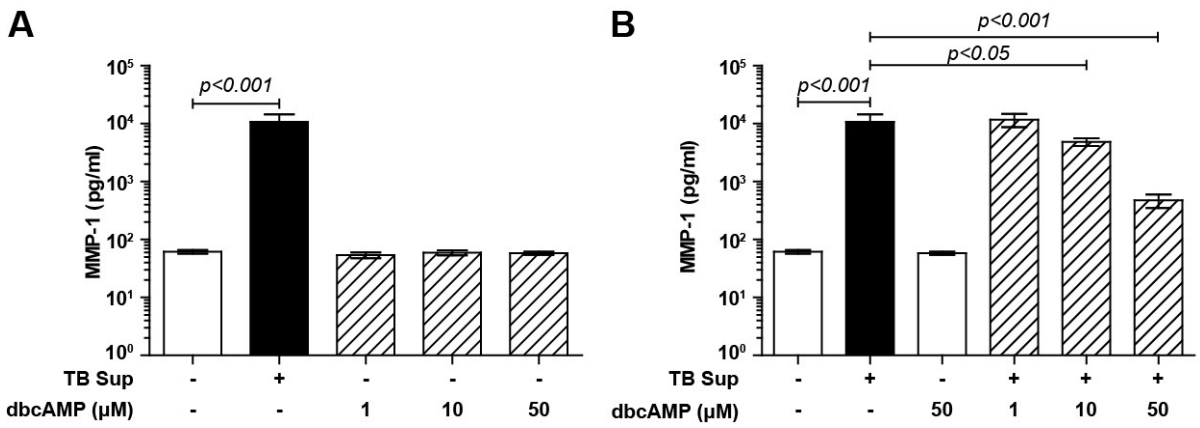

Figure 79. High Concentrations of dbcAMP unexpectedly reduced MMP-1 secretion by blood-derived human macrophages: (A) TB Sup substantially and significantly increased MMP-1 secretion by human blood-derived macrophages. Exogenous cAMP, in the form dbcAMP did not affect MMP-1 secretion in isolation. **(B)** When dbcAMP was added to TB Sup stimulated macrophages, MMP-1 secretion did not increase. At higher concentrations (10μm and 50μm), dbcAMP led to a reduction in MMP-1 secretion. *(Statistical Analysis, one-way ANOVA with Tukey post-test comparison, n=3).*

6.3. Even in minimally stimulated cells, exogenous cAMP does not increase MMP-1 secretion

McCarthy *et al.* had previously described that very high levels (100-500µM) of dbcAMP resulted in a decreased in collagenase secretion in LPS stimulated macrophages (235). Elkington *et al.* demonstrated that *M. tb* infection of macrophages leads to PGE_2 production, which then leads to increased host adenylate cyclase activity and increased host cAMP production (114). The results in section 6.3 suggested that perhaps endogenous cAMP was already reaching a level that led to maximal MMP-1 secretion. It was hypothesised that reducing this stimulus, may allow for easier identification of a role for exogenous cAMP in driving MMP-1 secretion. In order to select an appropriate stimulatory dose of TB Sup, a dose response analysis was performed (Figure 80A).

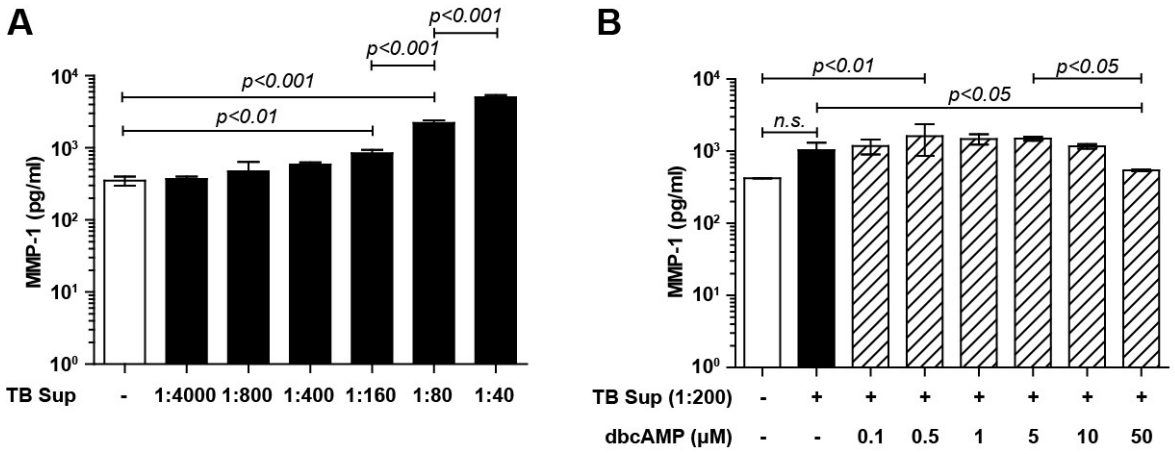

Figure 80. TB Sup exhibited a dose response effect on MMP-1 secretion by human macrophages, which was not significantly enhanced by low concentrations of dbcAMP, and was reduced by high concentrations of dbcAMP: (A) Although an upwards trend was observed at a 1:800 dilution, the difference did not become statistically different until a dilution of 1:160. **(B)** dbcAMP did not significantly enhance TB Sup driven MMP-1 secretion. A dose of 1:200 of TB Sup did not significantly upregulate MMP-1 expression, however, when this dilution of TB Sup was combined with 5µM of dbcAMP this upregulation became significant. A significant decrease in MMP-1 secretion was observed when dbcAMP secretion was increased from 1 to 50µM. *(Statistical Analysis, one-way ANOVA with Tukey post-test comparison, n=3).*

This demonstrated that increasing the concentration of TB Sup resulted in more MMP-1 secretion in a dose dependent fashion. It was decided that a TB Sup dilution of 1:200 should be used for further experiments, as this allows for an observable increase in MMP-1 secretion. Additionally, a larger range of dbcAMP concentrations was used to evaluate the effect of cAMP on MMP-1 secretion in

this low-stimulation model. Figure 80B shows that exogenous cAMP did not substantially increase MMP-1 secretion from TB Sup stimulated cells, even when the stimulus was reduced to allow for an increase in MMP-1 secretion. A significant but small increase in MMP-1 secretion at low concentrations of dbcAMP (0.1-5.0μM) may be masked in this data by the increased variability of the TB only stimulated cells in this experiment (black bar). This data does not suggest that cAMP contributes substantially to MMP-1 secretion, and also confirms that at high concentrations MMP-1 secretion is inhibited by the presence of exogenous cAMP.

6.4. Artificially increasing host derived cAMP, by utilising the phosphodiesterase inhibitor IBMX, does not increase MMP-1 secretion

In order to confirm the observation that increasing cytoplasmic levels of cAMP were not associated with increased MMP-1 secretion, the phosphodiesterase inhibitor IBMX (3-isobutyl-1-methylxanthine), was utilised to indirectly increase endogenous cAMP levels. Eight PDEs regulate host cAMP levels by converting cAMP to AMP. IBMX inhibits all but one of these PDEs and has been shown to reliably increase intracellular cAMP levels (236). IBMX was placed onto the macrophages 2 hours prior to stimulation with TB Sup or infection with live *M. tb H37Rv* (Figure 81).

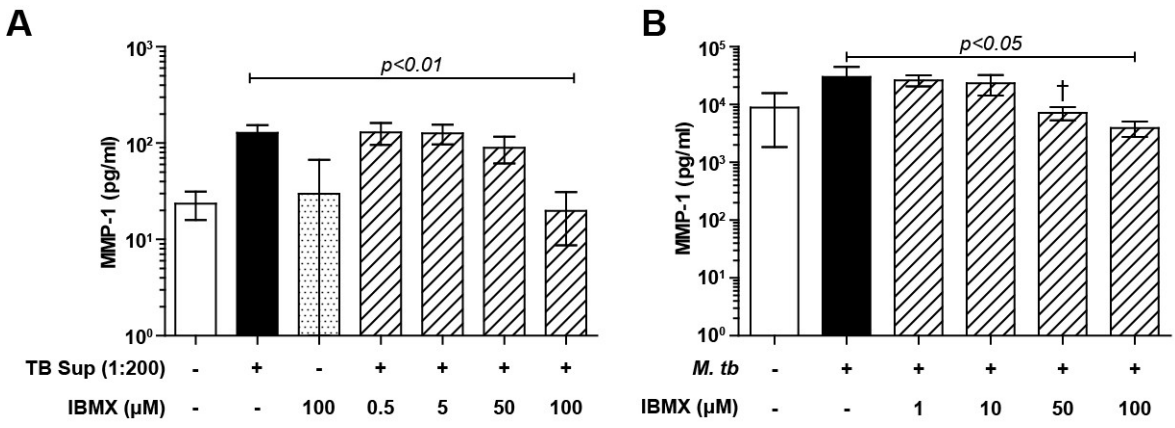

Figure 81. Phosphodiesterase inhibition did not enhance MMP-1 secretion from blood-derived human macrophages: (A) Inhibition of host phoshodiesterases by IBMX did not increase MMP-1 secretion. At 100μM IBMX, MMP-1 secretion is significantly reduced. **(B)** In live *M. tb H37Rv* infection (*M. tb*), a downwards trend in MMP-1 secretion was observed with increasing IBMX concentrations, which reached significance at a dose of 100 μM of IBMX. *(Statistical Analysis, one-way ANOVA with Tukey post-test comparison, n=3). (†: n=2: this point was excluded from statistical analysis).*

It was observed that in both in live infection, and in TB Sup stimulated cells, increasing endogenous cAMP did not increase MMP-1 secretion. It was again observed that at high concentrations of IBMX (which correspond to high endogenous cAMP levels), MMP-1 secretion was decreased.

6.5. dbcAMP cannot be used to enhance MMP-1 secretion even with a cAMP free stimulus

Broth culture of *M. tb* contains cAMP derived from the bacteria (234). This experiment aimed to provide an entirely cAMP free stimulus in which cAMP concentrations could be absolutely controlled by supplementing with dbcAMP. *M. tb H37Rv* killed by UV irradiation (UVTB) was spun at 10000g for 5 minutes, prior to washing 3x in PBS and then resuspended in either 7H9 (wUVTB) or the original supernatant (UVTB). The wUVTB should contain whole bacteria devoid of any secreted mediators. The UVTB served as a positive control. MMP-7, which is upregulated by *M. tb* infection in a cAMP independent manner (114) was also measured.

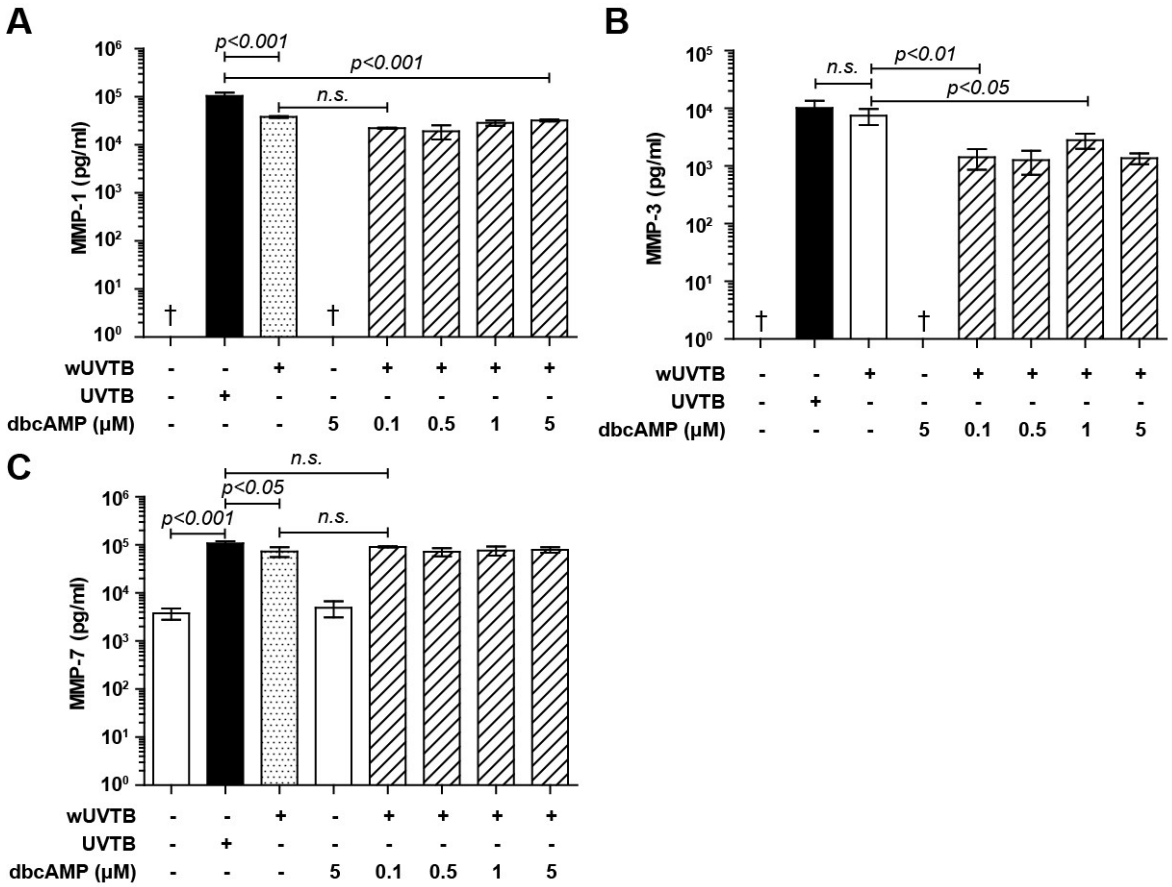

Figure 82. *M. tb* supernatant specifically enhanced MMP-1 secretion by primary human macrophages, whereas cAMP does not: (A) Ultraviolet light-killed *M. tuberculosis H37Rv* (UVTB) caused MMP-1 secretion from human primary monocyte derived macrophages. When the supernatant was removed and replaced with fresh media after the bacteria had been killed (wUVTB), MMP-1 production was reduced approximately 6 fold. dbcAMP did not increase MMP-1 secretion from wUVTB infected cells. **(B)** MMP-3 secretion was not dependent on the presence of supernatant, and was decreased in the presence of dbcAMP. **(C)** MMP-7 secretion was also significantly upregulated by UVTB, a small but statistically significant increase in MMP-7 secretion was seen with the addition of supernatant. As expected, MMP-7 secretion is remains unaffected by the addition of dbcAMP. *(Statistical Analysis, one-way ANOVA with Tukey post-test comparison,* †; *below the threshold of detection, which is approximately 10pg/ml, n=3).*

The addition of dbcAMP did not alter MMP-1 secretion, suggesting that exogenous cAMP does not increase MMP-1 secretion (figure 82A). In the same samples MMP-3 and -7 did not change significantly suggesting that a component of the supernatant (Figure 82B and C), which is not cAMP specifically up-regulates MMP-1 secretion. The observation that MMP-1 secretion is dependent on

both a cellular and supernatant component of the stimulus, but that MMP-3 and -7 secretion is not, indicated that enhanced MMP-1 secretion is dependent on a component of TB sup that is not cAMP.

6.6. MMP-1 secretion is PKA dependent during tuberculosis infection

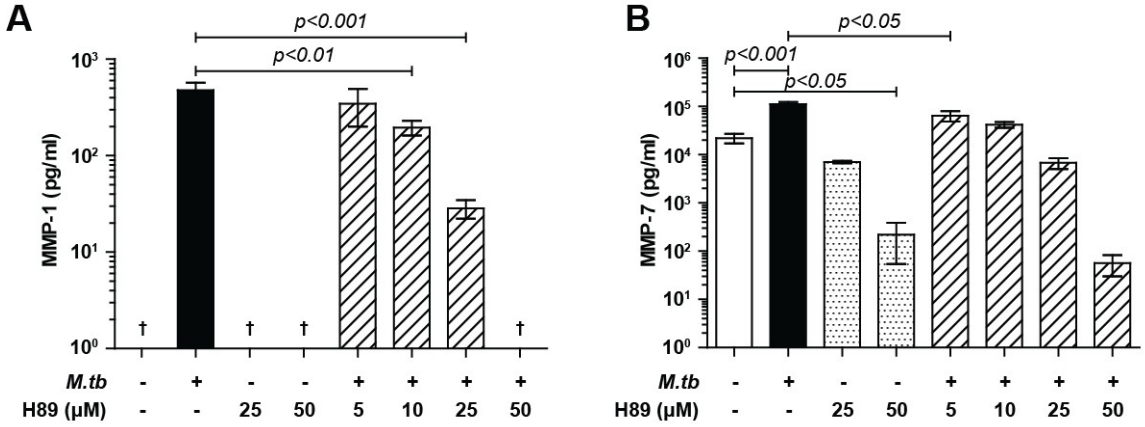

Figure 83. MMP-1 and MMP-7 secretion are PKA dependent: (A) A dose dependent reduction in MMP-1 secretion was observed when the PKA inhibitor H89 was added to *M. tb* infected macrophages. The reduction became statisically significant at 10μM of H89 **(B)** MMP-7 secretion was reduced by addition of the same inhibitor. Baseline MMP-7 secretion was not significantly reduced by the addition of 25μM of H89, however, *M. tb* driven MMP-7 secretion was reduced by 5μM of H89. *(Statistical Analysis, one-way ANOVA with Tukey post-test comparison, n=3). (†: below the threshold of detection, which is approximately 10pg/ml).*

PKA is a downstream signalling molecule from cAMP (via PGE_2). The PKA inhibitor H89 caused a dose dependent reduction in MMP-1 secretion occurs (Figure 83), indicating that MMP-1 secretion from *M. tb* infected macrophages is likely regulated in a cAMP dependent manner; although it is possible that cAMP independent mechanism for PKA activation may exist.

6.7. TNF secretion is reduced by dbcAMP in primary human macrophages

Because Agarwal *et al.* demonstrated that bacteria derived cAMP led to an increase in TNFα secretion (234) an investigation into whether TNFα secretion was increased in the presence of additional dbcAMP was performed. Agarwal had demonstrated this effect in mouse bone-derived monocyte-macrophages, and the human monocytic cell line THP-1. Surprisingly, in human blood-derived macrophages, TNFα secretion was decreased by increasing concentrations of dbcAMP (Figure 83), both at 24 and 48 hours post infection. These time points were used to match the experiments by Agarwal *et al.*

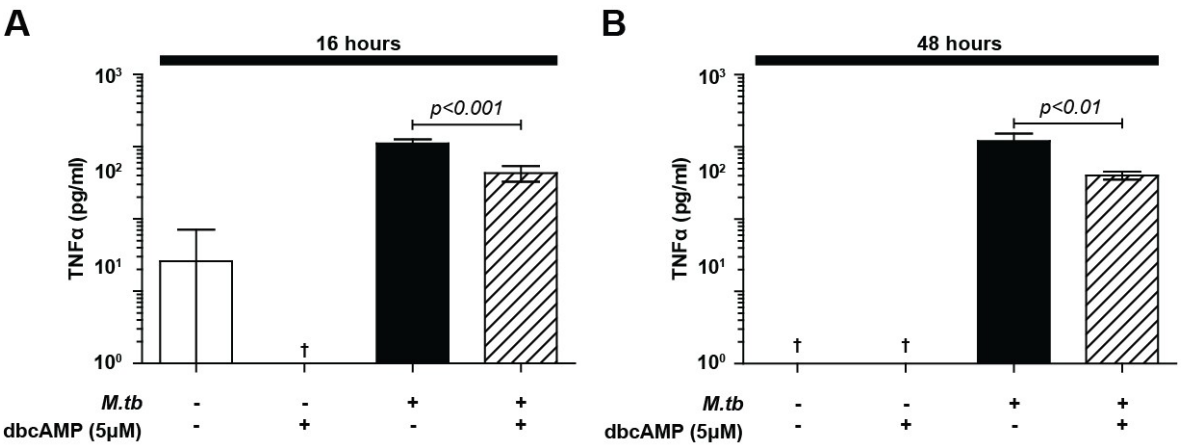

Figure 84. TNFα secretion by human blood derived macrophages is reduced by dbcAMP: H37Rv infection at an MOI of 1 led to a significant increase in the levels of TNFα as measured by ELISA. This was reduced by the addition of 5uM of dbcAMP, an effect that was observed at 16hours **(A)** and 48hours **(B)** post-infection. *(Statistical Analysis, one-way ANOVA with Tukey post-test comparison, n=3).*

This data suggests that despite the involvement of cAMP in regulating MMP-1 secretion, bacterial derived cAMP is not the main contributor to MMP-1 secretion during TB infection. However, the observations in figure 81, that the cultured supernatant led to a substantial increase in MMP-1 secretion, indicate that some mediator in this supernatant alters MMP-1 secretion.

6.8. MMP-1 and -3 secretion are specifically augmented by culture supernatant, whereas MMP-7 secretion remains unchanged

To confirm whether the culture supernatant contained a mediator (which could be protein, lipid, nucleotide or a small molecule) with the potential to augment MMP-1 secretion, the following experiment was performed: Differing concentrations of UVTB and wUVTB were used to stimulate primary macrophages (figure 84). A dose response effect was observed with both UVTB and wUVTB (Figure 84A and B). Surprisingly a dose response effect was not seen with MMP-7 secretion. This is most likely due to MMP-7 secretion being maximal, even at the lowest dose of UVTB used. This speculation is supported by the observation that a downwards trend is observed in MMP-7 secretion with decreasing concentration of the stimulus (Figure 84C). MMP-1 and -3 secretion differed significantly between equal concentrations of UVTB and wUVTB at all concentrations tested ($p<0.01$) whereas MMP-7 secretion was unchanged. This is a strong indicator that both cellular and secreted components of *M.tb* act synergistically to cause MMP-1 and -3, but not MMP-7 secretion.

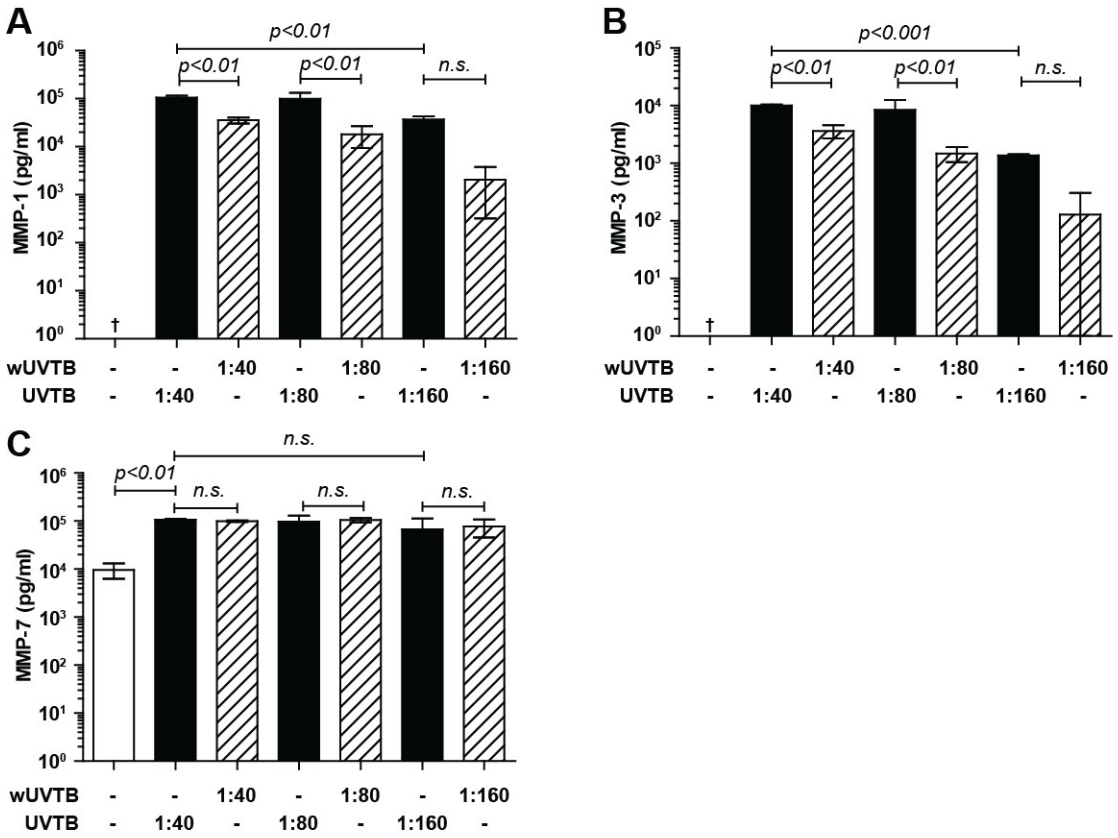

Figure 85. MMP-1 and MMP-3 secretion is lower in the absence of broth culture supernatant, whereas MMP-7 secretion is unchanged: (A) MMP-1 secretion in response to UV killed *M. tuberculosis* (UVTB) was dose dependent. At all concentrations of UVTB/wUVTB tested MMP-1 secretion was greater if its original supernatant was present, than if that supernatant was replaced by media alone. **(B)** MMP-3 secretion in the presence of UVTB was dose dependent. At all concentrations of UVTB/wUVTB tested MMP-3 secretion was greater if its original supernatant was present, than if that supernatant was replaced by media alone. **(C)** MMP-7 secretion did not change at the concentrations tested, and is not dependent on the presence of supernatant. *(Statistical Analysis, one-way ANOVA with Tukey post-test comparison, n=3). (†, below the threshold of detection, which is approximately 10pg/ml).*

6.9. Summary

In this model *M. tb* infection, which uses primary human macrophages, it was unexpectedly observed that exogenous cAMP, in the form of dbcAMP does not alter MMP-1 secretion. At high concentrations, it appears that exogenous cAMP can even reduce MMP-1 secretion from primary macrophages in the context of *M. tb* infection. The reduction in MMP-1 secretion, occurs at cAMP concentrations greater than those observed during *M. tb* infection (234), and so is unlikely to be of relevance *in vivo*. cAMP can restore the reduction in MMP-1 production during *M. bovis BCG* infection to the levels seen during *M. tb* infection of macrophages (116). cAMP can also restore the reduction in MMP-1 secretion caused COX inhibition in *M. tb* infected macrophages (114). The data presented here shows that *M. tb* induced MMP-1 secretion is PKA dependent. Suggesting that cAMP (as a key mediator of PKA) may be required for MMP-1 secretion. However, the data presented here also suggest that exogenous cAMP alone cannot augment MMP-1 secretion. It would appear that cAMP has a role in MMP-1 secretion, but that bacterial cAMP does not feed directly into this pathway. This is confirmed by the observation that the Rv0386 transposon mutant (which lacks a functional adenylate cyclase shown to be involved in the secretion of cAMP into the host cell (234)) induces an equal amount of MMP-1 secretion to its parent strain *M. tb CDC1551* (PTG Elkington, unpublished observation).

Agarwal *et. al* demonstrated that picomolar increases in cAMP altered early TNFα secretion from both the human monocytic cell line, THP-1, and mouse macrophage-like cell line, J774 as well as mouse bone derived monocyte-macrophages (234). However, the data presented here show that in primary human macrophages stimulated with *M. tb*, exogenous cAMP appears to reduce TNFα secretion (figure 84). The fact that increased levels of cAMP appear to be associated with anti-inflammatory, rather than pro-inflammatory changes, is in-keeping with a large body of work on the subject (237-244). This raises questions as to why the two cellular models differ. The primary cell model acts as the most representative *in vitro* model of human responses to *M. tb*, but the inherent variability makes it unsuitable for studying extremely small changes in cell behaviour. As such, the

results shown here do not exclude the possibility that bacterial cAMP plays a role in MMP-1 secretion, but instead suggest that this 'exogenous' cAMP source is not likely to be a major contributor to MMP-1 secretion in man. Interestingly, the data suggests that a mediator secreted by *M. tuberculosis* may specifically drive MMP-1 secretion (figures 82 and 85).

The data show repeatedly that filtered supernatant from *M. tb* culture can induce MMP-1 secretion. In addition to this, supernatant from UV-killed *M. tb* augments secretion of MMP-1 and -3, but not MMP-7, from macrophages. This suggests that MMP-1/-3 are specifically up-regulated by some component of the supernatant of *M. tb* broth culture. The possibility of such a virulence factor warrants further investigation. This is particularly pertinent as ESAT-6 has been linked to MMP-9 secretion and cellular recruitment in the zebrafish model of TB (111). Induction of MMPs has also been suggested as a pathogenic mechanism in both *Pseudomonas aeruginosa* (245) and *Helicobacter pylori* (246, 247). The 'secretome' of *M. tb* has been thoroughly assessed by the vaccine community, looking to identify antigenic peptides (248). Few people have identified functional activities for components of the secretome. However, the possibility that secreted products modulate host immune responses has been explored by several groups who have identified small molecules (234), lipids (249), and proteins (111) that mediate specific immune responses.

Finally, and perhaps most clinically pertinent is that increasing the production of cAMP (the main function of commonly used phosphodiesterase inhibitors) may reduce MMP-1 secretion in the context of TB. This effect would not be revealed by mouse studies. Mouse trials have suggested that PDE inhibition may be effective adjunctive therapy (250, 251), and so it is possible, that this effect may be underestimating potential clinical benefit. It would be interesting to investigate if similar divergences in cAMP signalling occurred in rabbits, a mechanism which may explain why trials of PDE inhibitors in rabbits infected with *M. tb* reduced pathology and facilitated isoniazid activity (167).

7. Discussion and Future Directions

Tuberculosis is a preventable cause of death, and yet it kills more than 1.4 million people each year (1). 10 million children are orphaned each year by disease (2). It is estimated that the disease has a total economic cost of $519 billion in sub-Saharan Africa alone (4). Clearly, a monumental, co-ordinated effort is required to improve preventative measures and facilitate diagnosis and treatment, especially in the complex social settings where TB is most prevalent. Novel preventative, diagnostic and therapeutic approaches must be developed if we are to combat TB in the developing world.

Tissue destruction, in particular cavity formation, is a common phenotype of active tuberculosis (9, 10, 39, 60, 69, 71, 85, 118) and rarely occurs in other diseases (88). It contributes to morbidity (176-179), mortality (180-183), transmission (184, 185), and treatment failure (71, 86, 186). It is poorly understood, largely due to the paucity of animal models in which it can be rigorously studied.

Animal models provide proof-of-concept and safety information prior to performing trials in human beings. Reducing the risk of newly trialled therapies is especially important in tuberculosis, which is readily cured in the individual, with a suboptimal, but still relatively easily administered and tolerated, course of antibiotics. Combating the TB problem in regions with limited resources requires more easily implemented interventions, but the trial of novel strategies is challenging where it is the ethical duty of the researcher to ensure that those within a cohort receive at least optimal care. Careful use and interpretation of animal models can be used to select the best interventional candidates. In depth analysis of animal models may provide insight into mechanisms of disease.

This thesis describes modifications to, and investigations of, a cavity model of tuberculosis that can be used for preclinical trials. It describes the development of modalities to better assess this model, and the confirmation that collagen degrading enzymes are associated, at a tissue level, with cavity

formation. The hope is that this work will facilitate investigation of novel therapies to tackle this global epidemic.

7.1. A cavity model that recapitulates human pathology, in a manner which makes interventional trials feasible

The key contribution of the work outlined here is the introduction of a modified model of cavitary tuberculosis that *rapidly and reliably* recapitulates the cavitary phenotype in man (185, 252). Despite the highly artificial process that leads to cavity formation in this model, the endpoint is representative of human disease. The histology is similar (71, 73, 155); there is a fibrotic layer surrounded by lymphocytes, within which lies a layer of epithelioid macrophages which become increasingly necrotic towards the centre of the cavity. In the necrotic region high numbers of acid-fast bacteria are found. Multinucleate giant cells and foam cells are observed; although perhaps less commonly than in human specimens, perhaps because such cell types form at later time points. CT findings are similar to those found in human disease (252-254) – cavities they are thick-walled, with surrounding infiltrate and are associated with airway change. Crucially, viable bacteria localise to the cavity surface, as in human disease (69, 71, 83). The cavities developed in the model do not significantly differ in phenotype from those seen in 'natural' models, where aerosol infection is followed by chronic disease (155, 162, 163, 189). It is therefore logical to investigate the process cavity development in the new model, because it may reflect the process of natural cavity formation in man. Conveniently, the short time course in cavity development means that well matched comparisons can be made.

Experimental techniques designed to investigate if cavity formation correlates with transmission did not yield positive results. However, further modifications to these methods, or perhaps careful examination of the pattern of dissemination after cavity formation, may reveal whether this model can be used to better understand the role of cavity formation in transmission.

7.2. Simple imaging modalities allow for the monitoring of progression of disease in a single animal

In man, the severity of TB can be measured in many ways; mortality, symptom scores, DALYs (disability adjusted life years), QALYs (quality adjusted life years), sputum bacillary count, structural extent of disease, respiratory function, weight, immunological parameter change, transmissibility and many so forth. It is essential to remember that the aim in treating an individual, is to achieve the absence of disease (i.e. symptoms) in both the short and long-term, and that at a community level, (be it local or global) the aim is to prevent disease in unaffected individuals, either by preventing acquisition directly, or by preventing transmission from infectious sources (i.e treating infected individuals). If treatment strategies are to achieve this, better correlates for symptomatic disease and transmission must be found in animal models. Current readouts of TB models include mortality, histology, bacterial burden, immunological marker change and weight-change. All of these measures, are highly correlative with bacterial burden, which is only partially responsible for disease outcome in man (69, 71, 74, 75). These measures can therefore predict the efficacy of antibacterial agents, and the importance of bacterial virulence factors required for survival in the context of the model species' immune response (which is often largely ineffective against the pathogen). However, they still cannot universally predict antibiotic effectiveness in man (128, 255-257). They may also predict how well vaccines enhance clearance of infection by the host species; although it is clear that immune-mediated clearance in many animal species does not often predict outcome in humans (22, 258-260).

This thesis presents a structural imaging method to assess a functional correlate of disease in rabbits. Evaluation of novel therapeutic strategies in this model may help us better understand current clinical strategies, and design similarly efficacious strategies. Occasionally, functional imaging has been used to assess local inflammation in animal models of TB (133, 134, 165, 261); however, evaluation of disease extent by CT has not previously been performed. This is surprising since we observed that in our model, CT changes better predict disease outcome than PET (262, 263).

The breath-hold technique allows for quantification of pathology *in vivo*, and is a modification of a similar technique used in neonates (202). The analysis, which was a modification of methods previously used in humans (191), demonstrated clear changes in lung involvement, even over the short duration of these experiments. The presence of such readily measurable changes suggests that observable difference would occur with effective therapeutics. Additionally, an estimate of recruitable lung can be achieved by varying lung pressure, again, by modification a previously published technique (191). Finally, a disease specific method was developed to assess, in a non-biased manner, regions in which pathological change is observed, before and after infection. These give accurate measures of specifically diseased regions – which can then be visualised, allowing for subjective analysis of the quantified regions. This technique is clearly unrefined when combined to cutting edge regional pulmonary function analysis (210, 211), but represents a conceptual advance in the use of animal models for TB research.

7.3. Hypersensitivity to PPD is correlated with cavity development

The data presented here suggests that in rabbits, sensitisation as measured by TST reactivity (type IV hypersensitivity (39)), to PPD (as opposed to old tuberculin), increases the risk of cavity formation. This is in-keeping with previous investigations where sensitisation resulted in cavity formation (157-161, 168, 169, 264, 265). It is unclear how this observation correlates to sporadic cavity formation during chronic infection in rabbits (155, 162, 163, 165). A unifying theory is that chronic infection in itself causes sensitisation (189), and that when bacterial burden is sustained after sensitisation, then cavity formation occurs. This would explain the variety of outcomes seen in chronic infection. This would suggest that sensitised animals also mount a bactericidal immune response that is simultaneously protective in certain regions but destructive in others. Currently, little is known about why certain strains produce chronic infection when others (particular CDC1551) do not (156, 266). The best characterised strains which causes chronic infection in rabbits is HN878, and the only suggested mechanisms for its increased virulence in animal models are contradictory;, suggesting alternative roles for IFNα and β induction and delay in T_h1 responses (163, 267-269).

This hypothesis is in-keeping with molecular data from other model systems in which apparently paradoxical roles for a number of mediators of inflammation occur. TNF (136, 141, 270), Leukotriene A4 (142, 143, 271), PD-1 (272-274) and cAMP (167, 234, 250, 275) have all been shown to be associated with divergent disease outcomes. Sensitisation probably results in disruption of many of these responses, which will vary subtly in a lesion-to-lesion manner. The high-dose sensitisation regimen administered as part of these experiments, as well as consistent delivery of equal bacterial burdens, may provide a consistency in responses that does not occur with lower dose sensitisations, or aerosol infection. Careful dissection of the relevant pathways is warranted, and conveniently, pharmaceutical inhibitors and modulators of many of these pathways are available (276-279). Introduction of such inhibitors into the model system presented here may reveal functional outcomes that other animal models may not predict.

Finally, it is worth considering that Dannenberg claims that humans are '100 times more sensitive to tuberculin' than rabbits (189), if this estimate is true, lower dose exposure to mycobacterial products in man may have a dramatic effect in inducing hypersensitivity. The experimental data presented in this thesis suggest that TST-positivity is a risk factor for active TB, rather than a simple marker of exposure (9, 39, 280). Were this to be true in people, it would imply that latent disease (rather than latent infection) is indicated by a positive TST, and that, logically, subclinical infection need not be accompanied by a positive TST. Such subclinical infection is a low risk for active disease. This logic would explain why it is well documented that TST/IGRA negative individuals may develop active TB without a discernible new exposure when given anti-TNF therapy (281-284). This hypothesis would also provide an explanation for the surprising absence of TST-positivity in some highly exposed individuals (37, 285), and why TST-negative immunocompetent individuals have a low risk of disease. If this is true, then reinterpretation of studies where persistent lack of conversion was assumed to be the protective from infection (285) is needed. This consideration is extremely important in the context of vaccine use and development, since it would suggest that developing certain immune responses may dispose to more destructive disease, even if the vaccine is initially protective.

7.4. Pulmonary disease in the rabbit resulting from *M. bovis* and *M. tuberculosis* infection are phenotypically different from each other

The work in this thesis also investigated infection of rabbits with *Mycobacterium bovis ravenel* after sensitisation. It is apparent that *M. bovis* infection results in a fundamentally different disease from that caused by *M. tb* in rabbits (73-75). This difference is often overlooked (74, 75). *M. bovis*, but not *M. tb*, rapidly disseminates and establishes infection in multiple organ sites. This observation is important to consider because *M. bovis* has not been sustained in human populations whereas *M. tuberculosis* has, implying that intra-host dissemination in the life-cycle of *M. tb* is questionable importance. However, the data here also suggest that despite being less capable of causing disseminated disease, *M. tb* infection results in cavity formation more often. Because cavity formation is associated with disease transmission (184, 185), the preponderance for *M. tb* to develop cavitary disease, instead of disseminated disease, indicates a direct link between cavitation and *M. tb*, and strongly indicates that cavity formation is a bacterial driven process. *M. bovis* is primarily found in domestic animal populations, where the mechanism of transmission, although often assumed to be 'aerosol', may be uro/faecal-respiratory transfer, and through contaminated milk.

The data presented here suggest that the immune responses to *M. bovis ravenel* are highly inflammatory when compared to equivalent infection with *M. tb H37Rv*. This suggests that cavity formation is a distinct process from inflammation, and suggests that cavity formation, as opposed to general necrotic or inflammatory pathways, is driven by *M. tb*. This is evidenced by the observation that *M. tb* secretes a mediator that drives MMP-1 secretion by macrophages.

Although the focus of this thesis is on the importance of *M. tb* as a human pathogen, it must be remembered that the economic burden of *M. bovis* in livestock is an important subject (57, 58, 286-293). No conclusive evidence for aerosol transmission of *M. bovis* could be found, an observation that is in-keeping with the finding that human-to-human transmission is very rare; human infection is primarily through ingestion of contaminated milk or occupational exposure (294, 295). Lurie

demonstrated transmission of *M. bovis* from one rabbit to another across an air-gap, however, transmission did not occur if cages were regularly cleaned and less bedding was used (74, 75, 205), suggesting that the primary mechanism of transmission was via contaminated bedding and not direct exhalation of bacteria.

The differences between the *M. bovis* and *M. tb* must explain why *M. bovis* is not epidemic in man whereas *M. tb* is. This observation, and the data presented here, suggest that *M. bovis* lacks crucial traits required for successful transmission in man (since it is clearly virulent within man(295)) – and is therefore a very separate disease. Since *M. tb* strains can sustain infection in rabbits (155, 163-165), it seems that the use of the different *M. bovis* infection model for investigating TB is unwarranted. However, it is important that an understanding of the mechanisms involved in the pathogenesis of TB, and the disease caused by *M. bovis* are sought. By comparing the two infections, specific mechanisms that underlie their respective successes in the populations they affect may be revealed. Understanding such mechanisms may reveal novel therapeutic targets, which may be of particular interest to those seeking to prevent disease transmission.

7.5. Molecular characterisation of the modified cavity model suggests parallels to human disease and reveals potential therapeutic targets

The final component of the studies in this thesis examined molecular correlations between rabbit and human disease, focussing specifically on ECM-degrading enzymes. The correlates between disease in man and this model occur were impressive, with the model showing similar increases in MMP expression to that observed in humans (105, 107, 109). In particular, MMP-1, which is increased during active TB (105, 107, 109, 110, 114-117), was found to increase at both the transcriptional and protein level in cavitary rabbit disease. This correlated with transcriptional data from rabbit aerosol infection models with *M. tb HN878* (163, 275). Since this enzyme is targetable with an inhibitor (Ro32-3555/Trocade/Cipemastat) of proven safety in man (226, 296), the suggested trials of this drug (53, 84, 107, 109) can now be carried out in a relevant preclinical model of disease. Perhaps more pertinent to clinical use, the commonly used antibiotic doxycycline is an FDA approved inhibitor of MMP-1 (297-301), with partial antibiotic effectiveness against *M. tb* (107), and may represent a more-cost effective adjunctive therapy for TB. Other options may exist for reducing tissue damage, particularly by identifying the pathways involved in regulating MMP-1 expression.

In vitro regulation of MMP-1 was examined using a blood-derived human macrophage culture model. Having hypothesised that bacterial derived cAMP (234) may be a key mediator promoting MMP-1 secretion, it was discovered, surprisingly, that high levels of cAMP reduced MMP-1 secretion by infected macrophages. In keeping with this observation the experiments demonstrated that the pan-PDE inhibitor IBMX (which should cause an increase in intracellular cAMP) also decreased MMP-1 secretion. This data supports the observation that CC-3052, a PDE4 inhibitor, reduced MMP-1 expression in a rabbit model of TB (275). PDE inhibitors have shown adjunctive therapeutic potential for treatment of *M. tb* infection in mice (250, 251) and rabbits (167, 275). The benefit derived in the treatment of mice, suggests an MMP-1 independent mechanism, since mice do not express a functional homologue of MMP-1 in lung tissue (130). There benefit in the rabbit model may be MMP-1 dependent, but since extensive ECM degradation does not occur in this model at the time

points studied, this reduction does not establish if MMP-1 inhibition is important. Further to this, the data presented here also suggest that *M. tb* secretes a mediator that enhances MMP-1 secretion by macrophages. Further understanding of such a mechanism would be of great interest, as it may reveal a virulence factor essential for continued disease progression and transmission. One could speculate that neutralisation of such a factor could prevent disease progression, and would make a worthy vaccine target.

In addition to MMP-1, this study also identified Cathepsin K as another potential mediator of collagenolysis in TB. Cathepsin K is a cysteine protease with fibrillar collagenase activity at acidic pH (221) and the only non-MMP, type-I collagenase. Coincidently, cathepsin K was demonstrated to be associated with TB pathology by another group observing the role of multi-nucleate giant cells in various pathologies (173), although the data in this thesis confirms that cathepsin K expression is not limited to these cell types. Although cathepsin D has previously been associated with tissue destruction in rabbits (162) – this structurally related enzyme, has no known function in tissue destruction. There is a clinically safe drug, Odanacatib, awaiting FDA-approval, which targets this enzyme specifically (228-233).

Taken together the data suggests that the 70-day rabbit model represents tissue destructive processes in active TB. The work identifies a number of potential targets, for which clinically safe drugs can be repurposed for rapid clinical deployment.

7.6. Summary

This work documents the modification of a rabbit model of cavitary tuberculosis, to a point where it can easily be used for therapeutic trials. The model is representative of a number of features of human disease, in particular; bacterial localisation to the cavity surface, cellular organisation in response to *M. tb* infection and ECM changes associated with TB. This thesis also outlines a simple way to collect, analyse and present imaging data in this model. Several molecular correlates with human disease were identified in this model, of which, at least two, are therapeutically relevant. This thesis presents a model for trialling these (and other) therapies for TB.

7.7. Future Directions

There are numerous future directions for this work, however, with the development of such a specific model of cavitary disease a number of investigations are imminently possible. Although this thesis followed a hypothesis surrounding the role of collagenases in tuberculosis, the applications for the model and technologies developed during the thesis are perhaps more relevant to several fundamental questions in tuberculosis treatment.

7.7.1. Understanding and improving antibiotic therapy

Investigating the relative contributions of antibiotics to the clearance of bacteria from cavities, may help us to understand why certain antibiotic regimens outperform others in man, despite similar in vitro activity (87, 126, 127, 164). One long-standing hypothesis is that the cavity microenvironment alters local antibiotic penetration and efficacy. This hypothesis has already been confirmed in granulomas during *M. tb* infection of rabbits (164, 166) using multiple-reaction-monitoring matrix-assisted laser desorption-ionisation mass spectrometry imaging (MRM-SELDI-MSI), to investigate relative drug concentrations in rabbit lesions. As of yet, no formal study of the cavity compartment has been completed. This method is fraught with challenges, as it provides only relative concentrations, and even with the establishment of such concentrations – it still does not give compartmental information (for example whether the antibiotic concentrates in macrophage vacuoles, where M. tuberculosis may persist). The current model allows for antibiotic exposure in the cavity setting to be monitored using either MRM-SELDI-MSI, or more conveniently, by evaluating bacterial burdens after antibiotic treatment - a measure of actual efficacy, rather than regional drug distribution. Such studies may help design novel therapeutic regimens that provide optimal cover of all compartments in which bacteria are found in man.

7.7.2. Protease inhibition as a therapeutic strategy

The next obvious investigation is the trial of these highly specific drugs Odanacatib and Cipemastat; such trials will establish whether cathepsin K and MMP-1 contribute to tissue destruction, or are merely associated with tissue destruction. If these therapies do prevent tissue destruction they

could potentially be used therapeutically in XDR-TB – where such drugs may reduce morbidity. Secondly, trialling such drugs may reveal mechanisms by which these enzymes regulate immune function,which may be relevant not only to understanding TB, but immunopathology in general. This may be especially relevant to inflammatory conditions where tissue destruction is the hallmark. Thirdly, these drugs could be trialled in combination with antibiotic regimens, as alterations to pathology may improve antibiotic penetration.

7.7.3. Understanding the bacterial factors involved in cavity formation

The final consideration is whether the model can be used to investigate bacterial factors which contribute to cavity formation, and thus identify cavity specific virulence factors. The identification of bacterial factors which contribute to cavitary disease either through direct induction of ECM-degrading factors, or through enhancing hypersensitivity reactions can now be tested in a relevant animal model. Further exploration of this concept, may provide novel vaccine targets that aim to neutralise the disease, rather than the bacteria itself. Although it is unlikely to lead to total disease eradication, this efficacy may be enough to break the cycle of epidemic transmission, or accelerate bacterial clearance in conjunction with antibiotic therapy, and thus shorten the duration of treatment.

References

1. Global Tuberculosis Report 2012. Geneva: World Health Organization2012.

2. Global Tuberculosis Control: WHO Report 2010. Report2010.

3. Juniarti N, Evans D. A qualitative review: the stigma of tuberculosis. J Clin Nurs. 2011 Jul;20(13-14):1961-70.

4. Laxminarayan R, Klein E, Dye C, Floyd K, Darley S, Adeyi O. Economic Benefit of Tuberculosis Control. Policy Research Working Paper. Washington, D.C.: World Bank2007 Contract No.: 4295.

5. Global Tuberculosis Report 2012: Annex 2, Country Profiles. Geneva: World Health Organization 2012.

6. Gandhi NR, Moll A, Sturm AW, Pawinski R, Govender T, Lalloo U, et al. Extensively drug-resistant tuberculosis as a cause of death in patients co-infected with tuberculosis and HIV in a rural area of South Africa. Lancet. 2006 Nov 4;368(9547):1575-80.

7. Fenner F, Henderson DA, Arita I, Jezek Z, Ladnyi ID. Smallpox and its Eradication. Geneva: World Health Organization; 1988.

8. World Health Organization. Global Commission for the Certification of Smallpox Eradication. The global eradication of smallpox : final report of the Global Commission for the Certification of Smallpox Eradication, Geneva, December 1979. Geneva: World Health Organization ; Albany, N.Y. : WHO Publications Centre distributor; 1980.

9. Fauci AS. Harrison's principles of internal medicine. 17th ed. New York: McGraw-Hill; 2008.

10. Kumar PJ, Clark ML. Kumar & Clark's clinical medicine. 8th ed. Edinburgh: Saunders Elsevier; 2012.

11. Snider GL. Tuberculosis then and now: a personal perspective on the last 50 years. Ann Intern Med. 1997 Feb 1;126(3):237-43.

12. Miramontes R, Pratt R, Price SF, Navin TR, Lo TQ. Trends in Tuberculosis - United States, 2012. Centers for Disease Control and Prevention; 2013 [updated 22/03/201309/06/2013]; Available from: http://www.cdc.gov/mmwr/preview/mmwrhtml/mm6211a2.htm?s_cid=mm6211a2_w.

13. GDP per capita, PPP (current international $) The World Bank; 2013; Available from: http://data.worldbank.org/indicator/NY.GDP.PCAP.PP.CD.

14. Copenhagen Consensus 2012: Expert Panel Findings. Copenhagen, Denmark 2012.

15. Baily GV. Tuberculosis prevention Trial, Madras. Indian J Med Res. 1980 Jul;72 Suppl:1-74.

16. Comstock GW, Woolpert SF, Livesay VT. Tuberculosis studies in Muscogee County, Georgia. Twenty-year evaluation of a community trial of BCG vaccination. Public Health Rep. 1976 May-Jun;91(3):276-80.

17. Comstock GW, Livesay VT, Woolpert SF. Evaluation of BCG vaccination among Puerto Rican children. Am J Public Health. 1974 Mar;64(3):283-91.

18. Dye C. Global epidemiology of tuberculosis. The Lancet. 1999;367(9514):938-40.

19. Scriba TJ, Tameris M, Smit E, van der Merwe L, Hughes EJ, Kadira B, et al. A phase IIa trial of the new tuberculosis vaccine, MVA85A, in HIV- and/or *Mycobacterium tuberculosis*-infected adults. Am J Respir Crit Care Med. 2012 Apr 1;185(7):769-78.

20. Abel B, Tameris M, Mansoor N, Gelderbloem S, Hughes J, Abrahams D, et al. The novel tuberculosis vaccine, AERAS-402, induces robust and polyfunctional CD4+ and CD8+ T cells in adults. Am J Respir Crit Care Med. 2010 Jun 15;181(12):1407-17.

21. Hawkridge T, Scriba TJ, Gelderbloem S, Smit E, Tameris M, Moyo S, et al. Safety and immunogenicity of a new tuberculosis vaccine, MVA85A, in healthy adults in South Africa. J Infect Dis. 2008 Aug 15;198(4):544-52.

22. Tameris MD, Hatherill M, Landry BS, Scriba TJ, Snowden MA, Lockhart S, et al. Safety and efficacy of MVA85A, a new tuberculosis vaccine, in infants previously vaccinated with BCG: a randomised, placebo-controlled phase 2b trial. Lancet. 2013 Feb 1.

23. Trunz BB, Fine PEM, Dye C. Effect of BCG vaccination on childhood tuberculous meningitis and miliary tuberculosis worldwide: a meta-analysis and assessment of cost-effectiveness. The Lancet. 2006;367(9517):1173-80.

24. Escombe AR, Oeser CC, Gilman RH, Navincopa M, Ticona E, Pan W, et al. Natural ventilation for the prevention of airborne contagion. PLoS Med. 2007 Feb;4(2):e68.

25. Riley RL, Mills CC, O'Grady F, Sultan LU, Wittstadt F, Shivpuri DN. Infectiousness of air from a tuberculosis ward. Ultraviolet irradiation of infected air: comparative infectiousness of different patients. Am Rev Respir Dis. 1962 Apr;85:511-25.

26. Sultan L, Nyka W, Mills C, O'Grady F, Wells W, Riley RL. Tuberculosis disseminators. A study of the variability of aerial infectivity of tuberculous patients. Am Rev Respir Dis. 1960 Sep;82:358-69.

27. Torok ME, Reuter S, Bryant J, Koser CU, Stinchcombe SV, Nazareth B, et al. Rapid whole-genome sequencing for investigation of a suspected tuberculosis outbreak. J Clin Microbiol. 2013 Feb;51(2):611-4.

28. Gardy JL, Johnston JC, Sui SJH, Cook VJ, Shah L, Brodkin E, et al. Whole-Genome Sequencing and Social-Network Analysis of a Tuberculosis Outbreak. New England Journal of Medicine. 2011;364(8):730-9.

29. Roetzer A, Diel R, Kohl TA, Rückert C, Nübel U, Blom J, et al. Whole Genome Sequencing versus Traditional Genotyping for Investigation of a *Mycobacterium tuberculosis* Outbreak: A Longitudinal Molecular Epidemiological Study. PLoS Med. 2013;10(2):e1001387.

30. Alonso PL, Lindsay SW, Armstrong JR, Conteh M, Hill AG, David PH, et al. The effect of insecticide-treated bed nets on mortality of Gambian children. Lancet. 1991 Jun 22;337(8756):1499-502.

31. Valdiserri RO, Lyter DW, Leviton LC, Callahan CM, Kingsley LA, Rinaldo CR. AIDS prevention in homosexual and bisexual men: results of a randomized trial evaluating two risk reduction

interventions. AIDS. 1989 Jan;3(1):21-6.

32. Gralton J, McLaws ML. Protecting healthcare workers from pandemic influenza: N95 or surgical masks? Crit Care Med. 2010 Feb;38(2):657-67.

33. Shine KI, Rogers B, Goldfrank LR. Novel H1N1 Influenza and Respiratory Protection for Health Care Workers. New England Journal of Medicine. 2009;361(19):1823-5.

34. Jefferson T, Del Mar CB, Dooley L, Ferroni E, Al-Ansary LA, Bawazeer GA, et al. Physical interventions to interrupt or reduce the spread of respiratory viruses. Cochrane Database Syst Rev. 2011(7):CD006207.

35. Biscotto CR, Pedroso ER, Starling CE, Roth VR. Evaluation of N95 respirator use as a tuberculosis control measure in a resource-limited setting. Int J Tuberc Lung Dis. 2005 May;9(5):545-9.

36. Escombe AR, Moore DA, Gilman RH, Navincopa M, Ticona E, Mitchell B, et al. Upper-room ultraviolet light and negative air ionization to prevent tuberculosis transmission. PLoS Med. 2009 Mar 17;6(3):e43.

37. Andrews JR, Morrow C, Wood R. Modeling the role of public transportation in sustaining tuberculosis transmission in South Africa. Am J Epidemiol. 2013 Mar 15;177(6):556-61.

38. Cohen T, Murray M, Wallengren K, Alvarez GG, Samuel EY, Wilson D. The prevalence and drug sensitivity of tuberculosis among patients dying in hospital in KwaZulu-Natal, South Africa: a postmortem study. PLoS Med. 2010 Jun;7(6):e1000296.

39. Robbins SL, Kumar V. Robbins and Cotran pathologic basis of disease. 8th ed. Philadelphia, PA: Saunders/Elsevier; 2010.

40. Dowdy DW, Basu S, Andrews JR. Is passive diagnosis enough? The impact of subclinical disease on diagnostic strategies for tuberculosis. Am J Respir Crit Care Med. 2013 Mar 1;187(5):543-51.

41. WHO. WHO endorses rapid tuberculosis test. Geneva2010 [cited 2013 12/06/2013]; Available from: http://www.who.int/mediacentre/news/releases/2010/tb_test_20101208/en/index.html

42. Dai Y, Feng Y, Xu R, Xu W, Lu W, Wang J. Evaluation of interferon-gamma release assays for the diagnosis of tuberculosis: an updated meta-analysis. Eur J Clin Microbiol Infect Dis. 2012 Nov;31(11):3127-37.

43. Diel R, Loddenkemper R, Nienhaus A. Predictive value of interferon-gamma release assays and tuberculin skin testing for progression from latent TB infection to disease state: a meta-analysis. Chest. 2012 Jul;142(1):63-75.

44. Fan L, Chen Z, Hao XH, Hu ZY, Xiao HP. Interferon-gamma release assays for the diagnosis of extrapulmonary tuberculosis: a systematic review and meta-analysis. FEMS Immunol Med Microbiol. 2012 Aug;65(3):456-66.

45. Metcalfe JZ, Everett CK, Steingart KR, Cattamanchi A, Huang L, Hopewell PC, et al. Interferon-gamma release assays for active pulmonary tuberculosis diagnosis in adults in low- and middle-income countries: systematic review and meta-analysis. J Infect Dis. 2011 Nov 15;204 Suppl 4:S1120-

9.
46. Nash DR, Douglass JE. Anergy in active pulmonary tuberculosis. A comparison between positive and negative reactors and an evaluation of 5 tu and 250 tu skin test doses. CHEST Journal. 1980;77(1):32-7.

47. Tuberculosis in the UK: Annual Report on Tuberculosis in the UK, 2012. London: Health Protection Agency 2012.

48. Lee M, Lee J, Carroll MW, Choi H, Min S, Song T, et al. Linezolid for Treatment of Chronic Extensively Drug-Resistant Tuberculosis. New England Journal of Medicine. 2012;367(16):1508-18.

49. Gler MT, Skripconoka V, Sanchez-Garavito E, Xiao H, Cabrera-Rivero JL, Vargas-Vasquez DE, et al. Delamanid for Multidrug-Resistant Pulmonary Tuberculosis. New England Journal of Medicine. 2012;366(23):2151-60.

50. Diacon AH, Pym A, Grobusch M, Patientia R, Rustomjee R, Page-Shipp L, et al. The Diarylquinoline TMC207 for Multidrug-Resistant Tuberculosis. New England Journal of Medicine. 2009;360(23):2397-405.

51. Diacon AH, Donald PR, Pym A, Grobusch M, Patientia RF, Mahanyele R, et al. Randomized pilot trial of eight weeks of bedaquiline (TMC207) treatment for multidrug-resistant tuberculosis: long-term outcome, tolerability, and effect on emergence of drug resistance. Antimicrob Agents Chemother. 2012 Jun;56(6):3271-6.

52. Jawahar MS, Banurekha VV, Paramasivan CN, Rahman F, Ramachandran R, Venkatesan P, et al. Randomized clinical trial of thrice-weekly 4-month moxifloxacin or gatifloxacin containing regimens in the treatment of new sputum positive pulmonary tuberculosis patients. PLoS One. 2013;8(7):e67030.

53. Paige C, Bishai WR. Penitentiary or penthouse condo: the tuberculous granuloma from the microbe's point of view. Cell Microbiol. 2010 Mar;12(3):301-9.

54. Yoder MA, Lamichane G, Bishai WR. Cavitary pulmonary tuberculosis: The Holy Grail of disease transmission. Bangalore, INDE: Current Science Association; 2004.

55. Cobo J, Asensio A, Moreno S, Navas E, Pintado V, Oliva J, et al. Risk factors for nosocomial transmission of multidrug-resistant tuberculosis due to *Mycobacterium bovis* among HIV-infected patients. Int J Tuberc Lung Dis. 2001 May;5(5):413-8.

56. Evans JT, Smith EG, Banerjee A, Smith RMM, Dale J, Innes JA, et al. Cluster of human tuberculosis caused by Mycobacterium bovis: evidence for person-to-person transmission in the UK. The Lancet. 2007;369(9569):1270-6.

57. Torgerson P, Torgerson D. Does risk to humans justify high cost of fighting bovine TB? Nature. 2008;455(7216):1029-.

58. Michel AL, Müller B, van Helden PD. *Mycobacterium bovis* at the animal–human interface: A problem, or not? Veterinary Microbiology. 2010;140(3–4):371-81.

59. Rocha A, Elias AR, Sobral LF, Soares DF, Santos AC, Marsico AG, et al. Genotyping did not evidence any contribution of *Mycobacterium bovis* to human tuberculosis in Brazil. Tuberculosis (Edinb). 2011 Jan;91(1):14-21.

60. Lim EKS, Loke YK, Thompson AM. Medicine & surgery : an integrated textbook. Edinburgh ; New York: Churchill Livingstone/Elsevier; 2007.

61. Bucher HC, Griffith LE, Guyatt GH, Sudre P, Naef M, Sendi P, et al. Isoniazid prophylaxis for tuberculosis in HIV infection: a meta-analysis of randomized controlled trials. AIDS. 1999;13(4):501-7.

62. Rom WN, Garay SM. Tuberculosis. 2nd ed. Philadelphia: Lippincott Williams & Wilkins; 2004.

63. Gardam MA, Keystone EC, Menzies R, Manners S, Skamene E, Long R, et al. Anti-tumour necrosis factor agents and tuberculosis risk: mechanisms of action and clinical management. The Lancet Infectious Diseases. 2003;3(3):148-55.

64. Hsu KK. Thirty years after isoniazid: Its impact on tuberculosis in children and adolescents. JAMA. 1984;251(10):1283-5.

65. Ena J, Valls V. Short-Course Therapy with Rifampin plus Isoniazid, Compared with Standard Therapy with Isoniazid, for Latent Tuberculosis Infection: A Meta-analysis. Clinical Infectious Diseases. 2005 March 1, 2005;40(5):670-6.

66. Adetifa IM, Ota MO, Jeffries DJ, Lugos MD, Hammond AS, Battersby NJ, et al. Interferon-gamma ELISPOT as a biomarker of treatment efficacy in latent tuberculosis infection: a clinical trial. Am J Respir Crit Care Med. 2013 Feb 15;187(4):439-45.

67. Pai M, Joshi R, Dogra S, Mendiratta DK, Narang P, Dheda K, et al. Persistently elevated T cell interferon-gamma responses after treatment for latent tuberculosis infection among health care workers in India: a preliminary report. J Occup Med Toxicol. 2006;1:7.

68. Takenami I, Finkmoore B, Machado A, Jr., Emodi K, Riley LW, Arruda S. Levels of interferon-gamma increase after treatment for latent tuberculosis infection in a high-transmission setting. Pulm Med. 2012;2012:757152.

69. Rich AR. The Pathogenesis of Tuberculosis. 2 ed. Springfield, Illinois: Thomas; 1951.

70. Stedman's Medical Dictionary. 28 ed. Baltimore, MD: Lippincott Williams & Wilkins; 2006.

71. Canetti C. The tubercle bacillus in the pulmonary lesion of man: histobacteriology and its bearing on the therapy of pulmonary tuberculosis. New York, New York: Springfield; 1955.

72. Laennec RTH. A treatise on the diseases of the chest in which they are described according to their anatomical characters, and their diagnosis, established on a new principle by means of acoustick instruments. London: T. and G. Underwood; 1821.

73. Hunter RL. Pathology of post primary tuberculosis of the lung: an illustrated critical review. Tuberculosis (Edinb). 2011 Nov;91(6):497-509.

74. Lurie MB. Resistance to Tuberculosis: Experimental Studies in Native and Acquired Defensive Mechanisms: Harvard University Press, Cambridge, Massachusetts; 1964.

75. Dannenberg AM, Jr. Pathogenesis of human pulmonary tuberculosis : insights from the rabbit model. Washington, D.C.: ASM Press; 2006.

76. Russell DG, Barry CE, 3rd, Flynn JL. Tuberculosis: what we don't know can, and does, hurt us. Science. 2010 May 14;328(5980):852-6.

77. Russell DG. *Mycobacterium tuberculosis* and the intimate discourse of a chronic infection. Immunol Rev. 2011 Mar;240(1):252-68.

78. Russell DG, Cardona PJ, Kim MJ, Allain S, Altare F. Foamy macrophages and the progression of the human tuberculosis granuloma. Nat Immunol. 2009 Sep;10(9):943-8.

79. Russell DG. Who puts the tubercle in tuberculosis? Nat Rev Microbiol. 2007 Jan;5(1):39-47.

80. Reece ST, Kaufmann SH. Floating between the poles of pathology and protection: can we pin down the granuloma in tuberculosis? Curr Opin Microbiol. 2012 Feb;15(1):63-70.

81. Ernst JD. The immunological life cycle of tuberculosis. Nat Rev Immunol. 2012;12(8):581-91.

82. Ramakrishnan L. Revisiting the role of the granuloma in tuberculosis. Nat Rev Immunol. 2012 May;12(5):352-66.

83. Kaplan G, Post FA, Moreira AL, Wainwright H, Kreiswirth BN, Tanverdi M, et al. Mycobacterium tuberculosis growth at the cavity surface: a microenvironment with failed immunity. Infect Immun. 2003 Dec;71(12):7099-108.

84. Elkington PT, D'Armiento JM, Friedland JS. Tuberculosis immunopathology: the neglected role of extracellular matrix destruction. Sci Transl Med. 2011 Feb 23;3(71):71ps6.

85. Price NM, Farrar J, Tran TT, Nguyen TH, Tran TH, Friedland JS. Identification of a matrix-degrading phenotype in human tuberculosis in vitro and in vivo. J Immunol. 2001 Mar 15;166(6):4223-30.

86. Singla R, Srinath D, Gupta S, Visalakshi P, Khalid UK, Singla N, et al. Risk factors for new pulmonary tuberculosis patients failing treatment under the Revised National Tuberculosis Control Programme, India. Int J Tuberc Lung Dis. 2009 Apr;13(4):521-6.

87. Benator D, Bhattacharya M, Bozeman L, Burman W, Cantazaro A, Chaisson R, et al. Rifapentine and isoniazid once a week versus rifampicin and isoniazid twice a week for treatment of drug-susceptible pulmonary tuberculosis in HIV-negative patients: a randomised clinical trial. Lancet. 2002 Aug 17;360(9332):528-34.

88. Gadkowski LB, Stout JE. Cavitary pulmonary disease. Clin Microbiol Rev. 2008 Apr;21(2):305-33, table of contents.

89. Price AP, England KA, Matson AM, Blazar BR, Panoskaltsis-Mortari A. Development of a decellularized lung bioreactor system for bioengineering the lung: the matrix reloaded. Tissue Eng Part A. 2010 Aug;16(8):2581-91.

90. Petersen TH, Calle EA, Zhao L, Lee EJ, Gui L, Raredon MB, et al. Tissue-engineered lungs for in vivo implantation. Science. 2010 Jul 30;329(5991):538-41.

91. Hynes RO. The extracellular matrix: not just pretty fibrils. Science. 2009 Nov 27;326(5957):1216-9.

92. Greenlee KJ, Werb Z, Kheradmand F. Matrix Metalloproteinases in Lung: Multiple, Multifarious, and Multifaceted. Physiological Reviews. 2007 January 1, 2007;87(1):69-98.

93. Werb Z. ECM and Cell Surface Proteolysis: Regulating Cellular Ecology. Cell. 1997;91(4):439-42.

94. Parks WC, Shapiro SD. Matrix metalloproteinases in lung biology. Respir Res. 2001;2(1):10-9.

95. Davey A, McAuley DF, O'Kane CM. Matrix metalloproteinases in acute lung injury: mediators of injury and drivers of repair. European Respiratory Journal. 2011 October 1, 2011;38(4):959-70.

96. Ra HJ, Parks WC. Control of matrix metalloproteinase catalytic activity. Matrix Biol. 2007 Oct;26(8):587-96.

97. Nagase H, Woessner JF, Jr. Matrix metalloproteinases. J Biol Chem. 1999 Jul 30;274(31):21491-4.

98. Nagase H, Visse R, Murphy G. Structure and function of matrix metalloproteinases and TIMPs. Cardiovascular Research. 2006 February 15, 2006;69(3):562-73.

99. Chang JC, Wysocki A, Tchou-Wong KM, Moskowitz N, Zhang Y, Rom WN. Effect of *Mycobacterium tuberculosis* and its components on macrophages and the release of matrix metalloproteinases. Thorax. 1996 Mar;51(3):306-11.

100. Huntley GW. Synaptic circuit remodelling by matrix metalloproteinases in health and disease. Nat Rev Neurosci. 2012 Nov;13(11):743-57.

101. Siefert SA, Sarkar R. Matrix metalloproteinases in vascular physiology and disease. Vascular. 2012 Aug;20(4):210-6.

102. Troeberg L, Nagase H. Proteases involved in cartilage matrix degradation in osteoarthritis. Biochim Biophys Acta. 2012 Jan;1824(1):133-45.

103. Austin KM, Covic L, Kuliopulos A. Matrix metalloproteases and PAR1 activation. Blood. 2013 Jan 17;121(3):431-9.

104. Fields GB. Interstitial Collagen Catabolism. Journal of Biological Chemistry. 2013 March 29, 2013;288(13):8785-93.

105. Ugarte-Gil CA, Elkington P, Gilman RH, Coronel J, Tezera LB, Bernabe-Ortiz A, et al. Induced sputum MMP-1, -3 & -8 concentrations during treatment of tuberculosis. PLoS One. 2013;8(4):e61333.

106. Seddon J, Kasprowicz V, Walker NF, Yuen HM, Sunpath H, Tezera L, et al. Procollagen III N-terminal Propeptide and Desmosine are Released by Matrix Destruction in Pulmonary Tuberculosis. J Infect Dis. 2013 Aug 9.

107. Walker NF, Clark SO, Oni T, Andreu N, Tezera L, Singh S, et al. Doxycycline and HIV Infection Suppress Tuberculosis-induced Matrix Metalloproteinases. Am J Respir Crit Care Med. 2012 Feb 16.

108. Sakamoto K, Kim MJ, Rhoades ER, Allavena RE, Ehrt S, Wainwright HC, et al. Mycobacterial Trehalose Dimycolate Reprograms Macrophage Global Gene Expression and Activates Matrix Metalloproteinases. Infect Immun. 2012 Dec 21.

109. Elkington P, Shiomi T, Breen R, Nuttall RK, Ugarte-Gil CA, Walker NF, et al. MMP-1 drives immunopathology in human tuberculosis and transgenic mice. J Clin Invest. 2011 May;121(5):1827-33.

110. O'Kane CM, Elkington PT, Jones MD, Caviedes L, Tovar M, Gilman RH, et al. STAT3, p38 MAPK, and NF-kappaB drive unopposed monocyte-dependent fibroblast MMP-1 secretion in tuberculosis. Am J Respir Cell Mol Biol. 2010 Oct;43(4):465-74.

111. Volkman HE, Pozos TC, Zheng J, Davis JM, Rawls JF, Ramakrishnan L. Tuberculous granuloma induction via interaction of a bacterial secreted protein with host epithelium. Science. 2010 Jan 22;327(5964):466-9.

112. Ganachari M, Ruiz-Morales JA, Gomez de la Torre Pretell JC, Dinh J, Granados J, Flores-Villanueva PO. Joint effect of MCP-1 genotype GG and MMP-1 genotype 2G/2G increases the likelihood of developing pulmonary tuberculosis in BCG-vaccinated individuals. PLoS One. 2010;5(1):e8881.

113. Wang CH, Lin HC, Lin SM, Huang CD, Liu CY, Huang KH, et al. MMP-1(-1607G) polymorphism as a risk factor for fibrosis after pulmonary tuberculosis in Taiwan. Int J Tuberc Lung Dis. 2010 May;14(5):627-34.

114. Rand L, Green JA, Saraiva L, Friedland JS, Elkington PT. Matrix metalloproteinase-1 is regulated in tuberculosis by a p38 MAPK-dependent, p-aminosalicylic acid-sensitive signaling cascade. J Immunol. 2009 May 1;182(9):5865-72.

115. Elkington PT, Green JA, Emerson JE, Lopez-Pascua LD, Boyle JJ, O'Kane CM, et al. Synergistic up-regulation of epithelial cell matrix metalloproteinase-9 secretion in tuberculosis. Am J Respir Cell Mol Biol. 2007 Oct;37(4):431-7.

116. Elkington PT, Nuttall RK, Boyle JJ, O'Kane CM, Horncastle DE, Edwards DR, et al. Mycobacterium tuberculosis, but not vaccine BCG, specifically upregulates matrix metalloproteinase-1. Am J Respir Crit Care Med. 2005 Dec 15;172(12):1596-604.

117. Elkington PT, Emerson JE, Lopez-Pascua LD, O'Kane CM, Horncastle DE, Boyle JJ, et al. Mycobacterium tuberculosis up-regulates matrix metalloproteinase-1 secretion from human airway epithelial cells via a p38 MAPK switch. J Immunol. 2005 Oct 15;175(8):5333-40.

118. Elkington PT, Ugarte-Gil CA, Friedland JS. Matrix metalloproteinases in tuberculosis. Eur Respir J. 2011 Aug;38(2):456-64.

119. Dufour A, Overall CM. Missing the target: matrix metalloproteinase antitargets in inflammation and cancer. Trends in Pharmacological Sciences. 2013;34(4):233-42.

120. Overall CM, Kleifeld O. Tumour microenvironment - opinion: validating matrix metalloproteinases as drug targets and anti-targets for cancer therapy. Nat Rev Cancer. 2006 Mar;6(3):227-39.

121. Rosenbaum E, Zahurak M, Sinibaldi V, Carducci MA, Pili R, Laufer M, et al. Marimastat in the treatment of patients with biochemically relapsed prostate cancer: a prospective randomized,

double-blind, phase I/II trial. Clin Cancer Res. 2005 Jun 15;11(12):4437-43.

122. Sparano JA, Bernardo P, Stephenson P, Gradishar WJ, Ingle JN, Zucker S, et al. Randomized phase III trial of marimastat versus placebo in patients with metastatic breast cancer who have responding or stable disease after first-line chemotherapy: Eastern Cooperative Oncology Group trial E2196. J Clin Oncol. 2004 Dec 1;22(23):4683-90.

123. Bramhall SR, Hallissey MT, Whiting J, Scholefield J, Tierney G, Stuart RC, et al. Marimastat as maintenance therapy for patients with advanced gastric cancer: a randomised trial. Br J Cancer. 2002 Jun 17;86(12):1864-70.

124. Ghate JV, Turner ML, Rudek MA, Figg WD, Dahut W, Dyer V, et al. Drug-induced lupus associated with COL-3: report of 3 cases. Arch Dermatol. 2001 Apr;137(4):471-4.

125. Box GEP, Draper NR. Empirical model-building and response surfaces. New York: Wiley; 1987.

126. Grosset J, Almeida D, Converse PJ, Tyagi S, Li SY, Ammerman NC, et al. Modeling early bactericidal activity in murine tuberculosis provides insights into the activity of isoniazid and pyrazinamide. Proc Natl Acad Sci U S A. 2012 Sep 11;109(37):15001-5.

127. Rosenthal IM, Tasneen R, Peloquin CA, Zhang M, Almeida D, Mdluli KE, et al. Dose-ranging comparison of rifampin and rifapentine in two pathologically distinct murine models of tuberculosis. Antimicrob Agents Chemother. 2012 Aug;56(8):4331-40.

128. Rosenthal IM, Zhang M, Williams KN, Peloquin CA, Tyagi S, Vernon AA, et al. Daily dosing of rifapentine cures tuberculosis in three months or less in the murine model. PLoS Med. 2007 Dec;4(12):e344.

129. Lun S, Guo H, Adamson J, Cisar JS, Davis TD, Chavadi SS, et al. Pharmacokinetic and in vivo Efficacy Studies of the Mycobactin Biosynthesis Inhibitor Salicyl-AMS in Mice. Antimicrob Agents Chemother. 2013 Jul 15.

130. Balbin M, Fueyo A, Knauper V, Lopez JM, Alvarez J, Sanchez LM, et al. Identification and enzymatic characterization of two diverging murine counterparts of human interstitial collagenase (MMP-1) expressed at sites of embryo implantation. J Biol Chem. 2001 Mar 30;276(13):10253-62.

131. Lemaitre V, O'Byrne TK, Dalal SS, Tall AR, D'Armiento JM. Macrophage-specific expression of human collagenase (MMP-1) in transgenic mice. Ann N Y Acad Sci. 1999 Jun 30;878:736-9.

132. Pan H, Yan BS, Rojas M, Shebzukhov YV, Zhou H, Kobzik L, et al. Ipr1 gene mediates innate immunity to tuberculosis. Nature. 2005 Apr 7;434(7034):767-72.

133. Davis SL, Be NA, Lamichhane G, Nimmagadda S, Pomper MG, Bishai WR, et al. Bacterial thymidine kinase as a non-invasive imaging reporter for *Mycobacterium tuberculosis* in live animals. PLoS One. 2009;4(7):e6297.

134. Davis SL, Nuermberger EL, Um PK, Vidal C, Jedynak B, Pomper MG, et al. Noninvasive pulmonary [18F]-2-fluoro-deoxy-D-glucose positron emission tomography correlates with bactericidal activity of tuberculosis drug treatment. Antimicrob Agents Chemother. 2009 Nov;53(11):4879-84.

135. Harper J, Skerry C, Davis SL, Tasneen R, Weir M, Kramnik I, et al. Mouse model of necrotic tuberculosis granulomas develops hypoxic lesions. J Infect Dis. 2012 Feb 15;205(4):595-602.

136. Skerry C, Harper J, Klunk M, Bishai WR, Jain SK. Adjunctive TNF inhibition with standard treatment enhances bacterial clearance in a murine model of necrotic TB granulomas. PLoS One. 2012;7(6):e39680.

137. Vilaplana C, Marzo E, Tapia G, Diaz J, Garcia V, Cardona PJ. Ibuprofen Therapy Resulted in Significantly Decreased Tissue Bacillary Loads and Increased Survival in a New Murine Experimental Model of Active Tuberculosis. J Infect Dis. 2013 May 3.

138. Driver ER, Ryan GJ, Hoff DR, Irwin SM, Basaraba RJ, Kramnik I, et al. Evaluation of a mouse model of necrotic granuloma formation using C3HeB/FeJ mice for testing of drugs against Mycobacterium tuberculosis. Antimicrob Agents Chemother. 2012 Jun;56(6):3181-95.

139.

140. Ramakrishnan L. Looking within the zebrafish to understand the tuberculous granuloma. Adv Exp Med Biol. 2013;783:251-66.

141. Swaim LE, Connolly LE, Volkman HE, Humbert O, Born DE, Ramakrishnan L. *Mycobacterium marinum* infection of adult zebrafish causes caseating granulomatous tuberculosis and is moderated by adaptive immunity. Infect Immun. 2006 Nov;74(11):6108-17.

142. Roca FJ, Ramakrishnan L. TNF dually mediates resistance and susceptibility to mycobacteria via mitochondrial reactive oxygen species. Cell. 2013 Apr 25;153(3):521-34.

143. Tobin DM, Roca FJ, Oh SF, McFarland R, Vickery TW, Ray JP, et al. Host genotype-specific therapies can optimize the inflammatory response to mycobacterial infections. Cell. 2012 Feb 3;148(3):434-46.

144. Tobin DM, Vary JC, Jr., Ray JP, Walsh GS, Dunstan SJ, Bang ND, et al. The lta4h locus modulates susceptibility to mycobacterial infection in zebrafish and humans. Cell. 2010 Mar 5;140(5):717-30.

145. Watral V, Kent ML. Pathogenesis of Mycobacterium spp. in zebrafish (*Danio rerio*) from research facilities. Comparative Biochemistry and Physiology Part C: Toxicology & Pharmacology. 2007;145(1):55-60.

146. Prouty MG, Correa NE, Barker LP, Jagadeeswaran P, Klose KE. Zebrafish-*Mycobacterium marinum* model for mycobacterial pathogenesis. FEMS Microbiol Lett. 2003 Aug 29;225(2):177-82.

147. Padilla-Carlin DJ, McMurray DN, Hickey AJ. The guinea pig as a model of infectious diseases. Comp Med. 2008 Aug;58(4):324-40.

148. Flynn JL, Capuano SV, Croix D, Pawar S, Myers A, Zinovik A, et al. Non-human primates: a model for tuberculosis research. Tuberculosis (Edinb). 2003;83(1-3):116-8.

149. Ford CB, Lin PL, Chase MR, Shah RR, Iartchouk O, Galagan J, et al. Use of whole genome sequencing to estimate the mutation rate of *Mycobacterium tuberculosis* during latent infection. Nat Genet. 2011 May;43(5):482-6.

150. Lin PL, Myers A, Smith L, Bigbee C, Bigbee M, Fuhrman C, et al. Tumor necrosis factor neutralization results in disseminated disease in acute and latent *Mycobacterium tuberculosis*

infection with normal granuloma structure in a cynomolgus macaque model. Arthritis Rheum. 2010 Feb;62(2):340-50.

151. Lin PL, Rodgers M, Smith L, Bigbee M, Myers A, Bigbee C, et al. Quantitative comparison of active and latent tuberculosis in the cynomolgus macaque model. Infect Immun. 2009 Oct;77(10):4631-42.

152. Lin PL, Dartois V, Johnston PJ, Janssen C, Via L, Goodwin MB, et al. Metronidazole prevents reactivation of latent *Mycobacterium tuberculosis* infection in macaques. Proc Natl Acad Sci U S A. 2012 Aug 28;109(35):14188-93.

153. Mehra S, Pahar B, Dutta NK, Conerly CN, Philippi-Falkenstein K, Alvarez X, et al. Transcriptional reprogramming in nonhuman primate (*rhesus macaque*) tuberculosis granulomas. PLoS One. 2010;5(8):e12266.

154. Manabe YC, Dannenberg AM, Jr., Tyagi SK, Hatem CL, Yoder M, Woolwine SC, et al. Different strains of Mycobacterium tuberculosis cause various spectrums of disease in the rabbit model of tuberculosis. Infect Immun. 2003 Oct;71(10):6004-11.

155. Manabe YC, Kesavan AK, Lopez-Molina J, Hatem CL, Brooks M, Fujiwara R, et al. The aerosol rabbit model of TB latency, reactivation and immune reconstitution inflammatory syndrome. Tuberculosis (Edinb). 2008 May;88(3):187-96.

156. Leong FJWM, Dartois V, Dick T. A color atlas of comparative pathology of pulmonary tuberculosis. Boca Raton: CRC Press; 2011.

157. Subbian S, Tsenova L, O'Brien P, Yang G, Kushner NL, Parsons S, et al. Spontaneous latency in a rabbit model of pulmonary tuberculosis. Am J Pathol. 2012 Nov;181(5):1711-24.

158. Nakamura S, Ogawa Y, Hirayama M, Taka K, Yasaka S, Yamamura Y. [Histological studies on the tuberculous cavity experimentally produced in the rabbit's lung; experimental studies on the tuberculous allergy. II]. Kekkaku. 1954 Jun;29(6):205-10; English abstract, 33.

159. Yamaguchi M, Ogawa Y, Endo K, Takeuchi H, Nakamura S, Yasaka S, et al. [Experimental formation of tuberculous cavity in rabbit lung. V. Experimental production of tuberculous cavity by chemical constituents of tubercle bacilli]. Kekkaku. 1958 Jan;33(1):12-6; English abstract 48.

160. Yamaguchi M, Ogawa Y, Endo K, Takeuchi H, Yasaka S, Nakamura S, et al. [Experimental formation of tuberculous cavity in rabbit lung. IV. Cavity formation by paraffine oil extract prepared from heat killed tubercle bacilli]. Kekkaku. 1955 Sep;30(9):521-4.

161. Yamamura Y, Yasaka S, Nakamura S, Ogawa Y, Yamaguchi M, Endo K, et al. Experimental studies on the tuberculous allergy. III. Experimental formation of the tuberculous cavity in the rabbit's lung by killed tubercle bacillus. Kekkaku. 1954 Sep;29(9):361-7; English abstract, 76-7.

162. Yamamura Y, Yasaka S, Yamaguchi M, Endo K, Iwakura H, Nakamura S, et al. Experimental formation of the tuberculous cavity in the rabbit's lung; experimental study on the tuberculous allergy. I. Kekkaku. 1954 Apr;29(4):143-6; English abstract, 53-4.

163. Converse PJ, Dannenberg AM, Jr., Estep JE, Sugisaki K, Abe Y, Schofield BH, et al. Cavitary tuberculosis produced in rabbits by aerosolized virulent tubercle bacilli. Infect Immun. 1996 Nov;64(11):4776-87.

164. Subbian S, Tsenova L, Yang G, O'Brien P, Parsons S, Peixoto B, et al. Chronic pulmonary cavitary tuberculosis in rabbits: a failed host immune response. Open Biol. 2011 Dec;1(4):110016.

165. Kjellsson MC, Via LE, Goh A, Weiner D, Low KM, Kern S, et al. Pharmacokinetic evaluation of the penetration of antituberculosis agents in rabbit pulmonary lesions. Antimicrob Agents Chemother. 2012 Jan;56(1):446-57.

166. Via LE, Schimel D, Weiner DM, Dartois V, Dayao E, Cai Y, et al. Infection dynamics and response to chemotherapy in a rabbit model of tuberculosis using [(18)F]2-fluoro-deoxy-D-glucose positron emission tomography and computed tomography. Antimicrob Agents Chemother. 2012 Aug;56(8):4391-402.

167. Prideaux B, Dartois V, Staab D, Weiner DM, Goh A, Via LE, et al. High-Sensitivity MALDI-MRM-MS Imaging of Moxifloxacin Distribution in Tuberculosis-Infected Rabbit Lungs and Granulomatous Lesions. Anal Chem. 2011 Feb 18.

168. Subbian S, Tsenova L, O'Brien P, Yang G, Koo MS, Peixoto B, et al. Phosphodiesterase-4 inhibition combined with isoniazid treatment of rabbits with pulmonary tuberculosis reduces macrophage activation and lung pathology. Am J Pathol. 2011 Jul;179(1):289-301.

169. Nedeltchev GG, Raghunand TR, Jassal MS, Lun S, Cheng QJ, Bishai WR. Extrapulmonary dissemination of *Mycobacterium bovis* but not *Mycobacterium tuberculosis* in a bronchoscopic rabbit model of cavitary tuberculosis. Infect Immun. 2009 Feb;77(2):598-603.

170. Jassal MS, Nedeltchev GG, Osborne J, Bishai WR. A modified scoring system to describe gross pathology in the rabbit model of tuberculosis. BMC Microbiol. 2011;11:49.

171. Suckow MA, Schroeder V. The laboratory rabbit. 2nd ed. Boca Raton: CRC Press; 2010.

172. Elkington PT, Friedland JS. Matrix metalloproteinases in destructive pulmonary pathology. Thorax. 2006 Mar;61(3):259-66.

173. Ramakers C, Ruijter JM, Deprez RH, Moorman AF. Assumption-free analysis of quantitative real-time polymerase chain reaction (PCR) data. Neurosci Lett. 2003 Mar 13;339(1):62-6.

174. Park JK, Rosen A, Saffitz JE, Asimaki A, Litovsky SH, Mackey-Bojack SM, et al. Expression of cathepsin K and tartrate-resistant acid phosphatase is not confined to osteoclasts but is a general feature of multinucleated giant cells: systematic analysis. Rheumatology (Oxford). 2013 May 14.

175. Dannenberg AM, Jr. Pathogenesis of Human Tuberculosis: Insights from the Rabbit Model. Washington, DC: American Society for Microbiology Press; 2006.

176. Kesavan AK, Mendez SE, Hatem CL, Lopez-Molina J, Aird K, Pitt ML, et al. Effects of dexamethasone and transient malnutrition on rabbits infected with aerosolized *Mycobacterium tuberculosis CDC1551*. Infect Immun. 2005 Oct;73(10):7056-60.

177. Rhee CK, Yoo KH, Lee JH, Park MJ, Kim WJ, Park YB, et al. Clinical characteristics of patients with tuberculosis-destroyed lung. Int J Tuberc Lung Dis. 2013 Jan;17(1):67-75.

178. Massard G, Olland A, Santelmo N, Falcoz PE. Surgery for the sequelae of postprimary tuberculosis. Thorac Surg Clin. 2012 Aug;22(3):287-300.

179. Alsina L, Gala-Peralta S, Noguera A, Pons M, culi JL, Mu, et al. Neonatal pulmonary

tuberculosis evolving to a destroyed lung [Case Study]. The International Journal of Tuberculosis and Lung Disease. 2008;12(5):573-5.

180. Ralph AP, Ardian M, Wiguna A, Maguire GP, Becker NG, Drogumuller G, et al. A simple, valid, numerical score for grading chest x-ray severity in adult smear-positive pulmonary tuberculosis. Thorax. 2010 October 1, 2010;65(10):863-9.

181. Stebbings AE, Lim TK. Cause, treatment and outcome of patients with life-threatening haemoptysis. Singapore Med J. 1999 Feb;40(2):67-9.

182. Anuradha C, Shyamkumar NK, Vinu M, Babu NR, Christopher DJ. Outcomes of bronchial artery embolization for life-threatening hemoptysis due to tuberculosis and post-tuberculosis sequelae. Diagn Interv Radiol. 2011 Jun 15.

183. Krishnan B, Shaukat A, Chakravorty I. Fatal haemoptysis in a young man with tuberculous mediastinal lymphadenitis. A case report and review of the literature. Respiration. 2009;77(3):333-6.

184. Ryu YJ, Lee JH, Chun EM, Chang JH, Shim SS. Clinical outcomes and prognostic factors in patients with tuberculous destroyed lung. Int J Tuberc Lung Dis. 2011 Feb;15(2):246-50, i.

185. Visser ME, Stead MC, Walzl G, Warren R, Schomaker M, Grewal HM, et al. Baseline predictors of sputum culture conversion in pulmonary tuberculosis: importance of cavities, smoking, time to detection and W-Beijing genotype. PLoS One. 2012;7(1):e29588.

186. Golub JE, Bur S, Cronin WA, Gange S, Baruch N, Comstock GW, et al. Delayed tuberculosis diagnosis and tuberculosis transmission. The International Journal of Tuberculosis and Lung Disease. 2006;10(1):24-30.

187. Wang JY, Lee LN, Yu CJ, Chien YJ, Yang PC. Factors influencing time to smear conversion in patients with smear-positive pulmonary tuberculosis. Respirology. 2009 Sep;14(7):1012-9.

188. Lamichhane G, Zignol M, Blades NJ, Geiman DE, Dougherty A, Grosset J, et al. A postgenomic method for predicting essential genes at subsaturation levels of mutagenesis: application to *Mycobacterium tuberculosis*. Proc Natl Acad Sci U S A. 2003 Jun 10;100(12):7213-8.

189. Lamichhane G, Tyagi S, Bishai WR. Designer arrays for defined mutant analysis to detect genes essential for survival of Mycobacterium tuberculosis in mouse lungs. Infect Immun. 2005 Apr;73(4):2533-40.

190. Converse PJ, Dannenberg AM, Jr., Shigenaga T, McMurray DN, Phalen SW, Stanford JL, et al. Pulmonary bovine-type tuberculosis in rabbits: bacillary virulence, inhaled dose effects, tuberculin sensitivity, and *Mycobacterium vaccae* immunotherapy. Clin Diagn Lab Immunol. 1998 Nov;5(6):871-81.

191. Seibert FB, Crumb C, Dufour EH. Antigenic differences in two tuberculin protein fractions. J Infect Dis. 1951 Nov-Dec;89(3):252-8.

192. Gattinoni L, Caironi P, Cressoni M, Chiumello D, Ranieri VM, Quintel M, et al. Lung recruitment in patients with the acute respiratory distress syndrome. N Engl J Med. 2006 Apr 27;354(17):1775-86.

193. Lewinsohn DM, Tydeman IS, Frieder M, Grotzke JE, Lines RA, Ahmed S, et al. High resolution

radiographic and fine immunologic definition of TB disease progression in the rhesus macaque. Microbes and Infection. 2006;8(11):2587-98.

194. Boneu B, Caranobe C, Cadroy Y, Dol F, Gabaig AM, Dupouy D, et al. Pharmacokinetic studies of standard unfractionated heparin, and low molecular weight heparins in the rabbit. Semin Thromb Hemost. 1988 Jan;14(1):18-27.

195. Martinic G. A technique for intragastric gavage of radiolabeled liquid cholesterol in rabbits (Oryctolagus cuniculus) using a pediatric feeding tube. Lab Anim (NY). 2008 Jul;37(7):323-8.

196. McCabe PM, Gonzales JA, Zaias J, Szeto A, Kumar M, Herron AJ, et al. Social environment influences the progression of atherosclerosis in the watanabe heritable hyperlipidemic rabbit. Circulation. 2002 Jan 22;105(3):354-9.

197. Szeto A, Gonzales JA, Spitzer SB, Levine JE, Zaias J, Saab PG, et al. Circulating levels of glucocorticoid hormones in WHHL and NZW rabbits: circadian cycle and response to repeated social encounter. Psychoneuroendocrinology. 2004;29(7):861-6.

198. Hara-Kudo Y, Morishita Y, Nagaoka Y, Kasuga F, Kumagai S. Incidence of diarrhea with antibiotics and the increase of clostridia in rabbits. J Vet Med Sci. 1996 Dec;58(12):1181-5.

199. Brown C. Nasogastric tube placement in the rabbit. Lab Anim (NY). 2010 Jan;39(1):14-5.

200. Perry-Clark LM, Meunier LD. Vascular access ports for chronic serial infusion and blood sampling in New Zealand white rabbits. Lab Anim Sci. 1991 Oct;41(5):495-7.

201. Kalender WA, Rienmuller R, Seissler W, Behr J, Welke M, Fichte H. Measurement of pulmonary parenchymal attenuation: use of spirometric gating with quantitative CT. Radiology. 1990 Apr;175(1):265-8.

202. Hayward J, Lisson P. Carbon Dioxide Tolerance of Rabbits and Its Relation to Burrow Fumigation. Wildlife Research. 1978;5(2):253-61.

203. Long FR, Castile RG, Brody AS, Hogan MJ, Flucke RL, Filbrun DA, et al. Lungs in infants and young children: improved thin-section CT with a noninvasive controlled-ventilation technique--initial experience. Radiology. 1999 Aug;212(2):588-93.

204. Rangayyan RM, Vu RH, Boag GS. Automatic delineation of the diaphragm in computed tomographic images. J Digit Imaging. 2008 Oct;21 Suppl 1:S134-47.

205. Xu Z, Bagci U, Kubler A, Luna B, Jain S, Bishai WR, et al. Computer-aided detection and quantification of cavitary tuberculosis from CT scans. Medical Physics. 2013;40(11):-.

206. Lurie MB, Heppleston AG, Abramson S, Swartz IB. Evaluation of the method of quantitative airborne infection and its use in the study of the pathogenesis of tuberculosis. Am Rev Tuberc. 1950 Jun;61(6):765-97.

207. Jones RM, Ashford R, Cork J, Palmer S, Wood E, Spyvee P, et al. Evaluation of a method to detect Mycobacterium bovis in air samples from infected Eurasian badgers (Meles meles) and their setts. Lett Appl Microbiol. 2013 May;56(5):361-5.

208. McMurray DN. Hematogenous reseeding of the lung in low-dose, aerosol-infected guinea pigs: unique features of the host-pathogen interface in secondary tubercles. Tuberculosis (Edinb).

2003;83(1-3):131-4.

209. Mutolo D, Bongianni F, Cinelli E, Pantaleo T. Role of excitatory amino acids in the mediation of tracheobronchial cough induced by citric acid inhalation in the rabbit. Brain Res Bull. 2009 Aug 28;80(1-2):22-9.

210. Mutolo D, Bongianni F, Evangelista S, Cinelli E, Pantaleo T. Effects of zofenopril and ramipril on cough reflex responses in anesthetized and awake rabbits. J Cardiovasc Pharmacol Ther. 2010 Dec;15(4):384-92.

211. Kaczka DW, Cao K, Christensen GE, Bates JH, Simon BA. Analysis of regional mechanics in canine lung injury using forced oscillations and 3D image registration. Ann Biomed Eng. 2011 Mar;39(3):1112-24.

212. Kaczka DW, Smallwood JL. Constant-phase descriptions of canine lung, chest wall, and total respiratory system viscoelasticity: effects of distending pressure. Respir Physiol Neurobiol. 2012 Aug 15;183(2):75-84.

213. Caradec J, Sirab N, Keumeugni C, Moutereau S, Chimingqi M, Matar C, et al. 'Desperate house genes': the dramatic example of hypoxia. Br J Cancer. 2010 Mar 16;102(6):1037-43.

214. Kamburov A, Pentchev K, Galicka H, Wierling C, Lehrach H, Herwig R. ConsensusPathDB: toward a more complete picture of cell biology. Nucleic Acids Res. 2011 Jan;39(Database issue):D712-7.

215. Kamburov A, Wierling C, Lehrach H, Herwig R. ConsensusPathDB--a database for integrating human functional interaction networks. Nucleic Acids Res. 2009 Jan;37(Database issue):D623-8.

216. Kanehisa M, Goto S, Sato Y, Furumichi M, Tanabe M. KEGG for integration and interpretation of large-scale molecular data sets. Nucleic Acids Res. 2012 Jan;40(Database issue):D109-14.

217. Kanehisa M, Goto S. KEGG: kyoto encyclopedia of genes and genomes. Nucleic Acids Res. 2000 Jan 1;28(1):27-30.

218. D'Eustachio P. Reactome knowledgebase of human biological pathways and processes. Methods Mol Biol. 2011;694:49-61.

219. Matthews L, Gopinath G, Gillespie M, Caudy M, Croft D, de Bono B, et al. Reactome knowledgebase of human biological pathways and processes. Nucleic Acids Res. 2009 Jan;37(Database issue):D619-22.

220. Vastrik I, D'Eustachio P, Schmidt E, Gopinath G, Croft D, de Bono B, et al. Reactome: a knowledge base of biologic pathways and processes. Genome Biol. 2007;8(3):R39.

221. Ashburner M, Ball CA, Blake JA, Botstein D, Butler H, Cherry JM, et al. Gene ontology: tool for the unification of biology. The Gene Ontology Consortium. Nat Genet. 2000 May;25(1):25-9.

222. Bromme D, Okamoto K, Wang BB, Biroc S. Human cathepsin O2, a matrix protein-degrading cysteine protease expressed in osteoclasts. Functional expression of human cathepsin O2 in *Spodoptera frugiperda* and characterization of the enzyme. J Biol Chem. 1996 Jan 26;271(4):2126-32.

223. Gelb BD, Shi GP, Chapman HA, Desnick RJ. Pycnodysostosis, a lysosomal disease caused by cathepsin K deficiency. Science. 1996 Aug 30;273(5279):1236-8.

224. Tschesche H, Knauper V, Kramer S, Michaelis J, Oberhoff R, Reinke H. Latent collagenase and gelatinase from human neutrophils and their activation. Matrix Suppl. 1992;1:245-55.

225. Qi JH, Ebrahem Q, Moore N, Murphy G, Claesson-Welsh L, Bond M, et al. A novel function for tissue inhibitor of metalloproteinases-3 (TIMP3): inhibition of angiogenesis by blockage of VEGF binding to VEGF receptor-2. Nat Med. 2003 Apr;9(4):407-15.

226. Snoek-van Beurden PA, Von den Hoff JW. Zymographic techniques for the analysis of matrix metalloproteinases and their inhibitors. Biotechniques. 2005 Jan;38(1):73-83.

227. Close DR. Matrix metalloproteinase inhibitors in rheumatic diseases. Ann Rheum Dis. 2001 Nov;60 Suppl 3:iii62-7.

228. Broadhurst MJ, Brown PA, Lawton G, Ballantyne N, Borkakoti N, Bottomley KMK, et al. Design and synthesis of the cartilage protective agent (CPA, Ro32-3555). Bioorganic & Medicinal Chemistry Letters. 1997 Sep 9;7(17):2299-302.

229. Stoch SA, Zajic S, Stone J, Miller DL, Van Dyck K, Gutierrez MJ, et al. Effect of the cathepsin K inhibitor odanacatib on bone resorption biomarkers in healthy postmenopausal women: two double-blind, randomized, placebo-controlled phase I studies. Clin Pharmacol Ther. 2009 Aug;86(2):175-82.

230. Jensen AB, Wynne C, Ramirez G, He W, Song Y, Berd Y, et al. The cathepsin K inhibitor odanacatib suppresses bone resorption in women with breast cancer and established bone metastases: results of a 4-week, double-blind, randomized, controlled trial. Clin Breast Cancer. 2010 Dec 1;10(6):452-8.

231. Bone HG, McClung MR, Roux C, Recker RR, Eisman JA, Verbruggen N, et al. Odanacatib, a cathepsin-K inhibitor for osteoporosis: a two-year study in postmenopausal women with low bone density. J Bone Miner Res. 2010 May;25(5):937-47.

232. Eisman JA, Bone HG, Hosking DJ, McClung MR, Reid IR, Rizzoli R, et al. Odanacatib in the treatment of postmenopausal women with low bone mineral density: three-year continued therapy and resolution of effect. J Bone Miner Res. 2011 Feb;26(2):242-51.

233. Langdahl B, Binkley N, Bone H, Gilchrist N, Resch H, Rodriguez Portales J, et al. Odanacatib in the treatment of postmenopausal women with low bone mineral density: five years of continued therapy in a phase 2 study. J Bone Miner Res. 2012 Nov;27(11):2251-8.

234. Brixen K, Chapurlat R, Cheung AM, Keaveny TM, Fuerst T, Engelke K, et al. Bone density, turnover, and estimated strength in postmenopausal women treated with odanacatib: a randomized trial. J Clin Endocrinol Metab. 2013 Feb;98(2):571-80.

235. Agarwal N, Lamichhane G, Gupta R, Nolan S, Bishai WR. Cyclic AMP intoxication of macrophages by a *Mycobacterium tuberculosis* adenylate cyclase. Nature. 2009 Jul 2;460(7251):98-102.

236. McCarthy JB, Wahl SM, Rees JC, Olsen CE, Sandberg L, Wahl LM. Mediation of macrophage collagenase production by 3'-5' cyclic adenosine monophosphate. J Immunol. 1980 May;124(5):2405-9.

237. Soderling SH, Beavo JA. Regulation of cAMP and cGMP signaling: new phosphodiesterases and new functions. Curr Opin Cell Biol. 2000 Apr;12(2):174-9.

238. Katakami Y, Nakao Y, Koizumi T, Katakami N, Ogawa R, Fujita T. Regulation of tumour necrosis factor production by mouse peritoneal macrophages: the role of cellular cyclic AMP. Immunology. 1988 Aug;64(4):719-24.

239. Renz H, Gong JH, Schmidt A, Nain M, Gemsa D. Release of tumor necrosis factor-alpha from macrophages. Enhancement and suppression are dose-dependently regulated by prostaglandin E2 and cyclic nucleotides. J Immunol. 1988 Oct 1;141(7):2388-93.

240. Tannenbaum CS, Hamilton TA. Lipopolysaccharide-induced gene expression in murine peritoneal macrophages is selectively suppressed by agents that elevate intracellular cAMP. J Immunol. 1989 Feb 15;142(4):1274-80.

241. Taffet SM, Singhel KJ, Overholtzer JF, Shurtleff SA. Regulation of tumor necrosis factor expression in a macrophage-like cell line by lipopolysaccharide and cyclic AMP. Cell Immunol. 1989 May;120(2):291-300.

242. Endres S, Fulle HJ, Sinha B, Stoll D, Dinarello CA, Gerzer R, et al. Cyclic nucleotides differentially regulate the synthesis of tumour necrosis factor-alpha and interleukin-1 beta by human mononuclear cells. Immunology. 1991 Jan;72(1):56-60.

243. Zhong WW, Burke PA, Drotar ME, Chavali SR, Forse RA. Effects of prostaglandin E2, cholera toxin and 8-bromo-cyclic AMP on lipopolysaccharide-induced gene expression of cytokines in human macrophages. Immunology. 1995 Mar;84(3):446-52.

244. Donnelly LE, Tudhope SJ, Fenwick PS, Barnes PJ. Effects of formoterol and salmeterol on cytokine release from monocyte-derived macrophages. Eur Respir J. 2010 Jul;36(1):178-86.

245. Aronoff DM, Canetti C, Serezani CH, Luo M, Peters-Golden M. Cutting edge: macrophage inhibition by cyclic AMP (cAMP): differential roles of protein kinase A and exchange protein directly activated by cAMP-1. J Immunol. 2005 Jan 15;174(2):595-9.

246. Miyajima S, Akaike T, Matsumoto K, Okamoto T, Yoshitake J, Hayashida K, et al. Matrix metalloproteinases induction by pseudomonal virulence factors and inflammatory cytokines in vitro. Microb Pathog. 2001 Dec;31(6):271-81.

247. Pillinger MH, Marjanovic N, Kim SY, Lee YC, Scher JU, Roper J, et al. *Helicobacter pylori* stimulates gastric epithelial cell MMP-1 secretion via CagA-dependent and -independent ERK activation. J Biol Chem. 2007 Jun 29;282(26):18722-31.

248. Bebb JR, Letley DP, Thomas RJ, Aviles F, Collins HM, Watson SA, et al. *Helicobacter pylori* upregulates matrilysin (MMP-7) in epithelial cells in vivo and in vitro in a Cag dependent manner. Gut. 2003 Oct;52(10):1408-13.

249. Gomez M, Johnson S, Gennaro ML. Identification of secreted proteins of *Mycobacterium tuberculosis* by a bioinformatic approach. Infect Immun. 2000 Apr;68(4):2323-7.

250. Geisel RE, Sakamoto K, Russell DG, Rhoades ER. In vivo activity of released cell wall lipids of *Mycobacterium bovis bacillus Calmette-Guerin* is due principally to trehalose mycolates. J Immunol. 2005 Apr 15;174(8):5007-15.

251. Maiga M, Agarwal N, Ammerman NC, Gupta R, Guo H, Maiga MC, et al. Successful shortening of tuberculosis treatment using adjuvant host-directed therapy with FDA-approved phosphodiesterase inhibitors in the mouse model. PLoS One. 2012;7(2):e30749.

252. Maiga M, Ammerman NC, Maiga MC, Tounkara A, Siddiqui S, Polis M, et al. Adjuvant Host-Directed Therapy with Types 3 and 5 but Not Type 4 Phosphodiesterase Inhibitors Shortens the Duration of Tuberculosis Treatment. J Infect Dis. 2013 May 21.

253. Lee ES, Park CM, Goo JM, Yim JJ, Kim HR, Lee HJ, et al. Computed tomography features of extensively drug-resistant pulmonary tuberculosis in non-HIV-infected patients. J Comput Assist Tomogr. 2010 Jul;34(4):559-63.

254. Lee J-J, Chong P-Y, Lin C-B, Hsu A-H, Lee C-C. High resolution chest CT in patients with pulmonary tuberculosis: Characteristic findings before and after antituberculous therapy. European journal of radiology. 2008;67(1):100-4.

255. Yeh JJ, Chen SC, Teng WB, Chou CH, Hsieh SP, Lee TL, et al. Identifying the most infectious lesions in pulmonary tuberculosis by high-resolution multi-detector computed tomography. Eur Radiol. 2010 Sep;20(9):2135-45.

256. Almeida DV, Converse PJ, Li SY, Tyagi S, Nuermberger EL, Grosset JH. Bactericidal activity does not predict sterilizing activity: the case of rifapentine in the murine model of *Mycobacterium ulcerans* disease. PLoS Negl Trop Dis. 2013;7(2):e2085.

257. Diacon AH, Dawson R, von Groote-Bidlingmaier F, Symons G, Venter A, Donald PR, et al. 14-day bactericidal activity of PA-824, bedaquiline, pyrazinamide, and moxifloxacin combinations: a randomised trial. Lancet. 2012 Sep 15;380(9846):986-93.

258. Rustomjee R, Diacon AH, Allen J, Venter A, Reddy C, Patientia RF, et al. Early bactericidal activity and pharmacokinetics of the diarylquinoline TMC207 in treatment of pulmonary tuberculosis. Antimicrob Agents Chemother. 2008 Aug;52(8):2831-5.

259. Tchilian EZ, Desel C, Forbes EK, Bandermann S, Sander CR, Hill AV, et al. Immunogenicity and protective efficacy of prime-boost regimens with recombinant (delta)ureC hly+ *Mycobacterium bovis BCG* and modified vaccinia virus ankara expressing *M. tuberculosis* antigen 85A against murine tuberculosis. Infect Immun. 2009 Feb;77(2):622-31.

260. Verreck FA, Vervenne RA, Kondova I, van Kralingen KW, Remarque EJ, Braskamp G, et al. MVA.85A boosting of BCG and an attenuated, phoP deficient *M. tuberculosis* vaccine both show protective efficacy against tuberculosis in rhesus macaques. PLoS One. 2009;4(4):e5264.

261. Griffiths KL, Pathan AA, Minassian AM, Sander CR, Beveridge NE, Hill AV, et al. Th1/Th17 cell induction and corresponding reduction in ATP consumption following vaccination with the novel *Mycobacterium tuberculosis* vaccine MVA85A. PLoS One. 2011;6(8):e23463.

262. Lin PL, Coleman T, Carney JP, Lopresti BJ, Tomko J, Fillmore D, et al. Radiologic responses in cynomolgous macaques for assessing tuberculosis chemotherapy regimens. Antimicrob Agents Chemother. 2013 Jun 24.

263. Dey B, Luna B, Miller-Jaster K, Foster B, Bagci U, Klunk M, et al., editors. Qualitative and Quantitative Analysis of Inflammation in Pulmonary Tuberculosis in Rabbit using F18-FDG-PET/CT Imaging: A multi-Parametric Approach. Molecular Imaging of Infectious Diseases: Current Status and

Future Challenges; 2012 09/21/2012; National Institutes of Health, Bethesda, MD, USA.

264. Luna B, Kubler A, Larsson C, Klunk M, Jain SK, Bishai WR, editors. Cavity Development in the Rabbit Model of Tuberculosis is Independent of Inflammation. Molecular Imaging of Infectious Diseases: Current Status and Future Challenges; 2012 09/21/2012; National Institutes of Health, Bethesda, MD, USA.

265. Nakamura S, Ogawa Y, Yamamura Y, Yasaka S. The experimental production of nontuberculous cavities in rabbit lungs of egg albumin. Am Rev Tuberc. 1957 Jan;75(1):99-104.

266. Lurie MB. Experimental epideminology of tuberculosis: the effect of a primary infection on contact tuberculosis in rabbits. J Exp Med. 1933 Aug 31;58(3):305-27.

267. Bishai WR, Dannenberg AM, Jr., Parrish N, Ruiz R, Chen P, Zook BC, et al. Virulence of *Mycobacterium tuberculosis CDC1551* and *H37Rv* in rabbits evaluated by Lurie's pulmonary tubercle count method. Infect Immun. 1999 Sep;67(9):4931-4.

268. Manca C, Tsenova L, Bergtold A, Freeman S, Tovey M, Musser JM, et al. Virulence of a *Mycobacterium tuberculosis* clinical isolate in mice is determined by failure to induce Th1 type immunity and is associated with induction of IFN-alpha /beta. Proc Natl Acad Sci U S A. 2001 May 8;98(10):5752-7.

269. Barczak AK, Domenech P, Boshoff HI, Reed MB, Manca C, Kaplan G, et al. In vivo phenotypic dominance in mouse mixed infections with *Mycobacterium tuberculosis* clinical isolates. J Infect Dis. 2005 Aug 15;192(4):600-6.

270. Ordway D, Henao-Tamayo M, Harton M, Palanisamy G, Troudt J, Shanley C, et al. The hypervirulent *Mycobacterium tuberculosis* strain HN878 induces a potent TH1 response followed by rapid down-regulation. J Immunol. 2007 Jul 1;179(1):522-31.

271. Keane J, Gershon S, Wise RP, Mirabile-Levens E, Kasznica J, Schwieterman WD, et al. Tuberculosis associated with infliximab, a tumor necrosis factor alpha-neutralizing agent. N Engl J Med. 2001 Oct 11;345(15):1098-104.

272. Curtis J, Kopanitsa L, Stebbings E, Speirs A, Ignatyeva O, Balabanova Y, et al. Association analysis of the LTA4H gene polymorphisms and pulmonary tuberculosis in 9115 subjects. Tuberculosis (Edinb). 2011 Jan;91(1):22-5.

273. Singh A, Mohan A, Dey AB, Mitra DK. Inhibiting the Programmed Death 1 Pathway Rescues *Mycobacterium tuberculosis*-Specific Interferon gamma-Producing T Cells From Apoptosis in Patients With Pulmonary Tuberculosis. J Infect Dis. 2013 Jun 5.

274. Barber DL, Mayer-Barber KD, Feng CG, Sharpe AH, Sher A. CD4 T cells promote rather than control tuberculosis in the absence of PD-1-mediated inhibition. J Immunol. 2011 Feb 1;186(3):1598-607.

275. Lazar-Molnar E, Chen B, Sweeney KA, Wang EJ, Liu W, Lin J, et al. Programmed death-1 (PD-1)-deficient mice are extraordinarily sensitive to tuberculosis. Proc Natl Acad Sci U S A. 2010 Jul 27;107(30):13402-7.

276. Subbian S, Tsenova L, O'Brien P, Yang G, Koo MS, Peixoto B, et al. Phosphodiesterase-4 inhibition alters gene expression and improves isoniazid-mediated clearance of *Mycobacterium*

tuberculosis in rabbit lungs. PLoS Pathog. 2011 Sep;7(9):e1002262.

277. Hamid O, Robert C, Daud A, Hodi FS, Hwu W-J, Kefford R, et al. Safety and Tumor Responses with Lambrolizumab (Anti–PD-1) in Melanoma. New England Journal of Medicine. 2013;369(2):134-44.

278. Nielsen OH, Ainsworth MA. Tumor necrosis factor inhibitors for inflammatory bowel disease. N Engl J Med. 2013 Aug 22;369(8):754-62.

279. Israel E, Dermarkarian R, Rosenberg M, Sperling R, Taylor G, Rubin P, et al. The effects of a 5-lipoxygenase inhibitor on asthma induced by cold, dry air. N Engl J Med. 1990 Dec 20;323(25):1740-4.

280. Leff JA, Busse WW, Pearlman D, Bronsky EA, Kemp J, Hendeles L, et al. Montelukast, a leukotriene-receptor antagonist, for the treatment of mild asthma and exercise-induced bronchoconstriction. N Engl J Med. 1998 Jul 16;339(3):147-52.

281. Kumar PJ, Clark ML. Kumar & Clark's clinical medicine. 7th ed. Edinburgh ; New York: Saunders Elsevier; 2009.

282. Jauregui-Amezaga A, Turon F, Ordas I, Gallego M, Feu F, Ricart E, et al. Risk of developing tuberculosis under anti-TNF treatment despite latent infection screening. J Crohns Colitis. 2013 Apr 1;7(3):208-12.

283. Jung YJ, Lyu J, Yoo B, Lee CK, Kim YG, Yang SK, et al. Combined use of a TST and the T-SPOT(R).TB assay for latent tuberculosis infection diagnosis before anti-TNF-alpha treatment. Int J Tuberc Lung Dis. 2012 Oct;16(10):1300-6.

284. Tannus Silva DG, Silva BD, Torres PP, Santana PJ, Jr., Junqueira-Kipnis AP, Fouad Rabahi M. Latent tuberculosis in rheumatoid arthritis: evaluating cellular response and high-resolution computed tomography. Arch Bronconeumol. 2012 May;48(5):144-9.

285. Park JH, Seo GY, Lee JS, Kim TH, Yoo DH. Positive conversion of tuberculin skin test and performance of interferon release assay to detect hidden tuberculosis infection during anti-tumor necrosis factor agent trial. J Rheumatol. 2009 Oct;36(10):2158-63.

286. Cobat A, Gallant CJ, Simkin L, Black GF, Stanley K, Hughes J, et al. Two loci control tuberculin skin test reactivity in an area hyperendemic for tuberculosis. J Exp Med. 2009 Nov 23;206(12):2583-91.

287. Donnelly CA, Woodroffe R, Cox DR, Bourne J, Gettinby G, Le Fevre AM, et al. Impact of localized badger culling on tuberculosis incidence in British cattle. Nature. 2003;426(6968):834-7.

288. Donnelly CA, Woodroffe R, Cox DR, Bourne FJ, Cheeseman CL, Clifton-Hadley RS, et al. Positive and negative effects of widespread badger culling on tuberculosis in cattle. Nature. 2006;439(7078):843-6.

289. Torgerson P, Torgerson D. Benefits of stemming bovine TB need to be demonstrated. Nature. 2009;457(7230):657-.

290. Gordon SV. Bovine TB: stopping disease control would block all live exports. Nature. 2008;456(7223):700-.

291. Donnelly CA, Woodroffe R. Epidemiology: Reduce uncertainty in UK badger culling. Nature. 2012;485(7400):582-.

292. Roper TJ. Ecology: Badger cull culled. Nature. 2003;426(6968):782-3.

293. Brumfiel G. Badger battle erupts in England. Nature. 2012 Oct 18;490(7420):317-8.

294. Woolhouse M, Wood J. Tuberculosis: Society should decide on UK badger cull. Nature. [Correspondence]. 2013;498(7455):434-.

295. de Kantor IN, LoBue PA, Thoen CO. Human tuberculosis caused by *Mycobacterium bovis* in the United States, Latin America and the Caribbean. Int J Tuberc Lung Dis. 2010 Nov;14(11):1369-73.

296. Cordova E, Gonzalo X, Boschi A, Lossa M, Robles M, Poggi S, et al. Human *Mycobacterium bovis* infection in Buenos Aires: epidemiology, microbiology and clinical presentation. Int J Tuberc Lung Dis. 2012;16(3):415-7.

297. Hemmings FJ, Farhan M, Rowland J, Banken L, Jain R. Tolerability and pharmacokinetics of the collagenase-selective inhibitor Trocade in patients with rheumatoid arthritis. Rheumatology (Oxford). 2001 May;40(5):537-43.

298. Cakir Y, Hahn KA. Direct action by doxycycline against canine osteosarcoma cell proliferation and collagenase (MMP-1) activity in vitro. In Vivo. 1999 Jul-Aug;13(4):327-31.

299. Koivunen AL, Maisi P, Konttinen YT, Prikk K, Sandholm M. Collagenolytic activity and its sensitivity to doxycycline inhibition in tracheal aspirates of horses with chronic obstructive pulmonary disease. Acta Vet Scand. 1997;38(1):9-16.

300. Shlopov BV, Stuart JM, Gumanovskaya ML, Hasty KA. Regulation of cartilage collagenase by doxycycline. J Rheumatol. 2001 Apr;28(4):835-42.

301. Smith GN, Jr., Mickler EA, Hasty KA, Brandt KD. Specificity of inhibition of matrix metalloproteinase activity by doxycycline: relationship to structure of the enzyme. Arthritis Rheum. 1999 Jun;42(6):1140-6.

302. Suomalainen K, Halinen S, Ingman T, Lindy O, Saari H, Konttinen YT, et al. Tetracycline inhibition identifies the cellular sources of collagenase in gingival crevicular fluid in different forms of periodontal diseases. Drugs Exp Clin Res. 1992;18(3):99-104.